41
Vol. 1

UNIVERSIDAD POLITÉCNICA SALESIANA

LA GRANJA 41

THE LIFE SCIENCE JOURNAL Num. (1)

SPECIAL ISSUE

CONNECTIVITY CORRIDORS A STRATEGY FOR TERRITORY CONSERVATION

ISSN impress:1390-3799 / ISSN electronic:1390-8596

MISCELLANEOUS

- Land use/land cover change in the Llanganates-Sangay connectivity corridor by 2030
- Presence of Poison Dart Frogs and some Insights for Their Conservation
- Rainfall characteristics and extreme events using a vertically pointing rain radar
- Urban photobioreactor for CO_2 sequestration and microalgal biomass production
- Identifying an antimicrobial peptide of *Chamaemelum nobile*

©Molestina / WWF-Ecuador

LA GRANJA

Index

Editorial 7

Scientific Paper

Special issue: Connectivity Corridors. A strategy for the conservation of territories

Analysis and prediction of land use/land cover change in the Llanganates-Sangay Connectivity Corridor by 2030 11
Luis Jaramillo, Andrea Mancheno Herrera, Adriana Guzmán and Juan Gabriel Mollocana Lara.

Multivariate analysis of Ecuadorian provinces and protected areas based on the presence of poison dart frogs (*Dendrobatidae*) and some insights for their conservation 32
Patricio Yánez-Moretta, Julio Gereda-García, Alexander Huaraca-Egas, Michael Baldeón-Morales and Darwin Quinteros-Sarmiento.

Conservation

Pesticides and their impact on entomofauna in Andean farmers' fields in Ecuador 51
Diego Mina, Jhenny Cayambe, Tatiana Cárdenas, Israel Navarrete and Olivier Dangles.

Earth Sciences

Rainfall Characteristics and extreme events in the Tropical Andes using a Vertically Pointing rain radar 69
Javier Chininín-Cabrera and Rolando Célleri.

Dichotomous contingent valuation of the water ecosystem service in an Andean microwatershed in Ecuador 82
Edison Campos Collaguazo and Luis Jimenez.

Biotechnology

Urban photobioreactor for CO_2 sequestration and microalgal biomass production 95
Saim Khan, Mehmood Ali, Atif Mustafa and Aqsa Iqbal.

Identification of an antimicrobial peptide from *Chamaemelum nobile* 112
Diana Daniela Portela Dussán, Sandra Mónica Estupiñan Torres and Silvio Alejandro Lopez-Pazos.

Veterinary Sciences

Assessment of Physicochemical, Microbial, and Hygienic Quality of Raw Cow Milk Produced in Dairy Herds from the Peruvian Andes 121
Fernando Arauco Villar, Leonor Guzmán Estremadoyro, Rafael Pantoja Esquivel, Noemí Mayorga Sánchez, Ide Unchupaico Payano and Alex Rubén Huamán de la Cruz.

Agricultural Sciences

Improvement of the nutritional value of *Lupinus mutabilis* Sweet foliage meal by solid-state fermentation with *Aspergillus niger* J1 and *Trichoderma viride* M5-2 strains 133
David Catagua, Julio Dustet Mendosa and Elaine Valiño Cabrera.

Planting Distance in *Zea mays* L. during the dry and rainy seasons on the central Coast of Ecuador 144
Camilo Alexander Mestanza Uquillas, Pánfilo José Cedeño Cárcamo, Diana Verónica Véliz Zamora, Santiago Cristóbal Vásquez Matute and John Jairo Pinargote Alava.

Guidelines 155

LA GRANJA:
REVISTA DE
CIENCIAS DE LA VIDA

Editorial

Dear reader,

It is an honor to present Volume 41 of *La Granja* journal. This special issue, titled "Connectivity Corridors: A Strategy for Territorial Conservation", highlights the efforts of researchers dedicated to understanding and promoting the importance of ecological connectivity as a key tool for conservation and land management.

Connectivity corridors are special areas for biodiversity conservation, established between the National System of Protected Areas (SNAP), National Forest Heritage, areas of hydrological importance, buffer zones, and other conservation areas recognized by international instruments ratified by Ecuador, such as RAMSAR sites and Key Biodiversity Areas (KBAs). Their objective is to mitigate the effects of landscape fragmentation and the risks associated with the isolation of flora and fauna populations by utilizing remnant habitats that maintain genetic flows and ecological processes. This ensures the connectivity of wild populations, ecosystem resilience, and the continuous provision of environmental services in areas outside protected zones, where varying levels of human pressures occur.

Ecuador has been a pioneer in establishing connectivity corridors as an innovative conservation approach. The country has implemented *Ministerial Agreement 0019*, which facilitates the design, recognition, and management of connectivity corridors. To date, the Ministry of Environment, Water, and Ecological Transition (MAATE) has officially recognized three connectivity corridors.

This recognition grants them significance in local territorial planning, as current regulations mandate their inclusion in development and land-use plans. Additionally, MAATE is leading a participatory process to define the best management tools for these corridors, acknowledging that planning instruments must be comprehensive, accessible, and easily applicable.

Their relevance lies in being complementary alternatives to traditional conservation schemes, whose long-term efficiency is often compromised by geographical isolation and human disturbances. Furthermore, the recognition of new protected areas is an increasingly evident technical and political challenge.

Therefore, the recognition of connectivity corridors, along with the establishment and strengthening of their priority conservation areas, collaboration with local communities and stakeholders in implementing sustainable land management practices, and participatory governance, enhances the effective connectivity area and promotes the coordination of local and regional actors.

This special issue includes studies that provide key evidence for understanding and strengthening connectivity corridors in Ecuador.

The first study, "Analysis and Prediction of Land Use and Cover Change in the Llanganates-Sangay Connectivity Corridor by 2030", employs advanced spatial modeling tools, such as MOLUSCE and artificial neural networks, to project future scenarios of land-use transformation in the Llanganates-Sangay Connectivity Corridor (CELS). While the results indicate lower deforestation rates in protected areas within the CELS, threats persist in non-protected zones. The recognition of the CELS presents an opportunity to consolidate conservation strategies in priority areas for connectivity and strengthen zones with official conservation schemes.

The second study, "Multivariate Analysis of Ecuadorian Provinces and Protected Areas Based on the Presence of Poison Dart Frogs (*Dendrobatidae*) and Considerations for Their Conservation", analyzes the distribution of 48 species of poison dart frogs, 32 of which are endemic to Ecuador. These species, considered key bioindicators, reflect the health status of ecosystems. Through classification and ordination analyses, the study identifies priority regions for the conservation of these amphibians and underscores the importance of ecological corridors in facilitating connectivity between fragmented populations.

In the journal's miscellaneous section, aligned with conservation themes, Diego Mina and his research team from the Pontificia Universidad Católica del Ecuador, the International Potato Center of Ecuador, and the Center for Functional and Evolutionary Ecology (UMR CEFE) in Montpellier, France, present a study on pesticide use and its impact on entomofauna in Andean farms in Ecuador. The study highlights the importance of improving agricultural practices and the rational use of pesticides, not only to enhance crop yields but also to preserve pollinator species vital for the agricultural sector's development.

Similarly, Edison Campos Collaguazo and Luis Alberto Jiménez from the National Agrarian University La Molina in Peru conduct a study on "Valuation of Hydrological Ecosystem Services in a Páramo Microbasin in Ecuador", using the contingent valuation method to determine the community's willingness to pay for this ecosystem service, thereby promoting its conservation.

From the earth sciences, Javier Chininín-Cabrera and Rolando Célleri, researchers from the University of Cuenca in Ecuador, conduct a study to determine rainfall characteristics and extreme events in the Tropical Andes using a vertically pointing radar. This region is characterized by its complexity and limited data availability, posing significant challenges for atmospheric models in simulating rainfall. This research contributes to understanding the vertical structure, diurnal cycle, and convective or non-convective origins of precipitation, potentially improving the prediction of extreme rainfall events.

From Pakistan, researchers Mehmood Ali Khan, Mustafa Atif, and Iqbal Aqsa from the University of Engineering and Technology in Karachi present an urban photobioreactor for CO_2 sequestration and microalgal biomass production, which has applications in biofuel production and other value-added products, making it an interesting contribution to climate change mitigation through greenhouse gas sequestration.

In the field of biotechnology, Diana Portela Dussán and her research team from the Universidad Antonio Nariño and the Universidad Colegio Mayor de Cundinamarca in Colombia present their research on the identification of an antimicrobial peptide from Roman chamomile. Using *in silico* and experimental approaches, they found that its apoplastic fluid inhibits the development of *R. solani*, representing a previously uncharacterized activity.

Finally, in agricultural sciences, Fernando Arauco Villar and a broad team of researchers from the National University of Central Peru, the Technological University of Peru, and the Peruvian Union University evaluate the physicochemical, microbial, and hygienic quality of cow's milk in the Peruvian Andes. Additionally, David Catagua, Julio Dustet Mendosa, and Elaine Valiño Cabrera, in a collaborative study between the Escuela Superior Politécnica del Litoral in Ecuador and the Technological University of Havana "José Antonio Echeverría" in Cuba, present their research on improving the nutritional value of chocho foliage flour through solid-state fermentation with lignocellulolytic fungal strains, finding significant improvements in the legume's nutritional value.

We are confident that this volume represents an unprecedented effort in compiling and disseminating scientific results that are relevant to strengthening ecological connectivity and advancing life and environmental sciences. It is clear that science must play a fundamental role in local and regional planning, providing solid foundations for the implementation and monitoring of conservation strategies with the involvement of local stakeholders and civil society. Specifically, this special issue demonstrates the imperative to continue generating research in these areas and to strengthen collaboration among the academic community, conservation institutions, protected area managers, private landowners, and decision-makers at local and national levels to promote informed land management decisions based on technical and scientific evidence.

Sincerely,

MSc. Andrea Mancheno Herrera
World Wildlife Fund (WWF), Ecuador
GUEST EDITOR

PhD. Gorki Ríos Alvear
University of Porto, Portugal
Universidad IKIAM, Ecuador
GUEST EDITOR

PhD. Rafael Antelo
Wildlife Connect Leader and PACHA Coordinator (WWF), Bolivia
GUEST EDITOR

PhD. Sheila Serrano Vincenti
Universidad Politécnica Salesiana, Ecuador
EDITOR-IN-CHIEF

PhD. Ignacio de los Ríos
Universidad Politécnica de Madrid, España
EDITOR-IN-CHIEF

La granja: Revista de Ciencias de la Vida
pISSN:1390-3799; eISSN:1390-8596
https://doi.org/10.17163/lgr.n41.2025.01

Special Issue / Edición Especial
Conectivity Corridors

Analysis and prediction of land use/land cover change in the Llanganates-Sangay Connectivity Corridor by 2030

Análisis y predicción del cambio de uso y cobertura de suelo en el Corredor de Conectividad Llanganates-Sangay para 2030

Luis Jaramillo[1,2], Andrea Mancheno Herrera[1,6], Adriana Guzmán*[3,4,6] and Juan Gabriel Mollocana Lara*[5]

[1] *World Wildlife Fund (WWF) Ecuador, Código Postal 170517, Quito, Ecuador.*
[2] *Nippon Koei Latin America- Caribbean Co. Ltd., Código Postal 170526, Quito, Ecuador.*
[3] *Facultad de Recursos Naturales. Escuela Superior Politécnica de Chimborazo ESPOCH, Código Postal EC060155, Riobamba, Ecuador.*
[4] *Centro de Estudios Integrales de Dinàmica Exògena CEIDE. Universidad Nacional de La Plata, Código Postal 1900, La Plata, Argentina.*
[5] *Grupo de Investigación Ambiental en el Desarrollo Sustentable GIADES, Ingeniería Ambiental. Universidad Politécnica Salesiana UPS, Quito, 170702, Ecuador.*
[6] *Red de Investigación del Corredor Ecológico Llanganates Sangay.*

*Corresponding author: catalina.guzman@espoch.edu.ec, jmollocana@ups.edu.ec

Received on October 1st, 2024. Accepted, after revision on February 14th, 2025. Published on March 1st, 2025.

Abstract

This paper analyses Land Use and Land Cover (LULC) change trends in the Llanganates-Sangay Connectivity Corridor (CELS) from 2018 to 2022 and predicts trends through 2030. MapBiomas LULC maps reveals annual change rates (2018–2022) of -0.37%/year (-1147.33 ha) for Forest Formation, -1.17%/year (-30.01 ha) for Non-Forest Natural Formation, 2.21%/year (906.19 ha) for Agriculture and Livestock Areas, 8.50%/year (250.84 ha) for Non-Vegetated Areas, and 0.17%/year (30.31 ha) for Water Bodies. The higher annual change rate inside Forest Formation is -0.58%/year (-990.35 ha) occurring in areas not designated under any conservation status. Projections for 2030 were made using the MOLUSCE tool, combining an Artificial Neural Network (ANN) model with Cellular Automata simulations. The ANN model was trained on five explanatory variables and LULC maps from 2018 and 2020, achieving a training error of 8.46%. Predictive accuracy was assessed by comparing the simulated 2022 LULC map with the 2022 MapBiomas map, resulting in a Kappa coefficient of 0.95, indicating excellent predictive accuracy. Additionally, LULC simulations from 2022 to 2030 predict annual rates of change of –0.27%/year (-1628.97 ha) for Forest Formation, -1.39%/year (-63.49 ha) for Non-Forest Natural Formation, 1.92%/year (1778.26 ha) for Agriculture and Livestock Areas, 0.97%/year (30.38 ha) for Non-Vegetated Areas, and 0.63%/year (-146.18 ha) for Water Bodies. The findings show that annual rates of deforestation will remain low and protected areas will have less deforestation than non-protected areas.

Keywords: Deforestation, CELS, MOLUSCE, LULC changes.

Resumen

Este estudio analiza las tendencias de cambio de uso y cobertura del suelo (LULC) en el Corredor de Conectividad Llanganates-Sangay (CELS) durante el período 2018-2022 y predice tendencias hasta 2030. Los mapas de LULC de MapBiomas revelan tasas anuales de cambio (2018-2022) de -0,37%/año (-1147.33 ha) para Formación de Bosque, -1,17%/año (-30,01 ha) para Formaciones Naturales No Boscosas, 2,21%/año (906.19 ha) para Áreas de Agricultura y Ganadería, 8,50%/año (250,84 ha) para Áreas sin Vegetación y 0,17%/año (30,31 ha) para Cuerpos de Agua. La mayor tasa de cambio anual dentro de Formación de Bosque, -0,58%/año (-990,35 ha), ocurre en áreas no protegidas. Las proyecciones para 2030 se realizaron utilizando la herramienta MOLUSCE, que combina una Red Neuronal Artificial (ANN) con simulaciones de Autómatas Celulares. La ANN fue entrenada con cinco variables explicatorias y mapas de LULC de 2018 y 2020, logrando un error de entrenamiento de 8,46%. La precisión predictiva se evaluó comparando el mapa simulado de LULC para 2022 con el mapa de MapBiomas 2022, obteniendo un coeficiente Kappa de 0,95, lo que indica una excelente precisión. Además, las simulaciones de LULC para 2022-2030 predicen tasas anuales de cambio de -0,27%/año (-1628,97 ha) para Formación de Bosque, -1,39%/año (-63,49 ha) para Formaciones Naturales No Boscosas, 1,92%/año (1778,26 ha) para Áreas de Agricultura y Ganadería, 0,97%/año (30,38 ha) para Áreas No Vegetadas y 0,63%/año (-146,18 ha) para Cuerpos de Agua. Los resultados sugieren que las tasas anuales de deforestación se mantendrán bajas y que las áreas protegidas tendrán menos deforestación que las áreas que no están protegidas.

Palabras clave: Deforestación, CELS, MOLUSCE, cambios de cobertura y uso de suelo.

Suggested citation: Jaramillo, L., Mancheno Herrera, A., Guzmán, A. and Mollocana Lara, J.G. (2025). Analysis and prediction of land use/land cover change in the Llanganates-Sangay Connectivity Corridor by 2030. *La Granja: Revista de Ciencias de la Vida.* Vol. 41(1):11-31. https://doi.org/10.17163/lgr.n41.2025.01.

Orcid IDs:

Luis Jonathan Jaramillo Coronel: https://orcid.org/0000-0002-3127-9855
Andrea Cecilia Mancheno Herrera: https://orcid.org/0009-0000-5525-1665
Adriana Catalina Guzmán Guaraca: https://orcid.org/0000-0003-0473-2041
Juan Gabriel Mollocana Lara: https://orcid.org/0000-0002-2430-8400

1 Introduction

Ecuador is known worldwide as one of the 13 most biodiverse countries in the world, but it faces a growing threat, as between 1990 and 2000 the country lost 15% of its native forest area, leading to one of the highest deforestation rates in Latin America (Rivas et al., 2024). This dynamic mainly affects the Amazon, considered one of the most biodiverse regions on the planet (Mainville et al., 2006). Forest losses compromise the country's capacity to keep global warming below 1.5°C, since this region stores between 367 and 733 Gt of CO_2 in its vegetation and soils (Vergara et al., 2022).

Deforestation and land use change have caused an accelerated fragmentation of natural vegetation areas in the Andes and the Ecuadorian Amazon. Between 1990 and 2018, with the main affected areas being the buffer zones of protected areas, 25.5% were lost in their surroundings (Kleemann et al., 2022). These dynamics compromise the effectiveness of conservation strategies, even in areas with high levels of protection. Fragmentation affects the provision of essential ecosystem services, such as water regulation, carbon storage and biodiversity conservation.

In this context, it is crucial to implement comprehensive measures that include forest conservation and sustainable management of buffer zones (Vergara et al., 2022). Nowadays, tools based on remote sensing and artificial intelligence allow progress in the analysis and prediction of LULC changes, both spatially and temporally. Classification techniques such as Random Forest (RF) and Support Vector Machines (SVM) have demonstrated high accuracy in the generation of land use and land cover mapping, facilitating the observation and analysis of deforestation processes and LULC transformation (Admas, 2024; Elagouz et al., 2020; Lukas et al., 2023; Tikuye et al., 2023).

In this study, we also used the *QGIS add-on MOLUSCE* (Modules for Land Use Change Evaluation), which combines spatial and temporal data with advanced modeling techniques, such as cellular automata (CA) and artificial neural networks (ANN). This tool allows simulating and predicting changes in land use and land cover. MOLUSCE has demonstrated its effectiveness in various contexts (Muhammad et al., 2022; Talukdar et al., 2020). The Llanganates-Sangay Connectivity Corridor (CELS) is a critical ecological link, connecting Llanganates National Park in the north, Sangay National Park in the south and several conservation areas recognized under diverse schemes within its boundaries. The CELS encompasses a significant ecotone, bridging the Andean highlands and the Amazon basin, and playing a pivotal role in preserving the region's unique ecosystems (Ríos-Alvear et al., 2024).

Relevant scientific research has been developed for more than 150 years in this area, with important results, such as the identification of 178 species of orchids and nearly 200 species of endemic plants, surpassing even the Galapagos Islands in botanical diversity (Jost, 2004). It is also home to nearly 700 species of birds and 285 species of reptiles and amphibians, surpassing the records of Yasuní National Park (INABIO et al., 2023). However, human activities have reshaped this area. For instance, late colonization processes in cities like Baños and Puyo, driving human settlement and economic activities such as tourism and agriculture, have significantly influenced land use changes in the region, leading to the conversion of natural areas into agricultural and urban spaces (Herrera and Rodríguez, 2016). Deforestation and LULC change have increased landscape fragmentation and significantly reduced ecosystem connectivity, putting the survival of species and the provision of ecosystem services at risk (Reyes-Puig et al., 2023).

This study aims to determine land use and land cover changes in the Llanganates-Sangay Connectivity Corridor (CELS) from 2018 to 2022 and project trends up to 2030 using the MOLUSCE tool. It focuses on quantifying forest cover loss during the analysis period and forecasting future scenarios of change in LULC, based on changes recorded between 2018 and 2022.

2 Materials and Methods

2.1 Study area

The Llanganates-Sangay Connectivity Corridor (CELS) spans the provinces of Tungurahua, Pastaza, and Morona Santiago (Figure 1) and encompasses 92,148 hectares (Viteri-Basso et al., 2024). The corridor serves as an ecological link, connecting Llanganates National Park in the north with Sangay National Park in the south. It forms a key transition zone between the eastern Andes and the western Amazon. This area was designated as a "Gift to the Earth" by WWF in 2002, recognizing its global importance for biodiversity. The CELS was officially recognized as a Connectivity Corridor in 2023 by Ecuador's Ministry of Environment and Natural Resources (Ríos-Alvear et al., 2024).

The CELS ranges in altitude from 760 and 3812 meters above sea level and has a rainy tropical climate (Viteri-Basso et al., 2024), with annual precipitation between 2500 and 5500 mm and temperatures ranging between 9 and 22°*C*. These climatic and altitudinal variations favor the formation of habitats that foster exceptional biodiversity (Gaglio et al., 2017; Ríos-Alvear et al., 2024). This area plays an important role in providing water resources for the Pastaza and Napo River basins that are vital for local communities, agricultural and tourism activities, and hydroelectric energy generation (Gaglio et al., 2017).

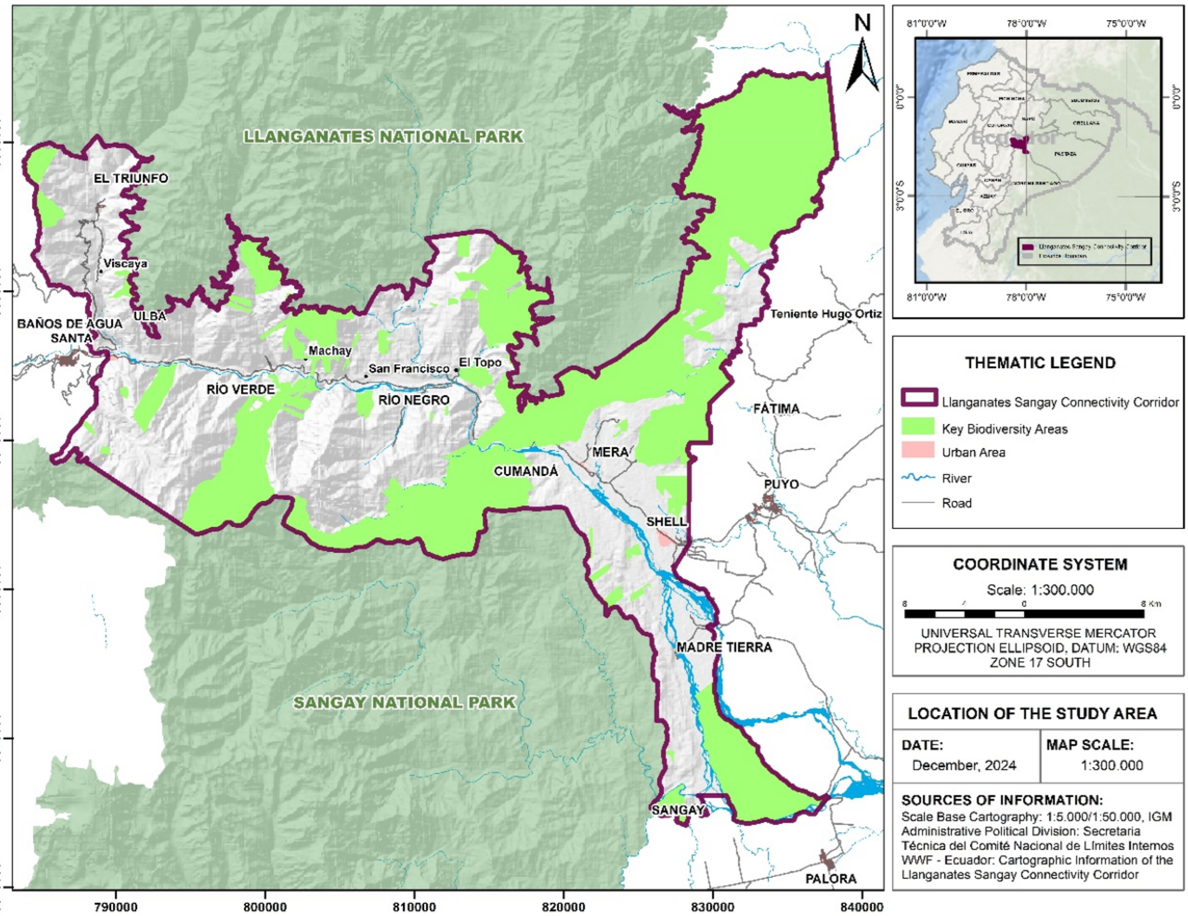

Figure 1. Location map of the CELS.

The primary economic activities in this area include agriculture, cattle ranching, tourism, fish farming, and timber production. While these activities are critical to the local economy, they have significantly impacted ecosystems, leading to deforestation and habitat fragmentation (Delgado Fernández et al., 2023).

Over the past two decades, various conservation initiatives have been implemented in this area, led by local, national, and international organizations such as EcoMinga Foundation, local governments, the Ministry of Environment, Water and Ecological Transition of Ecuador (MAATE), WWF, among others. Ecotourism initiatives within CELS can be found in the geoportal *https://geocels-upsq.hub.arcgis.com/*

Conservation strategies have included, for instance, the establishment of officially recognized protected areas, the management of privately conserved areas not officially recognized but designated for ecosystem conservation, and collaboration with local communities to promote sustainable land management practices. The latter includes supporting the adoption of agroecological practices to prevent soil degradation, maintain fertility, and curb agricultural frontier expansion (Aneloa et al., 2024). Additionally, nature-based tourism has been boosted as a sustainable development strategy to enhance local livelihoods while preserving natural ecosystems.

Despite these efforts, there remains the need to further integrate local communities into sustainable management strategies that effectively balance socioeconomic development with environmental conservation (Alvarado, 2020; Aneloa et al., 2024).

2.2 Data collection

Satellite imagery is essential for monitoring rainfall, deforestation, land use changes, and environmental impacts (Perea-Ardila et al., 2021). However, the high cloud cover in the Ecuadorian Amazon, located within the intertropical convergence zone, limits spatial data availability (Heredia-R et al., 2021). To address this, *MapBiomas* Collection 1.0 (MapBiomas, 2024) was chosen for its extensive temporal coverage (1985–2022) and ability to avoid a cloud cover category, which occupies nearly 10% of the CELS in other datasets. This improves differentiation between land use and land cover classes.

The *MapBiomas* 1.0 Collection provides annual land use and land cover (LULC) maps for Ecuador at a 30-meter resolution. These maps are generated through supervised classification using the Random Forest algorithm applied at the pixel level, based on satellite image mosaics from the Landsat series 4, 5, 7, 8, and 9. It uses a standardized legend tailored to Ecuador's specific land cover, dividing land into five main categories: Forest Formation, Non-Forest Natural Formation, Agriculture and Livestock Areas, Non-Vegetated Areas, and Water Bodies (Table 1). Natural forests fall under Forest Formation, while forest plantations, including silviculture, are classified as Agriculture and Livestock Areas. For detailed LULC category definitions, see Borja et al. (2023).

2.3 LULC change analysis and prediction by 2030

To achieve the objectives of this study, LULC maps from 2018 to 2022 were obtained from the MapBiomas platform and relevant explanatory variables related to LULC changes were generated using official data sources. The LULC maps from 2018 to 2022 were used to perform the LULC change analysis. Additionally, the LULC maps from 2018, 2020, and 2022, along with explanatory variables maps, were used to develop and validate a model designed to predict LULC changes through simulations up to 2030. The LULC change analysis, modeling, validation, and simulations were performed using the MOLUSCE tool (Figure 2).

Table 1. Classification of categories by land uses and land covers.

N°	Categories	Land Use/ Land Cover
1	Forest formation	Forest, open forest, mangrove and floodable forest.
2	Non-forest natural formation	Non-Forest wetland, grassland, rocky outcrop, other non-forest formations
3	Agriculture and Livestock Areas	Silviculture, Mosaic of cropland and pasture
4	Non-Vegetated Areas	Mining, urban areas, other non-vegetated areas
5	Water Bodies	Rivers, lakes, glaciers, aquaculture

2.3.1 LULC changes analysis

To describe LULC changes from 2018 to 2022, MapBiomas LULC maps were analyzed at one-year intervals. This analysis enabled the identification of historical LULC changes, detecting trends, and calculating LULC's annual rate of change. MOLUSCE tool was used to compute the transition matrix from 2018 to 2022, and the annual rate of change was calculated using Equation 1 (Puyravaud, 2003), originally proposed for deforestation studies but applicable to any LULC change due to its general formulation (Kouassi et al., 2021). Where q is the annual rate of change (1/year or %/year), A_1 is the LULC area at year t_1 and A_2 is the LULC area at year t_2, with $t_2 > t_1$.

$$q = \left(\frac{A_2}{A_1}\right)^{\dfrac{1}{t_2 - t_1}} - 1 \tag{1}$$

2.3.2 MOLUSCE

The MOLUSCE tool was used to analyze and simulate LULC changes up to 2030. This QGIS plugin allows for calculating transition matrices and incorporates widely accepted algorithms for modeling and simulations, such as Artificial Neural Networks (ANN), Cellular Automata (CA), and the Kappa coefficient for validating the accuracy; this index ranges from 0 to 1, which is interpreted as poor and almost perfect, respectively (Gaur and Singh, 2023; Jain, 2024; Mollocana Lara and Paredes Obando, 2024). These algorithms have been widely applied in LULC modeling studies, such as those conducted by Souza et al. (2020); Xu et al. (2024).

ANN learns spatial patterns and relationships between historical data and explanatory variables, modeling the transition potential and CA simulates dynamic spatial processes by applying transition rules based on neighborhood conditions (Alipbeki et al., 2024; Tenorio et al., 2022).

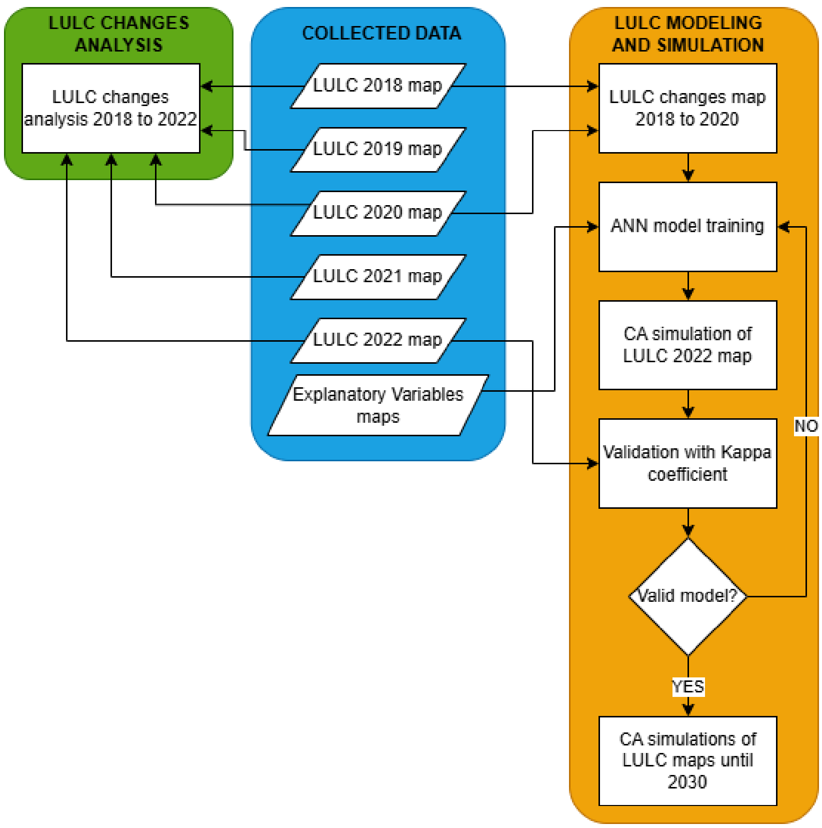

Figure 2. Methodology diagram for LULC analysis and prediction.

To predict LULC maps using the MOLUSCE tool, it is necessary to collect cartographic information representing explanatory variables related to LULC changes. This allows the Artificial Neural Network (ANN) algorithm within MOLUSCE to consider these variables during training, replicating learned behaviors and identifying spatial patterns (Al Mazroa et al., 2024). Five explanatory variables in raster format related to LULC changes were generated and integrated into the MOLUSCE tool. These variables are shown in Table 2.

Table 2. Definitions of explanatory variables for ANN training.

Variable	Definition
Proximity to roads	Raster representing the Euclidean distance in meters from each pixel to the nearest road
Proximity to settlements	Raster representing the Euclidean distance in meters from each pixel to urban centers
Protection level of natural areas	Raster representing the protection level of natural areas against natural cover removal on a scale from 0 to 5, where 0 indicates non-protected areas and 5 represents the highest level of protection
Altitude	Raster showing the height above sea level (m.a.s.l) for each pixel
Slope	Raster indicating the steepness or incline of the land for each pixel in degrees

Previous studies have identified proximity to roads and urban centers as key drivers of LULC change, as areas closer to these features tend to experience higher rates of natural cover loss due to increased accessibility and human activity (Gaur and Singh, 2023). Vegetation closer to roads and populated areas is more susceptible to removal due to the expansion of the agricultural frontier and the creation of pastures for livestock (Fischer et al., 2021).

Topographic features such as elevation and slope play an important role in determining the suitability of land for agriculture and development, as human activities are restricted or face difficulties in high-altitude or steep-slope areas (Xu et al., 2024). A significant portion of CELS is under some form of legal conservation, which acts as a major barrier against the advance of anthropogenic activities.

These explanatory variables are commonly used in LULC modeling because they can be obtained from accessible cartographic sources. In contrast, socioeconomic, law enforcement, or policy factors are less used due to data scarcity, complexity of spatial representation, and temporal mismatches. Despite these limitations, several studies have demonstrated good modeling results using only topographic and infrastructure variables, as seen in Barbosa de Souza et al. (2023); Alipbeki et al. (2024); Hasan et al. (2020).

While many studies have explored how protected areas help prevent deforestation, fewer studies have integrated protection levels as a variable in land use change models (Kim and Anand, 2021). Given that the CELS includes various types of protection and conservation areas, the protection level was integrated into the analysis to assess its influence on LULC dynamics. This level was determined through surveys conducted with three experts who were asked to evaluate, on a scale from 1 to 5, the effectiveness of different protection categories within the CELS in preventing deforestation. In this scale, 1 represents a low level of protection, while 5 indicates a high level of protection against deforestation.

For modelling and prediction purposes, a transition matrix from 2018 to 2020 (two-year interval) was calculated using the MOLUSCE tool. This matrix was used by MOLUSCE to create a change map, which, together with the explanatory variable rasters, served as inputs for the training of the ANN model that iteratively assesses its prediction accuracy and adjusts its structure to minimize errors. On the other hand, CA generates simulations based on the trained ANN model (Mustafa et al., 2021). In this study, each iteration of the CA algorithm produces a predicted LULC map two years in advance. The first iteration generated a LULC map for 2022, which was compared to the actual 2022 LULC map from MapBiomas to validate the model. Subsequently, four additional iterations were performed to produce a predicted LULC map for 2030. A transition matrix from the predicted LULC map for 2022 to that of 2030 was then calculated to analyze LULC changes and estimate annual rates of change using Equation 1.

After training the ANN model and generating a predicted LULC map for 2022 using the CA algorithm, it is essential to verify that the predictions made with the Cellular Automata algorithm and the ANN model are reliable enough to support decision-making (Bao Pham et al., 2024). To ensure this, the model was validated by comparing the predicted LULC map for 2022 generated by the algorithm with the actual LULC map from MapBiomas for the same year. The comparison was performed using Cohen's Kappa coefficient, a widely used metric for spatial data comparison (Mollocana Lara et al., 2021). MOLUSCE allows for multiple iterations of Kappa coefficient calculations, reducing errors caused by random sampling. The interpretation of the Kappa coefficient follows the criteria established in Santos et al. (2020).

3 Results and Discussion

3.1 LULC Changes Analysis from 2018 to 2022

The dynamics of land use and land cover change in the Llanganates-Sangay Connectivity Corridor (CELS) between 2018 and 2022 (Figure 3), shows the gradual decrease of Forest Formation areas stands out, especially in the CELS buffer zones. This suggests a process of deforestation, probably associated with human activities such as agricultural and livestock expansion, since this type of use shows a notable increase in the same area, indicating that the areas peripheral to the CELS have greater anthropic pressure. This change implies a significant transformation of forest ecosystems into more intensive uses.

The gradual loss of Forest Formation suggests an increase in landscape fragmentation, which affects ecological connectivity between montane and Amazonian ecosystems (Jokisch and Lair, 2002). Water Bodies and Non-Vegetated Areas remain relatively constant, with no perceptible changes in their extension, while Non-Forest Natural Formations show minor variations, which may be related to degradation or regeneration processes.

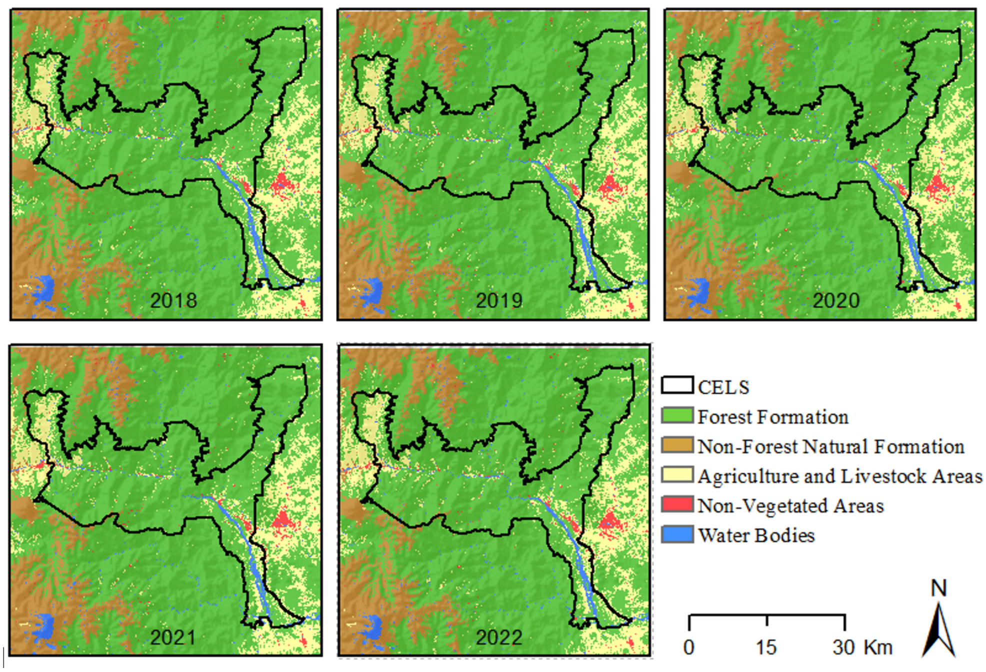

Figure 3. MapBiomas LULC maps from 2018 to 2022 (MapBiomas, 2024).

Table 3 and Figure 4 highlight the changes in LULC in CELS between 2018 and 2022, quantifying the transformation of the landscape. The Forest Formation category experienced an accumulated loss of 1,147.33 hectares, with an average annual rate of change of -0.37%, and its maximum value in 2021-2022 with -515.03 hectares (-0.67%/year).

This dynamic of decrease in the categories related to natural vegetation confirms that agriculture is the main driver of land use change, contributing significantly to deforestation and pressure on forest ecosystems that lose their ecological function in maintaining the diversity and connectivity of the landscape. Agricultural expansion, in turn, responds to economic stability that produces short-term fluctuations in the market.

Non-Vegetated Areas increased by 250.84 hectares (+8.50%/year), showing their greatest growth between 2021-2022 (+107.31 ha, +13.52%/year). This increase may reflect soil degradation processes related to erosion, urbanization and land abandonment, which alter the functionality of the corridor and generate a growing threat to natural ecosystems; this trend is consistent with other studies carried out in the Ecuadorian Amazon (Gutiérrez et al., 2016; Calvas et al., 2024; Viteri-Basso et al., 2024).

Table 3. CELS Land Use/Land Cover changes from 2018 to 2022.

Categories	Units	2018 to 2019	2019 to 2020	2020 to 2021	2021 to 2022	2018 to 2022
Forest Formation	ha	-266.94	-263.28	-102.09	-515.03	-1147.33
	q	-0.34	-0.34	-0.13	-0.67	-0.37
Non-Forest Natural Formation	ha	-8.96	-18.84	-7.32	5.12	-30.01
	q	-1.37	-2.92	-1.17	0.83	-1.17
Agriculture and Livestock Areas	ha	223.39	234.64	149.02	299.14	906.19
	q	2.26	2.32	1.44	2.85	2.21
Non-Vegetated Areas	ha	49.49	41.53	52.51	107.31	250.84
	q	7.61	5.94	7.09	13.52	8.50
Water bodies	ha	3.02	5.95	-92.12	103.46	20.31
	q	0.10	0.20	-3.09	3.58	0.17

*Negative symbol represents area reduction; ha represents change in hectares and q represents annual rate of change in %/year.

For their part, Water Bodies showed significant fluctuations, with losses in 2020-2021 (-3.09%/year) and a partial recovery in 2021-2022 (+3.58%/year). These dynamics, probably influenced by seasonal variations and sedimentation, require continuous hydrological monitoring to understand their causes and effects on the corridor.

Table 4 corresponds to the LULC transition matrix from 2018 to 2022. 96.93% (75577.18 ha) of the area occupied by the Forest Formation category remained stable, 2.49% changed to Agriculture and Livestock Areas and 0.15% to Non-Vegetated Areas. This reflects the fact that agricultural expansion is the main driver of deforestation.

The Non-Forest Natural Formation category has a permanence of 88.57% (578.7 ha), 7.55% changed to Forest Formation and 3.19% to Agriculture and Livestock Areas. Contrary to the above, 87.17% (8629.23 ha) remained as Agriculture and Livestock areas. They expanded by 1058.96 ha (10,7%) from Forest Formation and by 100.9 ha (1,02%) from Non-Vegetated Areas. This confirms that agriculture is the main transformation factor of the landscape of the non-vegetated areas 610,72 ha (93,95%) remained as non-vegetated areas, an increase of 120.57 ha (0,15%) from Forest Formation and 64.49 ha (2,17%) from Water Bodies, which could be associated with degradation and urbanization processes.

The category of water bodies has a permanence: 2589.5 ha (87,04%) remained as water bodies, 64.49 ha (2,17%) were reduced to non-vegetated areas and 130.54 ha (4,39%) to forest formation, possibly due to changes in water dynamics, sedimentation, seasonal timing of the Landsat satellite images used in the MapBiomas classification or inherent algorithmic errors.

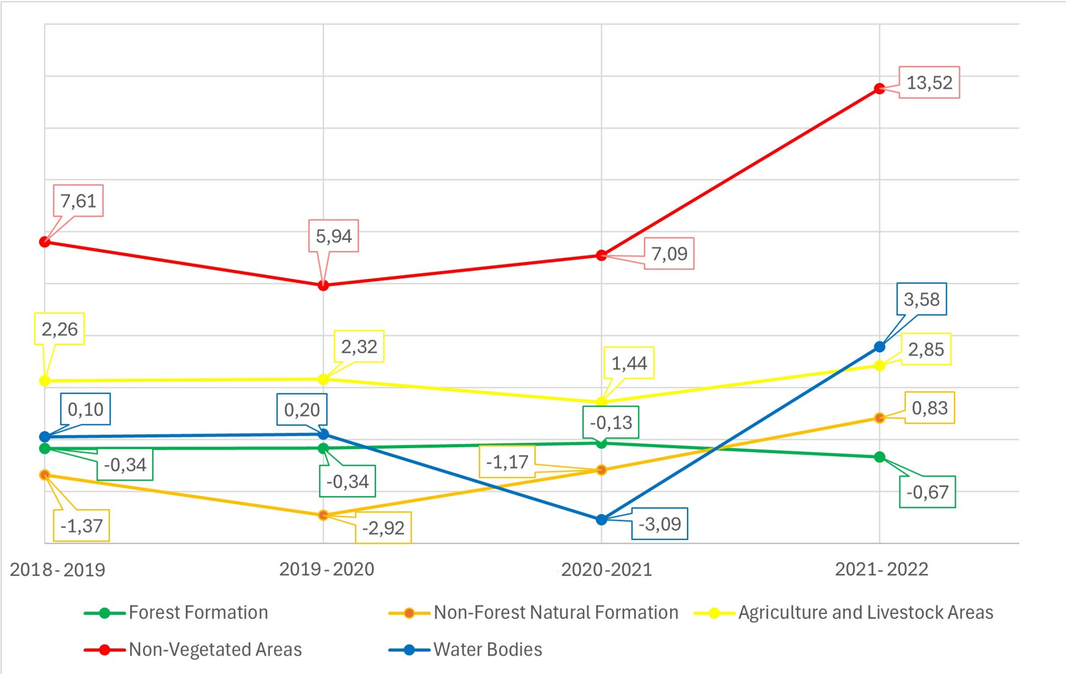

Figure 4. Evolution of annual LULC change rates (q %/year) at one-year intervals from 2018 to 2022.

The transition matrix shows that deforestation and conversion to agricultural land are the predominant dynamics in the CELS, driven by agricultural expansion. Additionally, the increase in non-vegetated areas reflects degradation processes that could intensify if sustainable management measures are not implemented.

Since Forest Formation annual rates of change are low, observing its area decrease (deforestation) is difficult. To improve this understanding, Figure 5 highlights the differences in Forest Formation changes between 2018 and 2019, as well as between 2018 and 2022.

3.2 Explanatory variables for 2030 LULC prediction

The rasters representing the explanatory variables for the prediction model are depicted in Figure 6 and Figure 7. Rasters proximity to roads, proximity to settlements, altitude and slope were generated from Military Geographic Institute (IGM) official information. The raster level of protection was generated based on information from the Ministry of Environment, Water, and Ecological Transition (MAATE), a conservation NGO supporting private areas in the CELS, and the expert opinions about the effective level of protection of different kinds of protected areas.

Not all conservation areas have the same level of protection against deforestation and the type of conservation areas varies significantly. Some are part of the National System of Protected Areas (SNAP), regulated by the Organic Environmental Code, which provides a robust legal framework that supports the conservation of these areas, and they have greater financial and technical capacity, which increases their level of protection. However, their effectiveness can be compromised by extractive activities permitted under legal exceptions, such as mining exploitation in certain protected areas.

Areas managed by local governments (GAD) have fewer resources and technical support, which limits their ability to implement effective conservation measures. In the case of privately owned areas, in some cases they are successful conservation models, which depend mainly on the commitment of the owners and lack a consolidated monitoring framework (Mendoza-Montesdeoca et al., 2022; Mestanza-Ramón et al., 2020).

Table 4. Transition matrix for LULC between 2018 and 2022.

2018 - 2022 Period	Forest formation	Non-forest natural formation	Agriculture and Livestock areas	Non-Vegetated areas	Water bodies	Total 2018
Forest formation	75577.18 (96.93 %)	23.6 (0.03 %)	1941.1 (2.49 %)	120.57 (0.15 %)	311.3 (0.4 %)	77973.75 (100 %)
Non-forest natural formation	49.31 (7.55 %)	578.7 (88.57 %)	20.86 (3.19 %)	4.21 (0.64 %)	0.27 (0.04 %)	653.34 (100 %)
Agriculture and Livestock areas	1058.96 (10.7 %)	19.03 (0.19 %)	8629.23 (87.17 %)	100.9 (1.02 %)	91.48 (0.92 %)	9899.6 (100 %)
Non-vegetated areas	10.43 (1.6 %)	0.37 (0.06 %)	25.71 (3.95 %)	610.72 (93.95 %)	2.84 (0.44 %)	650.05 (100 %)
Water bodies	130.54 (4.39 %)	1.65 (0.06 %)	188.9 (6.35 %)	64.49 (2.17 %)	2589.5 (87.04 %)	2975.09 (100 %)
Total 2022	76826.42	623.34	10805.80	900.89	2995.3	
Variation from 2018 to 2022	-1147.33	-30.01	906.19	250.84	20.31	

*The changes are expressed in hectares, with percentages in parentheses. Positive variation values indicate area gains, and negative values indicate losses.

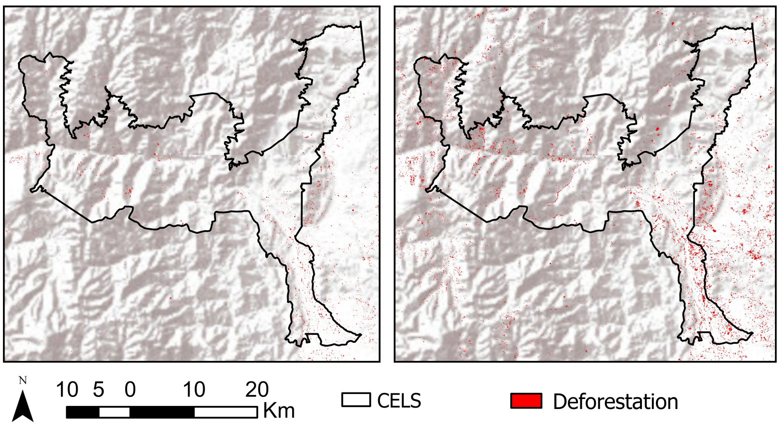

Figure 5. Deforestation represented as the transition from the Forest Formation class to any other LULC category between 2018–2019 (left) and 2018–2022 (right).

To account for these differences, three experts were polled to assess the level of protection against deforestation across various types of conservation areas. Selected experts have at least five years of experience in conservation and come from different institutions across Ecuador that have worked on officially recognized connectivity corridors (MAATE and two different NGO), providing varied perspectives and a broader understanding of conservation practices and challenges throughout the country. The results are presented in Table 5. Each protection level was rated on a scale of 1-5, with a value of 0 used for non-protected areas.

The importance of incorporating the protection level of a protected area into the model (Barreto et al., 2017; Pessôa et al., 2023) is demonstrated in Table 6, which shows its significant influence on deforestation rates. The annual change rates were calculated using the Equation 1. As expected, areas without any form of protection (protection level 0) experience the highest deforestation rates, followed by the Provincial Sustainable Development Ecological Area of Pastaza Province GAD (AEDSP), where sustainable productive activities are permitted (protection level 2). In contrast, protected areas such as ACMUS, APH, and Protective Forests (protection level 3) exhibit the lowest annual deforestation rates, followed by private protected areas (protection level 1).

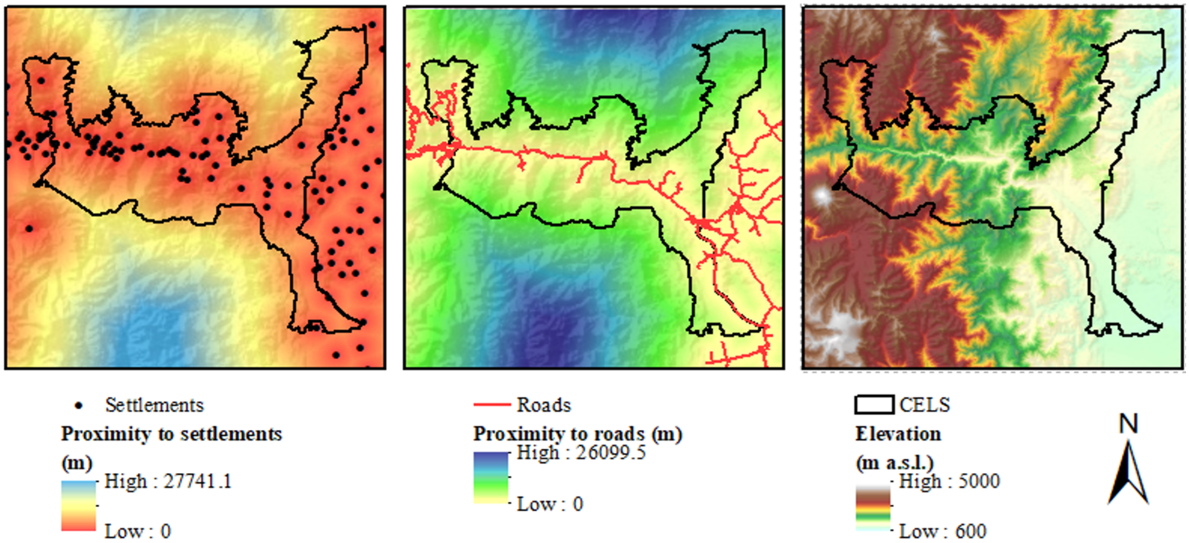

Figure 6. Proximity to settlements, proximity to roads and elevation explanatory variables.

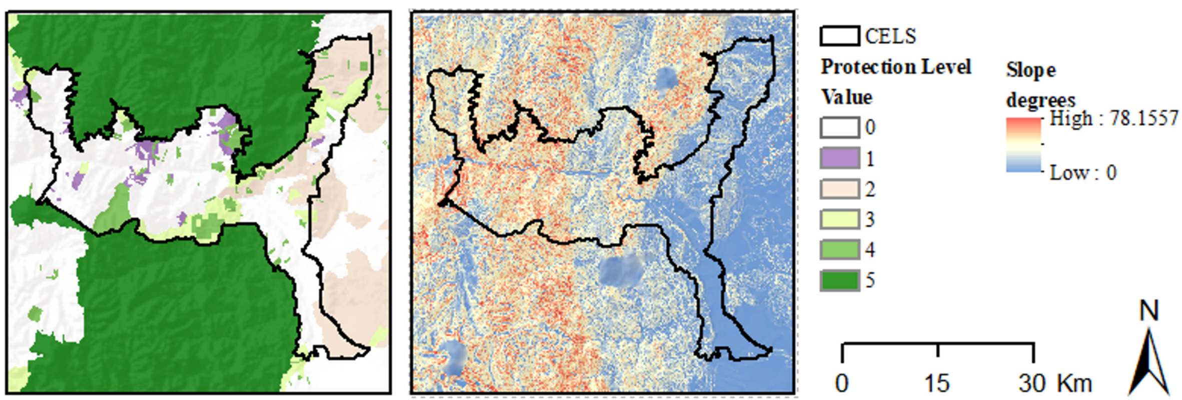

Figure 7. Protection level and slope explanatory variables.

Private protected areas exhibit a notable difference between the protection level reported by experts and the low deforestation rates calculated in this analysis. Two of the interviewed experts base their opinions on the lack of legal guarantees for long-term protection, as conservation status in private areas can change depending on the owner's vision. However, these areas often achieve higher conservation outcomes due to their specific focus, adaptability, and management by non-governmental organizations, families, or consortia, which implement rigorous conservation practices and reduce direct anthropogenic pressure. Despite these advantages, challenges persist, including tensions with local communities over restricted access to traditional resources and the vulnerability of conservation approaches to changes in ownership priorities (Iñiguez-Gallardo et al., 2021).

3.3 Artificial Neural Network model training

The ANN algorithm in the MOLUSCE tool was configured with a neighborhood size of 2 pixels and a learning rate of 0.002. Additionally, the momentum was set to 0.002 when these parameters help to stabilize learning and accelerate convergence. Figure 8 displays the learning curve illustrating the training process of the algorithm over 2000 iterations, with each iteration using 40,000 stratified sampling points to train and validate the neural network. The minimum error achieved by the neural network was 8.46 %.

Table 5. Results of a survey assessing the level of protection against deforestation, with 1 representing low level of protection and 5 high level of protection.

Type of conservation area	Protection level			
	Grade 1[a]	Grade 2[b]	Grade 3[a]	Rounded average
Private conservation areas	1	1	2	1
GAD conservation areas (ACMUS)	3	4	3	3
Water Protection Areas (APH)	3	3	4	3
Socio Bosque Program	4	4	3	4
Provincial Sustainable Development Ecological Area of Pastaza (AEDSP)	2	2	2	2
Protective Forests and Vegetation	1	4	4	3
National Parks (part of the SNAP)	5	5	5	5
Private Protected Areas (part of the SNAP)	3	5	5	4

[a]Specialists in Conservation- NGO.
[b]Specialist in Protected Areas– MAATE.

Table 6. Forest Formation annual rate of change according to the level of protection against deforestation of protected areas from 2018 to 2022.

Level of protection	Forest formation 2018	Forest formation 2022	Change 2018- 2022	
	ha	ha	ha	q (%/año)
0	42952.59	41962.24	-990.35	-0.58
1	3730.25	3727.59	-2.65	-0.02
2	13003.95	12889.33	-114.62	-0.22
3	9269.31	9264.46	-4.85	-0.01
4	8911.26	8876.59	-34.67	-0.10
5	106.39	106.21	-0.18	-0.04
Total	77973.75	76826.42	-1147.33	-0.37 %

*Negative values indicate area reduction.

3.4 Cellular Automata simulation

The predicted LULC maps from 2022 to 2030, at two-year intervals, are illustrated in Figure 9, while Table 7 details the transition for LULC predictions between 2022 and 2030 in hectares, with percentages in parentheses. Positive variation values indicate area gains, negative values indicate losses. Additionally, Figure 9 shows the evolution of predicted annual LULC change rates (%/year) at two-year intervals from 2022 to 2030 while Table 7 presents the corresponding transition matrix. In the other hand, Figure 10 shows the predicted future trends and variations in annual change rates of LULC categories from 2022 to 2030.

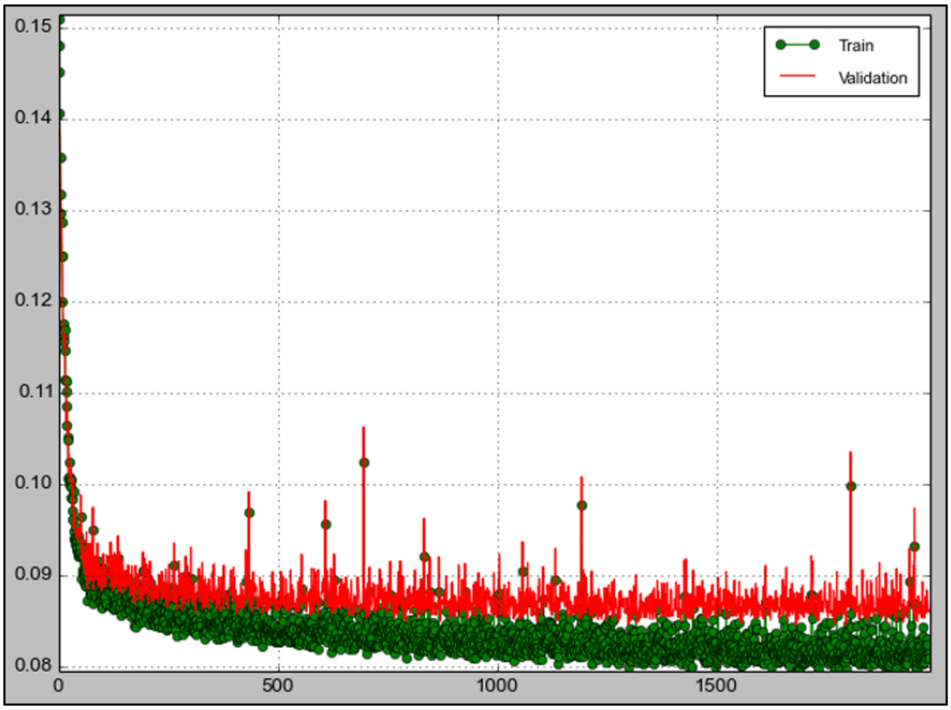

Figure 8. Artificial Neural Network learning curve.

Forest Formation, the largest land use, shows an area decrease (negative change rates), from 77025.39 ha in 2022 to 75396.42 ha in 2030, indicating ongoing but low reduction in forest cover, likely due to deforestation (Souza et al., 2020). The conversion of forests into pastures, agricultural land, and infrastructure is a key driver of deforestation, causing effects on ecosystems and climate. This process accelerates biodiversity loss, disrupts water systems, and releases stored carbon, intensifying climate change and altering local and regional environmental conditions (Kumar et al., 2022). Although most Forest Formation areas (95.59 %, 73628.13 ha) remained intact in the simulation, 3.72 % transitioned to Agriculture and Livestock Areas.

Similarly, 59.7 % of Non-Forest Natural Formations in 2022 persisted, while 21.04 % shifted to agriculture, indicating significant pressure on these ecosystems due to agricultural growth (Table 7). Decline in Non-Forest Natural Formation can lead to significant ecological consequences, including biodiversity loss and ecosystem degradation. For instance, the reduction of natural wetlands has been linked to decreased habitat quality and fragmentation, further exacerbating environmental degradation (Wilson et al., 2016).

Agriculture and Livestock Areas expand steadily, from 10804.52 ha in 2022 to 12582.78 ha in 2030, reflecting agricultural encroachment. Although Agriculture and Livestock Areas remained predominantly stable in the simulation (83.72 %, 9,045.19 ha), 1412.07 ha transitioned to Forest Formation. This shift may indicate the influence of conservation efforts and initiatives implemented in the CELS, such as promoting agroecological practices, which can facilitate forest restoration (Knapp and Sciarretta, 2023). Agriculture and Livestock Areas show positive but slightly deaccelerating change rates, indicating a continuous increase in agricultural land, albeit at a slower pace over time.

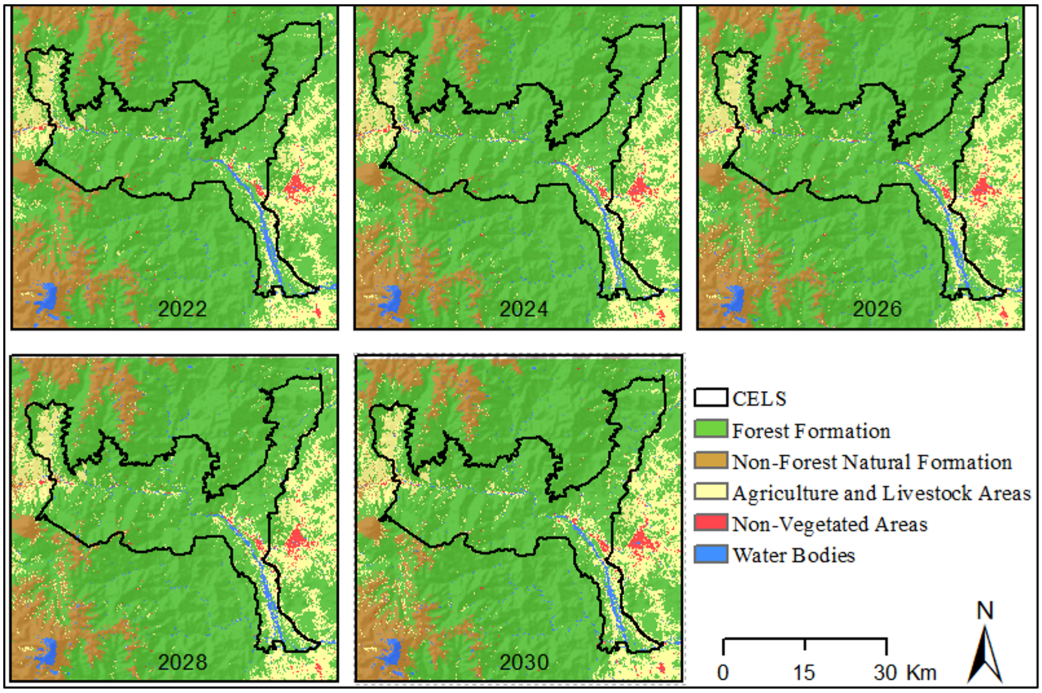

Figure 9. Predicted LULC maps from 2022 to 2030.

Table 7. Transition matrix for LULC predictions between 2022 and 2030.

2022 - 2030 Period	Forest formation	Non-forest natural formation	Agriculture and Livestock areas	Non-Vegetated areas	Water bodies	Total 2022
Forest formation	73628.13 (95.59 %)	82.88 (0.11 %)	2866.5 (3.72 %)	97.52 (0.13 %)	350.37 (0.45 %)	77025.39 (100 %)
Non-forest natural	112.06 (18.76 %)	356.68 (59.7 %)	125.69 (21.04 %)	2.01 (0.34 %)	1.01 (0.17 %)	597.45 (-100 %)
Agriculture and	1412.07 (13.07 %)	74.92 (0.69 %)	9045.19 (83.72 %)	130.45 (1.21 %)	141.88 (1.31 %)	10804.52 (100 %)
Non-vegetated areas	15.73 (2.1 %)	17.29 (2.31 %)	163.84 (21.86 %)	537.81 (71.77 %)	14.73 (1.97 %)	749.4 (-100 %)
Water bodies	228.42 (7.71 %)	2.2 (0.07 %)	381.56 (12.87 %)	41.99 (1.42 %)	2309.48 (77.93 %)	2963.65 (100 %)
Total 2030	75396.42	533.96	12582.78	809.77	2817.47	
Variation from 2022 to 2030	-1628.97	-63.49	1778.26	60.38	-146.18	

*The changes are expressed in hectares, with percentages in parentheses. Positive variation values indicate area gains, and negative values indicate losses.

In contrast, Non-Vegetated Areas exhibit positive and increasing change rates, reflecting a gradual expansion, likely associated with peri-urban growth (Souza et al., 2020) and other anthropogenic activity. This expansion could be also influenced by landslides and the increase in exposed river sandbanks, which become visible because of decreases in water bodies. Non-Vegetated Areas maintained 71.77 % of their coverage, however, the conversion of 163.84 ha into Agriculture and Livestock Areas could be attributed to land reclamation and ecological restoration efforts facilitating their transition to productive agricultural landscapes (Zine et al., 2024).

Water Bodies, while maintaining 77.93 % stability, experienced losses to both Forest Formation and Agriculture and Livestock Areas, likely driven by sedimentation processes and alterations in hydrological dynamics. Additionally, this trend may reflect the influence of the input data used to train the ANN, as the observed decline in Water Bodies from 2018 to 2022 appears to have guided the model to predict similar reductions in future scenarios. Further studies are needed to better understand the drivers behind these changes and to assess whether they represent temporary fluctuations, long-term trends, or potential errors in the modeling process. Figure 11 shows a comparison between the change from Forest Formation to any other LULC category between both periods 2022 - 2024 and 2022–2030.

3.5 Model validation

Using five iterations with 40,000 stratified sample points, an average Kappa coefficient of 0.95 was achieved, with stable values observed across all iterations. This indicates an excellent agreement between the predicted map and the 2022 MapBiomas map, suggesting that the model performs consistently and can be a useful tool in decision-making processes.

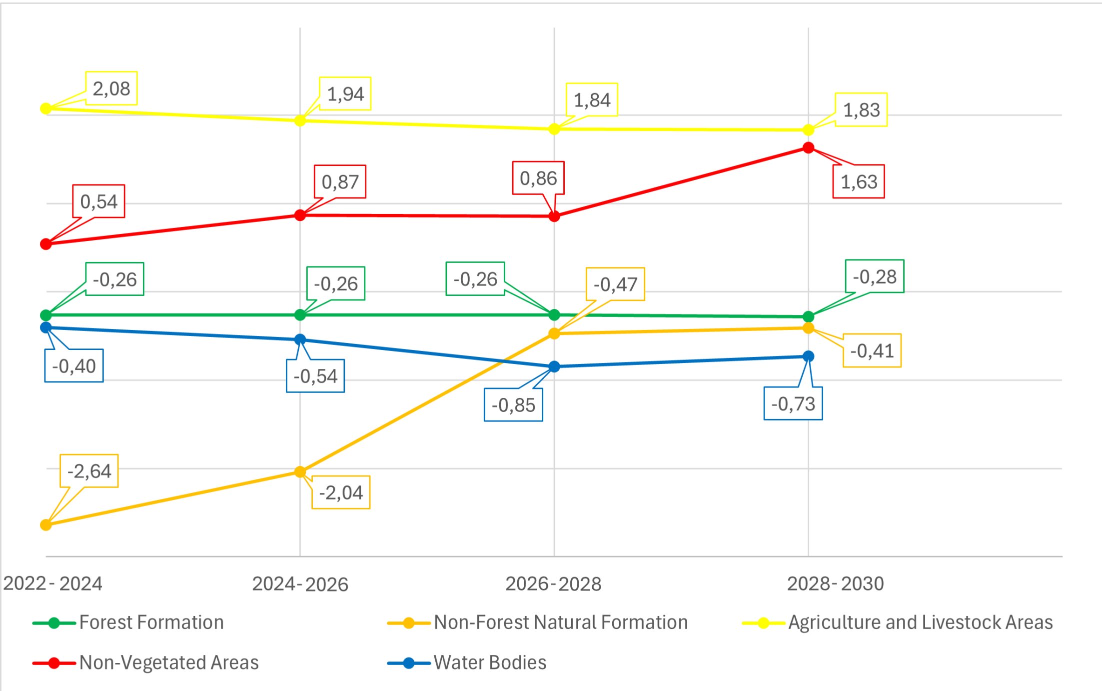

Figure 10. Evolution of predicted annual LULC change rates (%/year) at two-year intervals from 2022 to 2030.

3.6 Study limitations

The main limitations of this study include the low availability of satellite images due to the high cloud cover present during the analysis period. For this reason, land use and land cover maps generated by MapBiomas were used. Although this tool uses advanced image filtering and correction techniques, its cartography presents a margin of error with an accuracy of 80 %. Likewise, the use of the MOLUSCE tool, despite its robustness and frequent application to generate trends, includes an associated margin of error, with a Kappa coefficient of 0.95.

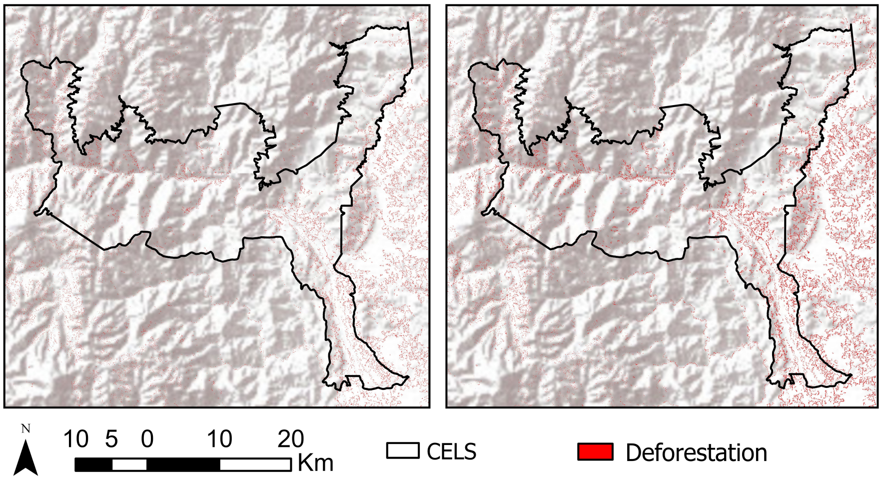

Figure 11. Predicted deforestation represented as the transition from the Forest Formation class to any other LULC category between 2022- 2024 (left) and 2022–2030 (right).

The naturalistic approach of the article prioritized the analysis of changes in natural cover and the different forms of conservation within the CELS. Socioeconomic, policy, political, and resource availability factors were not included in the analysis, due to the lack of readily available data and the complexities associated with integrating these variables into geospatial models. This represents an opportunity to carry out complementary research to address this limitation by incorporating data on population growth, economic activities, policy enforcement, resource availability and protected area management capacities to better capture the dynamics influencing LULC changes.

Despite these limitations, the results presented in this study reliably reflect the dynamics observed in the CELS. The variables used are widely applied in LULC modeling and the model was trained and validated using different data sets, reaching a high level of precision.

4 Conclusions

This study examined land use and land cover (LULC) maps sourced from the MapBiomas platform spanning 2018 to 2022. Predictive LULC maps for the period 2022 to 2030 were generated using the MOLUSCE tool in QGIS. Deforestation was represented as the transition from the Forest Formation class to any other LULC category. The findings confirm the expected trend of natural cover areas being replaced by anthropogenic uses, notably Agriculture and Livestock Areas expanding at the eastern and western boundaries of the CELS. To mitigate this, promoting sustainable anthropogenic practices such as agroecology is recommended.

Furthermore, it was observed that conservation areas exhibit lower deforestation rates, while most of the deforestation occurs in areas lacking any form of conservation status. Therefore, strengthening existing conservation areas, establishing new ones, and addressing the significant portion of unprotected natural cover within CELS are advisable strategies.

The relatively low deforestation rates found posed challenges in detecting changes in LULC maps. This challenge was also reflected in the Artificial Neural Network (ANN) algorithm, where training intervals had to be extended to two years due to minimal changes observed annually.

Using the ANN model and Cellular Automata simulation algorithm, the study estimated annual change rates between 2018 and 2022 as follows: a decrease of 0.37% per year, equivalent to 1147.33 hectares, for Forest Formation; a reduction of 1.17% per year, or 30.01 hectares, for Non-Forest Natural Formation; an increase of 2.21% per year, corresponding to 906.19 hectares, for Agriculture and Livestock Areas; a rise of 8.50% per year, representing 250.84 hectares, for Non-Vegetated Areas; and a slight increase of 0.17% per year, or 30.31 hectares, for Water Bodies. In contrast, LULC simulations for 2022 to 2030 predict an annual decrease of 0.27%, equal to 1628.97 hectares, for Forest Formation; a reduction of 1.39% per year, or 63.49 hectares, for Non-Forest Natural Formation; an increase of 1.92% per year, amounting to 1778.26 hectares, for Agriculture and Livestock Areas; a rise of 0.97% per year, adding 30.38 hectares, for Non-Vegetated Areas; and a slight decline of 0.63% per year, totaling 146.18 hectares, for Water Bodies. The model's predictive accuracy, evaluated using the Kappa coefficient, indicated excellent performance.

Acknowledgements

We extend our gratitude to the Hempel Foundation for funding the deforestation study in the Llanganates Sangay Connectivity Corridor, the process and results of which are presented in this article. We also thank WWF-Ecuador for their information and technical contributions. Special thanks go to the Universidad Politécnica Salesiana for its interest and efforts in disseminating knowledge about connectivity corridors, and to the CELS Research Network, of which ESPOCH is a part, for enabling this collaborative work opportunity.

Authors' contribution

L.J.J.C.: Conceptualization, Data curation, Formal analysis, Investigation, Methodology, Project administration, Supervision, Resources, Software, Validation, Visualization, Writing– original draft. A.C.M.H.: Conceptualization, Funding acquisition, Investigation, Methodology, Project administration, Resources, Supervision, Writing– original draft, Writing– review editing. A.C.G.G.: Formal analysis, Investigation, Methodology, Validation, Writing of introduction, methodology and results. J.G.M.L.: Data curation, Formal analysis, Investigation, Methodology, Validation, Visualization, Writing– review editing.

References

Admas, M. (2024). Predicting the impacts of land use/cover and climate changes on water and sediment flows in the megech watershed, upper blue nile basin. *Remote Sens*, 16:2385. Online:https://n9.cl/p2v51k.

Al Mazroa, A., Maashi, M., Kouki, F., Othman, K., Salih, N., Elfaki, M., and Begum, S. (2024). An analysis of urban sprawl growth and prediction using remote sensing and machine learning techniques for vila velha, brazil. *Journal of South American Earth Sciences*, 142:104988. Online:https://n9.cl/sseqj.

Alipbeki, O., Alipbekova, C., Mussaif, G., Grossul, P., Zhenshan, D., Muzyka, O., Turekeldiyeva, R., Yelubayev, D., Rakhimov, D., Kupidura, P., and Aliken, E. (2024). Analysis and prediction of land use/land cover changes in korgalzhyn district, kazakhstan. *Agronomy*, 14(2):268. Online:https://n9.cl/5tvd8.

Alvarado, O. (2020). La conservación neoliberal: otra cara de la economía verde. estudio de caso en el corredor ecológico llanganates sangay, ecuador. *Sociedad y ambiente*, (22):97–123. Online:https://n9.cl/0yycl.

Aneloa, W. E., Lara, J., Mendoza, C., Herrera, A., and Jacho, A. (2024). Development of a geoportal for the integrated management of cartographic information in the llanganates-sangay connectivity corridor. *Revista de Gestão Social e Ambiental*, 18(11):e08768. Online:https://n9.cl/wppfn.

Bao Pham, Q., Ajim Ali, S., Parvin, F., Van On, V., Mohd Sidek, L., Đurin, B., Cetl, V., Šamanović, S., and Nguyet Minh, N. (2024). Multi-spectral remote sensing and gis-based analysis for decadal land use land cover changes and future prediction using random forest tree and artificial neural network. *Advances in space research*, 74(1):17–47. Online:https://n9.cl/v4gdo.

Barbosa de Souza, K., Rosa dos Santos, A., Macedo Pezzopane, J., Machado Dias, H., Ferrari, J., Machado de Oliveira Peluzio, T., Toledo, J., Freire Carvalho, R., Rizzo Moreira, T., and França Araújo, E. (2023). Modeling dynamics in land use and land cover and its future projection for the amazon biome. *Forests*, 14(7):1281. Online:https://n9.cl/2egr1.

Barreto, J., González, T., and Armenteras, D. (2017). Dinámica espacio temporal de ocurrencia de incendios en zonas con diferentes tipos de manejo en el noroeste de la amazonia:¿ barrera efectiva? *Revista facultad de ciencias básicas*, 13(1):19–25. Online:https://n9.cl/susqb.

Borja, M., Holguín, W., Aguilar, C., Terán, K., Rodríguez, A., and Josse, C. (2023). Documento de bases teóricas de algoritmo (atbd) raisg - mapbiomas ecuador colección 1.0 de mapas anuales de cobertura y uso del suelo de ecuador. Online:https://n9.cl/89xt1.

Calvas, B., Castro, L., Kindu, M., Bingham, L., Pintado, K., Torres, J., Knoke, T., and Cueva-Ortiz, J. (2024). Large differences between observed and expected ecuadorian deforestation from 2001 to 2009: a counterfactual simulation approach. *Regional Environmental Change*, 24(2):1–15. Online:https://n9.cl/o4k9v.

Delgado Fernández, E., León Peralta, M., Cantos Guamán, C., and J., G. (2023). Effect of mining activity on biodiversity in a sector of the paquisha parish, province of zamora chinchipe-ecuador. *La Granja*, 38(2):106–123. Online:https://n9.cl/65gby.

Elagouz, M., Abou-Shleel, S., Belal, A., and El-Mohandes, M. (2020). Detection of land use/cover change in egyptian nile delta using remote sensing. *The Egyptian Journal of Remote Sensing and Space Science*, 23(1):57–62. Online:https://n9.cl/die101.

Fischer, R., Cordero, F., Luna, T., Velasco, R., DeDecker, M., Torres, B., Giessen, L., and Günter, S. (2021). Interplay of governance elements and their effects on deforestation in tropical landscapes: Quantitative insights from ecuador. *World Development*, 148:105665. Online:https://n9.cl/5x86g.

Gaglio, M., Aschonitis, V., Mancuso, M., Reyes Puig, J., Moscoso, F., Castaldelli, G., and Fano, E. (2017). Changes in land use and ecosystem services in tropical forest areas: a case study in andes mountains of ecuador. *Int. J. Biodivers. Sci. Ecosyst. Serv. Manag*, 13(1):264–279. Online:https://n9.cl/4q5fe.

Gaur, S. and Singh, R. (2023). A comprehensive review on land use/land cover (lulc) change modeling for urban development: current status and future prospects. *Sustainability*, 15(2):903. Online:https://n9.cl/9stqv.

Gutiérrez, R., Puig, J., Tapia, A., Terán, A., de Vargas, K., Bermudez, D., and Rodríguez, X. (2016). Desarrollo local y conservación en la vertiente oriental andina: corredor ecológico llanganates-sangay-valle del anzu. *Revista Amazónica. Ciencia y Tecnología*, 5(1):52–68. Online:https://n9.cl/wvv9v.

Hasan, S., Shi, W., Zhu, X., Abbas, S., and Khan, H. (2020). Future simulation of land use changes in rapidly urbanizing south china based on land change modeler and remote sensing data. *Sustainability*, 12(11):4350. Online:https://n9.cl/jhna4.

Heredia-R, M., Torres, B., Cabrera-Torres, F., Torres, E., Díaz-Ambrona, C., and Pappalardo, S. (2021). Land use and land cover changes in the diversity and life zone for uncontacted indigenous people: Deforestation hotspots in the yasuní biosphere reserve, ecuadorian amazon. *Forests*, 12(11):1539. Online:https://n9.cl/r3qb1.

Herrera, G. and Rodríguez, G. (2016). Resiliencia y turismo: El caso de la ciudad de baños de agua santa-ecuador. *Holos*, 3:229–250. Online:https://n9.cl/hso6tb.

INABIO, Ecominga Foundation, Sumak Kawsay In Situ, and Waska Amazonía (2023). *Amphibians and Reptiles of the Llanganates-Sangay Ecological Corridor*. National Biodiversity Institute Publication Series.

Iñiguez-Gallardo, V., Reyes-Bueno, F., and Peñaranda, O. (2021). Conservation debates: people's perceptions and values towards a privately protected area in southern ecuador. *Land*, 10(3):233. Online:https://n9.cl/147n4.

Jain, M. (2024). Future land use and land cover simulations with cellular automata-based artificial neural network: A case study over delhi megacity (india). *Heliyon*, 10(14):e34662. Online:https://n9.cl/zdry6.

Jokisch, B. and Lair, B. (2002). One last stand? forests and change on ecuador's eastern cordillera. *Geographical Review*, 92(2):235–256. Online:https://n9.cl/1o8235.

Jost, L. (2004). Explosive local radiation of the genus teagueia (orchidaceae) in the upper pastaza watershed of ecuador. *Lyonia*, 7(1):41–47. Online:https://n9.cl/kmuuf.

Kim, D. and Anand, A. (2021). Effectiveness of protected areas in the pan-tropics and international aid for conservation. *Geomatics*, 1(3):335–346. Online:https://n9.cl/m0dwx.

Kleemann, J., Zamora, C., Villacis-Chiluisa, A., Cuenca, P., Koo, H., Noh, J., Fürst, C., and Thiel, M. (2022). Deforestation in continental ecuador with a focus on protected areas. *Land*, 11(2):268. Online:https://n9.cl/8p6fh.

Knapp, J. and Sciarretta, A. (2023). Agroecology: protecting, restoring, and promoting biodiversity. *BMC Ecology and Evolution*, 23(1):29. Online:https://bit.ly/3Xgk2Ki.

Kouassi, J., Gyau, A., Diby, L., Bene, Y., and Kouamé, C. (2021). Assessing land use and land cover change and farmers' perceptions of deforestation and land degradation in south-west côte d'ivoire, west africa. *Land*, 10(4):429. Online:https://n9.cl/ke4z50.

Kumar, R., Kumar, A., and Saikia, P. (2022). *Environmental Degradation: Challenges and Strategies for Mitigation*, volume 104, chapter Deforestation and forests degradation impacts on the environment, pages 19–46. Springer.

Lukas, P., Melesse, A., and Kenea, T. (2023). Prediction of future land use/land cover changes using a coupled ca-ann model in the upper omo-gibe river basin, ethiopia. *Remote Sensing*, 15(4):1148. Online:https://n9.cl/o3xdi1.

Mainville, N., Webb, J., Lucotte, M., Davidson, R., Betancourt, O., Cueva, E., and Mergler, D. (2006). Decrease of soil fertility and release of mercury following deforestation in the andean amazon, napo river valley, ecuador. *Science of the Total Environment*, 368(1):88–98. Online:https://n9.cl/i2nwt.

MapBiomas (2024). Colección 1.0 de la serie de mapas anuales de cobertura y uso de suelo de ecuador. WebPage. Online: https://bit.ly/40GqWJu.

Mendoza-Montesdeoca, I., Rivera-Mateos, M., and Doumet-Chilán, Y. (2022). Políticas públicas ambientales y desarrollo turístico sostenible en las áreas protegidas de ecuador. *Revista de Estudios Andaluces*, (43):106–124. Online:https://n9.cl/eaxg3.

Mestanza-Ramón, C., Henkanaththegedara, S., Vásconez, P., Vargas, Y., Sánchez, M., Constante, D., Jimenez, M., Charco-Guamán, M., and Mestanza, P. (2020). In-situ and ex-situ biodiversity conservation in ecuador: A review of policies, actions and challenges. *Diversity*, 12(8):315. Online:https://n9.cl/56go9.

Mollocana Lara, J., Álvarez Mendoza, C., and Jaramillo Coronel, L. (2021). Evaluación de información relacionada con combustibles en el distrito metropolitano de quito para el modelado y simulación de incendios forestales, caso de estudio: Incendio del cerro atacazo. *La Granja. Revista de Ciencias de La Vida*, 34(2):45–62. Online:https://n9.cl/d57zh.

Mollocana Lara, J. and Paredes Obando, J. (2024). Assessment and selection of fuel models in areas with high susceptibility to wildfires in the metropolitan district of quito. In *International Conference on Innovation and Research*, pages 54–68. Online:https://n9.cl/j39e4z.

Muhammad, R., Zhang, W., Abbas, Z., Guo, F., and Gwiazdzinski, L. (2022). Spatiotemporal change analysis and prediction of future land use and land cover changes using qgis molusce plugin and remote sensing big data: a case study of linyi, china. *Land*, 11(3):419. Online:https://n9.cl/b0y84k.

Mustafa, A., Ebaid, A., Omrani, H., and McPhearson, T. (2021). A multi-objective markov chain monte carlo cellular automata model: Simulating multi-density urban expansion in nyc. *Computers, Environment and Urban Systems*, 87:101602. Online:https://n9.cl/1jt25.

Perea-Ardila, M., Leal-Villamil, J., and Oviedo-Barrero, F. (2021). Spectral characterization and monitoring of mangrove forests with remote sensing in the colombian pacific coast: Bajo baudó, chocó. *La Granja: Revista de Ciencias de la Vida.*, 34(2):27–44. Online:https://bit.ly/3CKfBA3.

Pessôa, A., Morelo, R., Silva-Junior, C., Doblas, J., Carvalho, N., Aragão, L., and Anderson, L. (2023). Protected areas are effective on curbing fires in the amazon. *Ecological Economics*, 214:107983. Online:https://n9.cl/82kct.

Puyravaud, J. (2003). Standardizing the calculation of the annual rate of deforestation. *Forest* *ecology and management*, 177(1-3):593–596. Online:https://n9.cl/yhlg7.

Reyes-Puig, J., Reyes-Puig, C., Pacheco-Esquivel, J., Recalde, S., Recalde, F., Recalde, D., Salazar, J., Peña, E., Paredes, S., Robalino, M., Flores, F., Paredes, V., Sailema, E., and Ríos-Alvear, G. (2023). First insights in terrestrial mammals monitoring in the candelaria and machay reserves in the ecuadorian tropical andes. *Biodiversity Data Journal*, 11:e98119. Online:https://n9.cl/bl2ojr.

Ríos-Alvear, G., Meneses, P., Ortega-Andrade, H., Santos, C., Muzo, A., López, K., Bentley, A., and Villamarín, F. (2024). Key connectivity areas in the llanganates-sangay ecological corridor in ecuador: A participative multicriteria analysis based on a landscape species. *Landscape and Urban Planning*, 246:105039. Online:https://n9.cl/w0pn4.

Rivas, C., Guerrero-Casado, J., and Navarro-Cerrillo, R. (2024). Functional connectivity across dominant forest ecosystems in ecuador: A major challenge for a country with a high deforestation rate. *Journal for Nature Conservation*, 78:126549. Online:https://n9.cl/msrhe.

Santos, F., Telles, L., Rosas, J., Gomes, A., Martins, R., Nascimento, A., and Sousa, E. (2020). Open source iterative bayesian classifier algorithm for quality assessment of processed coffee beans. *Nativa*, 8(1):118–123. Online:https://n9.cl/ugjvpj.

Souza, C., Z. Shimbo, J., Rosa, M., Parente, L., Alencar, A., Rudorff, B., Hasenack, H., Matsumoto, M., Ferreira, L., and Souza-Filho, P. (2020). Reconstructing three decades of land use and land cover changes in brazilian biomes with landsat archive and earth engine. *Remote Sensing*, 12(17):2735. Online:https://n9.cl/ybrqd.

Talukdar, S., Singha, P., Mahato, S., Pal, S., Liou, Y., and Rahman, A. (2020). Land-use land-cover classification by machine learning classifiers for satellite observations-a review. *Remote sensing*, 12(7):1135. Online:https://n9.cl/v7m3k.

Tenorio, C., Álvarez, G., Perez-Alania, M., Blanco, J., Paulino, C., Blanco, J., and Uribe, E. (2022). Bloom of prorocentrum cordatum in paracas bay, peru. *Diversity*, 14(10):844. Online:https://n9.cl/tkn7s.

Tikuye, B., Rusnak, M., Manjunatha, B., and Jose, J. (2023). Land use and land cover change detection using the random forest approach: The case of the upper blue nile river basin, ethiopia. *Global Challenges*, 7(10):2300155. Online:https://n9.cl/495uf.

Vergara, A., Arias, M., Gachet, B., Naranjo, L., Román, L., Surkin, J., and Tamayo, V. (2022). Informe de amazonía viva 2022. Technical report, WWF. Online:https://n9.cl/wov9ve.

Viteri-Basso, E., Puig, J., Reyes-Puig, C., and Ríos-Alvear, G. (2024). Shadows in the forest: Uncovering unusual colouration records in mammals from the ecuadorian tropical andes. *Biodiversity Data Journal*, 12:e137463. Online:https://n9.cl/z1aa5n.

Wilson, M., Chen, X., Corlett, R., Didham, R., Ding, P., Holt, R.and Holyoak, M., Hu, G., Hughes, A., and Jiang, L. (2016). Habitat fragmentation and biodiversity conservation: key findings and future challenges. *Landscape Ecology*, 31:219–227. Online:https://n9.cl/95fg8.

Xu, J., Jiao, C., Zheng, D., and Li, L. (2024). Agricultural land suitability assessment at the county scale in taiyuan, china. *Agriculture*, 14(1):16. Online:https://n9.cl/kiut6.

Zine, H., Hakkou, R., Papazoglou, E., Elmansour, A., Abrar, F., and Benzaazoua, M. (2024). Revegetation and ecosystem reclamation of post-mined land: toward sustainable mining. *Int. J. Environ. Sci. Technol.*, page 9775–9798. Online:https://n9.cl/rqhhbx.

LA GRANJA:
REVISTA DE
CIENCIAS DE LA VIDA
pISSN:1390-3799; eISSN:1390-8596
https://doi.org/10.17163/lgr.n41.2025.02

Special Issue / Edición Especial
CONNECTIVITY CORRIDORS

MULTIVARIATE ANALYSIS OF ECUADORIAN PROVINCES AND PROTECTED AREAS BASED ON THE PRESENCE OF POISON DART FROGS (*DENDROBATIDAE*) AND SOME INSIGHTS FOR THEIR CONSERVATION

ANÁLISIS MULTIVARIADO DE LAS PROVINCIAS Y ÁREAS PROTEGIDAS DE ECUADOR BASADO EN LA PRESENCIA DE RANAS DARDO VENENOSAS (*DENDROBATIDAE*) Y CONSIDERACIONES PARA SU CONSERVACIÓN

Patricio Yánez-Moretta*, Julio Gereda-García, Alexander Huaraca-Egas, Michael Baldeón-Morales and Darwin Quinteros-Sarmiento

Universidad de Investigación de Tecnología Experimental Yachay: Escuela de Ciencias Biológicas e Ingeniería, Urcuquí, Ecuador.

*Corresponding author: ayanez@yachaytech.edu.ec

Received on October 1st, 2024. Accepted, after revision on January 05th, 2025. Published on March 1st, 2025.

Abstract

Understanding the distribution patterns of species is crucial for developing effective conservation strategies, particularly in regions with high biodiversity and endemism like Ecuador. Amphibians, especially poison dart frogs (Dendrobatidae), serve as important bioindicators of environmental health, yet they face significant threats from habitat loss, climate change, and other anthropogenic factors. This study examines the distribution patterns of poison dart frog species across various provinces and protected areas in Ecuador, utilizing an updated database containing 48 species, 32 of which are endemic to the country. Cluster Analysis and Principal Component Analysis (PCA) were applied to compare provinces and protected areas based on species richness, effectively identifying regions with higher and lower poison dart frog species presence. Additionally, ecological factors and the influence of protected areas on the distribution of these frogs are discussed. The findings reveal regions of high species richness, underscore the potential effects of environmental changes on poison dart frog communities, and highlight the crucial role of protected areas in safeguarding biodiversity. This study underscores the importance of integrating these analyses into conservation planning and decision-making processes, aiming to protect poison dart frogs and their habitats. By addressing these challenges, this research contributes complementary perspectives into preserving Ecuador's unique amphibian diversity.

Keywords: Poison dart frogs, *Dendrobatidae*, multivariate analysis, biodiversity, Ecuadorian provinces, Ecuadorian protected areas.

Resumen

La comprensión de los patrones de distribución de las especies es fundamental para desarrollar estrategias de conservación efectivas, especialmente en regiones con alta biodiversidad y endemismo como Ecuador. Los anfibios, y en particular las ranas venenosas (Dendrobatidae), son importantes bioindicadores de la salud ambiental, pero enfrentan amenazas significativas como la pérdida de hábitat, el cambio climático y otros factores antropogénicos. Este estudio analiza los patrones de distribución de las especies de ranas venenosas en varias provincias y áreas protegidas de Ecuador, utilizando una base de datos actualizada que incluye 48 especies, 32 de las cuales son endémicas del país. Se emplearon técnicas de Análisis de Clasificación (Cluster analysis) y de Ordenamiento (Análisis de componentes principales) para comparar provincias y áreas protegidas en función de su riqueza de especies, identificando regiones con mayor y menor presencia de estas ranas venenosas. Además, se discuten los factores ecológicos y la influencia de las áreas protegidas en la distribución de estas especies. Los hallazgos revelan regiones con alta riqueza de especies, resaltan los posibles efectos de los cambios ambientales en las comunidades de ranas venenosas y subrayan el papel crucial de las áreas protegidas en la preservación de la biodiversidad. El presente estudio enfatiza la importancia de integrar estos análisis en la planificación de conservación y en los procesos de toma de decisiones, contribuyendo a la protección de las ranas venenosas y de sus hábitats, así como a la preservación de la singular diversidad de anfibios en Ecuador.

Palabras clave: Ranas dardo venenosas, *Dendrobatidae*, análisis multivariado, biodiversidad, provincias ecuatorianas, áreas protegidas de Ecuador.

Suggested citation:	Yánez-Moretta, P., Gereda-García, J., Huaraca-Egas, A., Baldeón-Morales, M. and Quinteros-Sarmiento, D. (2025). Multivariate analysis of Ecuadorian provinces and protected areas based on the presence of poison dart frogs (*Dendrobatidae*) and some insights for their conservation. *La Granja: Revista de Ciencias de la Vida.* Vol. 41(1):32-50. https://doi.org/10.17163/lgr.n41.2025.02.

Orcid IDs:

Patricio Yanez-Moretta: https://orcid.org/0000-0003-4436-7632
Julio Gereda-García: https://orcid.org/0000-0001-5065-3542
Alexander Huaraca-Egas: https://orcid.org/0000-0002-4439-6380
Michael Baldeón-Morales: https://orcid.org/0000-0002-2705-723X
Darwin Quinteros-Sarmiento: https://orcid.org/0000-0001-6137-2981

1 Introduction

Ecuador is an exceptionally diverse country, home to a wide variety of habitats and niches that support numerous vertebrate and invertebrate species. As of 2023, 676 amphibian species have been reported in Ecuador, of which 324 are endemic (Ron and Ortiz, 2024). The Dendrobatidae family, commonly known as the *poison dart frog* family, comprises neotropical frogs characterized by their conspicuous coloration (Figures 1-4), which is associated with toxic alkaloids present on their skin (Daly et al., 2005; Patocka et al., 1999).

Figure 1. A specimen of *Ameerega bilinguis* (Dendrobatidae) (Gallice, 2009).

Figure 2. A specimen of *Epipedobates anthonyii* (Dendrobatidae) (Tubifex, 2010).

Studying frogs from this family is relevant to numerous fields of research. Many alkaloids with potentially significant pharmacological properties have been isolated from the secretions of poison dart frogs (Daly et al., 1985, 2005; Spande et al., 1992). Species from the genus *Phyllobates* produce batrachotoxins, among the most potent non-peptide toxins, primarily targeting cardiac and nerve tissue by inducing irreversible membrane depolarization and disrupting normal signaling (Patocka et al., 1999). Conversely, species with lower amounts of skin toxins tend to exhibit duller or cryptic coloration (Santos et al., 2003).

According to a richness model created by Gómez (2017) the regions in Ecuador with highest Dendrobatidae species richness are the southeast and northwest amazonian region, the western foothills of the Ecuadorian Chocó and the eastern central Andean foothills. This shows a preference for humid and lowland areas, also reported by Valencia et al. (2009a,b).

Figure 3. A specimen of *Hyloxalus infraguttatus* (Dendrobatidae) (Klimsa, 2020).

Figure 4. A specimen of *Epipedobates machalilla* (Dendrobatidae) (Amphibiaweb, 2022).

The objectives of this research are: to analyze the distribution patterns of poison dart frog species across various provinces and protected areas in Ecuador, utilizing multivariate statistical methods such as Agglomerative Cluster Analysis and Principal Component Analysis to identify areas (provinces or protected areas) with high species richness and similarities between them. Also, to evaluate the influence of varying ecological conditions, as well as the role of protected areas on the presence, distribution, and conservation of poison dart frog species in Ecuador.

The provinces addressed in the study include Coastal provinces, Western Andean-Coastal, Eastern Andean-Amazonian, and Amazonian provinces. The protected areas included exclusively national parks and reserves that are part of the National System of Protected Areas (SNAP) (Ministerio del Ambiente, Agua y Transición Ecológica, 2023), which play a crucial official role in conserving amphibian biodiversity.

2 Materials and methods

2.1 Study Area

This study focuses on 23 provinces (Figure 5; Appendix 1) and 18 national protected areas (Figure 6; Appendix 2) across mainland Ecuador. The analysis covers a wide array of habitats, including lowland tropical rainforests and montane cloud forests, which are typical environments for poison dart frogs.

2.2 Data collection and processing

We considered a database consisting of the presence-absence of 48 Dendrobatidae frog species (Appendix 3), including 32 endemics to Ecuador, in the provinces and protected areas mentioned above. It is worth noting that the database was based on information from BioWeb, a webpage designed by the Museum of Zoology QCAZ (Ron and Ortiz, 2024). This website provides extensive information on amphibians in Ecuador, organized by families and species, as well as their geographical data.

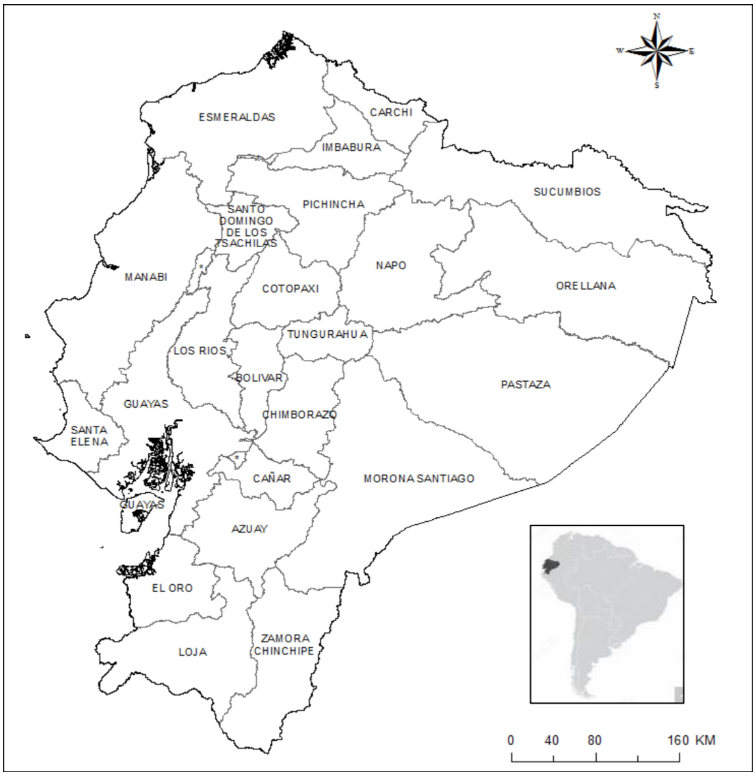

Figure 5. Provinces of mainland Ecuador: Detailed information about them available in Appendix 1.

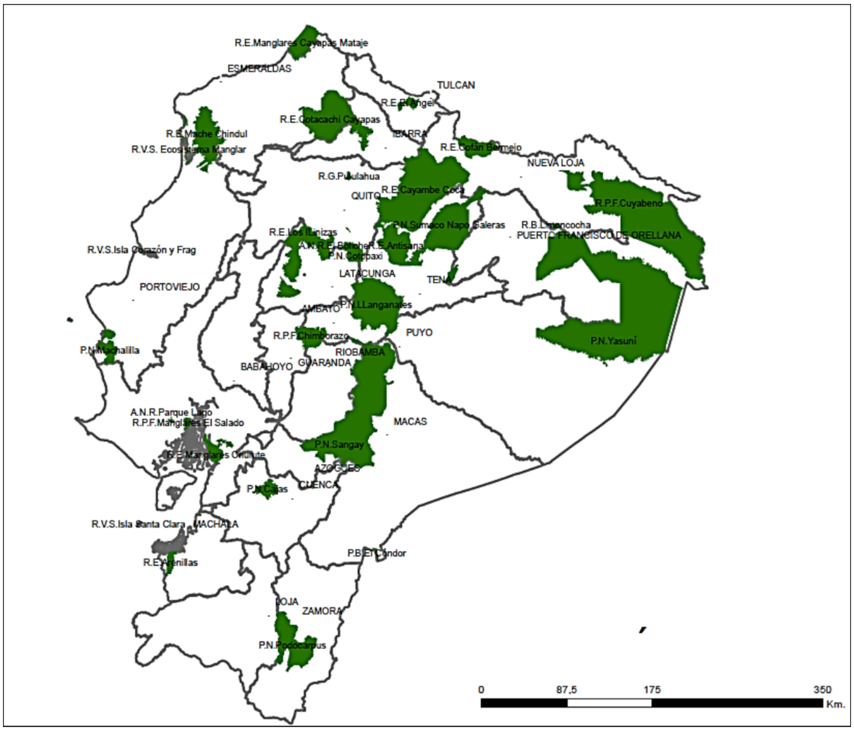

Figure 6. Protected Areas of mainland Ecuador belonging to the SNAP (National System of Protected Areas): Detailed information about them available in Appendix 2.

2.2.1 Cluster analysis

To achieve comparative analysis of the different provinces and SNAP protected areas of Ecuador depending on their similarity (based on the presence/absence of Dendrobatidae species) an Agglomerative Cluster Analysis was applied (using Community Analysis Package 4.0, Pisces Conservation Ltd., 2014).

The Agglomerative Cluster Analysis, in this case using the Bray-Curtis index as a measure of dissimilarity, is a statistical method employed to group elements or samples (provinces or protected areas). In this technique, this index could be used to quantify the difference between pairs of samples, focusing on the presence of dendrobatid species.

The analysis begins by treating each sample (a province or a protected area) as its own cluster and then iteratively merges the closest clusters with another sample until a predefined number of clusters or a suitable clustering solution is achieved. This method is particularly useful in ecological studies for classifying sites, communities or habitats by their species composition, revealing patterns of biodiversity and community structure (Legendre and Legendre, 2012; Yánez and Quishpe, 2013).

Agglomerative clustering techniques are widely used in ecology to create dendrograms that illustrate the formation of clusters among elements of interest, such as provinces or protected areas. These dendrograms visually represent how these elements resemble one another while differing from others, providing valuable findings into their relationships and patterns (Clarke et al., 2016; Kassambara, 2017).

This technique was used in the study to evaluate groups of provinces or protected areas that exhibit similarities in their frog species richness.

2.2.2 Principal component analysis

Principal component analysis (PCA) is a useful model that extracts the main patterns of a data set, considering variables and characteristics called principal components which are combined linearly in order to explain the variance of all variables (Greenacre et al., 2022; Wold et al., 1987).

PCA is also a statistical ordination technique used to simplify the complexity of high-dimensional data while retaining its essential patterns and relationships. It does this by transforming the original variables into a new set of uncorrelated variables called principal components, which are ordered so that the first few retain most of the variation present in the original variables. PCA helps in identifying the underlying structure of the data, reducing dimensionality, and highlighting important relationships between variables. It is a statistical technique that effectively summarize the essential information in the data (Jolliffe and Cadima, 2016) and it is widely used in various fields such as biology, ecology, and social sciences to make data analysis more manageable and insightful (Abdi and Williams, 2010; Jolliffe, 2002; Molina et al., 2018).

PCA was employed in this study (using Community Analysis Package 4.0, Pisces Conservation Ltd., 2014) to explore the relationships among dendrobatid species, as well as their associations with the provinces or protected areas of Ecuador. These relationships were visualized through two ordination plots, providing a clearer and more comprehensive representation of species distribution and their corresponding locations.

3 Results and Discussion

3.1 Similarity among provinces based on Dendrobatid species richness

The overall species richness by province is listed in Appendix 1. Notably, Morona Santiago and Napo (14 species each), Pastaza and Cotopaxi (13 each), Sucumbíos (11), and Santo Domingo and Pichincha (10 each) are the provinces where 10 or more species have been recorded.

The dendrogram displayed (Figure 7) illustrates the hierarchical clustering of Ecuadorian provinces based on the similarity of their dendrobatid species composition. Each individual branch represents a province, and the length of the branches reflects the level of dissimilarity between clusters. The horizontal axis represents a dissimilarity scale (Bray-Curtis index) ranging from 0 (complete similarity) to 1 (maximum dissimilarity). Provinces that form clusters at shorter branch lengths share more similar species compositions, indicating overlapping ecological characteristics or shared habitat types.

The ordination plot displayed (based on a Principal Components Analysis-Covariance Matrix; Figure 8) illustrates the relationships between dendrobatid species (green vectors) and the provinces of Ecuador (red squares). Provinces that are together share more similar species compositions, also indicating overlapping ecological characteristics or shared habitat types.

The analysis of dendrobatid species distributions across Ecuador's provinces reveals notable patterns of similarity, clustering provinces into four distinct groups (Figures 7-8). These groups illustrate how geographic, climatic, and ecological factors shape species richness and composition, providing a basis for understanding biogeographical trends and conservation needs.

Group 1: Azuay, Cañar, Bolívar, Chimborazo, Santa Elena, El Oro, Loja, and Guayas

This group is primarily characterized by species such as *Hyloxalus infraguttatus* (Hylinf), found in all eight provinces, *Hyloxalus elachyhistus* (Hylela), and *Epipedobates machalilla* (Epimac), both present in five provinces. Additionally, *Epipedobates anthonyi* (Epiant) is present in four provinces. These species are supported by shared environmental conditions, including similar altitudes and ecosystems (at least in the regions where these frog species were historically found).

Other species, such as *Hyloxalus vertebralis* (Hylver) and *Hyloxalus jacobuspetersi* (Hyljac), occur in fewer provinces but still contribute to the group's biodiversity. These patterns align with findings by Santos and Cannatella (2011) and Gómez (2017), which highlight the role of habitat connectivity in fostering shared species richness

Group 2: Carchi, Imbabura, Santo Domingo, Cotopaxi, Pichincha, Esmeraldas, Manabí, and Los Ríos

Provinces in this group exhibit high similarity due to the presence of species like *Epipedobates boulengeri* (Epibou), present in all eight provinces, *Hyloxalus* *awa* (Hylawa) and *Oophaga sylvatica* (Oopsyl), both found in seven provinces, and *Epipedobates espinosai* (Epiesp) in six provinces. Additionally, *Epipedobates machalilla* (Epimac) and *Hyloxalus infraguttatus* (Hylinf) are present in five and four provinces, respectively.

The proximity of these provinces and their shared lowland tropical and subtropical forest habitats support a high degree of overlap in dendrobatid species, as noted in other studies on amphibian distribution in Ecuador (Jongsma et al., 2014; Gómez, 2017).

Group 3: Morona Santiago, Pastaza, Napo, Sucumbíos, and Orellana

This cluster, encompassing Amazonian provinces, is characterized by *Ranitomeya ventrimaculata* (Ranven), *Ameerega hahneli* (Amehah), *Ranitomeya variabilis* (Ranvar), and *Hyloxalus sauteri* (Hylsau), all present in the five provinces. *Ameerega bilinguis* (Amebil) and *Ameerega parvula* (Amepar) appear in four provinces. The high species richness observed here reflects the continuous forest cover and the variety of ecological niches of the Amazon basin.

Studies by Myers et al. (2000) emphasize the Amazon's role as a biodiversity hotspot, underscoring the need to mitigate threats like deforestation and habitat fragmentation.

Group 4: Tungurahua and Zamora Chinchipe

This group is defined by *Hyloxalus shuar* (Hylshu), present in both provinces, alongside species such as *Hyloxalus anthracinus* (Hylant), *Hyloxalus marmoreoventris* (Hylmar), *Hyloxalus mystax* (Hylmys), *Hyloxalus exasperatus* (Hylexa), and *Leucostethus fugax* (Leufug), each found in one province. The distinct species composition suggests that altitudinal barriers and special microhabitats could play a pivotal role in shaping biodiversity in these areas.

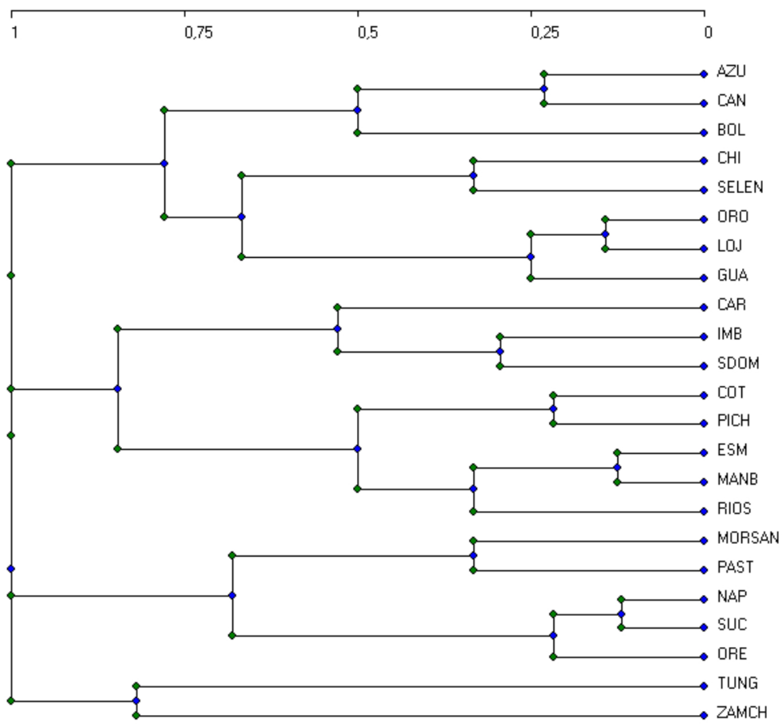

Figure 7. Dendrogram of 23 provinces of mainland Ecuador based on the presence-absence of 48 species of dendrobatids frogs. Method used: Hierarchical Agglomerative, Complete Linkage, and Bray-Curtis dissimilarities between provinces or groups of provinces (top axis).

These patterns align with conclusions from Ortiz et al. (2013), which highlight the Andes as centers of endemic amphibian diversity.

Regarding the situation in these two provinces, they are physically separated and share few similar environments, particularly in the eastern region of Tungurahua and the western region of Zamora Chinchipe. This geographic and ecological separation likely contributes to the low number of shared dendrobatid species between them, such as *Hyloxalus shuar*. Consequently, the similarity between these two provinces is among the lowest observed (Figure 7).

Necessary considerations

The clustering of provinces reflects biogeographical and ecological drivers of dendrobatid species distributions. The Amazonian provinces form cohesive clusters due to their uniform environmental conditions, while Andean and coastal provinces exhibit more distinct groupings influenced by altitudinal gradients, climatic variability, and habitat specialization. The dendrogram patterns underscore the interplay between geographic barriers and ecological connectivity in shaping biodiversity, offering critical insights for targeted conservation planning.

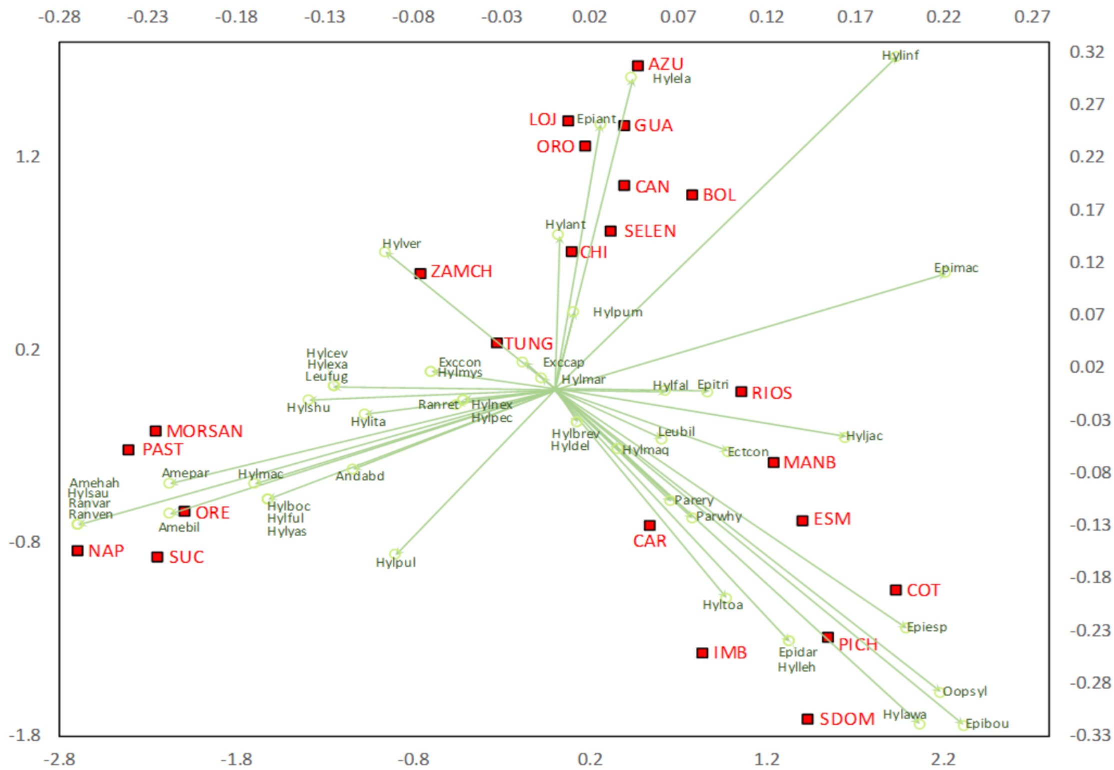

Figure 8. Ordination Plot (based on a PCA using a Covariance matrix) of the 23 provinces of Ecuador and their dendrobatids species richness (48). Note: F1 (horizontal axis) absorbed 43.4 % of the variance; F2 (vertical), 22.6 %.

The Amazon plays a pivotal role in preserving Ecuador's dendrobatid diversity, emphasizing the urgent need to safeguard its habitats from deforestation and other anthropogenic pressures. In contrast, Andean provinces such as Tungurahua, Chimborazo, and Bolívar host fewer dendrobatid species due to more difficult climatic conditions and more fragmented habitats. Coastal provinces, with relatively continuous ecosystems, facilitate species dispersal and persistence, yet face growing threats from agricultural expansion and urbanization, underscoring the necessity of targeted conservation measures.

Patterns of similarity and dissimilarity among provinces reveal the influence of biogeographic barriers on species distribution. For example, despite their relative proximity, Zamora Chinchipe and Napo exhibit distinct species assemblages shaped by microhabitat and environmental differences. Tools like Bray-Curtis index highlight these disparities, providing insights into the ecological and evolutionary drivers of dendrobatid distributions.

These findings stress the importance of spatial analyses in conservation planning. Andean and coastal provinces with unique species compositions require focused conservation strategies, while the high similarity among Amazonian provinces highlights the need to maintain habitat connectivity. Ecuador's exceptional dendrobatid diversity underscores the nation's role as a global amphibian biodiversity hotspot and the urgency of conserving microhabitats to protect vulnerable populations from human-induced pressures.

3.2 Similarity among SNAP's protected areas based on Dendrobatid species richness

The overall species richness by SNAP protected area is listed in Appendix 2. Remarkably, Yasuní National Park and Ilinizas Ecological Reserve (7 species each), Sangay National Park and Cuyabeno Reserve (5 each), and non-SNAP areas (mainly in private conservation zones) (21). These four protected areas also host the highest number of endemic species.

The dendrogram in Figure 9 illustrates the hierarchical clustering of Ecuadorian protected areas within the SNAP system, based on the similarity of their dendrobatid species composition, and one branch representing the areas outside this system (F-SNAP).

Each branch corresponds to a protected area, with branch lengths representing the degree of dissimilarity between clusters. The horizontal axis depicts the Bray-Curtis dissimilarity index, ranging from 0 (complete similarity) to 1 (maximum dissimilarity). Clusters formed at shorter branch lengths indicate protected areas with more similar species compositions, likely reflecting overlapping ecological characteristics or shared habitat types.

The ordination plot displayed (based on a principal component analysis-covariance matrix; Figure 10) illustrates the relationships between dendrobatid species (green vectors) and the SNAP's protected areas (red squares). Protected areas that are together share more similar species compositions, also indicating overlapping ecological characteristics or shared habitat types or geographic proximity.

The analysis of dendrobatid species distributions across Ecuador's protected areas (AAPP) reveals distinct patterns of similarity, clustering areas into eight groups based on shared species compositions (Figures 9–10). These groupings highlight the role of geographic proximity, habitat connectivity, and ecological characteristics in shaping species richness and diversity, offering critical insights into biogeographical trends and conservation priorities.

Group 1: Machalilla and Manglares Churute

This cluster of coastal protected areas is defined exclusively by the presence of *Epipedobates machalilla* (Epimac), a species endemic to this region. Shared lowland ecosystems and coastal forest remnants contribute to the group's composition, although habitat loss from urbanization and agriculture poses significant threats.

Group 2: Chimborazo and Pasochoa

Hyloxalus jacobuspetersi (Hyljac) is the sole species found in both areas, marking this cluster. The distinct altitudinal and climatic conditions of these regions may limit species richness but provide critical refuges for specialized taxa.

Group 3: Yasuní, Cuyabeno, and Limoncocha

This cluster is defined by the presence of four species: *Ameerega bilinguis* (Amebil), *Ameerega hahneli* (Amehah), *Hyloxalus sauteri* (Hylsau), and *Ranitomeya variabilis* (Ranvar), all found in the three areas. These species benefit from the extensive continuous forest cover of the Amazon basin, which facilitates dispersal and gene flow. These findings align with Myers et al. (2000), emphasizing the Amazon's significance as a biodiversity hotspot.

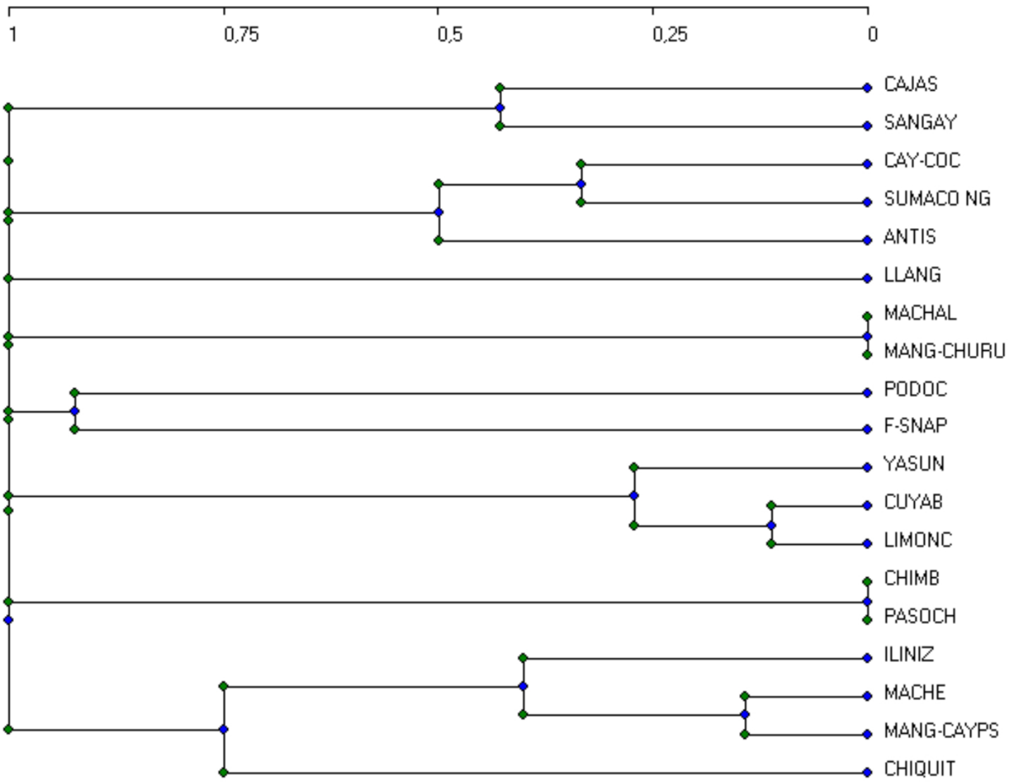

Figure 9. Dendrogram of 18 Protected Areas in Mainland Ecuador within the SNAP, Based on the Presence-Absence of 48 Dendrobatid Frog Species, and one general area for places outside the SNAP (F-SNAP). The analysis was conducted using the Hierarchical Agglomerative Method with Complete Linkage and Bray-Curtis dissimilarities (top axis).

Group 4: Mache-Chindul, Manglares Cayapas Mataje, Ilinizas, and La Chiquita

This group is characterized by *Epipedobates boulengeri* (Epibou), present in all four areas, alongside *Hyloxalus infraguttatus* (Hylinf) and *Oophaga sylvatica* (Oopsyl), found in three areas except La Chiquita. These species benefit from shared lowland tropical habitats and relatively high habitat connectivity across these protected areas.

Group 5: Sangay and Cajas

The shared presence of *Hyloxalus vertebralis* (Hylver) and *Hyloxalus anthracinus* (Hylant) characterizes this group. Both species are associated with mid-to relatively high-altitude habitats, highlighting the influence of Andean ecosystems on dendrobatid distributions. Similar altitudinal gradients and climatic conditions likely support the overlapping compositions observed.

Group 6: Cayambe-Coca, Sumaco-Napo Galeras, and Antisana

This group is primarily distinguished by *Hyloxalus pulchellus* (Hylpul) and *Hyloxalus bocagei* (Hylboc), present across the three areas. These protected areas share montane forest habitats, characterized by steep slopes, high precipitation, and a diverse array of ecological niches, fostering species persistence.

Group 7: Llanganates

Uniquely represented by *Hyloxalus maculosus* (Hylmac), Llanganates forms a solitary group, reflecting its distinct ecological and geographical conditions. The species' restricted range underscores the importance of preserving isolated Andean habitats.

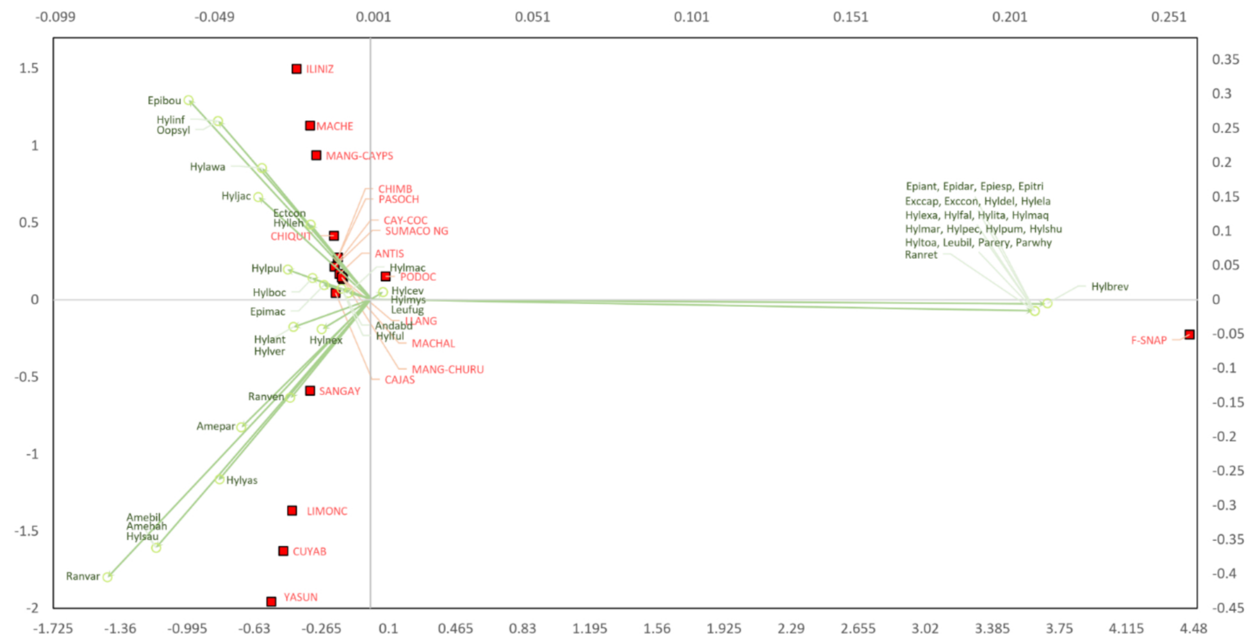

Figure 10. Ordination Plot (based on a PCA using a Covariance matrix) of the 18 Protected Areas of Mainland Ecuador (SNAP) and one general area for places outside the SNAP (F-SNAP) and their dendrobatids species richness (48). Note: F1 (horizontal) accounts for 31.5 % of the variance; F2 (vertical) explains 20.2 %.

Group 8: Podocarpus

Podocarpus stands alone, hosting *Hyloxalus cevallosi* (Hylcev), *Hyloxalus mystax* (Hylmys), and *Leucostethus fugax* (Leufug). This protected area shares *Hyloxalus breviquartus* (Hylbrev) with areas outside SNAP (F-SNAP). This species composition reflects the ecological complexity of Podocarpus, characterized by its relatively high-altitude cloud forests and endemic-rich flora and fauna.

The Podocarpus National Park joins very late in the Cladogram with the entity outside the SNAP (F-SNAP).

Beyond the SNAP system (F-SNAP), 21 dendrobatid species have been exclusively recorded in smaller conservation areas or wild environments outside formal national protection schemes. These include privately managed reserves (e.g., Bosque Protector Mindo Nambillo, Maquipucuna Reserve, Tesoro Escondido Reserve, Bilsa Biological Station, Río Palenque Research Center) and municipal or provincial conservation areas. These species are: *Epipedobates anthonyi, E. darwinwallacei, E. espinosai, E. tricolor, Excidobates captivus, E. condor, Hyloxalus delatorreae, H. elachyhistus, H. exasperatus, H. fallax, H. italoi, H. maquipucuna, H. marmoreoventris, H. peculiaris, H. pumilus, H. shuar, H. toachi, Leucostethus bilsa, Paruwrobates erythromos, P. whymperi, Ranitomeya reticulata*, all of them inhabiting these not-SNAP protected areas, emphasizing the importance of broader conservation strategies beyond the SNAP system.

Necessary considerations

The clustering of Ecuador's protected areas based on dendrobatid species composition reveals how ecological, geographic, and biogeographical factors influence biodiversity patterns. Amazonian areas exhibit high similarity due to their continuous forest cover, while Andean and coastal regions show distinct groupings shaped by altitudinal gradients, habitat specialization, and climatic variability.

The high level of dissimilarity among certain areas (or groups of areas) highlights the need for a networked approach to conservation. Methods such as network theory have proven effective for identifying and delimiting biogeographical regions, enabling more targeted and efficient conservation strategies (Vilhena and Antonelli, 2015). Each area contributes uniquely to the overall biodiversity, and protecting a diverse range of habitats is crucial as many species with restricted distributions depend on specific environmental conditions for their survival (Guisan et al., 2013).

These findings underscore the urgent need for conservation actions tailored to preserve Ecuador's exceptional amphibian diversity and address threats such as deforestation, habitat fragmentation, and human-induced pressures.

3.3 Distribution patterns and conservation implications for poison dart frogs included in threatened species categories

According to the information on Threatened Categories provided by the International Union for Conservation of Nature (International Union for Conservation of Nature, 2009) (Appendix 3), the following are the poison dart frog species classified under these categories:

3.3.1 Species in category Vulnerable

The following species are categorized as vulnerable: *Epipedobates espinosai*, *Hyloxalus infraguttatus*, *H. nexipus*, *H. peculiaris*, *H. pulchellus*, *H. shuar*, *H. toachi*, and *H. vertebralis*. These frogs are at risk of population decline due to factors such as habitat loss, environmental degradation, and climate change.

3.3.2 Species in category Endangered

The following species are categorized as endangered: *Ectopoglossus confusus*, *Epipedobates tricolor*, *Excidobates captivus*, *E. condor*, *Hyloxalus breviquartus*, *H. elachyhistus*, *H. fuliginosus*, *H. lehmanni*, *H. maculosus*, *H. marmoreoventris*, *H. mystax*, *Paruwrobates erythromos*, and *P. whymperi*. These species face severe risks of extinction in the wild if immediate conservation actions are not implemented. Habitat destruction and human activities are the primary drivers of their declining populations.

3.3.3 Species in category Critically Endangered

These species are at an extremely high risk of extinction due to their limited distributions, fragmented populations, and ongoing habitat destruction. Conservation efforts must urgently focus on their survival. The Critically Endangered species include *Andinobates abditus*, *Hyloxalus anthracinus*, *H. bocagei*, *H. delatorreae*, *H. exasperatus*, *H. fallax*, *H. jacobuspetersi*, *H. maquipucuna*, *H. marmoreoventris*, and *Hyloxalus pumilus*.

3.3.4 Importance of provincial and protected area data

Understanding the distribution of these species across provinces and protected areas is critical for identifying biodiversity hotspots and prioritizing conservation efforts.

In Ecuador, the hotspots for dendrobatid frogs are primarily located in these three regions (Tapia et al., 2017; Centro Jambatu de Investigación y Conservación de Anfibios, 2024):

- The Amazon Basin (eastern Ecuador): specially the provinces of Napo, Morona Santiago, and Sucumbíos, are known for their general high biodiversity. The dense rainforests and wetlands in this area provide the moisture and microhabitats needed for these frogs to thrive.
- The Chocó Bioregion (western Ecuador): specially the Esmeraldas and Pichincha provinces host many dendrobatid species thanks to the humid forests and diverse altitudinal gradients.
- The eastern Andean slopes, including Zamora-Chinchipe, Morona Santiago, and Azuay, also harbor dendrobatid, especially in cloud forests at varying altitudes.

Each province has unique ecological characteristics that influence the presence and survival of these frogs and other important species (Delgado et al., 2023; Crespo et al., 2022). By mapping their distribution, conservationists can pinpoint regions with the highest biodiversity or those with the most threatened populations, ensuring resources are allocated effectively. For example, provinces with high concentrations of Endangered or Critically Endangered species may require stricter habitat protection laws, targeted restoration projects, or the establishment of ecological corridors to maintain connectivity between populations.

4 Conclusions and Management implications

This study highlights the significant biodiversity of Ecuador's poison dart frogs, with distinct distribution patterns influenced by geographic, climatic, and ecological factors. The clustering of provinces and protected areas into groups based on species composition reveals clear biogeographic patterns, with Amazonian regions displaying high species richness and similarity. In contrast, Andean and coastal areas exhibit more unique species assemblages, shaped by altitudinal gradients and varying habitat conditions. These findings underscore the need for region-specific conservation efforts tailored to the unique environmental characteristics of each area or species composition.

The clustering of provinces also illustrates how the integrity of ecosystems is essential for maintaining amphibian biodiversity. In particular, the Amazonian provinces, which share continuous forest cover, support a greater diversity of species. In contrast, Andean provinces, which face harsher environmental conditions, show fewer species, emphasizing the vulnerability of these high-altitude ecosystems. The results suggest that protecting continuous forest habitats in lowland regions is critical to conserving Ecuador's amphibian diversity.

Additionally, the role of Ecuador's National System of Protected Areas (SNAP) in safeguarding biodiversity is evident. Protected areas such as Yasuní, Cuyabeno, and Sangay harbor a wide variety of species, demonstrating the importance of these areas in maintaining species richness. However, the dissimilarity observed among some SNAP areas indicates that some regions may require more targeted management strategies to address their unique ecological challenges. The identification of areas with lower species richness highlights the need for conservation actions that focus on habitat restoration, preventing further fragmentation.

While SNAP areas play a key role in biodiversity conservation, the study also reveals the importance of extending national conservation efforts beyond these formal protected spaces. Smaller reserves and privately managed areas, such as the Bosque Protector Mindo Nambillo and Maquipucuna Reserve, also host significant dendrobatid species. These areas, while outside the SNAP, are critical for maintaining connectivity and preserving species with limited distributions generally categorized as Threatened Species. Thus, a more integrated conservation approach, including private and community-led efforts, is essential for the long-term sustainability of Ecuador's amphibian populations.

The study's findings provide a comprehensive understanding of the distribution patterns of Ecuador's dendrobatid species and the ecological factors shaping them. Conservation planning should prioritize the preservation of continuous habitats, connectivity between protected areas, the presence of Dart Frog Threatened Species and the protection of specialized ecosystems, especially in Andean and coastal regions. A networked conservation approach, combining the efforts of SNAP and smaller conservation initiatives, is crucial to ensuring the future of Ecuador's exceptional amphibian biodiversity. Effective management strategies should focus on both the protection of existing habitats and the restoration of fragmented areas to prevent further biodiversity loss.

Acknowledgements

We would like to express our sincere gratitude to Universidad de Investigación de Tecnología Experimental Yachay for the approval provided through the research project BIO23-13. Its commitment to advancing scientific knowledge and fostering research initiatives has been instrumental in the successful development of this study.

Author's contribution

P.Y.M.: Conceptualization, Data curation, Formal analysis, Funding acquisition, Investigation, Methodology, Project administration, Computing resources, Supervision, Validation, Visualization, Writing– original draft, Writing– review editing. J.G.G.: Conceptualization, Data curation, Formal analysis, Investigation, Methodology, Validation, Writing– original draft, Writing– review editing. A.H.E., M.B.M., and D.Q.S. performed the Conceptualization, Data curation, Formal analysis, Investigation, Methodology, Validation, and Writing– original draft.

References

Abdi, H. and Williams, L. (2010). Principal component analysis. *Wiley interdisciplinary reviews: computational statistics*, 2(4):433–459. Online:https://n9.cl/j3ur5.

Amphibiaweb (2022). A specimen of Epipedobates machalilla (Dendrobatidae). Amphibiaweb. Online:https://bit.ly/3QwfETF.

Centro Jambatu de Investigación y Conservación de Anfibios (2024). Tres nuevas especies de ranas se suman a la riqueza de anfibios que hay en Ecuador. Anfibios Ecuador. Online:https://anfibiosecuador.ec/.

Clarke, K., Somerfield, P., and Gorley, R. (2016). Clustering in non-parametric multivariate analyses. *Journal of Experimental Marine Biology and Ecology*, 483:147–155. Online:https://n9.cl/7kqch.

Crespo, S., Solórzano, C., and Guerrero, J. (2022). Tráfico nacional de fauna silvestre y especies amenazadas: Un estudio descriptivo en Manabí (Ecuador). *LA GRANJA. Revista de Ciencias de la Vida*, 35(1):33–44. Online:https://n9.cl/p3gmx.

Daly, J., McNeal, E., Overman, L., and Ellison, D. (1985). A new class of cardiotonic agents: structure-activity correlations for natural and synthetic analogs of the alkaloid pumiliotoxin b (8-hydroxy-8-methyl-6-alkylidene-1-azabicyclo [4.3. 0] nonanes). *Journal of medicinal chemistry*, 28(4):482–486. Online:https://n9.cl/0i5l0.

Daly, J., Spande, T., and Garraffo, H. (2005). Alkaloids from amphibian skin: a tabulation of over eight-hundred compounds. *Journal of natural products*, 68(10):1556–1575. Online:https://n9.cl/2nbub.

Delgado, E., León, M., Cantos, C., and Guzmán, M. (2023). Efecto de la actividad minera sobre la biodiversidad en un sector del cantón Paquisha, provincia de Zamora Chinchipe-Ecuador. *La Granja*, 38(2):104–121. Online:https://n9.cl/51xta.

Gallice, G. (2009). A specimen of ameerega bilinguis (Dendrobatidae) in Coca, Orellana. Wikimedia Commons. Online:https://shorturl.at/Xdg9v.

Gómez, M. andd Ortega-Andrade, H. (2017). Biogeography of the Dendrobatidae family in Ecuador: Ecological Niche Models, diversity, endemism and threats. Master's thesis, Autonomous University of Barcelona.

Greenacre, M., Groenen, P., Hastie, T., d'Enza, A., Markos, A., and Tuzhilina, E. (2022). Principal component analysis. *Nature Reviews Methods Primers*, 2(1):100. Online:https://n9.cl/g8x5m.

Guisan, A., Tingley, R., Baumgartner, J., Naujokaitis-Lewis, I., Sutcliffe, P., Tulloch, A., Regan, T., Brotons, L., McDonald-Madden, E., and Mantyka-Pringle, C. (2013). Predicting species distributions for conservation decisions. *Ecology letters*, 16(12):1424–1435. Online:https://n9.cl/i8ae8.

International Union for Conservation of Nature (2009). The IUCN red list of threatened species. IUCN. Online:https://n9.cl/bk3tb.

Jolliffe, I. (2002). *Principal Component Analysis*. Springer Series in Statistics, 2nd ed edition.

Jolliffe, I. and Cadima, J. (2016). Principal component analysis: a review and recent developments. *Philosophical transactions of the royal society A: Mathematical, Physical and Engineering Sciences*, 374(2065):20150202. Online:https://n9.cl/6j3ha.

Jongsma, G., Hedley, R., Durães, R., and Karubian, J. (2014). Amphibian diversity and species composition in relation to habitat type and alteration in the mache-chindul reserve, northwest ecuador. *Herpetologica*, 70(1):34–46. Online:https://n9.cl/ltaoh.

Kassambara, A. (2017). Agglomerative hierarchical clustering. Data Novia. Online:https://shorturl.at/gP2g2.

Klimsa, E. (2020). A specimen of Hyloxalus infraguttatus (Dendrobatidae). iNaturalis. Online:https://shorturl.at/cLTOj.

Legendre, P. and Legendre, L. (2012). *Numerical Ecology*. Springer Series in Statistics, 3rd ed. edition.

Ministerio del Ambiente, Agua y Transición Ecológica (2023). A specimen of Hyloxalus infraguttatus (Dendrobatidae). Ministerio del Ambiente, Agua y Transición Ecológica. Online:https://n9.cl/1xvp9.

Molina, M., Terneus, E., Yánez, P., and Cueva, M. (2018). Resilience of phytoplankton community in the Andean Papallacta lagoon and its tributaries, eight years after an oil spill. *LA GRANJA. Revista de Ciencias de la Vida*, 28(2):67–83. Online:https://n9.cl/j79nwd.

Myers, N., Mittermeier, R., Mittermeier, C., Da Fonseca, G., and Kent, J. (2000). Biodiversity hotspots for conservation priorities. *Nature*, 403(6772):853–858. Online:https://bit.ly/3CNBAGz.

Ortiz, C., Páez, V., and Zapata, F. (2013). Temperature and precipitation as predictors of species richness in northern Andean amphibians from Colombia. *Caldasia*, 35(1):65–80. Online:https://n9.cl/ldo52.

Patocka, J., Wulff, K., and Palomeque, M. (1999). Dart poison frogs and their toxins. *ASA newsletter*, 74:16–18. Online:https://n9.cl/gxsq1.

Ron, S. andMerino-Viteri, A. and Ortiz, D. (2024). Anfibios del ecuador. version 2024.0. Museo de Zoología, Pontificia Universidad Católica del Ecuador. Online:https://n9.cl/iwiuj4.

Santos, J. and Cannatella, D. (2011). Phenotypic integration emerges from aposematism and scale in poison frogs. *Proceedings of the national academy of sciences*, 108(15):6175–6180. Online:https://n9.cl/0h77xr.

Santos, J., Coloma, L., and Cannatella, D. (2003). Multiple, recurring origins of aposematism and diet specialization in poison frogs. *Proceedings of the National Academy of Sciences*, 100(22):12792–12797. Online:https://n9.cl/f7isa.

Spande, T., Garraffo, H., Edwards, M., Yeh, H., Pannell, L., and Daly, J. (1992). Epibatidine: a novel (chloropyridyl) azabicycloheptane with potent analgesic activity from an Ecuadoran poison frog. *Journal of the American Chemical Society*, 114(9):3475–3478. Online:https://n9.cl/dgpmk1.

Tapia, E., Coloma, L., Pazmiño-Otamendi, G., and Peñafiel, N. (2017). Rediscovery of the nearly extinct longnose harlequin frog Atelopus longirostris (Bufonidae) in Junín, Imbabura, Ecuador. *Neotropical Biodiversity*, 3(1):157–167. Online:https://bit.ly/41ldIlY.

Tubifex (2010). A specimen of Epipedobates anthonyii (Dendrobatidae). Wikimedia Commons. Online:https://n9.cl/63j57.

Valencia, J., Betancourt, R., Yánez, P., Asanza, O., Benalcázar, Y., Hidalgo, J., and Campaña, J. (2009a). *Anfibios y Reptiles en ambientes cercanos a Pedro Vicente Maldonado y Balao*. Fundación Herpetológica Gustavo Orcés.

Valencia, J., Betancourt, R., Yánez, P., Olmedo, J., and Flores, R. (2009b). *Anfibios y Reptiles en ambientes cercanos a Nueva Loja y Lumbaquí*. Ecofondo y Fundación Herpetológica Gustavo Orcés.

Vilhena, D. and Antonelli, A. (2015). A network approach for identifying and delimiting biogeographical regions. *Nature communications*, 6(1):6848. Online:https://n9.cl/yvgyh.

Wold, S., Esbensen, K., and Geladi, P. (1987). Principal component analysis. Chimometrics and intelligent laboratory systems. In *Conference on Emerging Technologies Factory Automation Efta*, number 2, pages 704–706.

Yánez, P. and, B. J. and Quishpe, C. (2013). Multivariate characterization of the entities that make up the patrimony of natural areas of the Ecuadorian state: Phase i. *La Granja: Revista de Ciencias de la Vida*, 18(2):5–32. Online:https://n9.cl/xegcev.

Appendix

Appendix 1

Table 1. Provinces of mainland Ecuador addressed in the study

No.	Province	Region	Province Acronym used in multivariate analysis	Species richness of dendrobatid per province
1	Azuay	Andean	AZU	8
2	Bolívar	Andean	BOL	7
3	Cañar	Andean	CAÑ	5
4	Carchi	Andean	CAR	7
5	Chimborazo	Andean	CHI	1
6	Cotopaxi	Andean	COT	13
7	El Oro	Coastal and Western Andean	ORO	3
8	Esmeraldas	Coastal and Western Andean	ESM	9
9	Guayas	Coastal and Western Andean	GUA	4
10	Imbabura	Andean	IMB	7
11	Loja	Andean	LOJ	4
12	Los Ríos	Western Andean	RIOS	6
13	Manabí	Coastal and Western Andean	MANB	7
14	Morona Santiago	Amazonian and Eastern Andean	MORSAN	14
15	Napo	Amazonian and Eastern Andean	NAP	14
16	Orellana	Amazonian	ORE	9
17	Pastaza	Amazonian and Eastern Andean	PAST	13
18	Pichincha	Andean	PICH	10
19	Santa Elena	Coastal	SELEN	2
20	Santo Domingo de los Tsáchilas	Western Andean	SDOM	10
21	Sucumbíos	Amazonian and Eastern Andean	SUC	11
22	Tungurahua	Andean	TUNG	3
23	Zamora Chinchipe	Amazonian and Eastern Andean	ZAMCH	8

Appendix 2

Table 2. SNAP National Protected Areas addressed in the study

No.	Category of Protected Area	Protected Area	Region	Province Acronym used in multivariate analysis	Species richness of dendrobatid per area
1	Parque Nacional	PN Cajas	Andean	CAJAS	2
2	Parque Nacional	PN Cayambe Coca	Amazonian and Eastern Andean	CAY-COC	3
3	Parque Nacional	PN Llanganates	Amaznoian and Eastern Andean	LLANG	1
4	Parque Nacional	PN Machalilla	Coastal	MACHAL	1
5	Parque Nacional	PN Podocarpus	Amazonian and Eastern Andean	PODOC	4
6	Parque Nacional	PN Sangay	Amazonian and Eastern Andean	SANGAY	5
7	Parque Nacional	PN Sumaco Napo Galeras	Amazonian and Eastern Andean	SUMACO NG	3
8	Parque Nacional	PN Yasuní	Amazonian	YASUN	7
9	Reserva de Producción Faunística	RPF Chimborazo	Andean	CHIMB	1
10	Reserva de Producción Faunística	RPF Cuyabeno	Amazonian	CUYAB	5
11	Reserva Biológica	RB Limoncocha	Amazonian	LIMONC	4
12	Reserva Ecológica	RE Antisana	Eastern Andean	ANTIS	1
13	Reserva Ecológica	RE Ilinizas	Andean	ILINIZ	7
14	Reserva Ecológica	RE Mache Chindul	Coastal	MACHE	4
15	Reserva Ecológica	RE Manglares Cayapas Mataje	Coastal	MANG-CAYPS	3
16	Reserva Ecológica	RE Manglares Churute	Coastal	MANG-CHURU	1
17	Refugio de Vida Silvestre	RVS Pasochoa	Andean	PASOCH	1
18	Refugio de Vida Silvestre	RVS La Chiquita	Coastal	CHIQUIT	1
—	Only outside SNAP protected areas *	—	Various	F-SNAP	21

* Although some species of dendrobatid frogs were recorded outside the protected areas of the National System of Protected Areas (SNAP), it is worth mentioning that most of them were recorded in smaller private, provincial, or municipal conservation areas, such as protective forests or similar areas

Appendix 3

Table 3. Dendrobatidae frog species included in the study

No.	Species	Species Acronym used in Multivariate Analysis	Common name	Origin in relation to Ecuador	Conservation Category (IUCN, 2024)
1	*Ameerega bilinguis*	Amebil	Ecuador poison frog	Endemic	Least Concern
2	*Ameerega hahneli*	Amehah	Yurimaguas poison frog	Native	Least Concern
3	*Ameerega parvula*	Amepar	Valle Santiago rocket frog	Native	Least Concern
4	*Andinobates abditus*	Andabd	Collins' poison frog	Endemic	Critically Endangered
5	*Ectopoglossus confusus*	Ectcon	Confusing Rocket Frog	Endemic	Endangered
6	*Epipedobates anthonyi*	Epiant	Epibatidine poison frog	Native	Near Threatened
7	*Epipedobates boulengeri*	Epibou	Marbled poison-arrow frog	Native	Least Concern
8	*Epipedobates darwinwallacei*	Epidar	Darwin and Wallace poison frog	n.d.	n.d.
9	*Epipedobates espinosai*	Epiesp	Espinosa poison frog	Endemic	Vulnerable
10	*Epipedobates machalilla*	Epimac	Machalilla rocket frog	Endemic	Least Concern
11	*Epipedobates tricolor*	Epitri	Tricolor poison frog	Endemic	Endangered
12	*Excidobates captivus*	Exccap	Río Santiago poison frog	Native	Endangered
13	*Excidobates condor*	Exccon	Cóndor Poison Frog	Endemic	Endangered
14	*Hyloxalus anthracinus*	Hylant	South american rocket frog	Endemic	Critically Endangered
15	*Hyloxalus awa*	Hylawa	Awa rocket frog	Endemic	Near Threatened
16	*Hyloxalus bocagei*	Hylboc	Bocage's rocket frog	Endemic	Critically Endangered
17	*Hyloxalus breviquartus*	Hylbrev	Urrao rocket frog	Native	Endangered
18	*Hyloxalus cevallosi*	Hylcev	Palanda rocket frog	Endemic	Near Threatened
19	*Hyloxalus delatorreae*	Hyldel	Stella Rocket Frog	Endemic	Critically Endangered
20	*Hyloxalus elachyhistus*	Hylela	Loja rocket frog	Native	Endangered
21	*Hyloxalus exasperatus*	Hylexa	Yapitya rocket frog	Endemic	Critically Endangered
22	*Hyloxalus fallax*	Hylfal	Cotopaxi rocket frog	Endemic	Critically Endangered
23	*Hyloxalus fuliginosus*	Hylful	Quijos rocket frog	Endemic	Endangered

24	*Hyloxalus infraguttatus*	Hylinf	Chimbo rocket frog	Endemic	Vulnerable
25	*Hyloxalus italoi*	Hylita	Pastaza rocket frog	Endemic	Near Threatened
26	*Hyloxalus jacobuspetersi*	Hyljac	Quito rocket frog	Endemic	Critically Endangered
27	*Hyloxalus lehmanni*	Hylleh	Lehmann's rocket frog	Native	Endangered
28	*Hyloxalus maculosus*	Hylmac	Spotted rocket frog	Endemic	Endangered
29	*Hyloxalus maquipucuna*	Hylmaq	Maquipucuna rocket frog	Endemic	Critically Endangered
30	*Hyloxalus marmoreoventris*	Hylmar	Río Negro rocket frog	Endemic	Critically Endangered
31	*Hyloxalus mystax*	Hylmys	Cloud forest rocket frog	Endemic	Endangered
32	*Hyloxalus nexipus*	Hylnex	Los Tayos rocket frog	Native	Vulnerable
33	*Hyloxalus peculiaris*	Hylpec	Funny rocket frog	Endemic	Vulnerable
34	*Hyloxalus pulchellus*	Hylpul	Espada's rocket frog	Native	Vulnerable
35	*Hyloxalus pumilus*	Hylpum	San Vicente rocket frog	Endemic	Critically Endangered
36	*Hyloxalus sauli*	Hylsau	Santa Cecilia rocket frog	Native	Near Threatened
37	*Hyloxalus shuar*	Hylshu	Shuar rocket frog	Endemic	Vulnerable
38	*Hyloxalus toachi*	Hyltoa	Toachi rocket frog	Endemic	Vulnerable
39	*Hyloxalus vertebralis*	Hylver	Cuenca's rocket frog	Endemic	Vulnerable
40	*Hyloxalus yasuni*	Hylyas	Yasuní rocket frog	Endemic	Near Threatened
41	*Leucostethus bilsa*	Leubil	Bilsa white-chested frog	Endemic	Not Evaluated
42	*Leucostethus fugax*	Leufug	Pastaza rocket frog	Endemic	Near Threatened
43	*Oophaga sylvatica*	Oopsyl	Little-devil poison frog	Native	Near Threatened
44	*Paruwrobates erythromos*	Parery	Palenque poison frog	Endemic	Endangered
45	*Paruwrobates whymperi*	Parwhy	Tanti rocket frog	Endemic	Endangered
46	*Ranitomeya reticulata*	Ranret	Red-backed poison frog	Native	Near Threatened
47	*Ranitomeya variabilis*	Ranvar	Yellow striped poison frog	Native	Least Concern
48	*Ranitomeya ventrimaculata*	Ranven	Amazonian Poison Frog	Native	Least Concern

La granja:
Revista de
Ciencias de la Vida
pISSN:1390-3799; eISSN:1390-8596
https://doi.org/10.17163/lgr.n41.2025.03

Scientific paper/ Artículo científico
Conservation

Pesticides and their impact on entomofauna in Andean farmers' fields in Ecuador

Pesticidas y su impacto sobre la entomofauna en fincas de agricultores andinos de Ecuador

Diego Mina*[1], Jhenny Cayambe[2], Tatiana Cárdenas[3], Israel Navarrete[4] and Olivier Dangles[3]

[1]Pontificia Universidad Católica del Ecuador. 170143, Quito-Ecuador.
[2]Pontificia Universidad Católica del Ecuador sede Ibarra. 100150, Ibarra-Ecuador.
[3]UMR CEFE. 1919 route de Mende. 34090 Montpellier-France.
[4]Centro Internacional de la Papa. 170143, Quito-Ecuador.

*Corresponding author: diego.mina@ird.fr

Received on May 12th, 2022. Accepted, after revision on September 14th, 2024. Published on March 1st, 2025.

Abstract

Ignorance of the rational use of insecticides leads farmers in developing countries such as Ecuador to exceed the limit of permitted applications. In addition, little is known about the effect of insecticides on entomofauna of *Lupinus mutabilis* (lupine). This study aims to analyze the effect of insecticides on pests and beneficial insects, with special emphasis on pollinators, without neglecting the effect on crop yield. The entomofauna associated with Andean Lupin was used as a reference. Seventy-nine agricultural fields were evaluated in Cotopaxi-Ecuador, with the treatments with chemicals, without chemicals, and without any control. Once the experiment was presented to the participating group, the farmers chose the management treatment for their fields with recommendations from the researchers. For insect monitoring, yellow sticky and plate traps were used to obtain variables of insect abundance and diversity. The use and application of pesticides was recorded using surveys developed with Survey 123. The results showed that the application of insecticides was not always effective in controlling the pests studied. In addition, the treatments evaluated had different effects according to the type of insect pollinator analyzed. On the other hand, the study also showed that certain pests, especially borers, could induce a positive response (70% more flowers) that can actually benefit the final yield. These results suggest that pest controls for this crop should be more targeted and carried out before flowering to avoid causing damage to pollinators and borers, as well as natural enemies of pests.

Keywords: lupin, insecticides, pollinators, yield, entomofauna.

Resumen

El desconocimiento del uso racional de insecticidas conlleva a que agricultores de países en desarrollo como Ecuador sobrepasen el límite de aplicaciones permitidas. Además, poco se conoce del efecto que tienen los insecticidas sobre la entomofauna de *Lupinus mutabilis* (chocho). Este estudio busca analizar el efecto de los insecticidas sobre plagas e insectos benéficos con especial énfasis en polinizadores, sin descuidar el efecto sobre el rendimiento del cultivo. Se tomó como referencia la entomofauna asociada al cultivo de chocho. Se evaluaron 79 campos agrícolas en Cotopaxi-Ecuador, con tratamientos con químico, sin químico y sin ningún control. Una vez socializado el experimento, los agricultores eligieron el manejo para sus campos con las recomendaciones de los investigadores. Para el monitoreo de insectos se usaron trampas pegantes y de plato de color amarillo. Se obtuvieron variables de abundancia y diversidad de insectos. El uso y aplicación de plaguicidas se registró usando encuestas desarrolladas con Survey 123. Los resultados muestran que la aplicación de insecticidas no siempre fue efectiva en el control de las plagas analizadas. Además, los tratamientos evaluados tuvieron efectos distintos según el tipo de insecto polinizador analizado. Por otro lado, se observó que ciertas plagas, en especial barrenadores podrían inducir un efecto de respuesta positivo (70% más de flores) que beneficiaría el rendimiento final. Estos resultados podrían sugerir que los controles de plagas para este cultivo deberían ser más dirigidos y realizarse antes de la floración, esto evitaría causar daños a polinizadores, barrenadores y probablemente enemigos naturales de plagas.

Palabras clave: chocho, insecticidas, polinizadores, rendimiento, entomofauna.

Suggested citation: Mina, D., Cayambe, J., Cárdenas, T., Navarrete, I. and Dangles, O. (2025). Pesticides and their impact on entomofauna in Andean farmers' fields in Ecuador. *La Granja: Revista de Ciencias de la Vida.* Vol. 41(1):51-68. https://doi.org/10.17163/lgr.n41.2025.03.

Orcid IDs:

Diego Mina: https://orcid.org/0000-0001-8821-6575
Jhenny Cayambe: https://orcid.org/0000-0001-7413-2151
Tatiana Cárdenas: https://orcid.org/0000-0001-9956-3169
Israel Navarrete: https://orcid.org/0000-0002-9779-4809
Olivier Dangles: https://orcid.org/0000-0002-1987-8433

1 Introduction

The use of pesticides is a global practice, predominantly present in low-income countries. Factors such as lack of training, low education levels among farmers, limited alternatives to pesticides, and the influence of vendors are some of the reasons behind this (Berni et al., 2021; Jallow et al., 2017; Khan et al., 2015). According to the FAO (2017), global pesticide consumption reached over 4.11 million tons that year. FAO data shows that in the last 20 years, countries like Italy, France, and Japan have reduced pesticide use by an average of 36 %. In contrast, countries such as Malawi, Bangladesh, and Ethiopia have seen a 1325 % increase in demand. In Latin America, more than 5 kg of pesticide per hectare are used, while in countries like Ecuador, pesticide application increased by over 1500 % between 1990 and 2017 (FAO, 2017). Most studies place the blame for pesticide misuse on farmers (Damte and Tabor, 2015; Mengistie et al., 2017). The lack of basic understanding and an integrated perspective on pests contributes to this "misuse" by farmers (Wyckhuys et al., 2019), without accounting for external influencing factors such as government actions, universities, NGOs, and private companies (Pan et al., 2021). However, at the individual level, pesticide decision-making and resistance management are not solely the responsibility of farmers (Gould et al., 2018); all actors in the supply and consumption chain share this responsibility. In fact, farmers themselves acknowledge being blamed for the decline in insects, biodiversity loss, and pesticide overuse. However, they also consider this a holistic problem that should address multiple causes (Busse et al., 2021).

Pesticide application has numerous impacts, including soil contamination, human health risks, and environmental damage (Budzinski and Couderchet, 2018). In fact, pesticide use is one of the most damaging agricultural practices for agrobiodiversity (Mengistie et al., 2017). Studies confirm the negative impact of insecticides on entomofauna, showing declines and/or losses (Catarino et al., 2019; Goulson, 2019). Scientists attribute the most extensive harmful effects to insecticide use (Chemnitz, 2022). Intensive insecticide use is believed to accelerate pest adaptation while making beneficial insects more vulnerable (Potts et al., 2010; Chivian and Bernstein, 2015). For example, the synergy of IBE fungicides and neonicotinoids has caused higher mortality rates in solitary bees *Osmia lignaria*, the bumblebee *Bombus terrestres*, and *Apis mellifera* (Botías and Sánchez-Bayo, 2018). This points to a global crisis in the abundance, diversity, and biomass of insects, particularly pollinators, caused in part by anthropogenic activities in industrialized agricultural landscapes (Forister et al., 2019).

It is estimated that 35 % of global food production depends on animal pollination (Klein et al., 2007; Sawe et al., 2020). In fact, between 5 % and 8 % of global crop production would be lost without insect pollination (Aizen et al., 2009). Economically, agricultural production resulting from animal pollination is valued between \$ 235 and \$ 577 billion (Sawe et al., 2020). The detrimental effect of pesticides on beneficial entomofauna, specifically pollinators, and its impact on final crop yield has been well documented (Pacífico da Silva et al., 2015; Stanley et al., 2015; de Oliveira et al., 2019). Understanding the composition of entomofauna and their interactions could help improve farmers' knowledge and change their agricultural practices (Magrach et al., 2019).

Combining many elements such as biological control, inter- and intraspecific botanical diversity, synthetic volatile compounds, and induced defense, Integrated Pest Management (IPM) has been one of the most commonly used strategies (Stenberg, 2017). However, IPM has not traditionally considered insects like pollinators, which are also affected by agricultural practices. Consequently, there is a demonstrated need to incorporate strategies that protect pollinators within IPM to reduce their exposure to pesticides (Egan et al., 2020). These authors have proposed transitioning from IPM to IPPM (the second "P" for pollinators).

This approach was integrated into the representation of the interrelationships among the "4P": pesticides, pests, pollinators, and productivity (Figure 1). Pesticides in agriculture are used to control pests (Figure 1a), given their negative impact on productivity (Figure 1b). For many farmers, the use of pesticides is seen as necessary to improve (or prevent the decline of) crop productivity (Figure 1c). Similarly to pests, pesticides generally have a negative effect on pollinators (Figure 1d). Depending on the crop, pollinators can have a neutral or positive effect on productivity (Figure 1e). These relationships demonstrate the need to consider both pest and beneficial insects when evaluating the impact of insecticides on crop productivity.

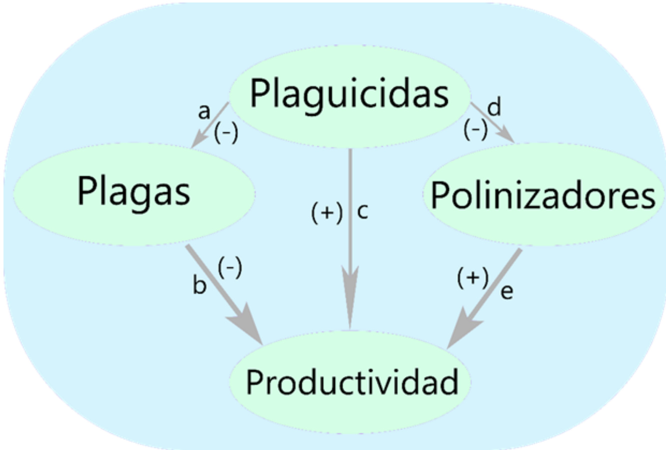

Figure 1. Relationships between the effect of pesticide use on entomofauna and productivity. Figure modified from Struelens et al. (2021).

It is interesting to analyze the transition from IPM to IPPM in an agricultural system where these relationships are represented. In a previous study, Struelens et al. (2021) reported that in Ecuador, insecticide applications affect entomofauna in small-scale Andean farmers' *Lupinus mutabilis* Sweet (chocho) systems. These authors found a significant impact on reducing pollinators due to the number of pesticide applications ($p = 0.021$; path coefficient = -0.892), without a clear reduction in pest populations. However, these conclusions are based on a limited number of fields (fewer than 20 in total), and the relationships between insecticides, pests, pollinators, and crops need further exploration. Although chocho is a self-pollinating plant, its production quality can significantly depend on insect pollinators. Therefore, it is an interesting crop model to analyze the combined effects of insecticides and their impact on entomofauna. Cowling et al. (1998) reported a cross-pollination rate of 4 to 11%, while Caligari et al. (2000) found an outcrossing rate of up to 58.8% in their experiments. Struelens et al. (2021) reported a 10.5% increase in the number of chocho seeds due to visits from pollinating insects.

Chocho is cultivated in several Andean countries. In Ecuador, the main production areas are Cotopaxi, Chimborazo, Pichincha, and Imbabura (SINAGAP, 2014). Its seeds are rich in protein (41-51%) and essential fatty acids (3-14%) (Nicklin et al., 2006). Its symbiosis with the bacterium *Bradyrhizobium* fixes atmospheric nitrogen (between 30 and 70 kg of N/ha), enriching the soil (Alandia, 2018).

However, in Ecuador, agricultural intensification of this crop has been accompanied by an increase in phytosanitary issues, primarily herbivore attacks (Caicedo and Peralta, 2000). In 2015, approximately 7825.59 ha of chocho were planted, with a trend of increasing acreage in subsequent years (INEC, 2015). Although there are few reports and studies on pests in the area, previous surveys by the authors mainly report borers, such as the stem borer (Agromyzidae) and the shoot fly (Anthomyiidae), which are present throughout almost the entire phenological cycle of the crop (Mina et al., 2017). Interestingly, the attack of this pest could suggest increased growth of reproductive organs in chocho, known as an overcompensation effect (Struelens et al., 2021). García and Eubanks (2019) document 86 studies showing examples of overcompensation in response to insect herbivory across 67 plant species representing 26 families.

Insecticide application is often the first, main, and sometimes the only option for Ecuadorian farmers to control pests. A common practice is to mix several pesticides into "cocktails". Sherwood et al. (2005), for example, reported that farmers mixed up to seven products in one "brew", sometimes with the same active ingredient or mechanism of control. In theory, these cocktails save time and labor while increasing efficacy in controlling pests and diseases. However, without clear information on the chemical labels, mixing these products is risky (Mengistie et al., 2017). Pesticide mixtures are a particular concern for human health due to their potential synergistic effects on toxicity. Pesticide mixtures with the same mode of action (MoA) often exhibit additive effects, while those with different MoAs produce effects that are difficult to predict (Hernández et al., 2017). In Ecuador, the problem is exacerbated as the government reports that many of the foods consumed exceed the Maximum Residue Limits (MRL) for pesticides allowed for human consumption.

This study is designed to address three main questions:

(i) How does insecticide use affect pests and pollinators (relationships a and d in Figure 1)?

(ii) Does insecticide use and its impact on entomofauna affect crop yields (relationships b, c in Figure 1)?

(iii) What is the relationship between the level of major pests (borers) and chocho yield (relationship d in Figure 1)?

2 Materials and Methods

2.1 Study sites

The study was conducted in 79 farmers' fields between January and November 2021 in the central-northern highlands of Ecuador (Figure 2). The fields were located in the parishes of Alaquez, Cochapamba, Cusubamba, Eloy Alfaro, Guaytacama, Juan Montalvo, La Matriz, and Pujilí (Table 1).

The study areas and farmers were selected based on: i) Levels of intensification in the agricultural landscape (planting density and/or number of species present in a given area); ii) Agricultural practices (e.g., use or non-use of insecticides); iii) Previous research and training work with farmers in the area; and iv) The farmers' interest in participating in the research.

2.2 Study Desing

Three activities were carried out. The first was the monitoring of insecticide applications in farmers' fields, the second was the monitoring of insect populations, and the third was the study of yield variability.

2.2.1 Recording of Insecticide Applications in Farmers' Fields

Two treatments were initially established: i) With chemicals; fields with synthetic chemical insecticide applications, and ii) Without chemicals; fields with organic insecticide applications. However, fields were also identified where farmers applied no pest control. Ultimately, 39 fields were designated as chemical, 34 as non-chemical, and 6 as no control.

Each farmer chose the treatment to apply, including irrigation, weeding, and the frequency of pest control measures, all financed by the farmers themselves. In all fields, seeds of the chocho variety INIAP-450 Andino were used, disinfected with the chemical recommended and used by local technicians (Tiabendazole + Thiamethoxam). Non-chemical fields used organic-biological strategies such as mineral broths and plant extracts, provided by the farmers and the local university. For the chemical treatments, active ingredients commonly used by farmers were applied (Table 2).

70 % of the farmers who applied chemical treatments used organophosphate and pyrethroid insecticides, with a range of 1 to 4 applications before the flowering stage. On the other hand, 95 % of the fields without chemical treatments used mineral broths and plant extracts (Table 2).

2.2.2 Data Collection

Data on the use and application of chemical products (active ingredient, dosage, frequency of application) were collected through surveys. The study was authorized by the Research Ethics Committee (CEISH) of the Pontificia Universidad Católica del Ecuador (PUCE). Each farmer signed an informed consent form regarding the research activities.

Table 1. Bioclimatic characteristics and treatments applied at the study sites, Cotopaxi 2021.

	Sites	Alaquez	Carrillo	Chan	Cuturivi	Guaytacama	La Merced	Cachipata	Yugshiloma	Total fields evaluated
	Average size of evaluated fields evaluados (m^2)	1850	1387	2125	985	1218	2367	2944	846	
	Main crops	Bean, fava bean, maize	Maize	Pea, bean	Pea, barley, potato	Pea, bean, maize	Maize	Maize, potato	Maize	
Bioclimatic characteristics	Altitude (masl)	3044	3032	2918	3503	2948	2950	3336	2900	
	Average precipitation during monitoring days (mm/day)	8.67	7.88	8.15	10.22	7.68	8.44	8.9	9.75	
	Temperature (°C)	12	11	13	11	11	13	10	11	
Number of treatments	With chemicals	4	6	1	13	5	2	9	2	42
	Chemical free	8	4	2	6	6	1	1	3	31
	No pest control	2		1	1	1	1	0	0	6

In addition to workshops, regular visits and monitoring of each experimental field were conducted. During these workshops, information about the experiment's activities was provided, and each farmer was responsible for applying their chosen treatment (Figure 3E). In-person sessions were held between March and November 2021, following a preestablished biosecurity protocol due to the pandemic.

2.2.3 Monitoring of Insect Populations in Farmers' Fields

Sticky traps and plate traps were used to capture flying insects reported as entomofauna associated with chocho (*Lupinus mutabilis*) (Mina et al., 2017). Yellow plastic sticky traps, A4 size (21 × 29.7 cm) (Ali et al., 2019), were used to sample pest insects and placed at crop height (Figure 3A). The number of traps and their distribution were based on the field's area, with one trap per 1000 m^2 (Heinz et al., 1992; Willett et al., 2020).

Sticky traps were placed 10 to 12 weeks after planting and were left in the field once for 72 hours (Shah et al., 2020). To analyze the effect of insecticides on pests, two insect species identified as pests at this crop stage were selected: i) the shoot borer (Diptera/Anthomyiidae, possibly *Lasiomma* sp. see (Struelens et al., 2021)) (Figure 3C) and ii) the black lady beetle (Coleoptera/Melyridae, *Astylus bourgeoisi*). A third pest, Agromyzidae (possibly *Liriomyza* sp.), was recorded during destructive sampling.

To record pollinating insects, yellow plate traps were placed at flower height (Figure 3B). Each trap contained 200 mL of water and 5 mL of neutral liquid soap (Saunders and Luck, 2013; Padron et al., 2021). Traps were collected after 72 hours (Shah et al., 2020), and the insects were preserved in sealed jars with 70% alcohol for later morphological identification. Insect identification was supported by taxonomic keys and the citizen science tool "iNaturalist" (Inaturalist, 2022).

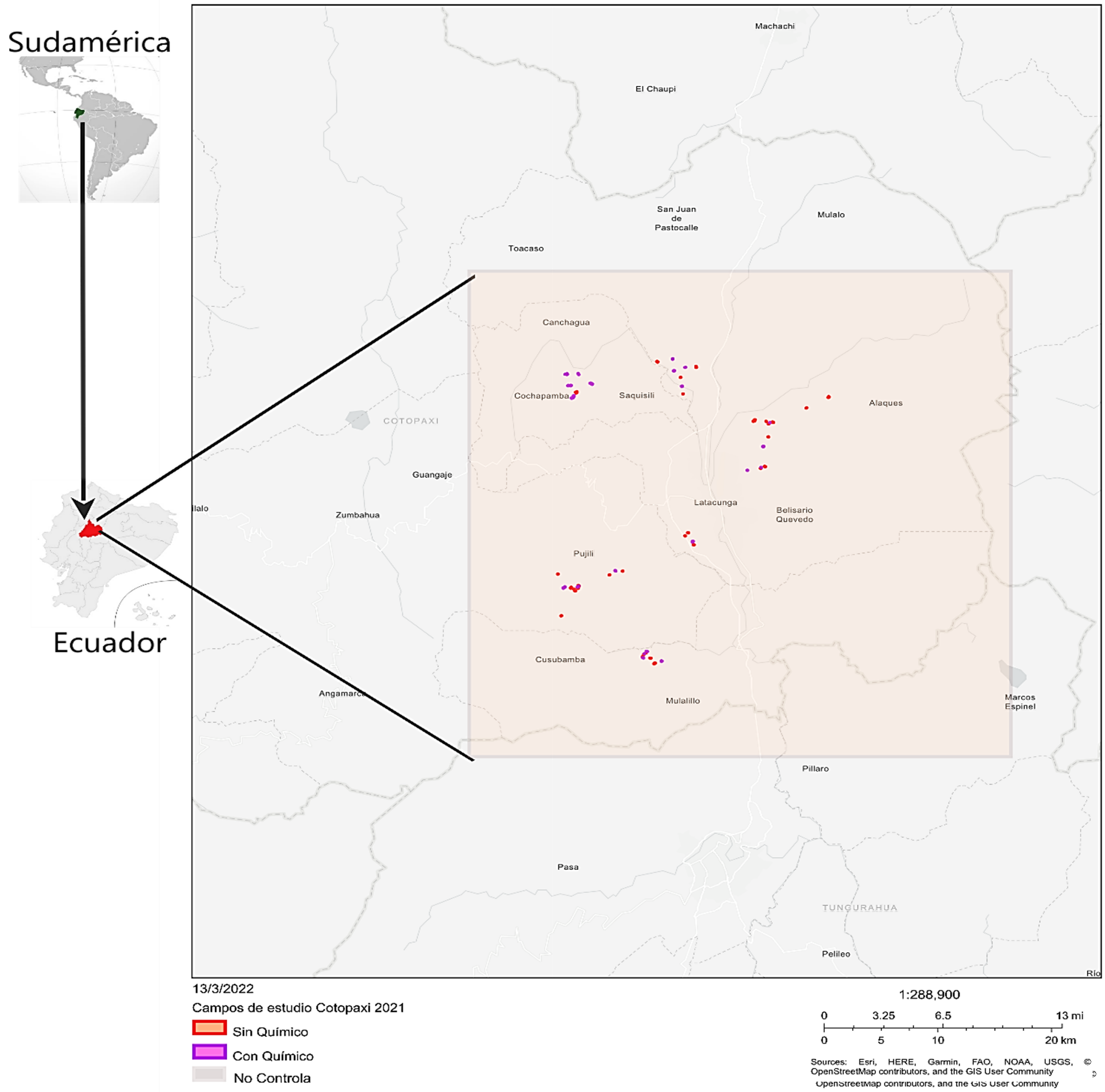

Figure 2. Continental and regional location of the study sites in the Ecuadorian highlands. Distribution of experimental fields according to the applied treatment.

2.3 Recording Variables Related to Damage and Yield

Additionally, damage levels were evaluated by marking 10 plants per field during the vegetative stage for destructive sampling. The height of each plant in reference to the central stem and the number of branches were recorded. These variables are related to the plants' response to the characteristic attack of the borers studied (Struelens et al., 2021). Height was measured in centimeters from the base of the stem to the apex of the central axis. The number of branches was recorded by counting those with reproductive organs (pods and/or flowers) (Garibaldi et al., 2016). These variables were complemented by the abundance of three pests found during destructive sampling: i) shoot borer (Diptera/Anthomyiidae), ii) stem borer (Diptera/Agromyzidae), and iii) moths (Lepidoptera).

Table 2. Treatments used by farmers for insect pest control, Cotopaxi 2021.

	Insect to control	**Chemical treatment Chemical group (GQ) Toxicological class (CT) Mode of action (MA)**	**Chemical-free treatment**
SEEDING	*Delia platura* *Agrotis* sp. *Agriotes* sp.	GQ: Oxime carbamates CT: Ib Highly hazardous MA: Cholinesterase inhibitors	Neem Oil Organic Insecticide 2-2-1 (ginger + chili + garlic) Microbes with Bitter Herb Extracts
		GQ: Pyrethroids and Pyrethrins CT: II Moderately hazardous MA: Insecticidal activity by contact and ingestion, affecting the nervous system	
		GQ: Organophosphates CT: II Slightly hazardous MA: hazardous inhibitor	
		GQ: Organophosphates CT: III Slightly hazardous MA: Acetylcholinesterase inhibitor	
VEGETATIVE STAGE	*Lasiomma* sp. *Liriomyza* sp.	GQ: Neonicotinoids + Phenylpyrazoles (Fiproles) CT: II Moderately hazardous MA: Fipronil, blocks the effect of the GABA (γ-aminobutyric acid) neurotransmitter	Application of Lime Sulfur Sprays Application of Ash Sprays Foliar Fertilizers (Amino Acids)
		GQ: Nereistoxin analogs CT: II Moderately hazardous MA: Stomach and contact action insecticide	

2.4 Data Analysis

Comparisons were made based on the treatment applied by the farmer during the crop cycle. Differences in pest and pollinator abundances between each type of treatment were analyzed using an Analysis of Variance (ANOVA). For pest insects (*Astylus bourgeoisi* and Anthomyiidae), sticky trap counts were used, while for Agromyzidae and pollinators, plate trap counts were used.

The nine most abundant groups of flower-visiting insects recorded across the 79 fields were selected. The effect of the treatments on crop yield, as reported by farmers after harvest, was also evaluated.

In addition to analyzing the impact of insecticides on pests, pollinators, and productivity, the relationship between pests and plant productivity (relationship d in Figure 1) was analyzed. A Productivity Index (PI) was created by summing the flowers and pods of each plant; this value was divided by the number of plants evaluated in each field.

In the 10 plants where productivity was assessed, the total number of borers was also counted through destructive sampling. All larvae of Anthomyiidae, Agromyzidae, and moths were summed. These counts were compared to the productivity index obtained for each field using a non-linear Poisson model. To fit the data to a linear model, a logarithmic transformation (Log +1) was performed for normal distribution and homoscedasticity of variance. All statistical analyses were conducted using the Past 4 project software (Hammer et al., 2001) and R v1.3.959 software (R Core Team 2020).

Figure 3. Methods used in this study (a) sticky traps, (b) plate traps, (c) shoot borer fly (Anthomyiidae/pest), (d) *Eristalis tenax* (Syrphidae/pollinator), (e) farmer applying pest control treatments.

3 Results

Abundance and Diversity of Sampled Entomofauna

In this experiment, 13 morphospecies of insects associated with chocho fields were identified. These were classified into two functional groups: pests and pollinators, either direct or indirect. Four orders and 12 families of insects were identified from a total of approximately 12,000 individuals collected. The order with the highest abundance was Diptera, accounting for 74 %, followed by Coleoptera at 18 %, and the remaining 8 % were Hymenoptera and Lepidoptera. The following are the main results that help address the questions posed in this study.

3.1 Effect of Pesticides on Pests, Pollinators, and Yield

The treatments applied showed variability in the response of the three pest insects analyzed. In all three cases, the "no control"treatment (no application of any pest control) appeared to have the lowest pest abundance. On the other hand, for *A. bourgeoisi* and Agromyzidae, there was a slight trend toward lower abundance in the "non-chemical", a trend not observed for Anthomyiidae. However, statistically, no significant effects of the treatments on the abundance of the three pests were found (p >0.05, Figure 4).

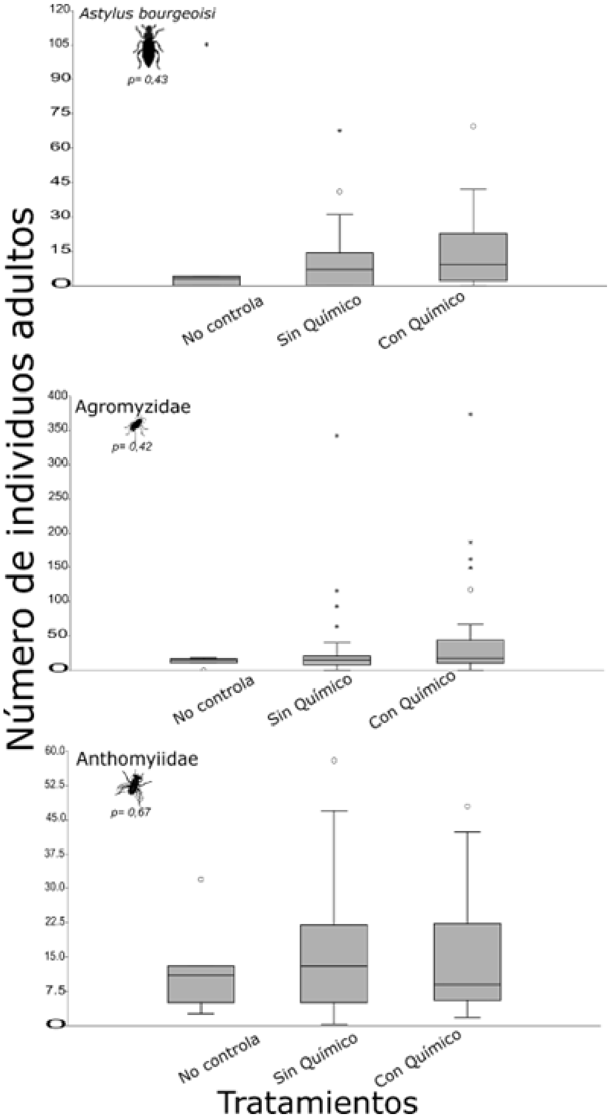

Figure 4. Effect of treatments on the abundance of pest insects monitored with sticky traps (A and C) and plate traps (B).

For pollinators, the 9 most abundant insect groups, reported as pollinators of various flowering crops, were considered. The insects analyzed included *Eristalis* sp., *Apis mellifera*, and flies from the families Stratiomyidae, Tachinidae, Sarcophagidae, Calliphoridae, Bibionidae, Syrphidae, and hymenopterans from the family Halictidae. However, all the insects sampled and uploaded to the iNaturalist app resulted in 52 different morphospecies (Inaturalist, 2022).

Some species of interest as pollinators include *Eristalis tenax* and *Eristalis bogotensis* (Syrphidae), *Cynomya cadaverina, Lucilia sericata, Calliphora vicina*, and *Chrysomya megacephala* (Calliphoridae), *Augochlorella aurata, Caenohalictus* sp., *Pseudaugochlora* sp., and *Neocorynura* sp. (Halictidae). Other identified insects included genera such as *Hedriodiscus* sp., *Netelia* sp., *Megachile* sp., *Eriothrix* sp., *Peralia* sp., and *Panzeria* sp.

The effect of the 3 treatments on the abundance of pollinators varied depending on the insect group. For insects such as *Apis mellifera, Stratiomyi-*

dae, Tachinidae, Sarcophagidae, Bibionidae, and *Syrphidae*, no statistical differences in abundances were found (ANOVA, *p* >0.05, Table 1). In contrast, for insects such as *Eristalis* sp., Calliphoridae, and Halictidae, lower abundances were found in chemically treated fields (ANOVA, *p* <0.05, Figure 5).

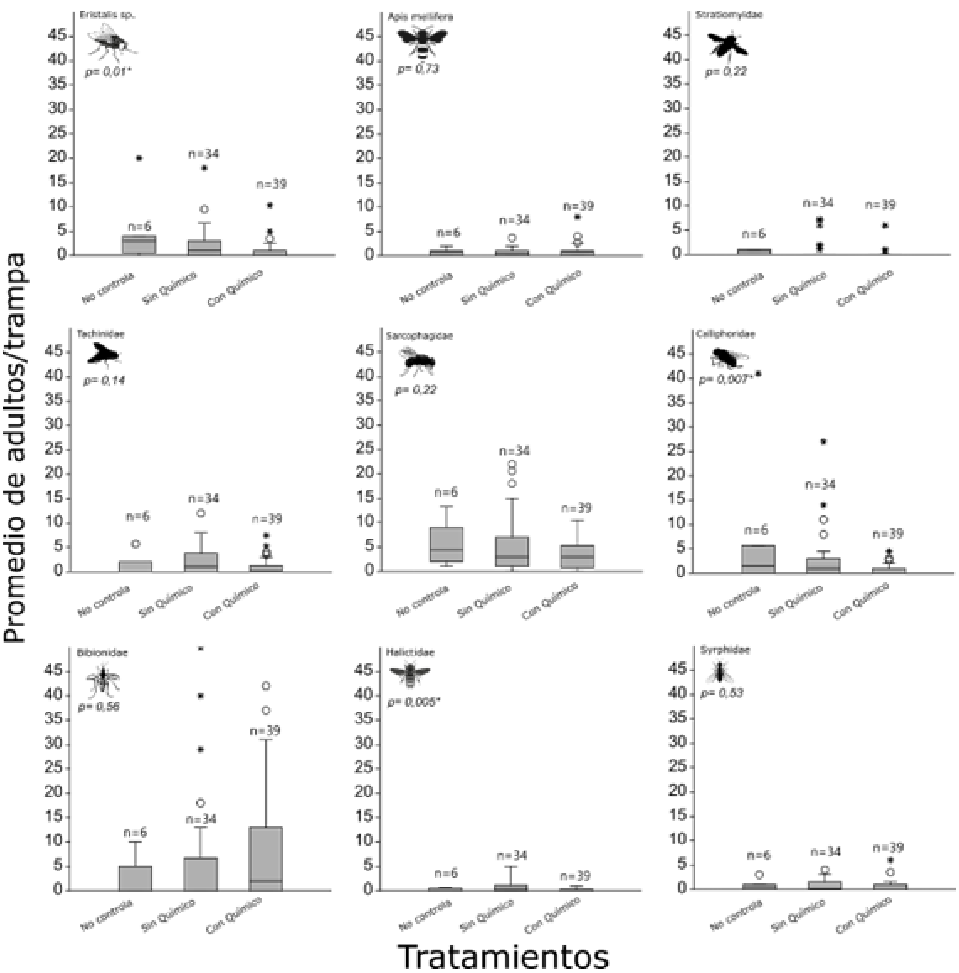

Figure 5. Effect of treatments on the abundance of beneficial insects monitored with plate traps.

Pairwise comparisons of treatments yielded the following results: i) No control vs. non-chemical was not significant (ANOVA, *p* <0.17), ii) No control vs. chemical was significant, with Tukey's test at 5% showing that the treatment with the lowest abundance of beneficial insects was the chemical treatment, with an average of 1.78 insects (ANOVA, *p* <0.002), iii) Non-chemical vs. chemical was significant, with Tukey's test at 5% showing the lowest abundance of beneficial insects in the chemical treatment (ANOVA, *p* <0.004).

The average height of the evaluated plants was 0.97 m, with a standard deviation of 0.24. The average number of branches was calculated to be 9.37, with a standard deviation of 2.45. Regarding the damage caused by borer pests on the main stem (measured as plant height), no significant effect of the treatments was found in the studied fields ($p = 0.903$; Figure 6A). On the other hand, it was observed that fields where chemical insecticides were applied had chocho plants with a greater number of branches (ANOVA, $p = 0.038$; Figure 6B).

Regarding estimated *chocho* productivity, where flowers and pods were counted on 10 randomly selected plants per field, significant variability was observed across the different fields, with no significant effect from any treatment (p >0.05, Figure 7). However, a positive correlation ($r = 0.19$) was found between the final yield reported by the farmers and the calculated productivity index.

3.2 Pest-Productivity Relationship

A weak positive linear relationship was calculated between the number of borers ($r^2 = 0.047$; Figure 8) and the calculated productivity index. There is a trend where a higher number of borers within the plant correlates with greater productivity. However, there is considerable variability in the results, and some plants with few borers also had productivity indices as high as plants with many borers. Figure 8 shows a slightly steeper slope after a certain pest threshold (log borers = 1.5), which may suggest that overcompensation begins after a certain level of pest attack.

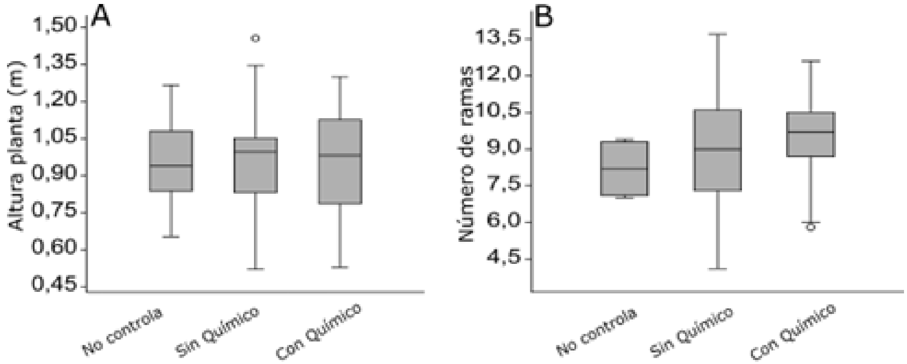

Figure 6. Relationship between treatments and borer pest damage measurements. (A) Plant height in meters, (B) Number of branches.

4 Discussion and conclusions

Several factors were not accounted for, such as soil heterogeneity, the management of surrounding crops, the residual effects of systemic insecticides, and natural habitats that could be adjacent to the study fields. On the other hand, it is noteworthy that the sample size provides a level of analysis that confirms hypotheses proposed in previous studies by the same research team. However, it is important to highlight the limitations of the experimental method, which generally analyzes a limited number of variables at a time.

Effect of Insecticides on Pest Insects

This study showed that for pest insects, no significant effects of any treatment on pest abundances were found, as noted by Struelens et al. (2021) in a previous study. This result was observed even in the treatment where the farmer did not implement any pest management actions. In other words, both the chemical and organic insecticides applied during this study were not effective in controlling the pests, with no reduction in their populations. The hypothesis is that these results could be related to two conditions: i) The active ingredients applied by the farmers were not appropriate for controlling the types of pests evaluated, and ii) The ecology of the three analyzed pests, where insecticide applications likely reached the larval stages inside the stem at sublethal doses, resulting in limited control.

In the first case, it is important to mention that 79.6% of the fields managed with chemical treatments used only three active ingredients: profenofos (acetylcholinesterase inhibitor), lambda-cyhalothrin, and cypermethrin (sodium channel modulators), all three being contact insecticides. Sixty-one percent of the fields managed in the experiment received advice from a chemical vendor or an agronomist to purchase a chemical product. As noted by Aga (2018), farmers' reliance on chemical vendors' advice is critical when it comes to controlling their pests. Zibaee Malagoli (2020) concluded that in cases of ineffective control, sublethal dose effects could exist but have yet to be evaluated for these pests. All these factors likely contribute to the development of resistance to these active ingredients.

Previous studies and surveys have demonstrated the presence of the shoot borer pest throughout much of the crop cycle (Mina et al., 2017). The hole created by the shoot borer is often used as an entry point for the other two borers found during destructive sampling. There is even evidence of trophic relationships between pests, where larvae of certain moth borers prey on larvae/pupae of the shoot borer fly.

Effect of Insecticides on Pollinators

This study indicates a negative effect of the insecticides used on the abundances of certain chocho pollinators. This effect was observed in dipterans like *Eristalis* sp., *Calliphoridae*, and hymenopterans from the *Halictidae* family, all of which are relatively large insects that contribute to the direct or indirect pollination of legumes, as noted by Miguel-Peñaloza et al. (2019). Studies like Catarino et al. (2019) have also reported varying effects depending on the pollinator and the chemical active ingredient analyzed. Another point to consider is the residual effect of systemic chemicals like neonicotinoids on pollinators (Wen et al., 2021). In the case of chocho, some farmers have opted to use such products to disinfect their seeds during planting, so considering the residuality variable would be of interest.

In the case of *Eristalis* sp. (Figure 3D; Figure 5) and other syrphid flies, adult visits to chocho flowers were observed. However, it is necessary to determine how much they contribute to the pollination of this crop, along with *Calliphoridae* and *Halictidae*. Nevertheless, the results show that fields where chemical products were used had lower pollinator abundance ($\bar{x} = 1$; SD = 1.9) compared to the control treatment ($\bar{x} = 5.1$; SD = 7.5). Syrphid flies are important pollinators with high floral visitation rates and pollen transport capabilities. In fact, *Eristalis* sp. is the most representative floral visitor among syrphid flies (Dunn et al., 2020). *Eristalis* sp. flies from May to October, which is when chocho is in bloom. They are cosmopolitan and do not always act as direct pollinators, pollinating a wide variety of plants, including legumes (Temreshev et al., 2017).

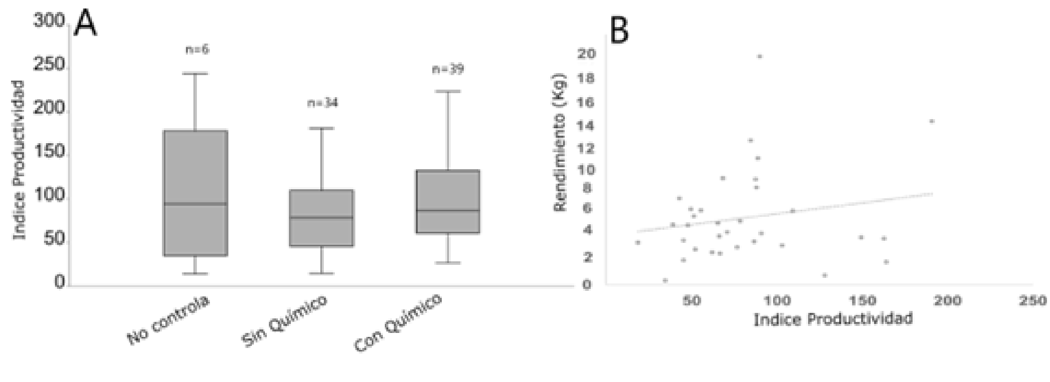

Figure 7. Relationship between treatments and yield. (A) Treatments vs. productivity index, (B) Productivity index vs. yield.

Pollinator analyses often focus exclusively on bees; however, this study highlights the role of other groups, such as these flies. Compared to bees, flies are less sensitive to habitat degradation and fragmentation, so their role as pollinators is enhanced in degraded agricultural habitats (Chakraborty et al., 2021). Studies like Garibaldi et al. (2020) have demonstrated that crop yields increase linearly with pollinator richness (number of species). In the case of *L. mutabilis*, Caligari et al. (2000) reported that there may be at least 58.8 % outcrossing, which could be harnessed by the diversity of insects visiting this crop's flowers. This diversity of insects observed during flowering necessitates the development of a methodology to confirm their effectiveness in *Lupinus* pollination.

Effect of Pesticides on Yield and Possible Overcompensation

The number of branches, recorded as a response-damage variable, was higher in fields treated with chemicals (Figure 6B). This suggests that the use of the chemicals analyzed does not directly affect the pests in question (*Anthomyiidae, Agromyzidae*, and moths). It seems that the attack of these pests predisposes the plant to a response that ultimately can positively affect yield (García and Eubanks, 2019). The average number of pods/plant was compared between healthy plants and those attacked by borers, with the latter producing 70 % more flowers than healthy plants. The hypothesis is that borer attacks do not have a decisive negative impact by limiting the growth of the central stem, as 95 % of the evaluated plants were attacked by these pests. However, herbivory by these insects causes an increase in lateral branches, a greater number of flowers and pods, which theoretically enhances productivity.

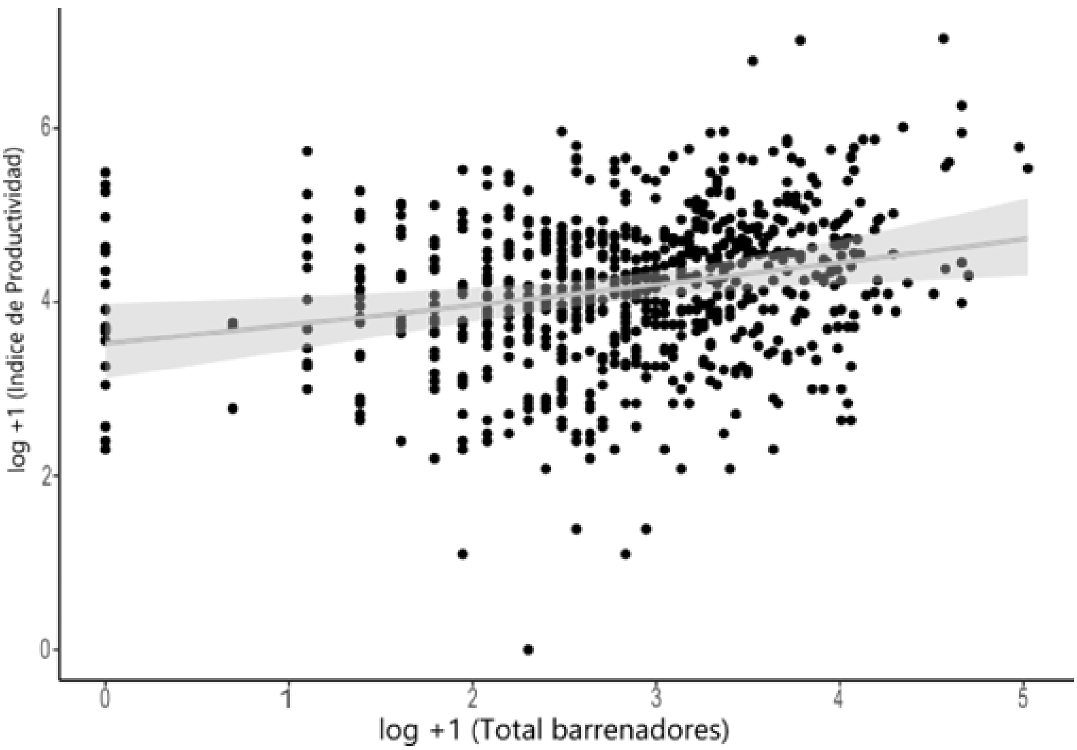

Figure 8. Relationship between the productivity index and the total number of borer pests found inside the evaluated plants (n = 770).

This possible overcompensation effect needs further analysis (in year 2 of this experiment) to understand the damage threshold, considering incidence and severity variables. Nonetheless, reports exist showing that overcompensation can double yields (comparing healthy vs. affected plants) (Poveda et al., 2018), in addition to meta-analyses providing evidence of both vegetative and reproductive overcompensation. Understanding these underlying mechanisms could be a pathway to improving integrated pest management and reducing insecticide use (García and Eubanks, 2019).

In conclusion, the interrelationships between insecticides, pests, pollinators, and crop productivity in the analyzed agroecosystem do not align as previously represented in Figure 1. The primary goal of insecticide use is to control pests (a), but as demonstrated, the most commonly recommended commercial insecticides for *chocho* cultivation do not have a clear control effect on the pests analyzed. The ecology of the main *chocho* pests, which develop by boring into stems and other plant organs, limits the effectiveness of control strategies, regardless of what they are.

It is also important to consider that insecticide application affects natural enemies (e.g., Pteromalidae microhymenopterans) found during destructive sampling. On the other hand, while pest insects are expected to negatively affect productivity (d), this can also be relative, as underlying mechanisms like overcompensation must be considered.

Regarding the relationship between insecticide use and pollinators (b), it is well known that chemicals have harmful effects on pollinators (Sánchez-Bayo and Wyckhuys, 2019). However, to better understand these effects, it is necessary to further explore pollinator-plant interactions, which are highly specialized in agricultural plants (Aguado et al., 2019), enabling a clearer understanding of the implicit ecological relationships. Regarding the insecticide-productivity relationship, as shown by Scarlato et al. (2022), pesticide use (especially insecticides) does not always have a strong relationship with crop yields.

It is crucial that results like those from this study are communicated to farmers (Wyckhuys et al., 2019). In this specific case, evidence of the poor or almost nonexistent control effects of insecticides on pests, as well as knowledge of mechanisms like overcompensation, can help reduce the use and dependence on agrochemicals. Furthermore, the social aspect and participatory research played a key role in this study, particularly in the application of treatments. In some cases, farmers did not follow the researchers' recommendations in a timely manner, and pest pressure compromised their crop health. Participatory research helps understand the variability and heterogeneity of the field, but it also poses a significant challenge, especially due to the immense variability introduced by each farmer's decisions. The year 2021 was highly atypical in terms of precipitation and temperature levels, which influenced the biology of the plants, pests, and pollinators.

Acknowledgments

This work was supported by the French Institute for Research and Development (IRD) and the McKnight Foundation's CCRP program (USA), within the framework of the research project: Agroecological Management of Crop Insects: Towards a Sustainable Collective Goal for Farmers (AMIGO). In addition, we would like to thank the field assistants and farmers who agreed to be part of the study.

Authors' contribution

D.M.: Conceptualization, Data curation, Investigation, Methodology, Project administration, Software, Validation, Writing– original draft; J.C.: Conceptualization, Investigation, Methodology, Supervision, Validation, Writing– review editing; T.C.: Data curation, Formal analysis, Methodology, Software, Writing– review editing; I.N.: Data curation, Formal analysis, Methodology, Software, Writing– review editing; O.D.: Conceptualization, Data curation, Funding acquisition, Investigation, Methodology, Project administration, Resources, Supervision, Validation, Writing– review editing.

References

Aga, A. (2018). Merchants of knowledge: Petty retail and differentiation without consolidation among farmers in maharashtra, india. *Journal of Agrarian Change*, 18(3):658–676. Online:https://n9.cl/8a1cxr.

Aguado, D., Gutierrez-Chacón, C., and Muñoz, M. (2019). Estructura funcional y patrones de especialización en las relaciones planta-polinizador de un agroecosistema en el valle del cauca, colombia. *Acta biológica colombiana*, 24(2):331–342. Online:https://n9.cl/smtz2.

Aizen, M., Garibaldi, L., Cunningham, S., and Klein, A. (2009). How much does agriculture depend on pollinators? lessons from long-term trends in crop production. *Annals of botany*, 103(9):1579–1588. Online:https://n9.cl/68tuya.

Alandia, G. (2018). *Los caminos del tarwi y la integración andina: Bolivia, Perú y Ecuador*. Ipdrs, HIVOS y Cipca Altiplano.

Ali, M., Bari, M., Haque, S., Kabir, M., Afrin, S., Nowrin, F., Islam, M., and Landis, D. (2019). Establishing next-generation pest control services in rice fields: eco-agriculture. *Scientific reports*, 9(1):10180. Online:https://n9.cl/043qob.

Berni, I., Menouni, A., El, I., Duca, R., Kestemont, M., Godderis, L., and Jaafari, S. (2021). Understanding farmers' safety behavior regarding pesticide use in morocco. *Sustainable Production and Consumption*, 25:471–483. Online:https://n9.cl/avoud3.

Botías, C. and Sánchez-Bayo, F. (2018). Papel de los plaguicidas en la pérdida de polinizadores. *Ecosistemas*, 27(2):34–41. Online:https://n9.cl/9f3an.

Budzinski, H. and Couderchet, M. (2018). Environmental and human health issues related to pesticides: from usage and environmental fate to impact. *Environmental Science and Pollution Research*, 25(15):14277–14279. Online:https://n9.cl/szbg0.

Busse, M., Zoll, F., Siebert, R., Bartels, A., Bokelmann, A., and Scharschmidt, P. (2021). How farmers think about insects: perceptions of biodiversity, biodiversity loss and attitudes towards insect-friendly farming practices. *Biodiversity and conservation*, 30:3045–3066. Online:https://n9.cl/00tiup.

Caicedo, V. and Peralta, I. (2000). *Zonificación potencial, sistemas de producción y procesamiento artesanal del chocho (Lupinus mutabilis Sweet) en Ecuador*. INIAP, Estación Experimental Santa Catalina.

Caligari, P., Römer, P., Rahim, M., Huyghe, C., Neves-Martins, J., and Sawicka-Sienkiewicz, E. (2000). *The potential of Lupinus mutabilis as a crop*, chapter Linking research and marketing opportunities for pulses in the 21st century: Proceedings of the third international food legumes research conference, pages 569–573.

Catarino, R., Bretagnolle, V., Perrot, T., Vialloux, F., and Gaba, S. (2019). Bee pollination outperforms pesticides for oilseed crop production and profitability. *Proceedings of the Royal Society B*, 286(1912):20191550. Online:https://n9.cl/ajrbl.

Chakraborty, P., Chatterjee, S., Smith, B., and Basu, P. (2021). Seasonal dynamics of plant pollinator networks in agricultural landscapes: how important is connector species identity in the network? *Oecologia*, 196(3):825–837. Online:https://n9.cl/wb0j2.

Chemnitz, C. (2022). *Pestizidatlas: Daten und Fakten zu Giften in der Landwirtschaft*. Heinrich-Böll-Stiftung.

Chivian, E. and Bernstein, A. (2015). *Preservar la vida: de cómo nuestra salud depende de la biodiversidad*. Fondo de Cultura Económica.

Cowling, W., Buirchell, B., and Tapia, M. (1998). *Lupin: Lupinus albus promoting the conservation and use of underutilized and neglected crops*. Institute of Plant Genetics and Crop Plant Research.

Damte, T. and Tabor, G. (2015). Small-scale vegetable producers' perception of pests and pesticide uses in east shewa zone, ethiopia. *International Journal of Pest Management*, 61(3):212–219. Online:https://n9.cl/f01ox.

de Oliveira, A., Junqueira, C., and Augusto, S. (2019). Pesticides affect pollinator abundance and productivity of sunflower (helianthus annuus l.). *Journal of Apicultural Research*, 58(1):2–8. Online:https://n9.cl/pdzin3.

Dunn, L., Lequerica, M., Reid, C., and Latty, T. (2020). Dual ecosystem services of syrphid flies (diptera: Syrphidae): pollinators and biological control agents. *Pest management science*, 76(6):1973–1979. Online:https://n9.cl/v799v.

Egan, P., Dicks, L., Hokkanen, H., and Stenberg, J. (2020). Delivering integrated pest and pollinator management (ippm). *Trends in Plant Science*, 25(6):577–589. Online:https://n9.cl/rpf74.

FAO (2017). Pesticide use, our world in data. FAO. Online:https://n9.cl/vgms3.

Forister, M., Pelton, E., and Black, S. (2019). Declines in insect abundance and diversity: We know enough to act now. *Conservation Science and Practice*, 1(8):e80. Online:https://n9.cl/4iztx.

García, L. and Eubanks, M. (2019). Overcompensation for insect herbivory: a review and meta-analysis of the evidence. *Ecology*, 100(3):e02585. Online:https://n9.cl/1p1uz.

Garibaldi, L., Carvalheiro, L., Vaissière, B., Gemmill-Herren, B., Hipólito, J., Freitas, B., Ngo, H., Azzu, N., Sáez, A., and Åström, J. (2016). Mutually beneficial pollinator diversity and crop yield outcomes in small and large farms. *Science*, 351(6271):388–391. Online:https://n9.cl/5d6lg.

Garibaldi, L., Sáez, A., Aizen, M., Fijen, T., and Bartomeus, I. (2020). Crop pollination management needs flower-visitor monitoring and target values. *Journal of Applied Ecology*, 57(4):664–670. Online:https://n9.cl/2x47x.

Gould, F., Brown, Z., and Kuzma, J. (2018). Wicked evolution: Can we address the sociobiological dilemma of pesticide resistance? *Science*, 360(6390):728–732. Online:https://n9.cl/6bon4.

Goulson, D. (2019). The insect apocalypse, and why it matters. *Current Biology*, 29(19):R967–R971. Online:https://n9.cl/olrlo4.

Hammer, Ø., Harper, D., and Ryan, P. (2001). Past: Paleontological statistics software package for education and data analysis. *Palaeontologia Electronica*, 4(1):1–9. Online:https://n9.cl/68tuya.

Heinz, K., Parrella, M., and Newman, J. (1992). Time-efficient use of yellow sticky traps in monitoring insect populations. *Journal of Economic Entomology*, 85(6):2263–2269. Online:https://n9.cl/s0f9p.

Hernández, A., Gil, F., and Lacasaña, M. (2017). Toxicological interactions of pesticide mixtures: an update. *Archives of toxicology*, 91:3211–3223. Online:https://n9.cl/wzje2.

Inaturalist (2022). Inpo-chocho (insectos polinizadores del chocho). iNaturalist. Online:https://n9.cl/j818t.

INEC (2015). Estadísticas agropecuarias. INEC. Online:https://n9.cl/y21b.

Jallow, M., Awadh, D., Albaho, M., Devi, V., and Thomas, B. (2017). Pesticide risk behaviors and factors influencing pesticide use among farmers in kuwait. *Science of the total environment*, 574:490–498. Online:https://n9.cl/421z7j.

Khan, M., Mahmood, H., and Damalas, C. (2015). Pesticide use and risk perceptions among farmers in the cotton belt of punjab, pakistan. *Crop Protection*, 67:184–190. Online:https://n9.cl/4rp16.

Klein, A., Vaissière, B., Cane, J., Steffan-Dewenter, I., Cunningham, S., Kremen, C., and Tscharntke, T. (2007). Importance of pollinators in changing landscapes for world crops. *Proceedings of the royal society B: biological sciences*, 274(1608):303–313. Online:https://n9.cl/schcs.

Magrach, A., Champetier, A., Krishnan, S., Boreux, V., and Ghazoul, J. (2019). Uncertainties in the value and opportunity costs of pollination services. *Journal of Applied Ecology*, 56(7):1549–1559. Online:https://n9.cl/azsye.

Mengistie, B., Mol, A., and Oosterveer, P. (2017). Pesticide use practices among smallholder vegetable farmers in ethiopian central rift valley. *Environment, Development and Sustainability*, 19:301–324. Online:https://n9.cl/umfug.

Miguel-Peñaloza, A., Delgado-Salinas, A., and Jiménez-Durán, K. (2019). Pollination biology and breeding system of desmodium grahamii (fabaceae, papilionoideae): functional aspects of flowers and bees. *Plant Systematics and Evolution*, 305:743–754. Online:https://n9.cl/jkmkg.

Mina, D., Struelens, Q., Carpio, C., Rivera, M., Rebai, N., Rebaudo, F., and Dangles, O. (2017). Lupin pest management in the ecuadorian andes: current knowledge and perspectives. *Outlooks on Pest Management*, 28(6):250–256. Online:https://n9.cl/wp8hs.

Nicklin, C., Rivera, M., and Nelson, R. (2006). Realizing the potential of an andean legume: roles of market-led and research-led innovations. *International Journal of Agricultural Sustainability*, 4(1):61–78. Online:https://n9.cl/p3s6j.

Pacífico da Silva, I., Oliveira, F., Pedroza, H., Gadelha, I., Melo, M., and Soto-Blanco, B. (2015). Pesticide exposure of honeybees (apis mellifera) pollinating melon crops. *Apidologie*, 46:703–715. Online:https://n9.cl/pcgb8.

Padron, P., Vásquez, C., Durán, S., Pezo, K., Loyola, N., and Junghanns, A. (2021). Use of colored pan traps method for monitoring insect (diptera and hymenoptera) diversity in the southern tropical andes of ecuador. *International Journal of Tropical Insect Science*, 41:643–652. Online:https://n9.cl/rbyekd.

Pan, Y., Ren, Y., and Luning, P. (2021). Factors influencing chinese farmers' proper pesticide application in agricultural products-a review. *Food Control*, 122:107788. Online:https://n9.cl/r12wx.

Potts, S., Biesmeijer, J., Kremen, C., Neumann, P., Schweiger, O., and Kunin, W. (2010). Global pollinator declines: trends, impacts and drivers. *Trends in ecology y evolution*, 25(6):345–353. Online:https://n9.cl/kbf401.

Poveda, K., Díaz, M., and Ramírez, A. (2018). Can overcompensation increase crop production? *Ecology*, 99(2):270–280. Online:https://n9.cl/98jm3.

Sánchez-Bayo, F. and Wyckhuys, K. (2019). Qué provoca el declive de los insectos. *Investigacion y Ciencia*, 517:12–14. Online:https://n9.cl/ezu5la.

Saunders, M. and Luck, G. (2013). Pan trap catches of pollinator insects vary with habitat. *Australian Journal of Entomology*, 52(2):106–113. Online:https://n9.cl/1xjra.

Sawe, T., Nielsen, A., and Eldegard, K. (2020). Crop pollination in small-scale agriculture in tanzania: Household dependence, awareness and conservation. *Sustainability*, 12(6):2228. Online:https://n9.cl/2moi8.

Scarlato, M., Dogliotti, S., Bianchi, F., and Rossing, W. (2022). Ample room for reducing agrochemical inputs without productivity loss: the case of vegetable production in uruguay. *Science of the Total Environment*, 810:152248. Online:https://n9.cl/ppl6v.

Shah, N., Junejo, I., Hullio, M., Maitlo, S., Daar, J., and Rajput, S. (2020). Evaluation of colored sticky traps for monitoring the population of whitefly bemisia tabaci (gennadius) on brinjal crop. *Pakistan journal of agricultural research*, 33(2):327–330. Online:https://n9.cl/4m7b8.

Sherwood, S., Cole, D., Crissman, C., and Paredes, M. (2005). From pesticides to people: improving ecosystem health in the northern andes. *The Pesticide Detox: towards a more sustainable agriculture*, pages 147–164. Online:https://n9.cl/o6d5u.

SINAGAP (2014). Resumen ejecutivo, zonificacion agroecológica económica del cultivo de chocho en ecuador, escala 1:250.000, 2014. Technical report, SINAGAP. Online:https://n9.cl/888qr.

Stanley, D., Garratt, M., Wickens, J., Wickens, V., Potts, S., and Raine, N. (2015). Neonicotinoid pesticide exposure impairs crop pollination services provided by bumblebees. *Nature*, 528(7583):548–550. Online:https://n9.cl/24v8ne.

Stenberg, J. (2017). A conceptual framework for integrated pest management. *Trends in plant science*, 22(9):759–769. Online:https://n9.cl/jtkey6.

Struelens, Q., Mina, D., and Dangles, O. (2021). Combined effects of landscape composition and pesticide use on herbivore and pollinator functions in smallholder farms. *CABI Agriculture and Bioscience*, 2(7):1–9. Online:https://n9.cl/x7d80.

Temreshev, I., Esenbekova, P., Kenzhegaliev, Y., Sagitov, A., Muhamadiev, N., and Homziak, J. (2017). Diurnal insect pollinators of legume forage crops in southeastern kazakhstan. *International Journal of Entomology Research*, 2(2):17–30. Online:https://n9.cl/8bkp6.

Wen, X., Ma, C., Sun, M., Wang, Y., Xue, X., Chen, J., Song, W., Li-Byarlay, H., and Luo, S. (2021). Pesticide residues in the pollen and nectar of oilseed rape (brassica napus l.) and their potential risks to honey bees. *Science of the Total Environment*, 786:147443. Online:https://n9.cl/0ngjr.

Willett, D., Filgueiras, C., Nyrop, J., and Nault, B. (2020). Field monitoring of onion maggot (delia antiqua) fly through improved trapping. *Journal of Applied Entomology*, 144(5):382–387. Online:https://n9.cl/kjpjkq.

Wyckhuys, K., Heong, K., Sanchez-Bayo, F., Bianchi, F., Lundgren, J., and Bentley, J. (2019). Ecological illiteracy can deepen farmers' pesticide dependency. *Environmental Research Letters*, 14(9):093004. Online:https://n9.cl/4usqq6.

La granja: Revista de Ciencias de la Vida
pISSN:1390-3799; eISSN:1390-8596
https://doi.org/10.17163/lgr.n41.2025.04

Scientific paper/ Artículo científico

Earth Sciences

Rainfall Characteristics and extreme events in the Tropical Andes using a Vertically Pointing rain radar

Características de lluvia y eventos extremos en los Andes Tropicales usando un radar de lluvia de Apuntamiento Vertical

Javier Chininín-Cabrera[1] and Rolando Célleri*[1,2]

[1]*Departamento de Recursos Hídricos y Ciencias Ambientales, Universidad de Cuenca, 010207, Cuenca, Ecuador.*
[2]*Facultad de Ingeniería, Universidad de Cuenca, 010203, Cuenca, Ecuador.*

*Corresponding author: rolando.celleri@ucuenca.edu.ec

Received on February 26th, 2023. Accepted, after revision on June 25th, 2024. Published on March 1st, 2025.

Abstract

Although the vertical structure of rain is relevant in aspects such as climate models (CM) and quantitative precipitation estimation (QPE), data about it is limited in the Andes. Within these aspects, extreme rainfall events are important due to their potential social impacts. Therefore, this study aims to characterize the vertical structure of rain and extreme events in the Tropical Andes using a Vertically Pointing Micro Rain Radar. For this, (i) the diurnal rainfall cycle was determined; (ii) the bright band was characterized; (iii) common characteristics of the vertical rain profile during extreme events, along with the average vertical reflectivity profiles of different development stages of a characteristic extreme event were studied. The study was performed using five years of data from a vertically pointing rain radar installed in Cuenca, Ecuador. The main results indicate that (i) rain events with high intensities are concentrated between 12:30 – 20:00 h (Local Time), during which 77% of the total rainfall occurs; (ii) the bright band has a thickness between 200 and 400 m, and its top (melting layer) is located between 4500 and 4900 m above sea level; (iii) rainfall shows a high variability in the water column: during the convective stage reflectivity values can increase up to 94% from the fusion layer to the ground. The results show the complexity of rainfall events in the Andean region and the need to consider these aspects into CM and QPE to improve their accuracy.

Keywords: Extreme events, melting layer, diurnal rainfall cycle, vertical structure of rain, tropical Andes.

Resumen

La información de la estructura vertical de la lluvia en los Andes es bastante limitada, a pesar de su importancia en aspectos como modelos de clima (MC) y estimación cuantitativa de lluvia (ECL). Dentro de estos aspectos, los eventos extremos conforman un punto de alto interés debido a la necesidad de mitigar los problemas sociales que pueden ocasionar. Por lo tanto, el objetivo de esta investigación es caracterizar la estructura vertical de la lluvia y eventos extremos en los Andes Tropicales usando un micro radar de lluvia de apuntamiento vertical. Para esto, (i) se determinó el ciclo diario de lluvia; (ii) se caracterizó la bright band; (iii) se caracterizó la columna de agua y los perfiles verticales promedio de reflectividad. Se utilizaron 5 años de datos medidos con un radar de apuntamiento vertical instalado en Cuenca, Ecuador. Los principales resultados indican que (i) los eventos de lluvia con altas intensidades se concentran entre las 12:30 – 20:00 h (Tiempo Local), y en este intervalo se registra el 77 % del total de lluvia; (ii) la bright band tiene un espesor entre 200 y 400 m y su parte superior (capa de fusión) se ubica entre 4500 y 4900 m snm; y (iii) la lluvia muestra una alta variabilidad en la columna de agua: durante la etapa convectiva los valores de reflectividad pueden aumentar hasta en un 94 % desde la capa de fusión hasta la superficie. Los resultados evidencian la alta complejidad de los eventos de lluvia de la zona andina y la necesidad de considerar estos aspectos para mejorar la precisión de MC y ECL.

Palabras clave: Eventos extremos, capa de fusión, ciclo diario de lluvia, estructura vertical de lluvia, Andes tropicales.

Suggested citation:	Chininín-Cabrera, J. and Célleri, R. (2025). Rainfall Characteristics and extreme events in the Tropical Andes using a Vertically Pointing rain radar. *La Granja: Revista de Ciencias de la Vida.* Vol. 41(1):69-81. https://doi.org/10.17163/lgr.n41.2025.04.

Orcid IDs:

Javier Chininín-Cabrera: https://orcid.org/0000-0003-3412-5576
Rolando Célleri: https://orcid.org/0000-0002-7683-3768

1 Introduction

Extreme rainfall events pose a significant challenge to society due to their potential consequences, such as flash floods, crop damage, erosion, landslides, and water contamination (Barlow et al., 2019; Mukherjee et al., 2018). This makes it essential to understand, characterize, and accurately estimate these events to mitigate their effects. However, in the Andes, the detailed study of such events and the processes governing rainfall has been limited by the sparse and unevenly distributed monitoring systems (Perry et al., 2017; Seidel et al., 2019) and by the fact that rainfall properties vary on temporal scales shorter than those captured by available climate data and models (Boucher et al., 2013; Seidel et al., 2019; Ward et al., 2011).

This issue increases by the high spatiotemporal variability of rainfall processes, influenced by the region's complex topography (Orellana-Alvear et al., 2017; Yarleque et al., 2016). These challenges are especially observed in the limited data and studies available on the Andes' vertical structure of rainfall (VSR), which describes rainfall from its origin in the clouds to when it reaches the ground.

The study of VSR has a significant impact on various aspects. First, it helps to understand the microphysics governing rainfall formation and evolution (Durán-Alarcón et al., 2019; Urgilés et al., 2021); moreover, features such as the bright band (BB) allow estimating the altitude at which rainfall originates, as it serves as an indicator of the melting layer (Endries et al., 2018; Konwar et al., 2012; Sumesh et al., 2019). In mountainous regions, radar and satellite products often suffer from accuracy deficiencies (Chen et al., 2022; Orellana-Alvear et al., 2019; Satgé et al., 2019; Ward et al., 2011), primarily due to the difference in altitude between the measurement location and the ground.

These inaccuracies are typically corrected using ground-based rain gauge data, but often without considering the vertical variation of rainfall properties (e.g., reflectivity) in the atmospheric column (Das and Maitra, 2016; Kirstetter et al., 2013; Peters et al., 2005). Therefore, the VSR provides crucial information for improving, comparing, and validating climate models and estimates obtained from radars and satellites (Durán-Alarcón et al., 2019).

Ground-based vertically pointing radars offer a suitable alternative for obtaining VSR data (Durán-Alarcón et al., 2019; Luo et al., 2020; Urgilés et al., 2021). In the Tropical Andes, studies using these radars are limited and can be classified into two groups: those directly describing the VSR and those using VSR for other purposes. In the first group, research has primarily focused on the melting layer or BB. Perry et al. (2017) calculated the frequency distribution of the melting layer height for Cusco, Peru (August 2014 – February 2015) and La Paz, Bolivia (October 2015 – December 2015), finding that most measurements in both locations fall between 4400 and 5100 meters above sea level (masl). Endries et al. (2018) used the same dataset for Cusco and an extended one for La Paz (October 2015 – February 2017) to study BB height based on time of day, finding that, consistent with surface temperature, it is higher in the afternoon and early evening. They also observed that the El Niño phenomenon in La Paz may have contributed to an increase in BB height during the 2015–2016 period.

Finally, Kumar et al. (2020) in Huancayo, Peru (2015–2018), reported that the BB is mostly found between 4000 and 5000 masl, but also, for the first time, determined the vertical variation of rainfall properties (reflectivity, intensity, liquid water content, and drop size distribution) for different surface rainfall intensities, revealing interesting behaviors especially for high intensities (20–200 mm/h). The second group of studies has focused mainly on classifying rainfall as stratiform, convective, or mixed using VSR, as done by Seidel et al. (2019) and Urgilés et al. (2021). Additionally, Bendix et al. (2006) in Loja, Ecuador, showed that mixed rainfall is a key feature of the region's precipitation, while Schauwecker et al. (2017), using the same dataset as Perry et al. (2017), determined that when the surface temperature is below 15°C, the melting layer can be relatively estimated using extrapolations with reanalysis data.

As noted, VSR information in the Tropical Andes obtained directly from ground-based radars is quite limited and is primarily concentrated in Peru and Bolivia. Furthermore, in no cases has VSR been used to study rainfall generation and dynamics during extreme events, despite its importance for both societal concerns and rainfall models and estimates.

Therefore, the objective of this research is to characterize the vertical structure of rainfall and extreme events in the Tropical Andes using a vertically pointing micro rain radar located in Cuenca, Ecuador. To achieve this, the study aims to (i) characterize the distribution of rainfall events throughout the day, especially those of high intensity, based on the study of the diurnal rainfall cycle; (ii) characterize the bright band based on its key features; and (iii) characterize the atmospheric column during extreme rainfall events and their temporal evolution.

2 Methodology

2.1 Study Area and Equipment

The study was conducted using data collected at the Balzay Meteorological Observatory (2°53’32” S, 79°02’10” W), located at 2600 meters above sea level in the Andes of Ecuador, in the city of Cuenca (Figure 1). The region experiences a bimodal precipitation pattern, with rainy months occurring in March-April and October-November (Campozano et al., 2016).

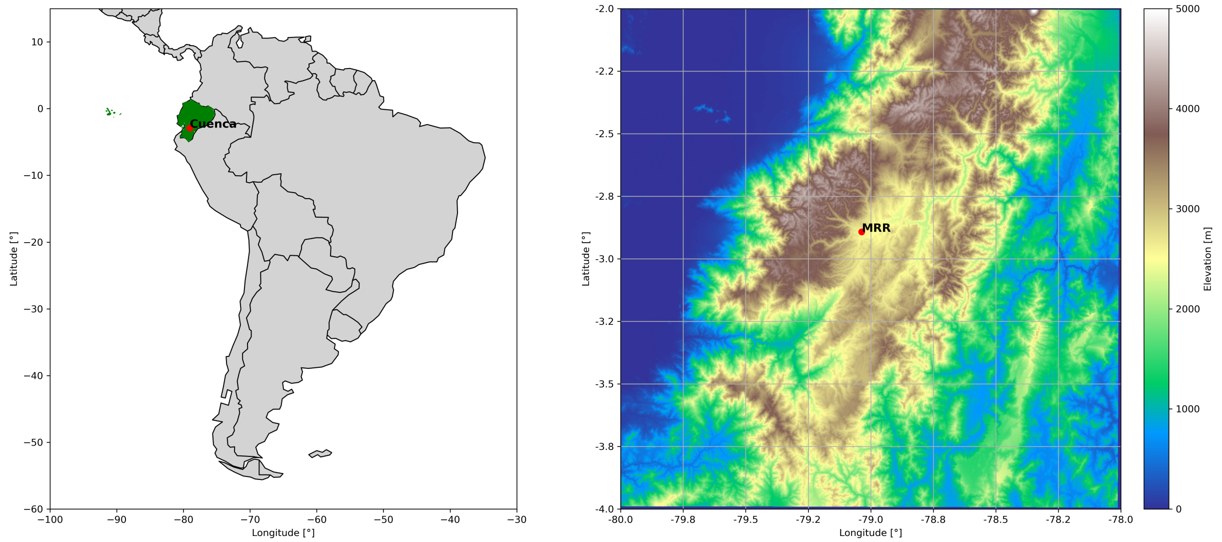

Figure 1. Study area in the Ecuadorian Andes.

The data used in this study come from a Micro Rain Radar (MRR), a compact radar with a vertically pointing parabolic antenna, operating at a frequency of 24 GHz, a wavelength of 12.5 mm, and an FM-CW operating mode (Löffler-Mang et al., 1999; METEK, 2009; Peters et al., 2002). The MRR uses the Doppler velocity spectrum as its measurement principle and derives the drop size distribution through the analytical relationship between terminal velocity and drop diameter, as described by Atlas et al. (1973). Based on this variable, the MRR calculates rainfall parameters such as reflectivity, liquid water content, rain intensity, and drop fall velocity; these relationships can be reviewed in detail in METEK (2009) and Peters et al. (2005). In each radar measurement, the atmospheric column is vertically discretized into 31 equal parts (bins), and for each bin, the five aforementioned variables are obtained. This measurement is referred to as the vertical profile (VP).

2.2 Data and Preprocessing

Five years of MRR measurements, from February 2017 to January 2022, were used. The MRR observations had a temporal resolution of 1 minute and an altitudinal resolution (bin thickness) of 100 meters. The MRR measures precipitation up to an altitude of 3100 meters above ground level (i.e., from 2600 to 5700 meters above sea level). The variables used in this study were reflectivity and rain intensity. To fill gaps and eliminate outliers in the rain intensity measurements at the lowest bin, data from a laser disdrometer (Thies Clima Laser) located at the same meteorological observatory were used. The percentage of missing measurements for this variable was reduced from 15.7% to 6.0%. A linear correlation was performed between the 5-minute accumulated rainfall from both instruments (Figure 2). Although the MRR measures the average intensity in a 100-meter bin from the surface, its variability can be explained by the disdrometer by 80%, as indicated by the coefficient of determination (R^2); furthermore, the p-value is less than 0.001.

On the other hand, no gap filling was applied to the vertical profiles (VP); however, a quality control process was implemented to remove incomplete measurements (i.e., VPs with one or more missing bins). Additionally, the two highest bins of the VPs were excluded from all analyses, as they often presented outliers due to electromagnetic interference.

2.3 Calculation of the Diurnal Rainfall Cycle

The characteristics of the diurnal rainfall cycle were studied in 30-minute intervals using the average precipitation amount (PA), precipitation frequency (PF), average precipitation intensity (PI), and accumulated average precipitation (PAQ). Based on the considerations of Zhou et al. (2008) and Zhang et al. (2017), PA was calculated for each 30-minute interval during the 5-year study period by dividing the accumulated precipitation by the number of valid measurements. PF was calculated as the ratio between the number of rainy measurements and the number of valid measurements, while PI was obtained by dividing the accumulated precipitation by the number of rainy measurements. Additionally, PAQ was calculated as the accumulated percentage of the total rainfall up to each interval. For this study, a 30-minute measurement was considered valid if 90% or more of the minutes within that interval had data, and considered rainy if a minimum of 0.1 mm of precipitation was recorded.

2.4 Characterization of the Bright Band

The bright band (BB) was characterized by analyzing its thickness (BB_{th}) and the height of its upper boundary (melting layer; H_T), and how these two characteristics varied during the study period was calculated. To detect the presence of the BB during an event, the algorithm proposed by Cha et al. (2009) was implemented, which builds on previous studies by Klaassen (1988) and Fabry and Zawadzki (1995) but introduces a new concept called bright band sharpness. This algorithm is based on the use of the reflectivity VP and the variation in its gradient.

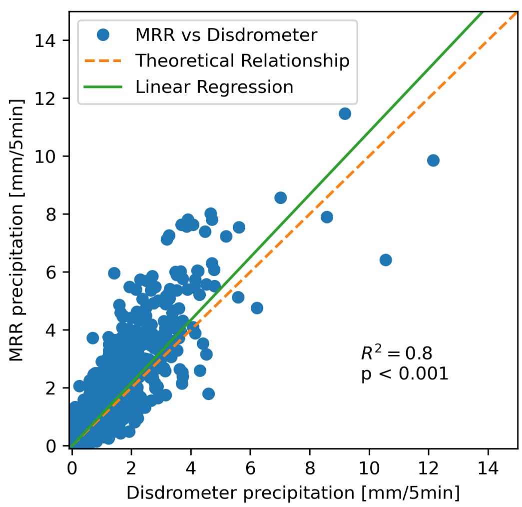

Figure 2. Correlation of cumulative rainfall every 5 minutes between disdrometer and MRR measurements in its first band above ground level (0-100 masl).

When the BB is detected in a measurement, H_T is defined as the altitude with the steepest negative gradient, and similarly, the lower boundary (H_B) is the altitude with the steepest positive gradient; BB_{th} is calculated as the difference between H_T and H_B. Additionally, the algorithm requires the peak reflectivity (Z_{peak}) from the VP; to obtain this, the first 500 meters from the ground were excluded, as it was verified that in some cases, Z_{peak} occurred at these heights (this is mainly due to coalescence and aggregation processes at these levels during different events, which can significantly increase reflectivity, exceeding that of the BB), which would erroneously discard a VP with an actual BB.

2.5 Vertical Rainfall Variability

The evolution of the reflectivity VP was visually inspected for all events where rain intensities greater than 100 mm/h per minute were recorded in the first bin. This threshold captures approximately the top 10.0% of the highest-intensity events recorded per minute during the study period, categorizing them as extreme rainfall events. From these, one representative high-intensity rainfall event was selected, and the characteristics of its average vertical reflectivity profile (AVRP) were thoroughly studied during its various developmental stages.

For each stage, the AVRP was calculated as the average reflectivity of each bin in the VPs, as shown by Das and Maitra (2016) and Peters et al. (2005). The developmental stages were classified as convective, stratiform with BB, and stratiform without BB. To distinguish between convective and stratiform stages, vertical velocity profiles and a fuzzy rule-based system were used, as described in Seidel et al. (2019). Measurements that could not be classified using this methodology were labeled as "Unclassified." Additionally, for the sub-classification of the stratiform stage, BB detection was performed using the algorithm described in Section 2.4.

3 Results

3.1 Diurnal rainfall cycle

Figure 3 shows the curves for precipitation amount (PA), precipitation frequency (PF), precipitation intensity (PI), and accumulated precipitation amount (PAQ) for the diurnal rainfall cycle. PA and PI clearly demonstrate the region's rainfall pattern, which exhibits a unimodal behavior, with the highest peaks occurring around 15:00 local time (LT; UTC-5). PA indicates that the accumulated rainfall for each interval begins to increase significantly after 12:30 LT and stabilizes around 20:00 LT, remaining relatively low during the rest of the day. Furthermore, 77% of the total rainfall occurs within this 7.5-hour window, as indicated by PAQ. Similarly, PI shows that the maximum average intensities, around 4 mm/h, are recorded between 14:00 and 14:30 LT.

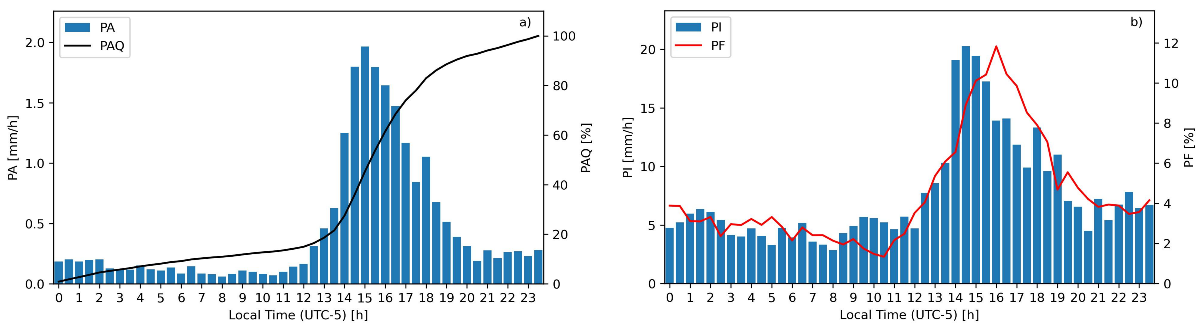

Figure 3. Diurnal rainfall cycle for the period 02/01/2017 – 01/31/2022. a) Precipitation amount (PA) and accumulated precipitation amount (PAQ); b) Precipitation frequency (PF) and precipitation intensity (PI).

While this intensity might be considered low, it should be noted that it represents the average of all events measured during this interval. The magnitude of the events occurring as well as in adjacent intervals can be seen by comparing PF and PA, as PF is approximately three times higher than during the night or morning hours, yet the accumulated rainfall can be up to 20 times greater. This suggests that high-intensity events occurring during these hours contribute significantly to the total precipitation.

3.2 Characterization of the Bright Band

Figure 4 presents the characterization of the BB in terms of a) Diurnal cycle, b) Variation and frequency of its upper boundary height (H_T) and c) Variation and frequency of its thickness (BB_{th}). The lowest occurrence of the BB is found between 09:00 and 12:00 LT. After this period, its frequency increases, reaching a peak at 18:00 LT, after which it begins to decline until the cycle repeats (Figure 4a).

On the other hand, H_T and BB_{th} exhibit relatively stable behavior, with variations centered around typical values. In the case of H_T (Figure 4b), it is found between 4500 and 4900 meters above sea level in 94.5%. Meanwhile, BB_{th} (Figure 4c) ranges between 200 and 400 meters 93.4% of the time. These characteristics indicate the height of the melting layer (where rain originates) and the distance required to complete the melting process of ice or snow into rain in the region. Additionally, the range of variation for H_T aligns with previous studies in the Andes of Bolivia and Peru (Endries et al., 2018; Kumar et al., 2020; Perry et al., 2017), indicating the stability of this height. The greatest differences are observed in southern Peru, where higher altitudes are recorded during the austral summer, which according to Schauwecker et al. (2017), may be caused by the Bolivian high-pressure system.

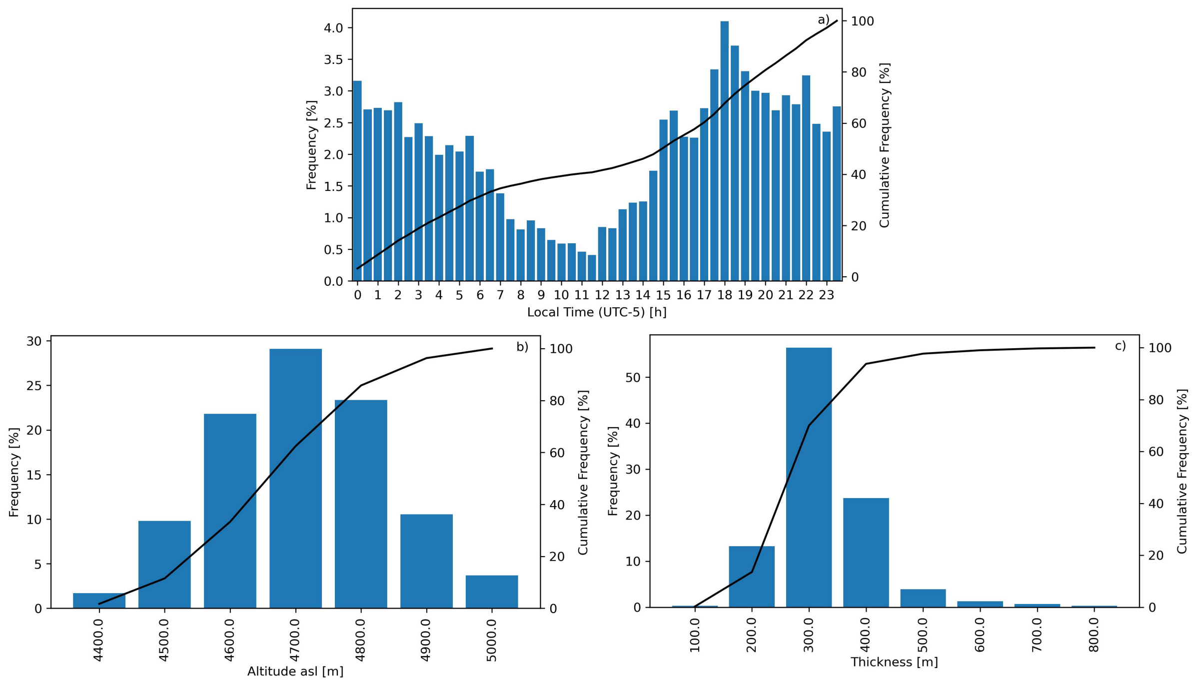

Figure 4. Characteristics of the bright band during the period 02/01/2017 – 01/31/2022. a) Diurnal cycle; b) Variation and frequency of its upper boundary height (H_T); c) Variation and frequency of its thickness (BB_{th}).

3.3 Vertical Rainfall Variability in Extreme Events

During the entire study period, there were 30 high-intensity rainfall events in which surface intensities exceeded 100 mm/h in a minute. All of these events exhibited convective stages during their evolution, with 90 % doing so in the early minutes of the storm, rapidly reaching high reflectivities of around 40 dBZ. Additionally, 50 % of the events displayed exclusively convective behavior, while the rest showed a combination of convective and stratiform stages. Out of the latter group, 80 % exhibited stratiform stages with a BB, which typically developed at the end of the storm.

On December 28, 2017, an event occurred that contained many of the characteristics mentioned above, and it was selected as a case study. Figure 5 shows the time evolution of its reflectivity profile, and the color bar above indicates the moments when convective stages, stratiform stages with BB, and stratiform stages without BB were recorded. Seidel et al. (2019) used this same event to illustrate the results of the methodology, described in section 2.5, for classifying storms into their convective or stratiform stages. Therefore, the analysis performed in this study also complements that work.

The average vertical reflectivity profiles (AVRP) for the different stages of the case study are shown in Figure 6. The AVRP for the convective stage presents significant differences compared to the stratiform stages, as it shows a much steeper negative gradient below 4700 meters above sea level. This results in a considerable increase in reflectivity from the melting layer to the surface (93.7 %), primarily due to the vertical winds characteristic of convective events, which promote rapid droplet growth with coalescence and aggregation processes dominating over others (Luo et al., 2020; Ramadhan et al., 2020; Rosenfeld and Ulbrich, 2003; Wen et al., 2017).

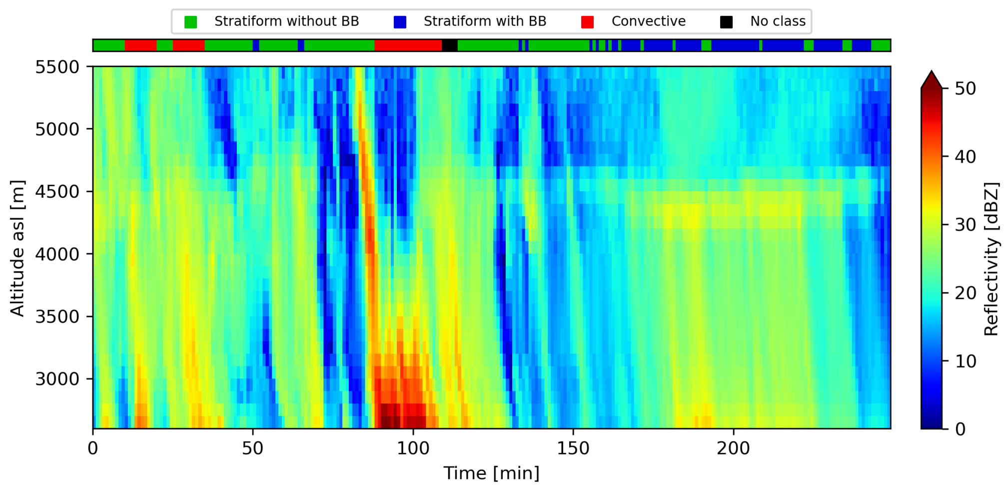

Figure 5. Vertical Reflectivity Profile and Development Stages of the Event Recorded on December 28, 2017, Between 14:50 and 19:10 LT.

In the case of the stratiform stages, the AVRP shows a significant increase in reflectivity between 4700 and 4200 meters above sea level, indicating that the rain is generated by the melting process (Massmann et al., 2017). However, the behavior diverges after reaching maximum reflectivity within this range, suggesting that rapid droplet growth occurs during the stage without BB, maintaining reflectivity close to its maximum. Additionally, the AVRP for these stages behaves similarly below 4200 meters above sea level, with relatively constant values until approaching the surface, where a negative gradient appears. This stable behavior is due to the balance between coalescence, droplet breakup, and evaporation processes, while the increase in reflectivity near the surface is explained by the dominance of coalescence and aggregation processes (Luo et al., 2020; Ramadhan et al., 2020; Wen et al., 2017). Above 4700 meters above sea level, all AVRPs exhibit relatively similar and constant behavior. This is likely because water exists in a solid state at this altitude, as described in Section 3.2, where the melting layer is generally located.

4 Discussion

4.1 Variability of Rainfall Characteristics

The diurnal rainfall cycle is consistent with previous results reported by Yang and Smith (2006), which found that peak rainfall tends to occur in the mid-afternoon in the continental tropics. The unimodal pattern of the diurnal cycle highlights the significant influence of afternoon convective events, mainly driven by surface heating (Bendix et al., 2006; Perry et al., 2014). In fact, all 30 extreme events identified during the study period occurred between 12:30 and 20:00 LT. This finding aligns with Hernandez-Deckers (2022), who showed that in northwestern South America (including parts of Ecuador), the diurnal cycle of convective events closely follows the pattern of PA.

It is worth noting that bimodal behaviors, with peaks in the early morning and late afternoon/evening, have been reported in the eastern foothills of the Andes in Colombia, Peru, and southern Ecuador. These behaviors are generally due to mesoscale instabilities (Bendix et al., 2006; Endries et al., 2018; Kumar et al., 2020, 2019; Poveda et al., 2005; Seidel et al., 2019).

On the other hand, low-intensity events, such as stratiform rainfall with or without BB, also play a significant role in the diurnal cycle. As Seidel et al. (2019) revealed, 91.9% of rainfall measurements in the region are stratiform, and 37.2% of those have BB. Their diurnal cycle (Figure 4a) shows persistent occurrence throughout the day, except in the mornings. This high frequency and persistence are particularly evident outside the 12:30–20:00 LT window, where rainfall amount and frequencies remain relatively low and stable.

4.2 Vertical Reflectivity Variability and Its Influence on Rainfall Estimates

While the vertical reflectivity variability reported in detail via AVRP in this study is limited to the case study, it highlights the importance of considering all event evolution stages for such analyses. Previous studies, such as Das and Maitra (2016), Kumar et al. (2020) and Peters et al. (2005), analyzed AVRP by grouping VPs according to surface rainfall intensity. However, this approach might lead to information loss in stratiform events with BB. This is because profiles with and without BB are averaged, potentially masking the reflectivity peak (Figure 6), which could lead to surface overestimations, as discussed later.

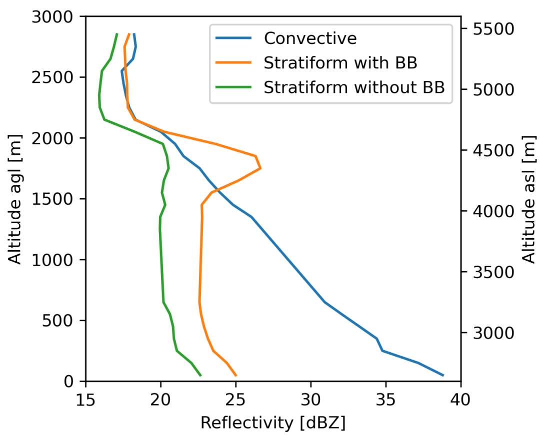

Figure 6. Average vertical reflectivity profiles (AVRP) for the stages of the storm recorded on December 28, 2017, between 14:50 and 19:10 LT

Conversely, grouping VPs according to event evolution stages, as done in this study, could also omit information for low-intensity events, where evaporation is more likely, leading to a positive gradient in the reflectivity VP, as shown in Das and Maitra (2016) and Kumar et al. (2020) for intensities between 0.02 and 2 mm/h. This type of gradient was not observed in this study's results, possibly due to specific event conditions or the averaging of VPs with opposite gradients.

In this context, we have found that reflectivity varies greatly within the atmospheric column and throughout the different stages of rainfall events. This underscores the need to account for these variations when estimating rainfall using ground-based radars or satellites in the region, as potential errors may arise depending on the altitude at which measurements are taken. Rainfall underestimation could occur due to: 1) Measurements above the melting layer during any stage of the event, as shown in the case study, where reflectivity above 4700 meters was lower than at the surface, with the greatest difference being 122.8%; and 2) Steep negative gradients in convective stages, where below the melting layer, this gradient caused a 93.7% increase in reflectivity down to the surface in the case study. On the other hand, overestimation can occur during stratiform stages at the BB height due to the reflectivity peak at that level, which does not represent surface conditions. Additionally, if evaporation occurs near the surface, this overestimation could be exacerbated because surface reflectivity would decrease, and the difference with the BB would be much greater than in the case study (Figure 6).

To avoid such errors, it would be ideal to classify the event as convective or stratiform—with or without BB—before estimating rainfall using Z–R relationships calibrated for these types, incorporating their vertical evolution and corresponding zone. However, this could be limited by the need for a network of instruments capable of making these classifications at multiple points. This highlights the importance of using new methods for estimating rainfall based on ground-based radar measurements, such as that shown in Orellana-Alvear et al. (2019), which improves the accuracy of the CAXX radar using estimates from random forest, a supervised machine learning algorithm. These models may indirectly account for differences based on rainfall types.

Based on the above, future research is recommended to compare the approaches for grouping VPs, either by intensity or by rainfall type. This will help determine the best way to group them to characterize their vertical evolution with the least amount of information loss. This will also be important for improving rainfall estimates using both traditional and alternative methods, as more efficient VP groupings could yield calibrated Z–R relationships, and if feasible, artificial intelligence models for each group.

5 Conclusions

The objective of this research was to characterize the vertical structure of rainfall and extreme events at one of the few sites in the Andes equipped with ground-based vertically pointing radars. To achieve this, the diurnal rainfall cycle was determined, the bright band was characterized, common features in the atmospheric column during high-intensity events were studied, and the average vertical reflectivity profiles of a representative event were analyzed. Based on this, the following conclusions can be drawn:

High-intensity events occur in the afternoon and are responsible for shaping the unimodal diurnal rainfall cycle, with a peak at 15:00. Seventy-seven percent of the total rainfall is recorded between 12:00 and 20:00 LT.

The BB exhibits consistent behavior and characteristics throughout the study period: (i) in 94.5% of cases, its upper boundary (melting layer) is located between 4500 and 4900 meters above sea level; (ii) 93.4% of the time, it has a thickness of 200 to 400 meters; and (iii) its diurnal cycle shows a significant decrease in occurrence only in the mornings.

High-intensity rainfall events are primarily sudden, as 90% of the studied events experienced a sharp increase in reflectivity immediately after the storm began. Additionally, half of the intense events exhibited combined convective-stratiform behavior.

Reflectivity exhibits high variability in the atmospheric column during high-intensity rainfall events. During the convective stage, reflectivity values can increase by up to 94 % from the melting layer to the surface.

Acknowledgments

This study was part of the SDG^{nexus} Network project (grant number 57526248), funded by the German Academic Exchange Service (DAAD) with support from the Federal Ministry for Economic Cooperation and Development (BMZ) under the "exceed - Excellence in Development Cooperation" program. The University of Cuenca co-financed this research through the Vice-Rectorate for Research.

Author Contribution

J.C.C.: Data curation, formal analysis, investigation, software, writing – original draft; R.C.: Conceptualization, funding acquisition, methodology, supervision, validation, writing – review and editing.

References

Atlas, D., Srivastava, R., and Sekhon, R. (1973). Doppler radar characteristics of precipitation at vertical incidence. *Reviews of Geophysics*, 11(1):1–35. Online:https://n9.cl/8t5da7.

Barlow, M., Gutowski, W., Gyakum, J., Katz, R., Lim, Y., Schumacher, R., Wehner, M., Agel, L., Bosilovich, M., Collow, A., Gershunov, A., Grotjahn, R., Leung, R., Milrad, S., and Min, S. (2019). North american extreme precipitation events and related large-scale meteorological patterns: a review of statistical methods, dynamics, modeling, and trends. *Climate Dynamics*, 53:6835–6875. Online:https://n9.cl/jovyd.

Bendix, J., Rollenbeck, R., and Reudenbach, C. (2006). Diurnal patterns of rainfall in a tropical andean valley of southern ecuador as seen by a vertically pointing k-band doppler radar. *International Journal of Climatology: A Journal of the Royal Meteorological Society*, 26(6):829–846. Online:https://n9.cl/57h73.

Boucher, O., Randall, D., Artaxo, P., Bretherton, C., Feingold, G., Forster, P., Kerminen, V., Kondo, Y., Liao, H., and Lohmann, U. (2013). *Climate change 2013: The physical science basis. Contribution of working group I to the fifth assessment report of the intergovernmental panel on climate change*, chapter Clouds and aerosols, pages 571–657. Cambridge University Press.

Campozano, L., Célleri, R., Trachte, K., Bendix, J., and Samaniego, E. (2016). Rainfall and cloud dynamics in the andes: A southern ecuador case study. *Advances in Meteorology*, 2016(1):3192765. Online:https://n9.cl/6c7l1.

Cha, J. W., Chang, K. H., Yum, S., and Choi, Y. J. (2009). Comparison of the bright band characteristics measured by micro rain radar (mrr) at a mountain and a coastal site in south korea. *Advances in Atmospheric Sciences*, 26:211–221. Online:https://n9.cl/4214z.

Chen, M., Huang, Y., Li, Z., Larico, A., Xue, M., Hong, Y., Hu, X., Novoa, H., Martin, E., McPherson, R., Zhang, J., Gao, S., Wen, Y., Perez, A., and Morales, I. (2022). Cross-examining precipitation products by rain gauge, remote sensing, and wrf simulations over a south american region across the pacific coast and andes. *Atmosphere*, 13(10):1666. Online:https://n9.cl/xfegq.

Das, S. and Maitra, A. (2016). Vertical profile of rain: Ka band radar observations at tropical locations. *Journal of Hydrology*, 534:31–41. Online:https://n9.cl/ldgsx.

Durán-Alarcón, C., Boudevillain, B.and Genthon, C., Grazioli, J., Souverijns, N., van Lipzig, N., Gorodetskaya, I., and Berne, A. (2019). The vertical structure of precipitation at two stations in east antarctica derived from micro rain radars. *The Cryosphere*, 13(1):247–264. Online:https://n9.cl/5c4zcy.

Endries, J., Perry, L., Yuter, S., Seimon, A., Andrade-Flores, M., Winkelmann, R., Quispe, N., Rado, M., Montoya, N., and Velarde, F. (2018). Radar-observed characteristics of precipitation in the tropical high andes of southern peru and bolivia. *Journal of Applied Meteorology and Climatology*, 57(7):1441–1458. Online:https://n9.cl/69im8.

Fabry, F. and Zawadzki, I. (1995). Long-term radar observations of the melting layer of precipitation and their interpretation. *Journal of the atmospheric sciences*, 52(7):838–851. Online:https://n9.cl/la1qq.

Hernandez-Deckers, D. (2022). Features of atmospheric deep convection in northwestern south america obtained from infrared satellite data. *Quarterly Journal of the Royal Meteorological Society*, 148(742):338–350. Online:https://n9.cl/ehh79.

Kirstetter, P., Andrieu, H., Boudevillain, B., and Delrieu, G. (2013). A physically based identification of vertical profiles of reflectivity from volume scan radar data. *Journal of applied meteorology and climatology*, 52(7):1645–1663. Online:https://n9.cl/w6d92h.

Klaassen, W. (1988). Radar observations and simulation of the melting layer of precipitation. *Journal of Atmospheric Sciences*, 45(24):3741–3753. Online:https://n9.cl/p5x3q.

Konwar, M., Maheskumar, R., Das, S., and Morwal, S. (2012). Nature of light rain during presence and absence of bright band. *Journal of earth system science*, 121:947–961. Online:https://n9.cl/38t3f.

Kumar, S., Castillo-Velarde, C., Valdivia Prado, J., Flores Rojas, J., Callañaupa Gutierrez, S., Moya Alvarez, A., Martine-Castro, D., and Silva, Y. (2020). Rainfall characteristics in the mantaro basin over tropical andes from a vertically pointed profile rain radar and in-situ field campaign. *Atmosphere*, 11(3):248. Online:https://n9.cl/cqkjhd.

Kumar, S., Vidal, Y., Moya-Álvarez, A., and Martínez-Castro, D. (2019). Effect of the surface wind flow and topography on precipitating cloud systems over the andes and associated amazon basin: Gpm observations. *Atmospheric Research*, 225:193–208. Online:https://n9.cl/dpba8.

Löffler-Mang, M., Kunz, M., and Schmid, W. (1999). On the performance of a low-cost k-band doppler radar for quantitative rain measurements. *Journal of Atmospheric and Oceanic Technology*, 16(3):379–387. Online:https://n9.cl/gq699.

Luo, L., Xiao, H., Yang, H., Chen, H., Guo, J., Sun, Y., and Feng, L. (2020). Raindrop size distribution and microphysical characteristics of a great rainstorm in 2016 in beijing, china. *Atmospheric Research*, 239:104895. Online:https://n9.cl/991oo.

Massmann, A., Minder, J., Garreaud, R., Kingsmill, D., Valenzuela, R.and Montecinos, A., and Fults, S.and Snider, J. (2017). The chilean coastal orographic precipitation experiment: Observing the influence of microphysical rain regimes on coastal orographic precipitation. *Journal of Hydrometeorology*, 18(10):2723–2743. Online:https://n9.cl/6yykb4.

METEK (2009). *MRR Physical Basics, Valid for MRR Service Version 5.2.0.1*.

Mukherjee, S., Aadhar, S., Stone, D., and Mishra, V. (2018). Increase in extreme precipitation events under anthropogenic warming in india. *Weather and climate extremes*, 20:45–53. Online:https://n9.cl/ilr75.

Orellana-Alvear, J., Célleri, R., Rollenbeck, R., and Bendix, J. (2017). Analysis of rain types and their z–r relationships at different locations in the high andes of southern ecuador. *Journal of Applied Meteorology and Climatology*, 56(11):3065–3080. Online:https://n9.cl/aujfbd.

Orellana-Alvear, J., Célleri, R., Rollenbeck, R., and Bendix, J. (2019). Optimization of x-band radar rainfall retrieval in the southern andes of ecuador using a random forest model. *Remote Sensing*, 11(14):1632. Online:https://n9.cl/2jmom.

Perry, L., Seimon, A., Andrade-Flores, M., Endries, J., Yuter, S., Velarde, F., Arias, S., Bonshoms, M., Burton, E., Winkelmann, I., Cooper, C., Mamani, G., Rado, M., Montoya, N., and Quispe, N. (2017). Characteristics of precipitating storms in glacierized tropical andean cordilleras of peru and bolivia. *Annals of the American Association of Geographers*, 107(2):309–322. Online:https://n9.cl/tmmwu.

Perry, L., Seimon, A., and Kelly, G. (2014). Precipitation delivery in the tropical high andes of southern peru: new findings and paleoclimatic implications. *International journal of Climatology*, 34(1):197–215. Online:https://n9.cl/deq83.

Peters, G., Fischer, B., and Andersson, T. (2002). Rain observations with a vertically looking micro rain radar (mrr). *Boreal environment research*, 7(4):353–362. Online:https://n9.cl/g4ihk.

Peters, G., Fischer, B., Münster, H., Clemens, M., and Wagner, A. (2005). Profiles of raindrop size distributions as retrieved by microrain radars. *Journal of Applied Meteorology and Climatology*, 44(12):1930–1949. Online:https://n9.cl/6lmqb.

Poveda, G., Mesa, O., Salazar, L., Arias, P., Moreno, H., Vieira, S., Agudelo, P., Toro, V., and Alvarez, J. (2005). The diurnal cycle of precipitation in the tropical andes of colombia. *Monthly Weather Review*, 133(1):228–240. Online:https://n9.cl/1rc7k.

Ramadhan, R., Marzuki, V., Vonnisa, M., Harmadi, Hashiguchi, H., and Shimomai, T. (2020). Diurnal variation in the vertical profile of the raindrop size distribution for stratiform rain as inferred from micro rain radar observations in sumatra. *Advances in Atmospheric Sciences*, 37:832–846. Online:https://n9.cl/tyyg4m.

Rosenfeld, D. and Ulbrich, C. (2003). *Radar and Atmospheric Science: A Collection of Essays in Honor of David Atlas*, chapter Cloud microphysical properties, processes, and rainfall estimation opportunities, page 237–258. Cambridge University Press.

Satgé, F., Ruelland, D., Bonnet, M., Molina, J., and Pillco, R. (2019). Consistency of satellite-based precipitation products in space and over time compared with gauge observations and snow-hydrological modelling in the lake titicaca region. *Hydrology and Earth System Sciences*, 23(1):595–619. Online:https://n9.cl/0iimn.

Schauwecker, S., Rohrer, M., Huggel, C., Endries, J., Montoya, N., Neukom, R., Perry, B., Salzmann, N., Schwarb, M., and Suarez, W. (2017). The freezing level in the tropical andes, peru: An indicator for present and future glacier extents. *Journal of Geophysical Research: Atmospheres*, 122(10):5172–5189. Online:https://n9.cl/nge5k.

Seidel, J., Trachte, K., Orellana-Alvear, J., Figueroa, R., Célleri, R., Bendix, J., Fernandez, C., and Huggel, C. (2019). Precipitation characteristics at two locations in the tropical andes by means of vertically pointing micro-rain radar observations. *Remote Sensing*, 11(24):2985. Online:https://n9.cl/rbmsh.

Sumesh, R., Resmi, E., Unnikrishnan, C., Jash, D., Sreekanth, T., Resmi, M., Rajeevan, K., Nita, S., and Ramachandran, K. (2019). Microphysical aspects of tropical rainfall during bright band events at mid and high-altitude regions over southern western ghats, india. *Atmospheric Research*, 227:178–19. Online:https://n9.cl/xjsco.

Urgilés, G., Célleri, R., Trachte, K., Bendix, J., and Orellana-Alvear, J. (2021). Clustering of rainfall types using micro rain radar and laser disdrometer observations in the tropical andes. *Remote Sensing*, 13(5):991. Online:https://n9.cl/wf0eoo.

Ward, E., Buytaert, W., Peaver, L., and Wheater, H. (2011). Evaluation of precipitation products over complex mountainous terrain: A water resources perspective. *Advances in water resources*, 34(10):1222–1231. Online:https://n9.cl/yb56c.

Wen, G., Xiao, H., Yang, H., Bi, Y., and Xu, W. (2017). Characteristics of summer and winter precipitation over northern china. *Atmospheric Research*, 197:390–406. Online:https://n9.cl/6mesf.

Yang, S. and Smith, E. (2006). Mechanisms for diurnal variability of global tropical rainfall observed from trmm. *Journal of climate*, 19(20):5190–5226. Online:https://n9.cl/r7p5o.

Yarleque, C., Vuille, M., Hardy, D., Posadas, A., and Quiroz, R. (2016). Multiscale assessment of spatial precipitation variability over complex mountain terrain using a high-resolution spatiotemporal wavelet reconstruction method. *Journal of Geophysical Research: Atmospheres*, 121(20):12–198. Online:https://n9.cl/atmk4.

Zhang, W., Huang, A., Zhou, Y., Yang, B., Fang, D., Zhang, L., and Wu, Y. (2017). Diurnal cycle of precipitation over fujian province during the pre-summer rainy season in southern china. *Theoretical and Applied Climatology*, 130:993–1006. Online:https://n9.cl/0tzid4.

Zhou, T., Yu, R., Chen, H., Dai, A., and Pan, Y. (2008). Summer precipitation frequency, intensity, and diurnal cycle over china: A comparison of satellite data with rain gauge observations. *Journal of Climate*, 21(16):3997–4010. Online:https://n9.cl/i6xgz.

LA GRANJA:
REVISTA DE
CIENCIAS DE LA VIDA
pISSN:1390-3799; eISSN:1390-8596
https://doi.org/10.17163/lgr.n41.2025.05

Scientific paper/ Artículo científico

EARTH SCIENCES

DICHOTOMOUS CONTINGENT VALUATION OF THE WATER ECOSYSTEM SERVICE IN AN ANDEAN MICRO-WATERSHED IN ECUADOR

VALORACIÓN CONTINGENTE DICOTÓMICA DEL SERVICIO ECOSISTÉMICO HÍDRICO EN UNA MICROCUENCA ANDINA DEL ECUADOR

Edison Campos Collaguazo* and Luis Jimenez

Universidad Nacional Agraria La Molina, Lima, Perú.

*Corresponding author: edicampos84@gmail.com

Received on February 24th, 2022. Accepted, after revision on July 18th, 2023. Published on March 1st, 2025.

Abstract

The moorland or paramo is a threatened ecosystem. The indiscriminate advance of the agricultural frontier is producing the loss of ecosystem services, especially water service. This research estimated the willingness to pay (WTP) of the water users corresponding to the Municipality of Riobamba for the conservation of the water service in the Micro-basin of the Chimborazo River (MCRCH). Four hundred and six surveys were applied by means of the double limit dichotomous contingent valuation method, using a maximum likelihood model in the Stata software. Four models were developed: simple limit, simple limit with other explanatory variables, double limit, and double limit with other explanatory variables, the latter being statistically more significant. As a result, it was determined that the WTP is USD 0.84 per month to conserve the water service of the MCRCH, value that increases if the home ownership variable is included in USD 0.04. The problem of climate change increases in USD 0.24, while the variable level of education decreases the WTP by USD 0.04.

Keywords: Contingent valuation, Dichotomous model, paramo or moorland, water Economy.

Resumen

El páramo es un ecosistema amenazado pues el avance indiscriminado de la frontera agrícola está produciendo la pérdida de servicios ecosistémicos, especialmente del servicio hídrico. Esta investigación estimó la disposición a pagar (DAP) de los usuarios de agua del Municipio de Riobamba, por la conservación del servicio hídrico de la Microcuenca del Río Chimborazo (MCRCH). Se aplicaron 406 encuestas, mediante el método de valoración contingente dicotómico de doble límite, usando un modelo de máxima verosimilitud en el software Stata. Se desarrollaron cuatro modelos de simple límite, de simple límite con otras variables explicativas, de doble límite y de doble límite con otras variables explicativas, siendo este último estadísticamente más significativo. Como resultado se determinó que la DAP es de USD 0,84 mensuales para conservar el servicio hídrico de la MCRCH, valor que se incrementa si se incluye la variable vivienda propia en USD 0,04 y al reconocer el problema del cambio climático en USD 0,24, mientras que la variable nivel de educación disminuye la DAP en USD 0,04.

Palabras clave: Valoración contingente, Modelo dicotómico, páramo, economía del agua.

Suggested citation:	Campos Collaguazo, E. and Jimenez, L. (2025). Dichotomous contingent valuation of the water ecosystem service in an Andean micro-watershed in Ecuador. *La Granja: Revista de Ciencias de la Vida.* Vol. 41(1):82-94. https://doi.org/10.17163/lgr.n41.2025.05.

Orcid IDs:

Edison Campos Collaguazo: https://orcid.org/0000-0002-3285-9907
Luis Jimenez: https://orcid.org/0000-0002-6082-1893

1 Introduction

The moorland in Ecuador holds significant ecological and economic importance (Hofstede et al., 2002). Millions of people depend directly or indirectly on its conservation. It is one of the most threatened ecosystems due to the expansion of agricultural areas, poor livestock management practices—including burning and overgrazing—the introduction of exotic species, mining, and hunting. These activities have transformed this fragile yet rich continuous landscape of peatlands, shrubs, and giant rosettes into a fragmented and degraded grassland ecosystem (Vuille et al., 2008).

A useful tool for highlighting the importance of an ecosystem is economic valuation, which translates changes in human well-being into monetary units based on variations in the quality or quantity of ecosystem goods and services. Economic valuation thus allows the quantification of the value of ecosystem goods and services in monetary terms, regardless of whether or not they have a price or market (Ministry of the Environment, 2015).

Environmental economic valuation is supported by a solid conceptual framework grounded in two branches of economic theory: microeconomics and welfare economics. In the first case, consumer preference theory is employed. In the second, monetary measures of well-being are derived and analyzed, as assessing the value of ecosystem goods and services requires linking them to changes in individual well-being (Ministry of the Environment, 2015). This type of valuation not only provides insights into their economic contribution but also determines whether people accept such investments and are willing to pay for the benefits obtained. Another decision-making approach for assessing the economic value of water involves evaluating non-structural or policy alternatives (Perez, 2010). Several studies on the economic valuation of water have been conducted worldwide in recent years, which are summarized in Table 1.

Table 1. Economic valuation studies of water worldwide in recent years.

Continent	Study	Author	WTP (USD)
America	Water springs under the direction of the local municipality of the city of Flagstaff.	Mueller (2014)	4.89
America	Application of the travel cost and contingent valuation methods to determine the willingness to pay for the conservation of water resources in Cajas National Park in the city of Cuenca.	Armijos Espinosa and Segarra Ortega (2016)	1.04
America	Contingent valuation in protected areas: The case of the Amazon sector, Ecuador.	Córdova et al. (2019)	5.15
America	Economic value of water from the Solís dam, located in Acámbaro, Guanajuato, Mexico.	Trujillo and Perales (2020)	1
Asia	Application of the contingent valuation method for a case study in Ramallah Governorate, Palestine, including urban, rural and refugee camps.	Awad and Holländer (2010)	189.37
Asia	Contingent valuation method using a simple dichotomous boundary model to measure average willingness to pay that seeks to raise funds to improve the water quality of the Swat River in Pakistan.	Shah (2013)	0.20
Asia	The willingness of farmers to pay to improve the water quality of the Aksu River in Kahramanmaras province.	Ikıkat (2020)	8.03

Africa	Applying a simple dichotomous boundary method to households in the Emuhaya district of Kenya.	Emily et al. (2013)	1.10
Africa	Assessment of household willingness to pay for a fluoride-safe water service connection in the Rift Valley region of Ethiopia.	Reta and Lee (2020)	6.84
Africa	Assessment of farmer households' willingness for better use of irrigation water in Southern Ethiopia.	Aman et al. (2020)	13.92
Africa	Determination of households' willingness to pay for improved operation and maintenance services in eight gravity-fed water systems on the island of Idjwi in the Democratic Republic of Congo.	Jimenez et al. (2021)	0.16
Africa	Use of the contingent valuation method to assess consumers' willingness to pay for improved continuous municipal water supply service in Chitungwiza.	Zvobgo (2021)	40
Africa	Analysis of the willingness to pay and participate in volunteer activities for the restoration of the Sosiani River in Eldoret, Kenya.	Wambui and Watanabe (2021)	1.54

Consequently, there is global information available on the contingent valuation method (CVM). Unfortunately, such studies are scarce in Ecuador, particularly those using double-bounded dichotomous models. Hanemann (1991) propose an alternative to improve the efficiency of estimations in dichotomous contingent valuations. This alternative is known as the double-bounded dichotomous choice method. In this approach, following the initial dichotomous contingent valuation question, a second follow-up question is asked. Specifically, if the respondent answers "yes" to the first question, they are asked about a higher amount. Conversely, if they answer "no" to the first question, they are offered a lower amount. This implies that the second question is endogenous, as it depends on the response to the first question, which is exogenous.

With this method, two responses are obtained from everyone, providing more information but simultaneously complicating the econometric analysis.

Given that y_i^1 and y_i^2 represent the responses to the first and second questions, respectively, the probability that an individual answers "Yes" to the first question and "No" to the second can be expressed as: $\Pr(y_i^1 = 1, y_i^2 = 0 \mid z_i) = \Pr(\text{Sí}, No)$, with similar expressions for the other three possible combinations. Assuming the function $WTP_i(z_i, u_i) = z_i\beta + u_i$ y $u_i \sim N(0, \sigma^2)$,, the likelihood of each case occurring is given by:

- Case 1: $y_i^1 = 1,\ y_i^2 = 0$

$$\begin{aligned}\Pr(\text{Yes}, No) &= \Pr(t^1 \leq WTP < t^2)\\ &= \Pr(t^1 \leq z_i{}'\beta + u_i < t^2)\\ &= \Pr\left(\frac{t^1 - z_i{}'\beta}{\sigma} \leq \frac{u_i}{\sigma} < \frac{t^2 - z_i{}'\beta}{\sigma}\right)\\ &= \Phi\left(\frac{t^2 - z_i{}'\beta}{\sigma} \leq \frac{u_i}{\sigma} < \frac{t^1 - z_i{}'\beta}{\sigma}\right)\end{aligned}$$

The last equality is obtained by using $\Pr(a \leq X < b) = F(b) - F(a)$, Therefore, using the symmetry property, we have that:

$$\Pr(\text{Yes}, No) = \Phi\left(z_i{}'\frac{\beta}{\sigma} - \frac{t^1}{\sigma}\right) - \Phi\left(z_i{}'\frac{\beta}{\sigma} - \frac{t^2}{\sigma}\right)$$

- Case 2: $y_i^1 = 1,\ y_i^2 = 1$

$$\begin{aligned}\Pr(\text{Yes}, \text{Yes}) &= \Pr(WTP > t^1, WTP \geq t^2)\\ &\Pr(z_i{}'\beta + u_i > t^1, z_i{}'\beta + u_i \geq t^2)\end{aligned}$$

Applying Bayes' rule, $\Pr(A,B) = \Pr(a \mid b) \times \Pr(B)$ it is held that:

$$\Pr(\text{Yes},\text{Yes}) = \Pr(z_i{}'\beta + u_i > t^1 \mid z_i{}'\beta + u_i \geq t^2) \times \Pr(z_i{}'\beta + u_i \geq t^2)$$

Since $t^2 > t^1$ and therefore $\Pr(z_i{}'\beta + u_i > t^1 \mid z_i{}'\beta + u_i \geq t^2) = 1$ then:

$$\begin{aligned}\Pr(\text{Yes},\text{Yes}) &= \Pr(u_i \geq t^2 - z_i{}'\beta)\\ &= 1 - \Phi\left(\frac{t^2 - z_i{}'\beta}{\sigma}\right)\end{aligned}$$

By symmetry:

$$\Pr(\text{Yes},\text{Yes}) = \Phi\left(z_i{}'\frac{\beta}{\sigma} - \frac{t^2}{\sigma}\right)$$

- Case 3: $y_i^1 = 0,\ y_i^2 = 1$

$$\begin{aligned}\Pr(\text{No},\text{Yes}) &= \Pr(t^2 \leq WTP < t^1)\\ &= \Pr(t^2 \leq z_i{}'\beta + u_i > t^1)\\ &= \Pr\left(\frac{t^2 - z_i{}'\beta}{\sigma} \leq \frac{u_i}{\sigma} < \frac{t^1 - z_i{}'\beta}{\sigma}\right)\\ &= \Phi\left(\frac{t^1 - z_i{}'\beta}{\sigma} - \Phi\frac{t^2 - z_i{}'\beta}{\sigma}\right)\\ \Pr(\text{No},\text{Yes}) &= \Phi\left(z_i{}'\frac{\beta}{\sigma} - \frac{t^2}{\sigma}\right) - \Phi\left(z_i{}'\frac{\beta}{\sigma} - \frac{t^1}{\sigma}\right)\end{aligned}$$

- Case 4: $y_i^1 = 0,\ y_i^2 = 0$

$$\begin{aligned}\Pr(\text{No},\text{No}) &= \Pr(WTP < t^1, WTP < t^2)\\ &= \Pr(z_i{}'\beta + u_i < t^1,\ z_i{}'\beta + u_i < t^2)\\ &= \Pr(z_i{}'\beta + u_i < t^2)\\ &= \Phi\left(\frac{t^2 - z_i{}'\beta}{\sigma}\right)\\ \Pr(\text{No},\text{No}) &= 1 - \Phi\left(z_i{}'\frac{\beta}{\sigma} - \frac{t^2}{\sigma}\right)\end{aligned}$$

Thus, the Lopez-Feldman (2012) model would depend on four conditional equations:

$$\Pr(y_i^1, y_i^2 \mid z_i) = \begin{cases} \Phi\left(z_i{}'\frac{\beta}{\sigma} - \frac{t^1}{\sigma}\right) - \Phi\left(z_i{}'\frac{\beta}{\sigma} - \frac{t^2}{\sigma}\right) & \text{si } y_i^1 = 1, y_i^2 = 0\\ \Phi\left(z_i{}'\frac{\beta}{\sigma} - \frac{t^1}{\sigma}\right) & \text{si } y_i^1 = 1, y_i^2 = 1\\ \Phi\left(z_i{}'\frac{\beta}{\sigma} - \frac{t^2}{\sigma}\right) - \Phi\left(z_i{}'\frac{\beta}{\sigma} - \frac{t^1}{\sigma}\right) & \text{si } y_i^1 = 0, y_i^2 = 1\\ 1 - \Phi\left(z_i{}'\frac{\beta}{\sigma} - \frac{t^2}{\sigma}\right) & \text{si } y_i^1 = 0, y_i^2 = 0 \end{cases}$$

The single-bounded dichotomous contingent valuation method can be estimated using the Probit model, a type of econometric model for binary choice— a choice between two options. This model is characterized by its reliance on the standard normal cumulative distribution. In contrast, the results for double-bounded dichotomous contingent valuation are obtained through the maximum likelihood method, which directly estimates the β coefficients used to calculate the mean willingness to pay (WTP). The doubleb command in Stata facilitates the analysis process (Lopez-Feldman, 2012).

For analyzing explanatory variables, the *stepwise* command can be used, which controls statistical criteria in stepwise procedures to build a model. This subcommand is ignored if no stepwise method is specified. It supports regression models where the selection of predictive variables is conducted through an automated process. This procedure involves a sequence of F-tests to select or remove explanatory variables (Lopez-Feldman, 2012).

The main objective of this study is to determine the economic cost, expressed in monetary terms, that the population assigns to the water service provided by the Chimborazo River Micro-basin (MCRCH) under current conditions, i.e., a real-world scenario. Respondents were given only the necessary information to descriptively introduce the valuation context. They were informed that the water reaching their homes originates from the MCRCH, thus explaining the implementation framework of the survey.

The hypothetical nature of the stated preference method assumes no real payment commitments from respondents, which often leads to exaggerated individual WTP estimates (Kjær, 2005). Cummings and Taylor (1999) suggest that this bias can be mitigated through a simple explanation provided before the question, highlighting the risks associated with exaggerated responses, particularly regarding WTP and income-related questions.

The sustainability of the moorland ecosystem, approached from a welfare economics perspective for natural resource conservation, offers an alternative framework. It evaluates the economic value of water, emphasizing the idea that conserving natural resources ensures true sustainable development.

Accordingly, this study conducted the economic valuation of the water service using a stated preference methodology-contingent valuation.

2 Materials and Methods

The study population consists of 32,739 urban households in the city of Riobamba, whose water consumption is primarily supplied by groundwater from the Chimborazo River Micro-basin (MCRCH). This population is classified as domestic consumers of the Public Water Company (EMAPAR). According to the 2020 database, EMAPAR had a total of 37,251 registered users, including all categories (residential, commercial, industrial, and others) (EMAPAR, 2020). For the purposes of this study, only the residential consumption category, which accounted for 90 % of the total, was considered. The other categories were excluded as they do not represent end users. In this context, water consumption meters were treated as the sampling units.

The survey was conducted using Google Forms by sending emails to registered potable water users. Respondents were distributed into four groups according to their respective urban parishes, as shown in Figure 1 (Group 1 = Lizarzaburu Parish, Group 2 = Maldonado Parish, Group 3 = Veloz Parish, and Group 4 = Velasco and Yaruquíes Parishes). The selected variant of the Contingent Valuation Method (CVM) aimed to determine the maximum WTP of consumers through a double-bounded dichotomous question format.

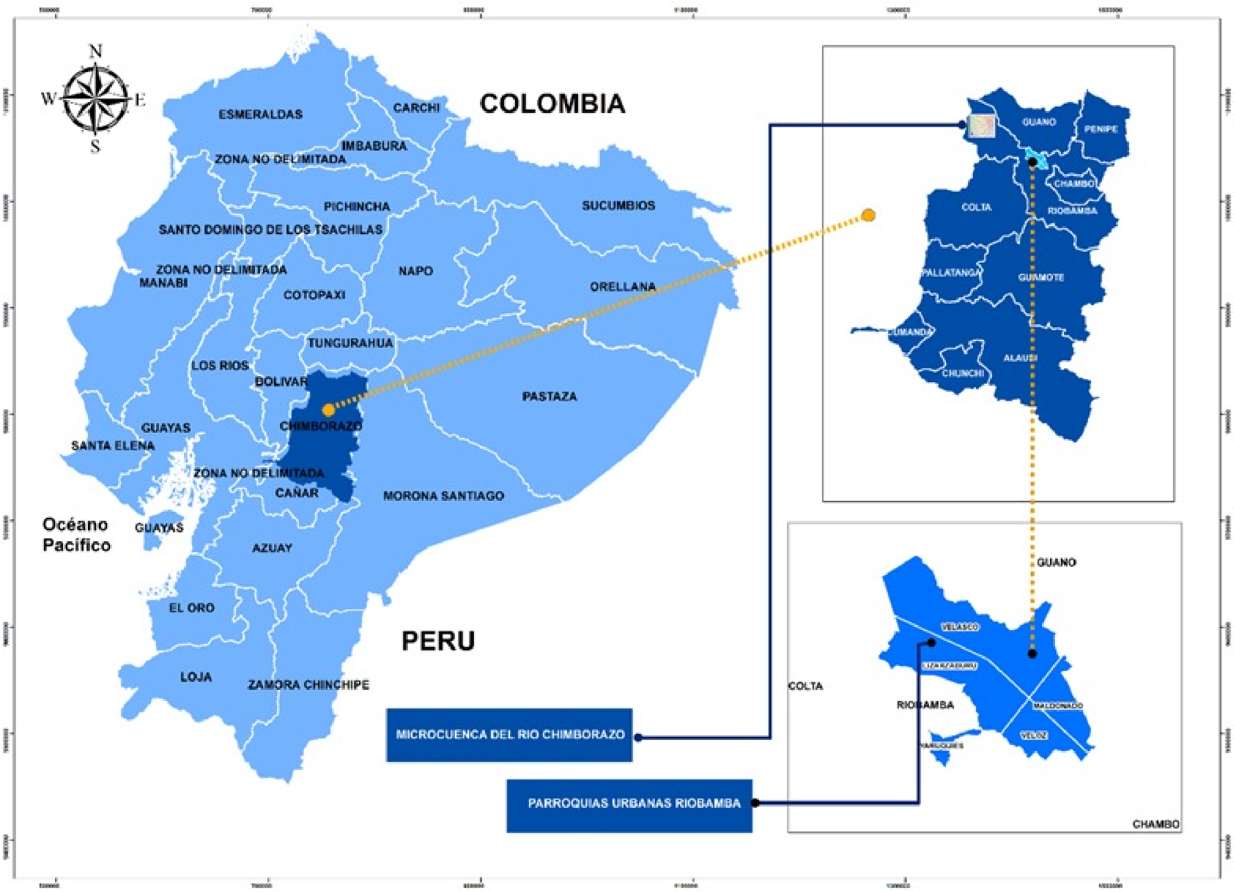

Figure 1. Chimborazo River micro-watershed - Riobamba urban parishes.

The first question asked: "*Would you be willing to pay an additional nn USD on your water bill to ensure the provision of water resources from the páramos of the Chimborazo River Micro-basin?*" The *nn* value was randomly selected from a vector of six values (USD 0.10, 0.25, 0.50, 0.75, 1.00, 1.25) and distributed evenly across the four groups, excluding the extreme values at both ends of the vector. Subsequently, a follow-up question presented the same inquiry with a second bid from the same vector, set as either the next higher or next lower value depending on whether the first response was positive or negative, respectively. A third, open-ended question related to the COVID-19 pandemic was included to verify the consistency of the responses. Since this question was endogenous to the previous ones, it did not affect the earlier results. The survey recognized respondents' monthly water consumption payment receipts as general evidence of their participation.

A pilot survey involving 40 participants was conducted to improve the clarity of certain questions, reduce their number due to time constraints, and make necessary adjustments to the bid vector. According to Sueki (2013), approximately 400 participants are required for a CVM with double-bounded dichotomous questions to minimize estimation errors and achieve statistically reliable WTP conclusions. Similarly, Alam (2013) established a sample size of 400 for a water-related CVM study, while Tentes and Damigos (2012) described their research with 310 cases.

For this study, formula (2) was used, where dichotomous responses provided a satisfactory approximation (Cochran, 1983). Considering the given conditions, p corresponded to an unbiased estimate of p, and the sample size was determined as follows:

$$N = \frac{no}{1} + \frac{no}{N} \tag{1}$$

So that,

$$no = \frac{z2\, p(1-p)}{e2} \tag{2}$$

Considering the population as N=32,739 water connection points for human consumption, a 95% confidence level (z=1.96), an acceptable margin of error (e=5%), and a 50% probability of approving the bid (p=50%), the required sample size was calculated to be 380 cases. This sample size was expanded to 406 respondents. For selecting the sampling elements, the option for managing complex models was utilized, applying a simple random sampling method followed by a homogeneous distribution across four groups from different sectors of the city, resulting in responses from 406 individuals.

The survey was structured into five sections, each including questions related to a specific topic, as follows:

- About Water
- About the Environment and Climate Change
- Willingness to Pay (WTP)
- Use of Public Resources
- Socioeconomic Information

This methodology enabled the development of four models (calculations included in the Stata software annex). Respondents were not informed they would be asked twice about their WTP. Therefore, the response to the first bid was exogenous to the second, allowing WTP estimation as if it were a single-bounded dichotomous question survey. For this case, the Probit model with a single explanatory variable (simple model, Model A) was used.

Model Descriptions:

Model A: Similar to a single-bounded dichotomous approach, this model excluded the second bid and included only one explanatory variable. The Probit model was used to estimate the WTP.

Model B: As in Model A, the second bid was not included, but all explanatory variables were considered. Using the stepwise command, only statistically significant variables were selected, and the Probit model was applied to determine WTP.

Model C: This model applied the maximum likelihood estimation method using the doubleb command. Only variables corresponding to the two bids and their respective responses were included, without considering additional explanatory variables. WTP was determined accordingly.

Model D: Statistically significant variables were selected using the stepwise command. Like Model

C, the maximum likelihood method was used with the doubleb command to determine WTP.

3 Results and Discussion

Before estimating the WTP using a CVM, various characteristics of the population were analyzed. It was determined that in the Riobamba canton, 96 % of users have a direct connection to the drinking water network, 95 % report receiving water service daily, 63 % have a cistern for water storage, and 54 % believe that the distribution issues stem from an inefficient drinking water network.

Regarding solutions to these issues and monthly water payments, 72 % of respondents feel that the Municipality of Riobamba, through EMAPAR, does not make effective decisions to address water scarcity problems. Additionally, 30 % reported paying more than USD 20 per month for drinking water service.

The average income of the surveyed group is USD 641.63, and the cost of drinking water per cubic meter is USD 0.49.

Simple limit (first offer only) with no other explanatory variables

Table 2. Simple Boundary Model A

WTP01	Coef.	Std. Err.	z	P>z	[95 % Coef.	Interval]
PRE1	-1.17	0.24	-4.81	0.00	-1.65	-0.70
Cons	1.31	0.18	7.15	0.00	0.95	1.67

With:
WTP01=Dichotomous response to first offer (explained variable).
PRE1=first offer (explanatory variable).
coef=constant value.

According to the total of PRE1 (-1.17), it can be observed that an increase in the offer leads to a lower probability of acceptance by the respondent.

Table 3. Simple boundary WTP Model A

WTP01	Coef.	Std. Err.	z	P>z	[95 % Coef.	Interval]
WTP	1.12	0.10	10.80	0.00	0.92	1.32

Based on the results shown in Table 2, the maximum WTP of USD 1.12 is obtained (Table 3), corresponding to the value from Model A, which is statistically significant. The estimation is based on a 95 % confidence level.

Model B: Simple limit (first offer only) with other explanatory variables

Table 4. Simple Boundary Model B with other explanatory variables

WTP01	Coef.	Std. Err.	Z	P>z	[95 % Coef.	Interval]
PRE1	-1.19	0.25	-4.80	0.00	-1.67	-0.70
SE06	-0.10	0.06	-1.75	0.08	-0.21	0.01
ACC04	0.40	0.18	2.20	0.03	0.04	0.76
SE07	0.10	0.05	1.94	0.05	0.00	0.19
Cons	1.11	0.31	3.55	0.00	0.49	1.73

For the analysis in Table 4, the following variable descriptions are important to consider:
PRE1: Value of the first bid.
SE06: Education level (Primary, Secondary, University, Master's, Doctorate).
ACC04: Climate change issue (Dichotomous).
SE07: Housing condition (Owned, Rented, Family-owned, Mortgaged).

These coefficients allowed for inferring the likelihood that a respondent would accept the first bid. Variables with positive coefficients increase this likelihood, while those with negative coefficients decrease it. However, in this study, this model serves as an intermediate step for estimating the average WTP.

Table 5. Simple Boundary Model B WTP

WTP01	Coef.	Std. Err.	z	P>z	[95 % Coef.	Interval]
WTP	1.13	0.10	10.74	0.00	0.92	1.33

It should be noted that if the respondent is aware of the climate change issue, their WTP increases by USD 0.40. Similarly, their housing condition raises the WTP by USD 0.09. However, education level, a variable with a negative coefficient, decreases the WTP by USD 0.09 (Table 4). In Model B, the estimated WTP is USD 1.13 (Table 5).

Model C: double-bounded dichotomous method (two bids) with no other explanatory variables.

Table 6. Double Boundary WTP Model C

		Coef.	Std. Err.	Z	P>z	[95% Coef. Interval]	
Beta	cons	0.84	0.03	30.05	0.00	0.78	0.89
Sigma	cons	0.50	0.03	17.23	0.00	0.44	0.55

Using the maximum likelihood model and the doubleb command, the average WTP is estimated at USD 0.84 for Model C, which, according to the analysis conducted in Stata, corresponds to the beta constant (Table 6). This value is lower than the results obtained in the two previous models.

Model D: double-bounded dichotomous method with other explanatory variables

Table 7. Double Boundary Model D

		Coef.	Std. Err.	z	P>z	[95% Coef. Interval]	
Beta	SE06	-0.04	0.02	-1.83	0.07	-0.08	0
	SE07	0.04	0.02	1.92	0.06	0	0.08
	ACC04	0.24	0.08	3.13	0	0.09	0.39
	cons	0.68	0.11	6.47	0	0.48	0.89
Sigma	cons	0.49	0.02	17.26	0	0.43	0.54

Table 8. Double Boundary D Model WTP

	Coef.	Std. Err.	Z	P>z	[95% Coef. Interval]	
Beta	0.84	0.03	30.42	0.00	0.78	0.89

It should be noted that homeownership increases the WTP by USD 0.04, and awareness of climate change issues raises it by USD 0.24. Conversely, variables with negative coefficients, such as education level, decrease the WTP by USD 0.04 (Table 7). The average WTP in Model D is USD 0.84 (Table 8).

Hanemann (1991), argue that using a CVM with single-bounded dichotomous questions is easier for respondents but is statistically less efficient than a double-bounded method, as it requires larger sample sizes to achieve a certain level of precision. The results generated by the four models provide a basis for identifying the most statistically significant WTP. Hanemann (1991) emphasize that the best models prioritize the impact on achieved precision, reflected in narrower confidence intervals. This aligns with Kjær (2005), who states that more precise estimates are associated with smaller confidence intervals and, consequently, greater statistical efficiency.

In agreement with the findings of Hanemann (1991) and Kjær (2005) regarding the precision achieved in confidence intervals and a lower standard error (Table 9), we can conclude that Model D is the most suitable for determining the maximum average WTP for the studied sample, which is USD 0.84 per month. It is worth highlighting that WTP values tend to be lower in double-bounded models. This phenomenon—where WTP decreases when information from the second question is introduced—is frequently observed (Lopez-Feldman, 2012).

Table 9. Statistics of the different models.

Model	WTP USD	Std. Err.	Z	P>∣z∣	[95% Intervalo de Conf.]	
A	1.12	0.10	10.8	0.00	0.92	1.32
B	1.13	0.10	10.74	0.00	0.92	1.33
C	0.84	0.03	30.05	0.00	0.78	0.89
D	0.84	0.03	30.42	0.00	0.78	0.89

In Ecuador, studies on dichotomous contingent valuation are scarce. Roldán (2017) conducted an economic evaluation of water resources for human consumption in the case of Cajas National Park in Ecuador, within the Tomebamba River Basin. The results established a monthly WTP of USD 3.44 using a double-bounded dichotomous question format. This value is higher than those determined in this research under Models C and D. It is important to consider that the economy of Azuay Province is stronger than that of Chimborazo Province, and the bid vectors used in Roldan's study were higher due to Azuay's greater environmental and economic awareness.

In Latin America, studies provide useful benchmarks for analysis, as these countries have developing economies and comparable ecosystems. Loyola Gonzales (2007) analyzed the WTP of families in the city of Arequipa, Peru, for the conservation of a protected mountainous area in the Andes, specifically the upper basin of the Chili River. The results showed a WTP of USD 1.41 per month using a single-bounded dichotomous question format. This value is 19.86 % higher than the estimates from Models A and B in this research, making it the most comparable study. It is undeniable that Peru's economy surpasses Ecuador's, with a GDP of USD 223,249 million for Peru and USD 106,165 million for Ecuador in 2021 (World Bank, 2021).

Avilés-Polanco et al. (2010) evaluated the hydrological service of the La Paz aquifer in Baja California, Mexico, using a double-bounded dichotomous question format. The average WTP per household was approximately USD 8.20 per month. Similarly, an economic evaluation of the water environmental services provided by the Río Pancho Poza Natural Area in Mexico, using a double-bounded dichotomous question format, yielded a WTP of USD 7.60 (Sánchez Bocarando, 2020). Both values exceed the estimates from Models C and D in this research. Mexico's GDP stands at USD 1,293,037 million (World Bank, 2021).

The USD 0.84 that individuals are willing to pay for the conservation of the MCRCH water service represents 0.13 % of the average income of respondents and a 4.2 % increase in their monthly water bill, assuming that over 30 % already pay more than USD 20 per month for water consumption. Charging USD 0.84 per month to potable water service users could generate a monthly budget of USD 27,500.76. According to Ecuador's Constitution, this budget could be managed by the Honorable Provincial Government of Chimborazo, which holds environmental jurisdiction. This fund could support socio-economic and productive programs as compensation for moorland landowners and for conservation, protection, restoration, afforestation, and reforestation efforts.

Lopez-Feldman (2012), recommends that when WTP estimates are used in cost-benefit analyses, the project's budget must be carefully assessed. For the conservation of the MCRCH, which requires an estimated USD 3,323,371.50 (Gobierno Autónomo Descentralizado de la Provincia de Chimborazo, 2019), Model B could be used as it generates the highest revenue for conservation compared to Model D, which produces a lower estimate. This reflects the difficulty in determining which set of estimates is more reliable (Lopez-Feldman, 2012).

In Europe, Söderberg and Barton (2013) detailed the results of a contingent valuation study aimed at improving recreational water quality in eutrophic lakes in southwestern Norway. The author concluded that WTP data for water quality could serve as a qualitative political indicator to support user-financed water quality measures rather than as a cardinal measure of marginal utility.

4 Conclusions

It is important to note that the WTP estimates obtained from Models C and D are lower compared to those from Models A and B. This phenomenon—where the average willingness to pay decreases, when information from the second question is introduced—is frequently observed. Determining which set of estimates is more reliable is challenging. On the one hand, estimates obtained using the follow-up model are expected to be more efficient; however, this does not rule out potential biases in the estimation process. The explanatory variables education level, climate change concerns, and housing conditions are significant in Models B and D.

The municipal company EMAPAR is responsible for water management in the city of Riobamba, which benefits from water sourced from the MCRCH. This study calculated the average WTP of households for the conservation of water services by developing four models. The first two models (A, B) used the single-bounded dichotomous method, focusing only on the first bid, either without (A) or with (B) explanatory variables. The latter two models (C, D) employed the double-bounded dichotomous method (two bids), also either without (C) or with (D) explanatory variables. Based on confidence intervals, Model D is the most robust and includes significant variables such as education level, housing conditions, and climate change concerns, estimating a WTP of USD 0.84 per month.

The contingent valuation analysis is being conducted as part of a cost–benefit analysis. Therefore, the various WTP estimates obtained can be used for sensitivity analysis. Model D yielded an annual economic value for the target population of USD 330,009.12 using the WTP estimate derived from the double-bounded dichotomous method with explanatory variables. On the other hand, using the information from Model B, which employs the single-bounded dichotomous method with explanatory variables, the annual economic value was USD 443,940.84.

To complete the sensitivity analysis, the conservation cost for the MCRCH is estimated at USD 3,323,371.50. In this case, regardless of which WTP version is used, the project will have a negative net economic benefit. Therefore, alternative funding sources will need to be sought to support the conservation of the ecosystem.

Authors' contribution

E.F.C.C.: Conceptualization, data curation, formal analysis, funding acquisition, investigation, methodology, project administration, resources, software, writing - original draft. L.A.J.D.: Supervision, validation, visualization, writing- review and editing.

References

Alam, K. (2013). Factors affecting public participation in river ecosystem restoration: using the contingent valuation method. *The Journal of Developing Areas*, 47(1):223–240. Online:https://n9.cl/bzicf.

Aman, M., Shumeta, Z., and Kebede, T. (2020). Economic valuation of improved irrigation water use: the case of meskan district, southern ethiopia. *Cogent Environmental Science*, 6(1):1843311. Online:https://n9.cl/mwdcd.

Armijos Espinosa, R. and Segarra Ortega, Y. (2016). Aplicación de los métodos de costo de viaje y valoración contingente para determinar la disposición a pagar para la conservación del recurso hídrico del parque nacional cajas de la ciudad de cuenca. Master's thesis, Universidad de Cuenca.

Avilés-Polanco, G., Huato Soberanis, L., Troyo-Diéguez, E., Murillo Amador, B., García Hernández, J., and Beltrán-Morales, L. (2010). Valoración económica del servicio hidrológico del acuífero de la paz, bcs: Una valoración contingente del uso de agua municipal. *Frontera norte*, 22(43):103–128. Online:https://bit.ly/3ZQG33G.

Awad, I. and Holländer, R. (2010). Applying contingent valuation method to measure the total economic value of domestic water services: A case study in ramallah governorate, palestine. *European Journal of economics, finance and administrative sciences*, 20:76–93. Online:https://n9.cl/zeu87.

Cochran, W. (1983). *Unbiased value estimates for environmental goods: A cheap talk design for the contingent valuation method*. Compañía Editorial Continental.

Córdova, J., Molina, E., Zurita, J., and Meza, E. (2019). Valoración contingente en áreas protegidas: caso sector amazónico, ecuador. *Opción: Revista de Ciencias Humanas y Sociales*, (90):581–606. Online:https://n9.cl/ot4rt.

Cummings, R. and Taylor, L. (1999). Unbiased value estimates for environmental goods: a cheap talk design for the contingent valuation method. *American economic review*, 89(3):649–665. Online:https://n9.cl/p0avs4.

EMAPAR (2020). Empresa pública de agua potable de riobamba rendición de cuentas. EMAPAR. Online:https://n9.cl/87ahv.

Emily, E., Kironchi, G., and Wangia, S. (2013). Willingness to pay for improved water supply due to spring protection in emuhaya disrict, kenya. *International Journal of Education and Research*, 1(7):1–14. Online:https://n9.cl/nsbbc.

Gobierno Autónomo Descentralizado de la Provincia de Chimborazo (2019). Plan de desarrollo y ordenamiento territorial de la provincia de chimborazo. riobamba: Gobierno autónomo descentralizado de la provincia de chimborazo. Technical report, Gobierno Autónomo Descentralizado de la Provincia de Chimborazo. Online:https://n9.cl/h4lt65.

Hanemann, W. (1991). Willingness to pay and willingness to accept: how much can they differ? *The American Economic Review*, 81(3):635–647. Online:https://n9.cl/m7bum.

Hofstede, R., Groenendijk, J., Coppus, R., Fehse, J., and Sevink, J. (2002). Impact of pine plantations on soils and vegetation in the ecuadorian high andes. *Mountain Research and Development*, 22(2):159–167. Online:https://n9.cl/8ja7dx.

Ikıkat, E. (2020). Willingness to pay for increasing river water quality in aksu river, turkey. *Environment, Development and Sustainability*, 22(7):6495–6503. Online:https://n9.cl/sps3v.

Jimenez, R., Arana, G., Landeta, B., and Larumbe, J. (2021). Willingness to pay for improved operations and maintenance services of gravity-fed water schemes in idjwi island (democratic republic of the congo). *Water*, 13(8):1050. Online:https://n9.cl/2dqiu.

Kjær, T. (2005). *A review of the discrete choice experiment - with emphasis on its application in health care*. Syddansk Universitet. Health Economics Papers.

Lopez-Feldman, A. (2012). Introduction to contingent valuation using stata. Online:https://n9.cl/p7oti.

Loyola Gonzales, R. (2007). *Valoración del Servicio Ambiental de Provisión de Agua con Base en la Reserva Nacional Salinas y Aguada Blanca - Cuenca del Río Chili*. PROFONANPE.

Ministry of the Environment (2015). *Manual de valoración económica del patrimonio natural. Lima, Perú*. Dirección General de Evaluación, Valoración y Financiamiento del Patrimonio Natural.

Mueller, J. (2014). Estimating willingness to pay for watershed restoration in flagstaff, arizona using dichotomous-choice contingent valuation. *Forestry*, 87(2):327–333. Online:https://n9.cl/9rfoi.

Perez, J. (2010). Centro interamericano de desarrollo e investigación ambiental y territorial. Mérida, Venezuela: CIDIAT. Universidad de los Andes.

Reta, B. and Lee, J. (2020). Estimation of household willingness to pay for fluoride-free water connection in the rift valley region of ethiopia: A model study. *Groundwater for sustainable development*, 10:100329. Online:https://n9.cl/h9ma9.

Roldán, D. (2017). Valoración económica de recursos hídricos para el suministro de agua potable. el caso del parque nacional cajas. la cuenca del rio tomebamba. Master's thesis, Universidad de Alicante.

Shah, S. (2013). *Valuation of freshwater resources and sustainable management in poverty dominated areas*. PhD thesis, Colorado State University.

Sánchez Bocarando, J. (2020). Valoración económica de los servicios ambientales hídricos provistos por el Área natural protegida río pancho poza. Master's thesis, Universidad Autónoma de México, México.

Söderberg, M. and Barton, D. (2013). Marginal wtp and distance decay: the role of 'protest'and 'true zero'responses in the economic valuation of recreational water quality. *Environmental and Resource Economics*, 59(3):389–405. Online:https://n9.cl/hb3au.

Sueki, H. (2013). Economic value of counseling services as perceived by university students in japan: A contingent valuation survey. *Journal of Psychology y Psychotherapy*, 3(5):127. Online:https://n9.cl/lm8av7.

Tentes, G. and Damigos, D. (2012). The lost value of groundwater: the case of asopos river basin in central greece. *Water resources management*, 26:147–164. Online:https://n9.cl/8xa41.

Trujillo, J. and Perales, A. (2020). Water economic valuation of solís dam for agricultural use. *Tecnología y ciencias del agua*, 11(4):339–369. Online:https://n9.cl/d411k.

Vuille, M., Francou, B., Wagnon, P., Juen, I., Kaser, G., Mark, B., and Bradley, R. (2008). Climate change and tropical andean glaciers: Past, present and future. *Earth-science reviews*, 89(3-4):79–96. Online:https://n9.cl/7ob94.

Wambui, A. and Watanabe, T. (2021). Willingness to pay and participate in improved water quality by lay people and factory workers: A case study of river sosiani, eldoret municipality, kenya. *Sustainability*, 13(4):1934. Online:https://n9.cl/1x1sm.

World Bank (2021). Pib (us$ to currently prices). World Bank. Online:https://n9.cl/9bot6.

Zvobgo, L. (2021). Consumer ability and willingness to pay more for continuous municipal water supply in chitungwiza. *Sustainable Water Resources Management*, 7(2):23. Online:https://n9.cl/y4z3rh.

Appendix

A Programming and estimating models and willingness to pay in STATA

```
// Contingent valuation double-limit dichotomous
method  //
// Distribution of the Initial Offer Amount
tabulate PRE1

// Fraction of respondents who answered YES to
the VC question //
tabulate DPA01

// Sensitivity to offers //
tabulate DPA01 PRE1, column nofreq

/// 1. // DAP estimation - without covariates //
probit DPA01 PRE1

// Calculation of the Willingness to Pay //
nlcom (DAP:- _b[_cons]/_b[PRE1]), noheader

// 2. // DAP estimation - with variables
probit DPA01 PRE1 AG01 AG07 AG11 ACC03 ACC04
ACC08 SE01 SE02 SE04 SE05 SE06 SE07 SE09 SE10
SE11

// Estimation of variables
probit DPA01 PRE1 SE06 SE07

// Estimation of variables
probit DPA01 PRE1 SE10 SE11

// Estimation of variables
probit DPA01 PRE1 AG01 AG07

// Estimation of variables
probit DPA01 PRE1 SE01 SE02

// Estimation of variables
probit DPA01 PRE1 SE01 SE02 SE06 SE11

// Estimation of variables
probit DPA01 PRE1 SE06 SE09

// Estimation of variables
probit DPA01 PRE1 SE06 SE10

// Estimation of variables
probit DPA01 PRE1 SE06 SE07

// After the analysis we remove the
non-significant figures and find the
willingness to pay//

// I get the means and generate a scalar for each
explanatory variable//

summarize SE06, meanonly
scalar SE06_M = r(mean)
summarize SE07, meanonly
scalar SE07_M = r(mean)

// We find the willingness to pay //

nlcom (DAP:- (_b[_cons]+SE06_M*_b[SE06]+SE07_M*_b[SE07])
/_b[PRE1]), noheader

//////////////////////////////
*---HAROLD - OTHER SPECIFICATION

stepwise, pr(.1): probit DPA01 PRE1 AG01 AG07 AG11
ACC03 ACC04 ACC08 SE01 SE02 SE04 SE05 SE06 SE07 SE09
SE10 SE11
probit DPA01 PRE1 SE06 SE07 ACC04

summarize SE06, meanonly
scalar SE06_M = r(mean)

summarize SE07, meanonly
scalar SE07_M = r(mean)

summarize ACC04, meanonly
scalar ACC04_M = r(mean)

nlcom (DAP:- (_b[_cons]+SE06_M*_b[SE06]+SE07_M*_b[SE07]+
ACC04_M*_b[ACC04])/_b[PRE1]), noheader //
//////////////////////////////////////////////////

// Maximum Likelihood Function//

generate DPA1 = 0
replace DPA1 = 1 if VAI==3 | VAI==4

// We generate a variable that tells us the answer
to the second question //

generate DPA2 = 0
replace DPA2 = 1 if VAI==2 | VAI==4

// We generate a single variable for the second
amount //

generate PRED = .
replace PRED = PRE2 if DPA1==1
replace PRED = PRE3 if DPA1==0

// Model without explanatory variables //
doubleb  PRE1 PRED DPA1 DPA2

// Model with explanatory variables //
doubleb  PRE1 PRED DPA1 DPA2 SE06 SE07 ACC04

// We find the willingness to pay //
nlcom (DAP:(_b[_cons]+SE06_M*_b[SE06]+SE07_M*_b[SE07]
+ACC04_M*_b[ACC04])), noheader

//// End ////
```

LA GRANJA:
REVISTA DE
CIENCIAS DE LA VIDA

pISSN:1390-3799; eISSN:1390-8596

https://doi.org/10.17163/lgr.n41.2025.06

Scientific paper/ Artículo científico

BIOTECHNOLOGY

URBAN PHOTOBIOREACTOR FOR CO_2 SEQUESTRATION AND MICROALGAL BIOMASS PRODUCTION

FOTOBIORREACTOR URBANO PARA EL SECUESTRO DE CO_2 Y LA PRODUCCIÓN DE BIOMASA MICROALGAL

Saim Khan[1], Mehmood Ali*[1], Atif Mustafa[1] and Aqsa Iqbal[2]

[1] *Department of Environmental Engineering, NED University of Engineering Technology, Karachi-75270, Pakistan.*
[2] *Department of Chemical Engineering, NED University of Engineering Technology, Karachi-75270, Pakistan.*

*Corresponding author: mehmood@neduet.edu.pk

Received on May 27th, 2024. Accepted, after revision on October 22nd, 2024. Published on March 1st, 2025.

Abstract

The growth system of microalgae photobioreactors (PBRs) has drawn a lot of interest as a viable and sustainable method for generating quality biomass for value-added products and biofuels. The objective of this research work is to cultivate microalgae species *Chlorella vulgaris* in a photobioreactor that was designed, fabricated, and powered by solar energy system. Three experimental conditions were compared with 1:4 ratios of microalgae culture (40L) and fresh water (10L) having 100mL of media (nutrients) used in each experiment with control sample (ambient air aeration) experiment # 1, injecting 200 g of CO_2 for 15 sec (experiment # 2), and 300g of CO_2 for 25 sec (experiment # 3) on alternate days during the cultivation period. All experiments showed the reduction of nutrients concentration (orthophosphate and nitrate) and enhancement of biomass productivity with respect to 10 days of cultivation period. Experiments 1, 2 and 3 showed removal of orthophosphate as 50%, 41.74% and 60.78% respectively, whereas nitrate removal was 22%, 48% and 58%. Biomass productivity from experiments 1, 2 and 3 after 10 days of cultivation period were 196.63 mg/L, 203.43 mg/L, 318.76 mg/L respectively. Statistical analysis revealed that supplying CO_2 from external source in experiment # 2 and experiment # 3 have same pattern of statistical significance with co-relationship between two groups of means with p-value of 6.306×10^{-14}. The maximum microalgal biomass was recovered from experiment # 3, with 7.98% by weight protein content yield and lipid content yield 37.4% by weight (1.87/ 5 g of dried biomass). Kinetic study showed volumetric mass transfer capacities of KO_2 and KCO_2 were found to be $1.763\times10^{-7} m^3/s$ and $1.676\times10^{-7} m^3/s$, with better result of KCO_2 gas transfer capacity of the system. In the extracted lipids favorable qualities of fatty acids for the production of microalgae biodiesel were found such as myristic (C14:0), palmitic (C16:0), palmitoleic (C16:1), oleic (C18:1), linoleic (C18:1), and linolenic acids (C18:3). The use of urban microalgae photobioreactors is an environmentally sustainable strategy that can contribute significantly to the bio-based economy and reduce the negative effects of traditional fossil fuel usage on the environment.

Keywords: Carbon sequestration, Urban photobioreactor, Carbon capture, Biomass productivity, CO_2 bio-fixation, *Chlorella vulgaris*, Biofuel production.

Resumen

El sistema de crecimiento de fotobiorreactores (PBRs) de microalgas es de gran interés pues es un método viable y sostenible para generar biomasa de calidad destinada a productos de valor agregado y biocombustibles. En este estudio se cultivó la especie de microalga *Chlorella vulgaris* en un fotobiorreactor diseñado, fabricado y alimentado por un sistema de energía solar. Se compararon tres condiciones experimentales con proporciones de 1:4 de cultivo de microalgas (40 L) y agua fresca (10 L), utilizando 100 mL de medio (nutrientes) en cada experimento: un experimento control (aireación con aire ambiente, experimento # 1), la inyección de 200 g de CO_2 durante 15 segundos (experimento # 2), y la inyección de 300 g de CO_2 durante 25 segundos (experimento # 3) en días alternos durante el periodo de cultivo. Todos los experimentos mostraron una reducción en la concentración de nutrientes (ortofosfato y nitrato) y un aumento en la productividad de biomasa tras un periodo de cultivo de 10 días. Los experimentos 1, 2 y 3 mostraron remociones de ortofosfato del 50 %, 41,74 % y 60,78 %, respectivamente, mientras que la remoción de nitrato fue del 22 %, 48 % y 58 %. La productividad de biomasa en los experimentos 1, 2 y 3 tras 10 días de cultivo fue de 196,63 mg/L, 203,43 mg/L y 318,76 mg/L, respectivamente. El análisis estadístico reveló que el suministro de CO_2 desde una fuente externa en los experimentos # 2 y # 3 sigue un patrón similar de significancia estadística, con una correlación entre ambos grupos de medias y un valor de p de $6\,306 \times 10^{-14}$. La mayor biomasa de microalgas fue recuperada del experimento # 3, con un contenido proteico del 7,98 % en peso y un contenido lipídico del 37,4 % en peso (1,87 g/5 g de biomasa seca). El estudio cinético mostró que las capacidades de transferencia volumétrica de masa de KO_2 y KCO_2 fueron de $1\,763\times10^{-7}$ m^3/s y $1\,676\times10^{-7}$ m^3/s, respectivamente, siendo más eficiente la capacidad de transferencia de KCO_2 del sistema. Los lípidos extraídos presentaron ácidos grasos favorables para la producción de biodiésel de microalgas, como ácido mirístico (C14:0), palmítico (C16:0), palmitoleico (C16:1), oleico (C18:1), linoleico (C18:1) y linolénico (C18:3). El uso de fotobiorreactores urbanos de microalgas es una estrategia ambientalmente sostenible que puede contribuir significativamente a la economía basada en recursos biológicos y reducir los efectos negativos del uso tradicional de combustibles fósiles sobre el medio ambiente.

Palabras clave: Secuestro de carbono, Fotobiorreactor urbano, Captura de carbono, Productividad de biomasa, Biofijación de CO_2, *Chlorella vulgaris*, Producción de biocombustibles.

Suggested citation: Khan, S., Ali, A., Mustafa, A. and Iqbal, A. (2025). Urban photobioreactor for CO_2 sequestration and microalgal biomass production. *La Granja: Revista de Ciencias de la Vida.* Vol. 41(1):95-111. https://doi.org/10.17163/lgr.n41.2025.06.

Orcid IDs:

Saim Khan: https://orcid.org/0009-0000-6256-4619
Mehmood Ali: https://orcid.org/0000-0002-1804-2677
Atif Mustafa: https://orcid.org/0000-0002-3815-0800
Aqsa Iqbal: https://orcid.org/0009-0001-7327-8877

1 Introduction

With over 75 % of all greenhouse gas emissions and almost 90 % of all carbon dioxide emissions coming from combustion of fossil fuels like coal, oil, and natural gas are by far the biggest cause of climate change. Greenhouse gas emissions cover the Earth, trapping heat from the sun, thus causing climate change and global warming. The world is now warming faster than at any point in recorded history. Over time, rising temperatures are altering weather patterns and upsetting the natural equilibrium of the environment. This poses many risks to human beings and all other forms of life on Earth (United Nations, 2024). Between 1900 and 2020, the Earth's atmosphere saw a temperature increase of around 1.1 °C, leading to changes in weather patterns and global warming, the global average temperature rises to 2 °C above the level of pre-industrial times, whilst pursuing efforts to limit the increase to 1.5 °C, was the stated objective in the Paris Agreement. This will also help to achieve the UN Sustainable Development Goal (SDG) goal 13 i.e., to combat climate action formulated in 2016.

The world's energy consumption is mostly fueled by fossil fuels, which account for around 85 % of all energy sources worldwide. Scientist have issued warnings about the risk of running out of finite fossil fuel supplies without creating a viable alternative energy source to take the place of the declining oil reserves. Another issue that has not received enough attention in many oil-producing nations is the pollution and emissions that come from the exploration and production of fossil fuels (Valavanidis, 2023). The challenges of depleting fossil fuel reserves and environmental crisis emanating from the use of fossil fuels, it is therefore increasingly necessary to find environmentally sustainable and clean fuels for future uses to mitigate climate change and global warming (Mahapatra et al., 2021; Rodionova et al., 2017). In order to reduce the impact of GHG's emissions from burning of fossil fuels, biofuels are produced directly or by biological processes or obtained via the chemical conversion of biomass as a replacement to fossil fuels (Rodionova et al., 2017). There are various types of biofuels, for example, first-generation biofuels consist of ethanol derived from starch-rich food crops or biodiesel created from residual animal fats like frying grease. The second generation is composed of bioethanol derived from non-food cellulosic material and biodiesel produced from oil-rich plant seeds like pongamia or jatropha. The most promising method to fulfill the world's energy demands is the third generation of biofuels, which are produced from microalgae, cyanobacteria, and other microorganisms (Rodionova et al., 2017).

The threat posed by air pollution causing climate change brought on by numerous human activities has gained attention from all around the world. Though formerly thought to be a promising technological solution to lessen this alarming situation, carbon capture and storage (CCS) techniques are now regarded as not economically feasible, and it is uncertain what effect they will have on the environment in the future (Sievert et al., 2023). As an alternative, the use of microalgae for the biological capture of carbon dioxide (CO_2) is seen to be a promising method for recycling the surplus CO_2 produced by vehicles, power plants, industries, volcanic eruptions, the breakdown of organic materials, and forest fires. Moreover, CO_2 can be taken up by microalgae and regenerated into biomass, which can then be used as a carbon source to make lipids for the synthesis of bioenergy and other products with added value (Sievert et al., 2023). The mass scale biomass can be achieved by microalgae cultivation, using two major cultivation systems such as open raceway pond and a photobioreactor system. The higher biomass productivity can be obtained through controlled environment using a photobioreactor. Considering the microalgae metabolism, it can be classified as photoautotrophic, photoheterotrophic, heterotrophic and mixotrophic. Sunlight, some basic inorganic elements like carbon dioxide (CO_2), and metal salts are necessary for the cell development or cultivation metabolism process of microalgae. Heterotrophic microalgae, on the other hand, require an additional source of certain organic compounds and nutrients, such as nitrogen (N) and phosphorus (P). Previous research demonstrates that growing Chlorella on a mixotrophic medium increases photosynthesis efficiency and provides exogenous organic resources. Furthermore, throughout the culture process, microalgal farming significantly lowers greenhouse gas (CO_2) emissions in addition to producing biomass and biofuels. On the other hand, wastewater from different sources can be used as a culture medium for microalgae. Microalgal strains that are photoheterotrophic, mixotrophic, or heterotrophic have grown in both light and dark media (Saratale et al., 2022).

For the cultivation of microalgae, photo bioreactor (PBR) is used having enclosed culture vessel with adjustable operational settings to regulate biomass. As a photosynthetic organism, microalgae can be grown in both closed (photobioreactor) and open (pond) systems. Better control over culture settings is possible with photobioreactors, which are being developed for maximum productivity, economic effectiveness, and minimum maintenance. The microalgae growth, photosynthesis, and lipid accumulation are dependent on a number of variables, including light, temperature, the medium's pH, the presence of CO_2, and macronutrients including potassium, phosphates, and nitrates (Saratale et al., 2022).

An urban photobioreactor is an alternative approach to greening that was created for urban environment where traditional greening is impractical because of space constraints, land values, and air pollution. It is based on the high CO_2 fixation and O_2 production efficiency of microalgae and photobioreactor technology. It is equal to one mature tree or 200 square meters of lawn, depending on the rate of carbon fixation. Because of its multipurpose nature, thoughtful design, and secure construction, it blends in with urban surroundings (Rehman et al., 2022). The microalgae cultivation in a photobioreactor includes number of factors such as microalgae species, photobioreactor design, choice of light source, mixing mechanisms, nutrient supply, temperature and pH control, and considerations for harvesting and processing. Emphasizing a high surface area to volume ratio is important in this design process. Given the light-dependent nature of the reaction, a greater surface area facilitates enhanced light penetration, which is fundamental requirement for photosynthesis (Stojiljković and Spasojević, 2023).

One sustainable method for capturing carbon dioxide and utilizing it to produce renewable products and reduce emissions is the use of photosynthetic microalgae. Past research study has mostly concentrated on the byproducts of microalgae, especially biofuels, rather than their capacity to sequester CO_2. *Chlorella sp.* was grown in an investigation at CO2 concentrations similar to those seen in the fuel gases from power plants. It was discovered that 5 % de CO_2 was the ideal concentration for the production of microalgae biomass. The cultures' CO_2 removal efficiency was then continuously observed using a nondispersive infrared sensor. Over the course of 14 days, the average CO_2 removal effectiveness was 17.5 %, which is significantly greater than the values reported in the literature when no direct real-time monitoring system is used (Scheufele et al., 2019). Microalgae have the ability to produce 10–20 times as much oil as vegetable oil seed crops, they are regarded as a promising feedstock for the production of third-generation biofuels (Leflay et al., 2021).

The cleaning of flue gas has generated a lot of interest because of the growing concerns about CO_2 emissions and environmental degradation. One method of reducing CO_2 emissions from flue gas that is seen to be promising is the use of microalgae for photosynthesis. On the other hand, the flue gas pollutants might prevent microalgal growth, which would reduce the rate of CO_2 fixation by microalgae. A steady pH level can help mitigate the inhibitory effects of SO_x, which contribute to the low pH, while NO_x can be used as a source of nitrogen to encourage the growth of microalgae once it dissolves and oxidizes in the culture medium. Fixing CO_2 from flue gas and using NO_x and SO_x as nutrients would generate microalgal biomass, which may be used as a suitable feedstock to make biofuels and bio-based chemicals (Ali et al., 2021). Microalgae can be used as a sustainable feedstock for the production of biodiesel by lipid extraction and a transesterification process because of their high lipid content and rapid growth rates. However, a number of obstacles need to be removed in order to produce biodiesel derived from microalgae, such as high production costs, low lipid productivity, and issues associated with large-scale growth and harvesting. The production of biodiesel from microalgae appears to have a promising future with possible uses in a number of sectors, including agriculture, energy, and transportation (Yen et al., 2015).

The current research study objectives are to design and fabricate a 250 L urban photobioreactor operated by solar energy system to cultivate *Chlorella vulgaris* in freshwater condition. The experiments included the control sample provided with ambient air aeration, while two experiments were conducted with introduction of intermittent CO_2 concentrations to investigate the influence of CO_2 on biomass productivity and its bio-fixation. On the alternate day basis measurements of the microalgae cultivation growth parameters were monitored and measured such as removal of nutrients, biomass productivity and CO_2 sequestration.

2 Materials and Methods

2.1 Microalgae culture and nutrient medium

The microalgae culture of *Chlorella vulgaris* was obtained from the Marine Resource Department, Pakistan Council of Scientific and Industrial Research (PCSIR) Laboratories Karachi, while the culture media (F/2) Guillards was prepared per liter having composition including 34g Sea salt, 84.15 mg $NaNO_3$, 6 mg $Na_2MoO_4.2H_2O$, 2.9 mg $FeCl_3.6H_2O$, 10 mg $Na_2EDTA.2H_2O$, 33 mg $Na_2SiO_3.9H_2O$, 1.96 mg $CuSO_4.5H_2O$, 4.4 mg $ZnSO_4.7H_2O$, 1.26 mg $Ma_2MoO_4.2H_2O$, 36 mg $MnCl_2.4H_2O$, 2 mg $CoCl_2.6H_2O$, 0.4 mg Vitamin B1, 0.002 mg Vitamin B12, 0.1 mg Biotin.

2.2 Designing of a photobioreactor

A photobioreactor for microalgae cultivation includes number of factors such as microalgae species, photobioreactor design, choice of light source, mixing mechanisms, nutrient supply, temperature and pH control, and considerations for harvesting and processing. In this design procedure, a high surface area to volume ratio is a critical factor. Given the light-dependent nature of the reaction, a greater surface area facilitates enhanced light penetration, which is fundamental requirement for photosynthesis. To achieve an optimal balance, the surface area to volume ratio can be heightened by employing geometrically efficient designs and configurations. This emphasis on optimizing the surface area to volume ratio underscores the significance of efficient light exposure and nutrient distribution. For a rectangular photobioreactor, based on its geometric specification, the surface area and volume can be calculated by the following equations (1) and (2):

$$A_s = 2HW + 2HL \tag{1}$$

$$V = HWL \tag{2}$$

Where W is the width, H is the height and L is the length of the flat panel photobioreactor. According to Equation 3, the bubble rise rate u_b and the mean bubble diameter d_b determine the shear rate of bubble cultures, or y-aeration. The velocity of bubbles depends on their size and the fluid's characteristics, therefore for medium-sized bubbles in water, 0.24 m/s is an acceptable value obtained by Hadamard–Rybczynski equation The bubble diameter can be estimated based on the fluid properties and conditions using the Calderbank Equation (Gaurav et al., 2024). This equation indicates that the smaller the bubble size, the larger the shear rate and the resulting damage to the microalgae cultures.

$$Y_{aeration} = \frac{2 \cdot u_b}{d_b} \tag{3}$$

Figure 1 shows the schematic diagram of an urban photobioreactor.

2.3 Experimental conditions of cultivating microalgae in a photobioreactor

A rectangular glass photobioreactor having dimensions height 90cm (35.43 inches), width 32cm (12.59 inches), length 121cm (47.63 inches) was designed with volume capacity of approximately $\sim$ 350 L, while its top cover is 97 cm (38.18 inches) and 178 cm (70 inches) having 500 W solar PV panel with size 58 inches $\times$ 26 inches $\times$ 1.5 inches (length $\times$ width and height). The solar PV panel was positioned at an angle of 30° on the top of the photobioreactor assembly to harnesses solar energy efficiently but also aligns with contemporary eco-friendly practices, contributing to a reduced carbon footprint. The photobioreactor was provided with a metallic frame for housing a battery, inverter, and an air pump. For microalgae species *Chlorella vulgaris* light source for photosynthesis being an essential component of the system; two LED of 7 W each operated by solar energy system were installed. The photobioreactor uses a combination of sunlight during the daytime and LED lights during the nighttime obtained from using solar energy obtained through a solar energy system. To maintain even dispersion of light and nutrients, air diffusers are provided for adequate aeration from the bottom of the photobioreactor.

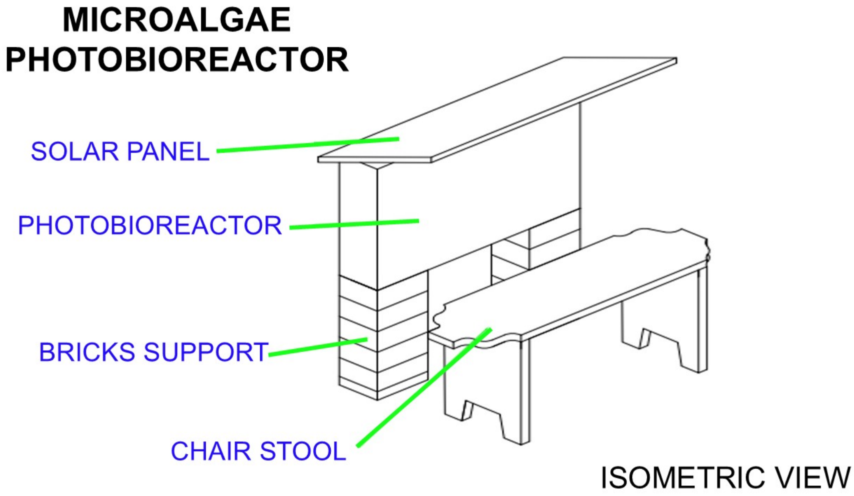

Figure 1. Showing an isometric view of design of an urban photobioreactor.

The microalgae cultivation had a working volume of 100 L. The nutrient (F/2 standard medium) were used as a growth additive for the experiments. The microalgae culture was kept under solar assisted light for 10 days cultivation time. The falling sunlight irradiance (Lux) on the photobioreactor and the solar PV panel and LEDs during the night were measured with a light intensity meter (MS6612T, Mastech, China). Each experiment with different ratios of culture, media (nutrients) and water with/ without carbon dioxide (CO_2), the parameters such as pH, TDS, temperature, and EC were measured using a pH/ORP/EC/TDS/temperature meter (EZ-9910, Multifunction, China).

Three experiments were conducted as per the following protocol by varying the concentration of carbon dioxide in the microalgae culture and water (see Table 1). Carbon dioxide (CO_2) with 98% purity concentration was dosed intermittently on alternate days. The mixing is achieved using air diffusers operated by an air pump (1780 GPH, Kulife Aquarium Air Pump, China), which supplies air in alternate hour for 15 min duration, powered by solar energy system. The microalgae cultivation with air aeration and with CO_2 (200 g y 300 g) enrichment (200 g and 300 g) of intermittent CO_2 injection were used in the subsequent runs of the experiment. This study involves three sets of experiments to investigate the growth of microalgae at various CO_2 concentration levels.

2.4 CO_2 bio-fixation by microalgae during cultivation

The flow rate of CO_2 introduced into the photobioreactor was measured using the continuity equation (4):

$$Q = A \times V \tag{4}$$

Where flow rate (Q), area of the pipe (A), and velocity of CO_2 gas (V) injected into the system through a rubber hose pipe having diameter (0.018 m) used to inject CO_2 in the photobioreactor was measured by using a vernier caliper through which the area was calculated. While the velocity of CO_2 injected into the photobioreactor tank was measured using a Weather Meter (Kestrel 4000NV, USA). The CO_2 was dosed for 15 sec in Experiment # 1 and 25 sec in (Experiment # 2) on alternate days. The volume of CO_2 injected is calculated by multiplying flow rate with dosing time, then the mass of CO_2 is computed by Density= Mass/ Volume.

The use of photosynthetic microalgae for carbon capture offers the potential for a sustainable capture system, which can both reduce emissions and produce renewable products (Borowitzka, 1999). The bio-fixation rate of carbon, R_{CO_2} (g_{CO_2} /L/ day) is calculated using the following mathematical equation (5):

$$R_{CO_2} = \%C \times PB\left(\frac{MW_{CO_2}}{MW_C}\right) \tag{5}$$

Where, R_{CO_2} refer to CO_2 bio-fixation rate, % C indicate total carbon content, PB is the biomass productivity (mg of biomass produced per L per day), MW_{CO_2} denote the molecular weight of CO_2 and MW_C is molecular weight of carbon. %C is the carbon content of the dry biomass, assumed at ~ 50 (Borowitzka, 1999).

2.5 Modelling of carbon dioxide (CO_2) volumetric mass transfer capacity in a photobioreactor

Mass transfer in a photobioreactor is the flow of substances between the gas and liquid phases, including gases (such carbon dioxide and oxygen) and nutrients. Mass transfer is greatly aided by aeration, which is usually accomplished by bubbling ambient air through the liquid medium. The interfacial area between the liquid and gas phases is increased as a result. The film theory is a common method that is used to explain mass transfer at the gas-liquid interface surface (Amaral et al., 2019). This hypothesis states that mass transfer takes place through a thin liquid coating that forms around gas bubbles. The rate at which a substance transitions from the gas phase to the liquid phase is measured by the mass transfer coefficient (k) in Equation 6. Its definition is the relationship between the thickness of the boundary layer (δ) at the gas-liquid interface and the substance's diffusion coefficient (D) in a liquid medium. The mass transfer coefficient for O_2 in photobioreactor is given by (Faruque et al., 2021).

$$k = \frac{D}{\delta} \tag{6}$$

By taking into account the impact of photobioreactor dimensions on mass transfer rates by including its surface area in the calculations. The photobioreactor's surface area directly impacts mass transfer rates because it determines the gas-liquid interface available for gas exchange. Considering the unique geometry of the reactor, the computed volumetric mass transfer capacity shows the rates at which molecules of carbon dioxide and oxygen can move from the gas phase to the liquid phase per unit area of the gas-liquid interface. This is calculated by the Equation 7 (Faruque et al., 2021):

$$k = \frac{D \times A}{\delta} \tag{7}$$

Surface area of a rectangular photobioreactor was calculated by the Equation 8:

$$A = 2\ (L \times W + L \times H + W \times H) \tag{8}$$

2.6 Measurement of microalgae growth parameters

2.6.1 Solar irradiance and Temperature

The falling solar irradiance (Lux) on the photobioreactor and LEDs during the night time were measured with a light intensity meter (MS6612T, Mastech, China).

Table 1. Water to media (nutrient) ratios utilized in the experimental study.

	Experiment # 1*	Experiment # 2*	Experiment # 3*
Water (L)	40	40	40
Microalgae culture (L)	10	10	10
F/2 standard nutrient media solution (mL)	100	100	100
Intermittent CO_2 injection time	0	15 sec (200 g of CO_2)	25 sec (300 g of CO_2)

*Each experiment was repeated twice, and the results of physical and chemical parameters are presented as an average value.

2.6.2 pH, TDS, TSS and Electrical conductivity

pH, TDS, TSS and electrical conductivity were by multi-functional meter (EZ-9910, Multifunction, China).

2.6.3 Nutrients removal (nitrates and orthophosphate)

Nitrate and orthophosphate concentrations were measured using a DR-500 UV-Vis spectrophotometer (Hach, USA). The nitrate amount was measured by adding powdered aluminum nitrate (Hach, USA) as a reagent to 10 mL of the sample to detect nitrate concentration. In order to measure the amount of nitrate at 425 nm, 10 mL of the prepared solution was introduced to the sample cell, similar to how samples were added and properly mixed by shaking with 8 mL of reagent solution combined with conventional procedures for testing water and wastewater in accordance with the proportions given for the ascorbic acid method (4500-P. E) to determine the concentration of orthophosphate (Amaral et al., 2019). A sample of 10 mL of the solution was added to the spectrophotometer's sample cell after 10 min, and the concentration was determined at 880 nm.

2.6.4 Biomass productivity

The biomass productivity was measured with a UV-Vis spectrophotometer (DR 5000, Hach, USA) at 680 nm from Hach (USA). According to the literature (Leflay et al., 2021), microalgae biomass yields were assessed alternately over the course of a 10-day growing period by measuring the optical density. *Chlorella vulgaris* standard dried biomass was used to plot the standard plot between the known concentration of microalgal biomass (mg/mL) vs absorbance at 680 nm.

2.7 Protein Extraction

The liquid sample with the highest biomass productivity was selected for protein detection and fatty acid analysis. For the protein detection, Lowry standard method was used to the extraction and quantification of proteins. Protein extraction analysis was conducted at the Food and Marine Resources Research Centre, PCSIR Laboratories, Karachi.

2.8 Lipid Extraction and fatty acids compositional analysis

A sample of 250 mL cultivated microalgae suspension was centrifuged at 3000 rpm using multipurpose centrifuge (1580 R, Lab-Tech, Italy) for 30 min to separate the liquid phase from the organic biomass content. Organic biomass was dried at 80 °C for 3 hrs in an oven (YCO-NO1, Gemmy Industrial corporation, Taiwan), after drying the dried biomass chips were pulverized in a mortar and pestle. The Bligh and Dyer procedure was followed to extract lipids from the dried microalgae biomass as per literature using n-hexane as an extraction organic solvent (Leflay et al., 2021) and extracted lipid yield by weight % was measured by weight using an electronic balance (AB 304-S, Mettler Tolendo, Switzerland).

3 Results and Discussion

3.1 Fabricated urban photobioreactor

An urban photobioreactor has been locally designed and fabricated, with dimensions height $\times$ width $\times$ length ($35.43 \times 12.59 \times 47.63$) inches, having total volume of 350 L showcasing an innovative structure tailored for efficient microalgae cultivation for climate change mitigation as depicted in Figure 2.

3.2 Analysis of microalgae growth parameters

3.2.1 Solar irradiance and temperature

In-depth research indicates that higher temperatures can enhance enzymatic activities involved in nutrient assimilation and lipid accumulation, crucial for biofuel production. However, there is an optimal temperature range for each algae species as excessively high temperatures might lead to thermal stress, disrupting cellular functions and impeding growth. Understanding and controlling temperature conditions are crucial for optimizing algae-based biofuel production systems. The results of experiment # 1 showed solar irradiation and temperature profile for the 10 days of cultivation time, measured average values 22.02 °C and 362.5 W/m^2 respectively (see Table 2).

Tables 3 and 4 show variation in temperature during the cultivation period between 22.3 to 24.0 °C and 23.9 to 25.3 °C for experiment # 2 and experiment # 3 respectively. The average solar irradiation measured for experiment # 1 and experiment # 2 were 391.9 and 430.4 W/m^2 respectively. Table 4 suggests that the optimal temperature range for higher biomass production lies between 24 to 25 °C, while solar irradiation of 430.4 W/m^2 yielding maximum 319.9 mg/L of microalgal biomass yield after 10 days of cultivation period.

Figure 2. Locally designed and fabricated urban photobioreactor.

3.2.2 pH, TDS, TSS and electrical conductivity

Algal growth and metabolism are influenced by pH level for both the performance of photobioreactors and the growth of microalgae. It plays a crucial role in determining the availability of nutrients, regulating metabolic activities, and overall health of microalgae within the growing medium (Shuler and Kargi, 2002). In addition to being dependent on CO_2 solubility, the pH value of the culture media appears to be influenced by nitrogen uptake, which is necessary for the development of algal cells and the subsequent consumption of nitrate by microalgae (Borowitzka, 1999).

The pH of the medium for experiment # 1 were between 7.9 to 8.3 giving an average of 8.12 which is greater than the desired value according to the literature (APHA, 2005), resulting in lesser biomass productivity. Whereas the average pH for the course of cultivation was determined to be 7.57 in experiments # 2 and 3 and were found in accordance with previous literature (APHA, 2005).

The growth medium's levels of electrical conductivity (EC) and total dissolved solids (TDS) are crucial in controlling the availability and solubility of essential nutrients, including nitrogen, phosphorus, potassium, and micronutrients. Imbalances in TDS and EC levels, either too high or too low, can impact the nutrient uptake by algae, potentially imposing limitations on their growth. Moreover, elevated TDS and EC levels may subject algae cells to osmotic stress caused due to higher concentration of solutes in the growth medium, differing from the cell's internal environment and affecting water balance and overall cell health.

Table 2 showed decreasing electrical conductivity from 1.34 to 0.98, this is due to EC directly related to the concentration of ions in the medium, including essential nutrients like nitrogen, phosphorus, and micronutrients reduced during the cultivation period. However, adequate nutrient availability is crucial for microalgae growth during its cultivation period (Brindhadevi et al., 2021). A considerable decrease in EC was observed in experiment # 2 and experiment # 3 between 1.13 to 0.82 and 1.34 to 0.95 respectively (see Table 3 and Table 4).

Table 2. Experiment # 1 (ratios used 80 % water and 20 % microalgae culture).

	Duration of cultivation				
Parameters	**Day 1**	**Day 3**	**Day 5**	**Day 7**	**Day 10**
Temperature (C)	21.8	22.7	21.9	21.3	22.4
Solar irradiation (W/m^2)	365.9	342.6	383	397.1	323.9
pH	8.1	8	8.3	7.9	8.3
EC (μs/cm)	1.34	1.33	1.15	1.11	0.98
TDS (mg/L)	610	600	580	550	540
TSS (mg/L)	71	82	93	98	100
Orthophosphate (mg/L)	104	100	73	60	52
Nitrate (mg/L)	10	9.5	8.8	8.2	7.8
Absorbance (abs)	0.11	0.14	0.16	0.2	0.23
Biomass productivity (mg/L)	113.3	134.4	148.4	176.5	196.63

It has been observed that TDS content decreases drastically in all three experiments # 1, 2, and 3 during cultivation period. The absorbance (light intensity) is found higher in experiment # 3 (with 300g of CO_2 introduced into the photobioreactor), ranging between 0.12 to 0.49 absorbance which subsequently decreases the electrical conductivity of salts in the system. While light intensity itself does not directly contribute to electrical conductivity, but having impact on photosynthesis, biomass growth, and metabolic activities can lead to changes in the ion composition of the culture medium (Morales et al., 2018; Nezammahalleh et al., 2016). Reduced TDS and EC levels can be interpreted as a positive outcome, indicating the utilization of nutrients by the microalgae for their growth and metabolic processes (Nezammahalleh et al., 2016).

The Total Suspended Solids (TSS) demonstrated a notable increasing trend, primarily attributed to the formation of insoluble biomass within the system as presented in Tables 2 to 4. This phenomenon contributes to the heightened turbidity of the system. Importantly, this observed increase in TSS serves not only as a consequence of biomass formation but also as a valuable indicator for quantifying biomass productivity. The rising TSS levels act as a tangible and easily measurable metric, offering a direct means to gauge the effectiveness of biomass production within the photobioreactor cultivation system. The biomass production of microorganisms such as *Chlorella vulgaris* throughout the cultivation phase can be significantly influenced by the levels of total suspended solids (TSS) and total dissolved solids (TDS) in water. During testing, the concentration of TSS increases from 71 to 100 mg/L (experiment 1), 74 to 105 mg/L (experiment 2) and 81 to 110 mg/L (experiment 3), from day one to day tenth during cultivation period. High levels of TSS can affect the light penetration into the water, reducing the availability of light for photosynthesis in *Chlorella vulgaris* cells, which can hinder the growth and biomass production (Morales et al., 2018).

3.2.3 Reduction of nutrients concentration during cultivation time

Adequate nutrient supply promotes algal growth and enhances biomass productivity. It is observed that an external nutrient concentration, or the nutrient concentration in the culture medium, controls the microalgae growth phase. Tables 2 to 4 showed the pattern of orthophosphate and nitrate removal by microalgae during its growth cycle. Experiment 1, 2 and 3 showed the % removal of orthophosphate from the water by microalgae was 50 %, 41.74 % and 60.78 % respectively, while the nitrate removal was 22 %, 48 % and 58 % respectively during the growth cycle of 10 days. In the current study, this variability in the percentage of removed phosphorus may result from variations in the initial amount of phosphorus in the culture media and the cultivation conditions (Barghbani et al., 2012). The overall nitrogen content in the media gradually drops during the course of the growth process for all enriched CO_2 feed concentrations. This might result from Chlorella's vulgaris rapid anabolism in the initial few days of the cultivation phase (Barghbani et al., 2012).

Table 3. Experiment # 2 (ratios used 80 % water and 20 % culture with Intermittent 200 g CO_2).

	Duration of cultivation				
Parameters	**Day 1**	**Day 3**	**Day 5**	**Day 7**	**Day 10**
Temperature (C)	23.8	22.5	22.9	22.3	24
Solar irradiation (W/m^2)	412.6	377.8	410.9	390.4	367.8
pH	7.8	8	7.5	7.1	7.37
EC (μs/cm)	1.13	1.06	0.97	0.91	0.82
TDS (mg/L)	690	670	60	620	570
TSS (mg/L)	74	78	89	93	105
Orthophosphate (mg/L)	103	77	70	59	60
Nitrate (mg/L)	10	9.3	8.5	7.4	5.2
Absorbance (abs)	0.091	0.11	0.135	0.21	0.24
Biomass productivity (mg/L)	115.3	142.4	163.1	183.5	203.43

Table 4. Experiment # 3 (ratios used 80 % water and 20 % culture with Intermittent 300 g CO_2).

	Duration of cultivation				
Parameters	**Day 1**	**Day 3**	**Day 5**	**Day 7**	**Day 10**
Temperature (C)	24.1	24.3	23.9	25.3	24
Solar irradiation (W/m^2)	426.5	428.6	398.3	463.9	434.7
pH	8.5	7.7	7.5	7.6	7.1
EC (μs/cm)	1.34	1.27	1.35	0.99	0.95
TDS (mg/L)	740	720	690	60	580
TSS (mg/L)	81	87	102	99	110
Orthophosphate (mg/L)	102	89	85	65	40
Nitrate (mg/L)	10	8.1	7.3	5.8	4.2
Absorbance (abs)	0.12	0.25	0.27	0.38	0.49
Biomass productivity (mg/L)	120.3	211.5	225.6	302.7	318.76

The *Chlorella vulgaris* has consumed the maximum quantity of orthophosphates, which is an essential nutrient for microalgae, and it is a crucial component of nucleic acids, ATP (adenosine triphosphate), and phospholipids, playing a vital role in various cellular processes. Adequate phosphorus availability supports the growth, metabolism, and reproduction of *Chlorella vulgaris* cells (Sriwiriyarat and Mukhthong, 2021). The results highlight the dynamic interaction between nutrient availability and microalgae intake consumption, with substantial reduction in orthophosphate and nitrate concentrations that underscore the successful utilization of these nutrients by the microalgae, demonstrating a positive nutrient supply that promotes their growth and biomass productivity (Tavares et al., 2023).

3.2.4 Biomass productivity rate

Biomass productivity results presented in Tables 2, 3, and 4 showed that the biomass productivity in the initial two experiments # 1 and 2 were having gradual increasing; however, it was observed that experiment # 3 with 300 g of intermittent CO_2 was having drastically increasing pattern with respect to cultivation period. The biomass increasing pattern showed from first day of cultivation 113.3, 115.3 to 10th day of cultivation 120.3 to 196.6, 203.4 and 318.7 mg/L respectively.

Though the biomass productivity was not too much, it can be improved by optimizing the microalgae culture's exposure to sunlight and increasing the supply of carbon dioxide, potentially from various exhaust emission sources. This strategic approach aligns with the research's acknowledgment that photoautotrophic species require substantial amounts of carbon to achieve optimal biomass output (Razzak, 2019).

Tabulated results from Experiment # 1 shows that biomass productivity increases over the cultivation time and maximum biomass concentration was found to be 197.5 mg/L, which is significantly lower than the findings of 2nd and 3rd experiments using CO_2 injections. Trial conducted at 200g CO_2 showed a progressive increase in biomass concentration during the cultivation phase.

The microalgae cultivated with ambient air and atmospheric CO_2 enrichment (referred to as atmospheric 0.03% CO_2), showed that the biomass concentration was slightly increased. Additionally, with 300 g of CO_2, the maximum concentration of biomass was obtained, this might be the result of the microalgae cultivated with higher concentration of CO_2 i.e., 300 g (Faruque et al., 2021).

3.3 Statistical analysis on biomass productivity

Tukey's Honest Significant Difference (HSD) test was used in the statistical analysis to determine the significance of differences between pairs of biomass productivity means at day 10 of cultivation period by using Minitab software (version 17) at a significance level of (α=0.05). The statistical analysis was conducted between control sample (experiment # 1) without CO_2 supplied from external source ($\times$1), experiment # 2 with 200 g of CO_2 supplied ($\times$2) and experiment # 3 with 300 g CO_2 supplied ($\times$3) into the photobioreactor cultivation system.

Table 5 showed that the p-value (6.306×10^{-14}) are highly significant and similar with difference between $\times$1 and $\times$3, followed by $\times$2 and $\times$3 as compared to control sample (experiment # 1) i.e., *p=0.0001*. Thus, it can be concluded that supplying CO_2 from external source in experiment # 2 and experiment # 3 have same pattern of statistical significance with co-relationship between two groups of means, having highly significant value with $\times$2 and $\times$3.

Table 5. Tukey HSD test comparative statement of difference of biomass productivity means.

Pair	Difference	SE	Q	Lower CI	Upper CI	Critical Mean	p-value
×1-×2	6.8	0.4679	14.5344	4.7699	8.8301	2.0301	0.0001221
×1-×3	122.5	0.4679	261.833	120.4699	124.5301	2.0301	6.306×10^{-14}
×2-×3	115.7	0.4679	247.2986	113.6699	117.7301	2.0301	6.306×10^{-14}

3.4 Protein and lipid extraction yields

The microalgal biomass sample for protein and lipid extraction was collected, exhibiting the highest biomass productivity. The dried microalgal biomass protein content of 7.98% by weight was obtained using Lowrys method, and lipid yield of 1.87 g/ 5 g of dry biomass was obtained using n-hexane in solvent extraction method. The protein result indicates a relatively lower protein content compared to other studies conducted in the past. This divergence in protein content could be attributed to the experimental parameters employed in this study using ambient air. Unlike most research focused on wastewater; the approach involved utilizing exhaust gases from atmosphere contain substantial quantities of nitrogen oxides. Microalgae's biological elimination of nitrogen oxides is a potential method for converting nitrogen oxides into protein (Lam and Lee, 2012).

In the present case, the atmospheric nitrogen was basically introduced into the photobioreactor with low concentration, which is a macronutrient for microalgae growth and thus lower production of protein was observed. Studies utilizing synthetic medium with the green microalga *Scenedesmus dimorphus* in BG-11 under both indoor and outdoor cultivation settings have been observed in earlier research that *S. dimorphus* may produce cell biomass in outdoor environments with up to 35% protein and 37% total lipid under specific growing conditions. It was successfully demonstrated that the highest yields for protein and carbohydrates were

0.2 and 0.7 g/ L/ day, respectively, and could be obtained in the early stages of cultivation. The highest yield for lipids, 0.17 g /L/day, occurred in a late stage of cultivation. These results were obtained through a combination of manipulating nitrogen availability, light intensity, and cell inoculation density (Çoban et al., 2021). The amount of nitrogen in a culture medium determines the microalgae's cell development rate and biochemical composition. Research showed that nitrogen starvation in a culture medium slows down the cell growth rate of microalgae and reduces protein synthesis by increasing lipid or carbohydrate content (Razzak, 2019).

Table 6. Major fatty acids identified in the extracted lipids.

Name of fatty acid	g/100g Total fatty acids
Myristic (C14:0)	11.39
Palmitic (C16:0)	34.03
Palmitoleic (C16:1)	9.16
Stearic (C18:0)	5.38
Oleic (C18:1n9c)	16.58
Linoleic (C18:2n6c)	4.52
g-linolenic (C18:3n6)	13.23
Euric (C22:1n9)	5.66

3.5 Fatty acids compositional analysis

The microalgae lipids were extracted, and fatty acids compositional analysis was conducted presented in Table 6. The lipid composition was identified to include myristic acid (C14:0), palmitic acid (C16:0), palmitoleic acid (C16:1), oleic acid (C18:1), linoleic acid (C18:1), and linolenic acid (C18:3). This detailed fatty acid profile provides information about the influence on biodiesel fuel properties. It is observed that all the major fatty acids were present in the extracted lipid, having favorable properties to produce microalgal biodiesel.

The literature emphasizes that the presence of long-chain saturated and monounsaturated fatty acids, particularly C18:2 and C18:3, significantly influences biodiesel cetane number, oxidation stability, and iodine content. It is commonly known that the qualities of biodiesel are closely related to the composition of free fatty acids. For example, oleic acid (C18:1) improves cold flow properties, whereas palmitic acid (C16:0) contributes to a lower iodine concentration and a larger cetane number. Additionally, the presence of linoleic acid (C18:2) and linolenic acid (C18:3) is associated with improved combustion properties, contributing to overall better fuel quality. The iodine value, a critical parameter for assessing biodiesel's chemical stability and susceptibility to oxidative rancidity, is significantly influenced by the presence of double-bonded fatty acids. A higher number of double bonds increases the polymerization potential, consequently reducing oxidation stability. This nuanced understanding of the fatty acid composition provides valuable insights into the potential applications and qualities of the biodiesel derived from the microalgae culture (Qie et al., 2019).

3.6 CO_2 injection into photobioreactor system

The intermittent CO_2 injected into the photobioreactor system with a velocity of 25 m/s of CO_2 for Experiment # 2 and Experiment # 3 represented 15 sec and 25 sec respectively. The area of the supply hose pipe was calculated as 2.54×10^{-4} m^2 and CO_2 velocity 25m/s, and the flow rate found was 6.36 $\times$ 10^{-3} m^3/s (using $Q = AV$). Now, this flow rate (Q) is multiplied by dosing time (t) using equation $V = Q \times t$, i.e., 15 sec and 25 sec to get the volume of CO_2 gas introduced into the photobioreactor cultivation system. The mass of CO_2 gas introduced into the photobioreactor tank were 200 g and 300 g, computed by ($D = M/V$) for Experiment # 2 and Experiment # 3 respectively.

3.7 Carbon dioxide (CO_2) bio-fixation by microalgae cultivation

The CO_2 bio-fixation rates (R_{CO_2}) are calculated using Equation 5 for all the three experiments conducted at alternative days. Therefore, in order to calculate the R_{CO_2}, the biomass productivity per day was calculated using the following regression equation obtained from a standard curve:

$$y = 0{,}7015x + 0{,}0362 \quad \left(R^2 = 0{,}9987\right) \tag{9}$$

The% C was assumed as 50% by dry weight of algal biomass as per literature (Scheufele et al., 2019) molecular weight of CO_2 44.01 g/mol and molecular weight of carbon is 12.01 g/mol.

Figure 3 showed that Experiment # 1 has a linear increasing trend in bio-fixation rate during the cultivation days with highest level to 362.07 mg/L/day.

Similarly, experiment # 2 also showed more or less a similar pattern but after 7th day of cultivation it increased to highest level to 374.92mg/L/day until 9th day of cultivation time. This increased level was due to introduction of intermittent CO_2 (200mg) into the photobioreactor for microalgae cultivation. Experiment # 3 showed a drastic increasing trend from 1st to 9th day of cultivation with introduction of 300mg of mass of CO_2 into the photobioreactor system. The lowest and highest level of bio-fixation rate were found to be 220.55 and 586.48 mg/L/day with 1st day and 9th day respectively.

High concentrations of carbon dioxide (CO_2) are essential for photosynthesis and have a direct impact on the growth rates at which microalgae is cultivated. The availability of CO_2 significantly impacts the efficiency of photosynthesis, thereby affecting biomass productivity. As a critical component of photosynthetic reactions, increased levels of CO_2 can enhance the efficiency of this process, ultimately leading to higher rates of biomass production (Wang et al., 2013). In the current study, it was found that introducing less CO_2 for a shorter amount of time causes it to dissolve completely due to the gas-liquid absorption process, whereas introducing more CO_2 for a longer amount of time reduces its ability to dissolve completely because the gas molecules cannot enter into the water molecules, reaching the equilibrium state (Razzak et al., 2024).

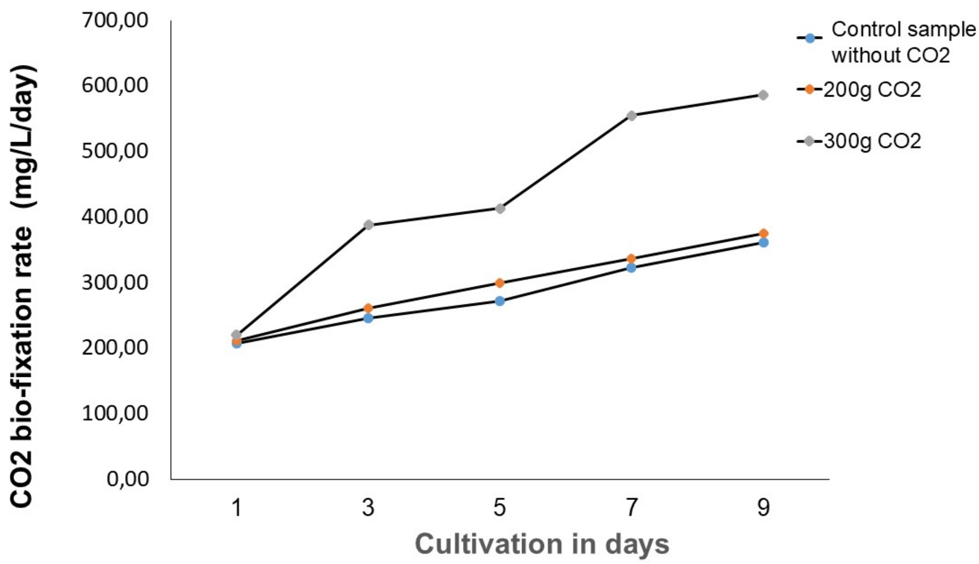

Figure 3. Microalgae CO_2 bio-fixation rate versus cultivation time.

3.8 Kinetic modelling of CO_2 volumetric mass transfer capacity

Multiplying the mass transfer coefficient of oxygen (k) by the surface area of the vessel in a photobioreactor provides an assessment of the system's capacity for both oxygen and carbon dioxide transfer. This combined product reflects the rate at which these gases can efficiently move into the culture medium within the photobioreactor, crucial for supporting the metabolic needs of the algae being cultured. The surface area of a rectangular photobioreactor with dimensions length (47.63 inch), width (12.6 inch) and height (35.43 inch) is calculated as 2734.08 inch^2 (1.763 m^2).

3.8.1 Volumetric Mass Transfer Capacity (k) for Oxygen:

Diffusion coefficient of oxygen in water (D_{O_2}) was 2×10^{-9} m^2 /s and thickness of the boundary layer (δ) is 0.02 meters.

$$k_{O_2} = \frac{2\times10^{-9}\times1{,}763}{0{,}02} = 1{,}763\times10^{-7}\ m^3/s \quad (10)$$

3.8.2 Volumetric Mass Transfer Capacity (k) for Carbon Dioxide:

Diffusion coefficient of carbon dioxide in water (D_{CO_2}) is 1.9×10^{-9} m^2 /s and thickness of the boundary layer (δ) is 0.02 m.

$$k_{CO_2} = \frac{1{,}9\times10^{-9}\times1{,}763}{0{,}02} = 1{,}676\times10^{-7}\ m^3/s \quad (11)$$

The rates at which oxygen and carbon dioxide molecules can move from the gas phase to the liquid phase of the gas-liquid interface are represented by the computed volumetric mass transfer capacity. A greater value denotes a faster gas transfer rate and higher quantity of gas transfer, which is necessary to sustain the algal metabolism, including photosynthesis.

4 Conclusion

This research study included the design and fabrication of an urban photobioreactor operated by solar energy system to cultivate microalgae species of *Chlorella vulgaris* for nutrient removal, biomass production, protein production and CO_2 sequestration. The research included monitoring of cultivation parameters for 10 days cultivation period. Three experimental conditions were compared, and it was found that experiment # 3 was having higher biomass productivity of 318.76 mg/L when introducing 300 g of intermittent CO_2 into cultivation system and nutrients removal efficiencies were 60.78% (orthophosphate) and 58% (nitrate). Statistical analysis found that introducing CO_2 from an external source in experiments # 2 and # 3 resulted in the same pattern of statistical significance, with a co-relationship between two sets of means (p value = 6.306×10^{-14}). The protein and lipid content yields were 7.98% and 37.4% by weight respectively. The O_2 and CO_2 volumetric mass transfer capacities for KO_2 and KCO_2 were 1.763×10^{-7} m^3/s and 1.676×10^{-7} m^3/s respectively.

The average O_2 and CO_2 transfer capability is improved by continuous agitation in a photobioreactor, essential for maintaining optimal conditions for the cultivation of microalgae. The extracted lipids contained favorable qualities of fatty acids for the production of microalgae biodiesel, myristic (C14:0), palmitic (C16:0), palmitoleic (C16:1), oleic (C18:1), linoleic (C18:1), and linolenic acids (C18:3). An urban microalgae photobioreactors is an environmentally friendly strategy that can greatly advance the biobased economy and lessen the damaging impacts of CO_2 produced by conventional fossil fuel combustion on the environment.

Acknowledgments

NED University of Engineering & Technology, Karachi is acknowledged by the authors for providing laboratory facilities and research funds for this research study. This research work was supported through financial grant provided by the Advanced Studies & Research Board, NED University of Engineering & Technology [Reference Number: Acad /50 (48) /4168].

Conflict of interest

The authors declare that they have no relevant conflicts of interest. All co-authors have examined the work and agree with its contents. They have no financial interests to report. Furthermore, the writers affirm that the submission is their original work and is not being reviewed for publication.

Author's contribution

S.K.: Research, methodology and writing original draft. M.A.: Conceptualization, supervision, funding acquisition, formal analysis and editing. A.M.: Writing -reviewing and editing. A.I.: Writing and data processing.

References

Ali, M., Masood, A., and Saleem, M. (2021). Microalgae cultivation in wastewater for simultaneous nutrients removal and biomass production. *International Journal of Energy and Environmental Engineering*, 12:475–485. Online:https://n9.cl/answax.

Amaral, A., Gillot, S., Garrido-Baserba, M., Filali, A., Karpinska, A., Plósz, B., De Groot, C., Bellandi, G., Nopens, I., and Takács, I. (2019). Modelling gas-liquid mass transfer in wastewater treatment: when current knowledge needs to encounter engineering practice and vice versa. *Water science and technology*, 80(4):607–619. Online:https://n9.cl/5vgwj.

APHA (2005). *Standard Methods for the Examination of Water and Wastewater*. American Public Health Association/American Water Works Association/Water Environment Federation, 21st edition edition.

Barghbani, R., Rezaei, K., and Javanshir, A. (2012). Investigating the effects of several parameters on the growth of chlorella vulgaris using taguchi's experimental approach. *International Journal of Biotechnology for Wellness Industries*, 1(2):128. Online:https://n9.cl/iohjx.

Borowitzka, M. (1999). Commercial production of microalgae: ponds, tanks, tubes and fermenters. *Journal of biotechnology*, 70(1-3):313–321. Online:https://n9.cl/shstm.

Brindhadevi, K., Mathimani, T., Rene, E., Shanmugam, S., Chi, N., and Pugazhendhi, A. (2021). Impact of cultivation conditions on the biomass and lipid in microalgae with an emphasis on biodiesel. *Fuel*, 284:119058. Online:https://n9.cl/9isnj.

Çoban, A., Şimşek, G., and Çetin, A. (2021). Effect of nitrogen source on growth and protein and lipid amounts of a freshwater microalga scenedesmus acutus. *Turkish Journal of Science and Technology*, 16(2):215–220. Online:https://n9.cl/m9igzn.

Faruque, M., Mohammed, K., Hossain, M., and Razzak, S. (2021). Influence of elevated co2 concentrations on growth, nutrient removal, and co2 biofixation using chlorella kessleri cultivation. *International Journal of Environmental Science and Technology*, 18:913–926. Online:https://n9.cl/qhk2pc.

Gaurav, K., Neeti, K., and Singh, R. (2024). Microalgae-based biodiesel production and its challenges and future opportunities: A review. *Green Technologies and Sustainability*, 2(1):100060. Online:https://n9.cl/znc4x.

Lam, M. and Lee, K. (2012). Microalgae biofuels: a critical review of issues, problems and the way forward. *Biotechnology advances*, 30(3):673–690. Online:https://n9.cl/w9fok.

Leflay, H., Pandhal, J., and Brown, S. (2021). Direct measurements of co2 capture are essential to assess the technical and economic potential of algalccus. *Journal of CO2 Utilization*, 52:101657. Online:https://n9.cl/ng2a3.

Mahapatra, S., Kumar, D., Singh, B., and Sachan, P. (2021). Biofuels and their sources of production: A review on cleaner sustainable alternative against conventional fuel, in the framework of the food and energy nexus. *Energy Nexus*, 4:100036. Online:https://n9.cl/8wa5y.

Morales, M., Sánchez, L., and Revah, S. (2018). The impact of environmental factors on carbon dioxide fixation by microalgae. *FEMS microbiology letters*, 365(3):fnx262. Online:https://n9.cl/h6rnz.

Nezammahalleh, H., Ghanati, F., Adams, T., Nosrati, M., and Shojaosadati, S. (2016). Effect of moderate static electric field on the growth and metabolism of chlorella vulgaris. *Bioresource technology*, 218:700–711. Online:https://n9.cl/5rotd.

Qie, F., Zhu, J., Rong, J., and Zong, B. (2019). Biological removal of nitrogen oxides by microalgae, a promising strategy from nitrogen oxides to protein production. *Bioresource technology*, 292:122037. Online:https://n9.cl/fmenw.

Razzak, S. (2019). In situ biological co2 fixation and wastewater nutrient removal with neochloris oleoabundans in batch photobioreactor. *Bioprocess and biosystems engineering*, 42(1):93–105. Online:https://n9.cl/yq31m7.

Razzak, S., Bahar, K., Islam, K., Haniffa, A., Faruque, M., Hossain, S., and Hossain, M. (2024). Microalgae cultivation in photobioreactors: Sustainable solutions for a greener future. *Green Chemical Engineering*, 5(4):418–439. Online:https://n9.cl/2lhn0.

Rehman, M., Kesharvani, S., Dwivedi, G., and Suneja, K. (2022). Impact of cultivation conditions on microalgae biomass productivity and lipid content. *Materials Today: Proceedings*, 56:282–290. Online:https://n9.cl/nl31us.

Rodionova, M., Poudyal, R., Tiwari, I., Voloshin, R., Zharmukhamedov, S., Nam, H., Zayadan, B., Bruce, B., Hou, H., and Allakhverdiev, S. (2017). Biofuel production: challenges and opportunities. *International Journal of Hydrogen Energy*, 42(12):8450–8461. Online:https://n9.cl/0xwr4.

Saratale, R., Ponnusamy, V., Jeyakumar, R., Sirohi, R., Piechota, G., Shobana, S., Dharmaraja, J., Lay, C.-H., Saratale, G., and Shin, H. (2022). Microalgae cultivation strategies using cost–effective nutrient sources: Recent updates and progress towards biofuel production. *Bioresource Technology*, 361:127691. Online:https://n9.cl/srjve.

Scheufele, F., Hinterholz, C., Zaharieva, M., Najdenski, H., Módenes, A., Trigueros, D., Borba, C., Espinoza-Quiñones, F., and Kroumov, A. (2019). Complex mathematical analysis of photobioreactor system. *Engineering in life sciences*, 19(12):844–859. Online:https://n9.cl/xtk4h.

Shuler, M. and Kargi, F. (2002). *Bioprocess Engineering- Basic Concepts*. Prentice-Hall, second edition edition.

Sievert, K., Cameron, L., and Carter, A. (2023). Why the cost of carbon capture and storage remains persistently high. Online:https://n9.cl/grhfk.

Sriwiriyarat, T. and Mukhthong, M. (2021). The feasibility study of using microalgae for polishing consumer-products industrial effluent containing high total dissolved solids. *Thai Environmental Engineering Journal*, 35(1):1–14. Online:https://n9.cl/9kjzb.

Stojiljković, D. and Spasojević, I. (2023). Urban photo-bioreactor liquid3. Green Product Award. Online:https://n9.cl/xx5ch.

Tavares, L., Nudi, M., Arroyo, P., Godoy, R., and Trevisan, E. (2023). Effect of different concentrations of phosphorus and nitrogen on the growth of the microalgae chlorella vulgaris. *International Journal of Energy and Environmental Engineering*, 14(4):563–572. Online:https://n9.cl/vmaxgx.

United Nations (2024). Causes and effects of climate change. United Nations. Online:https://n9.cl/nij3r.

Valavanidis, A. (2023). Extreme weather events exacerbated by the global impact of climate change. glimpse of the future, if climate change continues unabated. Online:https://n9.cl/5nffq.

Wang, L., Li, Y., Sommerfeld, M., and Hu, Q. (2013). A flexible culture process for production of the green microalga scenedesmus dimorphus rich in protein, carbohydrate or lipid. *Bioresource Technology*, 129:289–295. Online:https://n9.cl/ghase.

Yen, H., Ho, S., Chen, C., and Chang, J. (2015). Co2, nox and sox removal from flue gas via microalgae cultivation: A critical review. *Biotechnology journal*, 10(6):829–839. Online:https://n9.cl/dy725.

LA GRANJA:
REVISTA DE
CIENCIAS DE LA VIDA
pISSN:1390-3799; eISSN:1390-8596
https://doi.org/10.17163/lgr.n41.2025.07

Scientific paper/ Artículo científico
BIOTECHNOLOGY

IDENTIFICATION OF AN ANTIMICROBIAL PEPTIDE FROM *CHAMAEMELUM NOBILE*

IDENTIFICACIÓN DE UN PÉPTIDO ANTIMICROBIANO DE *CHAMAEMELUM NOBILE*

Diana Daniela Portela Dussán[1], Sandra Mónica Estupiñan Torres[2] and Silvio Alejandro Lopez-Pazos[1]*

[1]*Faculty of Sciences, Universidad Antonio Nariño, Carrera 3 Este 47A-15, Bogotá D.C., Colombia.*
[2]*Faculty of Health Sciences, Universidad Colegio Mayor de Cundinamarca, Calle 28 No. 5B-02 Bogotá D.C., Colombia.*

*Corresponding author: alejandrolopezpazos@uan.edu.co

Received on on July 14th, 2023. Accepted, after revision on April 2nd, 2024. Published on March 1st, 2025.

Abstract

Chamaemelum nobile, or Roman chamomile, is a plant containing anti-inflammatory and antimicrobial properties. Antimicrobial peptides (AMPs) are part of the plant defense system including lipid transfer peptides (LPTs). Our objective is to identify a LTP-related protein from *C. nobile* (cnLTP). PCR was performed on *C. nobile* DNA for identifying cnLTP gene. Bioinformatics was used for their characterization, and a sensitivity test was carried out on *Rhizoctonia solani*. cnLTP has 99 amino acids, 9.8 kDa, isoelectric point of 9.39, 33 aliphatic residues, aliphatic index of 85, hydropathicity of 0.127, four alpha-helices and four disulfide bridges. An inhibitory activity of apoplastic fluid of *C. nobile* was determined at 1 μg/mL on *R. solani*. This study contributes in the knowledge of a novel and non-characterized LTP using *in silico* and experimental related approaches.

Keywords: Roman chamomile, Antimicrobial peptide, Lipid transfer protein, *Rhizoctonia solani*.

Resumen

Chamaemelum nobile, o manzanilla romana, es una planta que contiene propiedades antiinflamatorias y antimicrobianas. Los péptidos antimicrobianos (AMP) son parte del sistema de defensa de las plantas, que incluye a los péptidos de transferencia de lípidos (LPT). Nuestro objetivo es identificar una proteína relacionada con LTP de *C. nobile* (cnLTP). Se realizó la PCR sobre el ADN de *C. nobile* para la identificación del gen cnLTP; se utilizó bioinformática para su caracterización, y una prueba de sensibilidad contra *Rhizoctonia solani*. cnLTP tiene 99 aminoácidos, 9,8 kDa, punto isoeléctrico de 9,39, 33 residuos alifáticos, índice alifático de 85, hidropaticidad de 0,127, cuatro hélices alfa y cuatro puentes disulfuro. Se encontró que el fluido apoplásico de *C. nobile* (1 μg/mL) inhibe el desarrollo de *R. solani*. Este estudio contribuye al conocimiento de un LTP novedoso y no caracterizado, utilizando enfoques *in silico* y experimentales.

Palabras clave: Manzanilla romana, péptido antimicrobiano, proteína de transferencia de lípidos, *Rhizoctonia solani*.

Suggested citation: Portela Dussán, D., Estupiñan Torres, S. and Lopez-Pazos, S. (2025). Identification of an antimicrobial peptide from *Chamaemelum nobile*. *La Granja: Revista de Ciencias de la Vida.* Vol. 41(1):112-120. https://doi.org/10.17163/lgr.n41.2025.07.

Orcid IDs:

Diana Daniela Portela Dussán: https://orcid.org/0000-0003-2949-7033
Sandra Mónica Estupiñan Torres: https://orcid.org/0000-0002-6937-4567
Silvio Alejandro Lopez-Pazos: https://orcid.org/0000-0002-3682-4162

1 Introduction

Pathogenesis-related proteins (PR) can be detected at the basal level in healthy tissues of plants, but increase their presence under the attack of pathogens. PRs activation may only begin after a phase of plant-pathogen interaction from recognition of molecular patterns associated with microorganisms (PAMPs) by recognition receptors of these patterns (PRR) present on the cell membrane of plants, or through the recognition of elicitors as nucleotide binding domain and leucine-rich repeat (NB-LRR) proteins. The concentration of PRs increases with the transduction of chemical signals as salicylic acid, ethylene and jasmonic acid during the first activation stage of defense mechanisms (Zhou and Zhang, 2020; Boyd et al., 2013). Antimicrobial peptides (AMPs) are one part of PRs, which have a molecular weight of less than 10 kDa and *in vitro* antimicrobial activity. AMPs are produced by microorganisms, animals and plants as defense mechanism against pathogens (Bin Hafeez et al., 2021).

AMPs comprise less than 200 amino acids are expressed constitutively and are inducible in susceptible tissues as leaf primordia, stomata and epidermis, e.g., it was evidenced in *Nicotiana megalosiphon* which after inoculation with *Peronospora hyoscyami* sp. *tabacina* over expressed in leaves a defensin gene, or *Brassica oleracea* inoculated with *Xanthomonas campestris* pv. *campestris* expressed on stem and leaves AMPs genes, and it was also observed that pepper inoculated with *X. campestris* pv. *vesicatory* caused high transcription in a CaAMP1 gene, and their expression generates tolerance to *Phytophthora sojae* (Sharma et al., 2022; Niu et al., 2020; Jiang et al., 2011; Portieles et al., 2010). It has been evidenced that cationic AMPs as alpha/beta thionins, defensins and lipid transfer peptides (LTPs) interact with anionic groups of the phospholipid bilayer in microorganisms. It also forms micelles to allow ion flow to the extracellular space with osmotic decompensation, cell lysis and death (Kovaleva et al., 2020).

Anionic AMPs, e.g., cyclotides, interact with the cytoplasmic membrane of pathogens through electrostatic forces between polar residues of an AMP and hydrophilic heads of phospholipids through recognition of the chiral glycerol backbone. The electrostatic force of this complex junction is determined by an ionic interaction between the ammonium group of phosphatidylethanolamine and the carboxyl group of a conserved glutamate from loop 1 of the AMP (Venkatesan and Roy, 2023; Troeira Henriques and Craik, 2017). The permeabilization suffered by the cytoplasmatic membrane in the microorganism/AMP interaction is not clear. Four possible mechanisms have been described: (i) it comprises peptide helices that form a bundle in the membrane with a central lumen; (ii) AMPs accumulate on the surface of a lipid bilayer interacting with the hydrophilic heads of phospholipids and covering the membrane like a carpet causing disorganization of the lipid bilayer; (iii) AMPs are inserted into the membrane, forming a pore and inducing continuous bending of the lipid monolayer, orienting the hydrophobic surface of the membrane towards the outside and the hydrophilic surface inwards, forming an aqueous channel with loss of polarity; (iv) AMP causes a competitive displacement of Ca2+ and Mg2+ (Boparai and Sharma, 2020; Li et al., 2012).

Roman chamomile *Chamaemelum nobile* (L.) is an aromatic perennial herb. The plant has a branched and elongated stem with a height ranging from 20 to 30 cm, which supports a floral head, formed by white leaves with segmented ligules and well-defined leaflets. It grows at temperate areas, and it is adaptable and used on several types of acidic soils with enough water. *C. nobile* contains some 0.24 - 1.9% volatile oils and 120 secondary metabolites, including flavonoids (quercetin, luteolin, apigenin, patuletine), alpha-bisabolol and bisabolol oxides A and B, azulenes (chamazulene), monoterpenes (alpha-pinene), sesquiterpenes (farnesene), coumarins (herniarina and umbelliferone). Its composition allows recognizing therapeutic properties (anti-inflammatory, spasmolytic, sedative, antioxidant, anticoagulant, antihyperlipidemic, repellent and antimicrobial). World production of *C. nobile* is over 1000 tonnes/year. To produce 0.8 - 1.5% of essential oils, 800 kg of floral stem/ha is used. Phenolic compounds and alkanes can be obtained from seed, fruit, or roots. *C. nobile* oils are effective *in vitro* against *Staphylococcus aureus* (0.1 mg/mL), *Escherichia coli* (0.1 mg/mL), *Bacillus subtilis* (0.05 mg/mL), *Pseudomonas aeruginosa* (12.5 and 25 mg/mL), *P. tolaasii* (300 mg/mL), *Candida albicans* (0.1 mg/mL), and fungi as *Aspergillus candidus*, *Penicillium* sp., *Fusarium culmorum* and *A. niger* (900 mg/mL) (Ghaedi et al., 2015; Kazemian et al., 2015; Srivastava et al., 2010; Saderi et al., 2005).

The aim of this research is to find a cationic AMP from *C. nobile* (named cnLTP) focused on attempting to identify the DNA sequence of a LTP. The parameters were bioinformatics and molecular tests, and evaluation on *Rhizoctonia solani*, a potato pathogen.

2 Materials and methods

2.1 *C. nobile* culture

Commercial Roman chamomile seeds were used in a propagation medium (Murashige and Skoog Salt and Vitamin Mixture (MS) supplemented with 20 mg/L sucrose, 0.1 mg/L, benzylaminopurine (BAP), 0.5 mg/L naphthaleneacetic Acid (NAA), 0.25 mg/L gibberellic acid (GA3). The seeds were maintained in a condition of constant temperature (20 °C) and humidity (70%).

2.2 PCR for detection of cnLTP gene

For DNA extraction, *C. nobile* leaves from *in vitro* plantlets were dipped in a tube containing lysis buffer (200 mM Tris HCl pH 7.5, 250 mM NaCl, 25 mM EDTA, 0.5% SDS), precipitation solution (isopropanol) and 1X TE buffer as diluent (Edwards et al., 1991). PCR was carried out using l X PCR buffer, 2.5 mM $MgCl_2$, 0.2 mM dNTPs, 0.4 μM of each primer and 0.2 U Taq DNA polymerase. Thermo cycle condition was a denaturation step at 95 °C for 5 min, 30 cycles consisting of denaturation (95 °C × 1 min), annealing (50 °C × 1 min), extension (72 °C × 1 min), and an final extension (72 °C × 5 min).

The PCR products were determined using 1.2% agarose electrophoresis, and sequenced (Macrogen, USA). The forward and reverse primers for LTP were 5'-GACTGCTCAACGGTTCAGTAAAGTTGA-3', and 5'-TCAACTTTACTGAACCGTTGAGCAGTC-3' respectively (Rojas, 2010). The obtained sequence data was deposited in GenBank (ID: MT294300).

2.3 *In silico* characterization of cnLTP

Nucleotide sequence of the cnLTP was employed to find its amino acid sequence, using Translate from Expasy server (http://web.expasy.org/translate/) (Artimo et al., 2012). To predict the feasible role of the AMP, a comparative analysis was completed using BLASTp (http://www.ncbi.nlm.nih.gov/BLASTp/) (Shah et al., 2018). The biochemical annotation of the cnLTP was done using ProtParam to find similar sequences in protein databases (https://web.expasy.org/protparam/) (Artimo et al., 2012). The homology modeling of the cnLTP was performed using I-TASSER server (https://zhanglab.ccmb.med.umich.edu/I-TASSER/) (Zhang, 2009). The best hit obtained on cnLTP annotation was found to LTP from *Nicotiana tabacum* and was taken as a template (PDB ID: 1T12A; 73% identity, 91% of query coverage; E-value of 7e-43). Figures were done by DeepView (https://spdbv.vital-it.ch/) (Johansson et al., 2012).

2.4 Susceptibility test for *R. solani* using *C. nobile* apoplastic fluid

Apoplast washing fluid (AWF) from *C. nobile* was extracted from leaves (Butt et al., 2019; Gentzel et al., 2019). Mature leaves (1 g) were first rinsed using sterile ddH_2O to remove cytoplasmic exudes from damage cells, and the fresh weight was then determined. Leaf segments were infiltrated in a bottle containing 250 mL of sterile ddH_2O at 4 °C and vacuum pressure of 20 kPa, which allows the air to escape and to facilitate the flow of water into the intercellular space, washing the AWF molecules. Once the pressure method was completed, the bottle was shaken slowly until it released air and vacuum to both reduce cell lysis and avoid cytoplasmic contamination.

The vacuum pressure was repeated until the leaves were completely infiltrated, its color turning to dark. The AWF was recovered from leaf segments dried with soft laboratory paper and wrapped in parafilm, and were centrifuged at 4 °C, 10000 rpm for 10 min. The Bradford assay was used to measure protein concentration (Bradford, 1976). Quality assessment for AWF peptides was performed by tricine-SDS-PAGE. The preliminary evaluation on the biological activity of the AWF on *R. solani* already completed by using 10 cm of the mycelium that was grown in PDA medium, and AWF lanes were added to each side and extended beyond the ends of the existing fungal structure on a gradually decreasing basis, using concentrations of 0.1 μg/mL - 1 μg/mL.

A suspension of *P. aeruginosa* strain PAO1 was used as a positive control (negative control - water instead of AWF as sample, data not shown). *R. solani* was incubated for five days at 30 °C. The effect of AWF proteins on *R. solani* was measured by the displacement of the mycelium situated in the Petri dish.

3 Results

Roman chamomile seeds were cultured in a MS medium supplemented with growth hormones to object of induce germination and growth of seedlings suitable for extracting genomic DNA. PCR identified a 300 pb product that could be determined by sequencing. This sequence was compared with the nucleotides entries recorded in the GenBank database using BLAST program (Shah et al., 2018). The DNA sequence (297 pb) had close linkage with tomato LTPs (identity 96%, E value 4e-57, coverage 96%, NCBI). This knowledge, in turn, enables deduction of the cnLTP sequence (99 residues) that the DNA then encodes. It only contains coding DNA sequences for mature peptide without signal peptide or polyadenylation site. The sequence of amino acids in the cnLTP, and hence protein function, is determined by eight C residues that are linked in four disulfide bonds (Figure 1A).

The theoretical molecular weight of cnLTP is 9.8 kDa, its isoelectric point is 9.39. In addition, the peptide is made up of 33 aliphatic residues (A, V, I, and L), and the aliphatic index of the cnLTP is 85. This index determines the volume occupied by aliphatic side chains, 12 positively charged residues given the cationic conformation of the cnLTP at neutral pH, and three negatively charged residues. The hydropathicity is 0.127, which indicates the presence of a hydrophobic cavity where interaction with lipids also takes place. cnLTP is made up of four alpha-helices. The first helix (P2-Q24) presents a H1A structure (P2-S5) formed by two folds in His3 and Gly4, and H1B (P18-L23) formed by four folds in Q11, G15, C19 and Y22. The second helix H2 (C32-L39) contains three folds in R34, G35, L39. The third helix H3 (P46-A62) comprises seven folds in D48, K50, A52, T54, L56, K57, A59, and N61. The fourth helix H4 (L68-C78) encloses a fold in G69, I74 and S76. The four alpha-helices are connected by three short loops, L1 (G25-G31), L2 (L40-T45) and L3 (I63-N67) (Figure 1B).

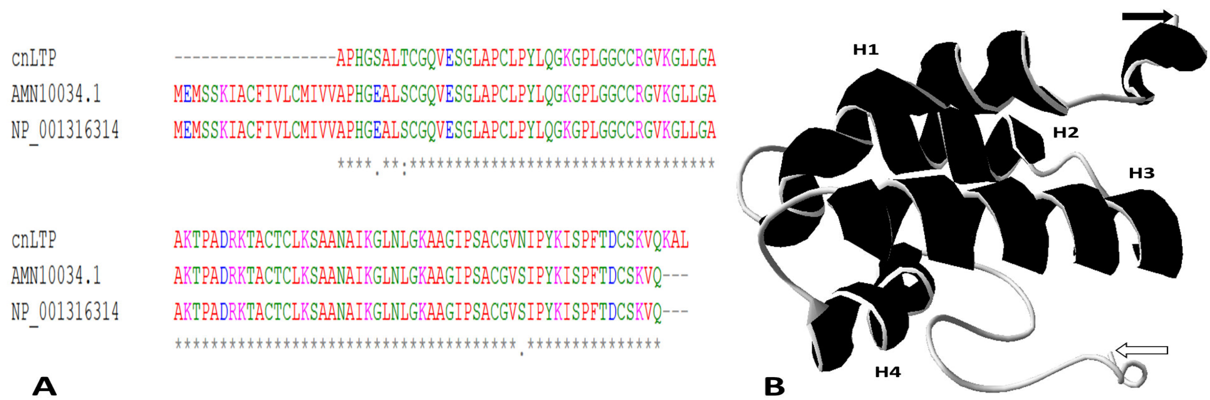

Figure 1. Structure of cnLTP. A. Alignment of two LTPs of tomato against cnLTP associated with physicochemical properties according to Clustal Omega (Sievers and Higgins, 2014): red is small plus hydrophobic (together with aromatic -Y), blue is acidic, magenta is basic – H, green is hydroxyl plus sulfhydryl plus amine plus G, gray corresponding to unusual amino and imino acids. B. 3D model of cnLTP, black arrow indicates the N-terminal, white arrow shows the C-terminal. Helices are indicated and colored in black.

cnLTP is stabilized by four disulfide bridges formed among C9-C33, C19-C55, C32-C78 and C53-C92, which were calculated throughout DISULFIND (http://disulfind.dsi.unifi.it/) (Ceroni et al., 2006). cnLTP has 50 hydrophobic residues: A, V, L, I, P, F and C, most of them are found inside of the peptide, forming a hydrophobic cavity which is a characteristic of AMPs (Li et al., 2012).

Biological evaluation of *C. nobile* apoplastic fluid was carried out considering the protein concentration (2.37 mg/mL), as well as the intrinsic presence of low molecular weight peptides of approximately 10 kDa, indicating that there are LTPs (Figure 2A). Antagonism tests indicated an inhibitory effect on *R. solani* at a concentration of 1 μg/mL (Figure 2B-2C).

4 Discussion

Peptides allow the bacteria to evade the host defense and proliferate by preventing cell signaling, cell migration and can even kill response cells directly. Peptides have complicated damage mechanisms on cell membranes (rupture), protein synthesis (inhibition), second messengers (activation), or a defense response (activation) (Yang and Yousef, 2018). It has been suggested that a specific biochemical characterization focused on specific biological activity, or a computer system-assisted design are relevant ways for the new biotechnological options discovery (Rondon-Villarreal and Pinzon-Reyes, 2018).

For LTPs, a signal sequence is responsible for directing the peptide towards the cytoplasmic membrane where it is cleaved at the N-terminus by an aminopeptidase, and the mature peptide is exported to the intercellular space where it exerts its biological activity (Pagnussat et al., 2012). The mature cnLTP has a conserved substitution (T-S), plus two semi-conserved substitutions (E-S, N-S). It has been reported that the conservation for S phosphorylation site (which could be exchanged with phosphorylatable T or E) would become one of the key residues to protein folding (Pearlman et al., 2011). The presence of the hydrophobic cavity is essential in the LTPs family, because it allows for binding and transferring lipids, e.g., a LTP from wheat, which had a hydrophobic cavity able to attract prostaglandin B2 and mobilize between microsomal fractions and mitochondria. The LTP hydrophobic cavity can be attached to saturated fatty acids (12–19 carbon atoms), unsaturated FAs of different chain length (16–18 carbon atoms) and geometry of unsaturation, lysolipids (14–16 carbon atoms), and jasmonic acid (Melnikova et al., 2016; Tassin-Moindrot et al., 2000).

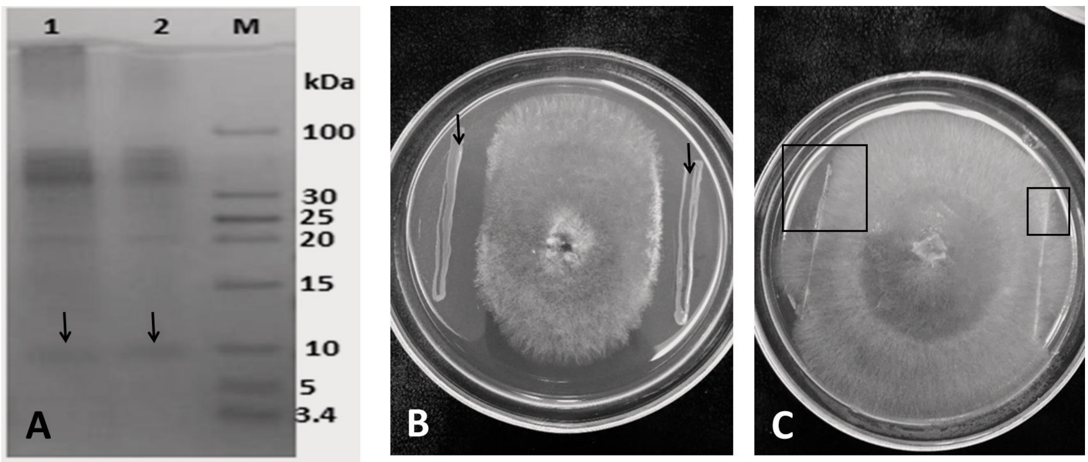

Figure 2. Bioassay of *C. nobile* AWF on *R. solani*. A. Tricine SDS-PAGE showed a band of 10 kDa related to LTPs in *C. nobile* AWF (lines 1 and 2, M is molecular weight marker). B. Positive control contained lanes with suspension of *P. aeruginosa* strain PAO1 (black arrows). C. *R. solani* mycelium with *C. nobile* AWF lanes to each side, which were gradually being extended on the medium; the squares showed inhibition areas.

LTPs are divided into two groups according to their molecular weight and structural conformation: (i) type 1 (9 -10 kDa) are made up of four alphahelices, characterized by having inhibitory activity on phytopathogens, (ii) type 2 (7.0 kDa) are made up of four alpha-helices, this type of peptides did not show inhibitory activity on plant pathogens (Finkina et al., 2016). cnLTP belongs to the LTP type

1 because of molecular weight (9.8 kDa) and its four alpha-helices. LTPs have biological activity against bacteria and fungi as *Clavibacter michiganensis, P. solanacearum, P. syringae, Alternaria brassicola, Ascochyta pisi, Colletotrichum lindemuthianum, F. solani, F. graminearum, F. culmorum, F. oxysporum, Botrytis cinerea, Sclerotinia sclerotiorum, Verticillium dahliae* (Finkina et al., 2016). Antagonism tests indicated an inhibitory effect of *C. nobile* AWF on *R. solani*, which has been verified and is as objective as possible, e.g., antimicrobial activity of oils of *C. nobile* has been evaluated on *Penicillium* sp., and *Aspergillus* sp. (Sharifzadeh et al., 2016). The location of a LTP in cell wall and their externalization toward the intercellular space by a signal sequence has suggested its presence in apoplastic fluid, as evidenced in *Arabidopsis thaliana*, *B. oleracea*, *Ricinus communis* and *Vigna unguiculata* (Missaoui et al., 2022). Two LTPs (IWFI and IWFI2) were isolated from intercellular washing fluid of *Beta vulgaris* with antifungal activity on *Cercospora beticola*, demonstrating their presence in AWF (Nielsen et al., 1996). I-TASSER can tell us how the cnLTP interact with cellular components, so cnLTP can be chemically attached to palmitic acid since it is also covers 30 % of all phospholipids (Carta et al., 2017).

5 Conclusions

This project explored the problem of identifying and characterizing a novel AMPs from *C. nobile*. It was possible to find relevant features of cnLTP (e.g., hydrophobic cavity or disulfide bridges), as well as to assess its activity on *R. solani*. Finally, medicinal plants as *C. nobile* may be a source of interesting AMPs to be used in Biotechnology, because they hold keys to improved synthesis of new or improved molecules by creating conditions for its successful adaptation.

Acknowledgements

This work was funded by the Universidad Antonio Nariño (project 2022207) and Universidad Colegio Mayor de Cundinamarca (Agreement 081 of 2020).

Author Contribution

DDPD; Conceptualization, investigation, data processing, visualization, writing the original draft. SMET; Project administration. SALP; Conceptualization, investigation, project administration, data processing, visualization, writing the original draft, writing-review and editing.

References

Artimo, P., Jonnalagedda, M., Arnold, K., Baratin, D., Csardi, G., De Castro, E., Duvaud, S., Flegel, V., Fortier, A., Gasteiger, E., Hernandez, C., Ioannidis, V., Kuznetsov, D., Liechti, R., Moretti, S., Mostaguir, K., Redaschi, N., Rossier, G., Xenarios, I., and Stockinger, H. (2012). Expasy: Sib bioinformatics resource portal. *Nucleic acids research*, 40(W1):W597–W603. Online:https://n9.cl/6qsqz.

Bin Hafeez, A., Jiang, X., Bergen, P., and Zhu, Y. (2021). Antimicrobial peptides: an update on classifications and databases. *International journal of molecular sciences*, 22(21):11691. Online:https://n9.cl/7j3e1.

Boparai, J. and Sharma, P. (2020). Mini review on antimicrobial peptides, sources, mechanism and recent applications. *Protein and peptide letters*, 27(1):4–16. Online:https://n9.cl/7ca86.

Boyd, L., Ridout, C., O'Sullivan, D., Leach, J., and Leung, H. (2013). Plant-pathogen interactions: disease resistance in modern agriculture. *Trends in genetics*, 29(4):233–240. Online:https://n9.cl/mzus9.

Bradford, M. (1976). A rapid and sensitive method for the quantitation of microgram quantities of protein utilizing the principle of protein-dye binding. *Analytical biochemistry*, 72(1-2):248–254. Online:https://n9.cl/dtt6o.

Butt, U., Naz, R., Nosheen, A., Yasmin, H., Keyani, R., Hussain, I., and Hassan, M. (2019). Changes in pathogenesis-related gene expression in response to bioformulations in the apoplast of maize leaves against fusarium oxysporum. *Journal of Plant Interactions*, 14(1):61–72. Online:https://n9.cl/47u486.

Carta, G., Murru, E., Banni, S., and Manca, C. (2017). Palmitic acid: physiological role, metabolism and nutritional implications. *Frontiers in physiology*, 8:902. Online:https://n9.cl/u84aoj.

Ceroni, A., Passerini, A., Vullo, A., and Frasconi, P. (2006). Disulfind: a disulfide bonding state and cysteine connectivity prediction server. *Nucleic acids research*, 34(Web Server issue. Online:https://n9.cl/n0oc5):W177–W181.

Edwards, K., Johnstone, C., and Thompson, C. (1991). A simple and rapid method for the preparation of plant genomic dna for pcr analysis. *Nucleic acids research*, 19(6):1349. Online:https://bit.ly/3UFvZb8.

Finkina, E., Melnikova, D., and Bogdanov, I. (2016). Lipid transfer proteins as components of the plant innate immune system: structure, functions, and applications. *Acta Naturae*, 8(2):47–61. Online:https://n9.cl/6pyyvl.

Gentzel, I., Giese, L., Zhao, W., Alonso, A., and Mackey, D. (2019). A simple method for measuring apoplast hydration and collecting apoplast contents. *Plant Physiology*, 179(4):1265–1272. Online:https://n9.cl/cd1nud.

Ghaedi, M., Naghiha, R., Jannesar, R., and Mirtamizdoust, B. (2015). Antibacterial and antifungal activity of flower extracts of urtica dioica, chamaemelum nobile and salvia officinalis: Effects of $Zn[OH]_2$ nanoparticles and hp-2-minh on their property. *Journal of Industrial and Engineering Chemistry*, 32:353–359. Online:https://n9.cl/5rvne.

Jiang, H., Song, W., Li, A., Yang, X., and Sun, D. (2011). Identification of genes differentially expressed in cauliflower associated with resistance to xanthomonas campestris pv. campestris. *Molecular biology reports*, 38:621–629. Online:https://n9.cl/djhw6.

Johansson, M., Zoete, V., Michielin, O., and Guex, N. (2012). Defining and searching for structural motifs using deepview/swiss-pdbviewer. *BMC bioinformatics*, 13:1–11. Online:https://n9.cl/gog0w7.

Kazemian, H., Ghafourian, S., Heidari, H., Amiri, P., Yamchi, J., Shavalipour, A., Houri, H., Maleki, A., and Sadeghifard, N. (2015). Antibacterial, anti-swarming and anti-biofilm formation activities of chamaemelum nobile against pseudomonas aeruginosa. *Revista da Sociedade Brasileira de Medicina Tropical*, 48:432–436. Online:https://n9.cl/w42wgt.

Kovaleva, V., Bukhteeva, I., Kit, O., and Nesmelova, I. (2020). Plant defensins from a structural perspective. *International Journal of Molecular Sciences*, 21(15):5307. Online:https://n9.cl/rs0vj.

Li, Y., Xiang, Q., Zhang, Q., Huang, Y., and Su, Z. (2012). Overview on the recent study of antimicrobial peptides: origins, functions, relative mechanisms and application. *Peptides*, 37(2):207–215. Online:https://n9.cl/lmj10.

Melnikova, D., Mineev, K., Finkina, E., Arseniev, A., and Ovchinnikova, T. (2016). A novel lipid transfer protein from the dill anethum graveolens l.: isolation, structure, heterologous expression, and functional characteristics. *Journal of Peptide Science*, 22(1):59–66. Online:https://n9.cl/p1gau.

Missaoui, K., Gonzalez-Klein, Z., Pazos-Castro, D., Hernandez-Ramirez, G., Garrido-Arandia, M., Brini, F., Diaz-Perales, A., and Tome-Amat, J. (2022). Plant non-specific lipid transfer proteins: An overview. *Plant Physiology and Biochemistry*, 171:115–127. Online:https://n9.cl/gyqyk.

Nielsen, K., Nielsen, J., Madrid, S., and Mikkelsen, J. (1996). New antifungal proteins from sugar beet (beta vulgaris l.) showing homology to non-specific lipid transfer proteins. *Plant Molecular Biology*, 31:539–552. Online:https://n9.cl/pvxezo.

Niu, L., Zhong, X., Zhang, Y., Yang, J., Xing, G., Li, H., Liu, D., Ma, R., Dong, Y., and Yang, X. (2020). Enhanced tolerance to phytophthora root and stem rot by over-expression of the plant antimicrobial peptide caamp1 gene in soybean. *BMC genetics*, 21:1–10. Online:https://n9.cl/f9rr6r.

Pagnussat, L., Burbach, C., Baluška, F., and de la Canal, L. (2012). An extracellular lipid transfer protein is relocalized intracellularly during seed germination. *Journal of experimental botany*, 63(18):6555–6563. Online:https://n9.cl/i93pf.

Pearlman, S., Serber, Z., and Ferrell, J. (2011). A mechanism for the evolution of phosphorylation sites. *Cell*, 147(4):934–946. Online:https://n9.cl/lh5n4.

Portieles, R., Ayra, C., Gonzalez, E., Gallo, A., Rodriguez, R., Chacon, O., Lopez, Y., Rodriguez, M., Castillo, J., and Pujol, M. (2010). Nmdef02, a novel antimicrobial gene isolated from nicotiana megalosiphon confers high-level pathogen resistance under greenhouse and field conditions. *Plant biotechnology journal*, 8(6):678–690. Online:https://n9.cl/f12lm.

Rojas, A. (2010). Identificación de genes tipo péptido antimicrobiano provenientes de solanum lycopersicum var. cerasiforme. Master's thesis, Universidad Nacional de Colombia.

Rondon-Villarreal, P. and Pinzon-Reyes, E. (2018). Computer aided design of non-toxic antibacterial peptides. *Current topics in medicinal chemistry*, 18(13):1044–1052. Online:https://n9.cl/je9o7g.

Saderi, H., Owlia, P., Hosseini, A., and Semiyari, H. (2005). Antimicrobial effects of chamomile extract and essential oil on clinically isolated porphyromonas gingivalis from periodontitis. In *III WOCMAP Congress on Medicinal and Aromatic Plants*, volume 6, pages 145–146. Acta horticulturae.

Shah, N., Altschul, S., and Pop, M. (2018). Outlier detection in blast hits. *Algorithms for Molecular Biology*, 13:1–9. Online:https://n9.cl/cwep59.

Sharifzadeh, A., Javan, A., Shokri, H., Abbaszadeh, S., and Keykhosravy, K. (2016). Evaluation of antioxidant and antifungal properties of the traditional plants against foodborne fungal pathogens. *Journal de Mycologie Médicale*, 26(1):e11–e17. Online:https://n9.cl/d8ldk.

Sharma, P., Kaur, J., Sharma, G., and Kashyap, P. (2022). Plant derived antimicrobial peptides: Mechanism of target, isolation techniques, sources and pharmaceutical applications. *Journal of Food Biochemistry*, 46(10):e14348. Online:https://n9.cl/n7751.

Sievers, F. and Higgins, D. (2014). Clustal omega. *Current protocols in bioinformatics*, 48(1):3–13. Online:https://n9.cl/1eihb.

Srivastava, J., Shankar, E., and Gupta, S. (2010). Chamomile: A herbal medicine of the past with a bright future. *Molecular medicine reports*, 3(6):895–901. Online:https://n9.cl/fqf5r.

Tassin-Moindrot, S., Caille, A., Douliez, J., Marion, D., and Vovelle, F. (2000). The wide binding properties of a wheat nonspecific lipid transfer protein: solution structure of a complex with prostaglandin b2. *European Journal of Biochemistry*, 267(4):1117–1124. Online:https://n9.cl/nky5q.

Troeira Henriques, S. and Craik, D. (2017). Cyclotide structure and function: The role of membrane binding and permeation. *Biochemistry*, 56(5):669–682. Online:https://n9.cl/sx0eik.

Venkatesan, J. and Roy, D. (2023). Cyclic cystine knot and its strong implication on the structure and dynamics of cyclotides. *Proteins: Structure, Function, and Bioinformatics*, 91(2):256–267. Online:https://n9.cl/qcmf6g.

Yang, X. and Yousef, A. (2018). Antimicrobial peptides produced by brevibacillus spp.: structure, classification and bioactivity: a mini review. *World journal of microbiology and biotechnology*, 34:1–10. Online:https://n9.cl/bqf5o.

Zhang, Y. (2009). I-tasser: Fully automated protein structure prediction in casp8. *Proteins: Structure, Function, and Bioinformatics*, 77(S9):100–113. Online:https://n9.cl/xo92s.

Zhou, J. and Zhang, Y. (2020). Plant immunity: danger perception and signaling. *Cell*, 181(5):978–989. Online:https://n9.cl/98e2d.

La granja: Revista de Ciencias de la Vida
pISSN:1390-3799; eISSN:1390-8596
https://doi.org/10.17163/lgr.n41.2025.8

Scientific paper/ Artículo científico

Veterinary Sciences

Assessment of Physicochemical, Microbial, and Hygienic Quality of Raw Cow Milk Produced in Dairy Herds from the Peruvian Andes

Evaluación de la calidad fisicoquímica, microbiana e higiénica de la leche de vaca producida por rebaños en los Andes peruanos

Fernando Arauco Villar*[1], Leonor Guzmán Estremadoyro[1], Rafael Pantoja Esquivel[1]†, Noemí Mayorga Sánchez[1], Ide Unchupaico Payano[1] and Alex Rubén Huamán de la Cruz[2,3]

[1] *Universidad Nacional del Centro del Perú, Facultad de Zootecnia, Av. Mariscal. Castilla N. 39 El Tambo, Huancayo, Perú.*
[2] *Universidad Tecnológica del Perú.*
[3] *Universidad Peruana Unión, Unidad de Posgrado.*

*Corresponding author: faraucov@gmail.com

Received on June 18th, 2021. Accepted, after revision on February 27th, 2024. Published on March 1st, 2025.

Abstract

The study was performed in Mantaro Valley, Junín, Perú, with the aim to evaluate the physicochemical, microbial, and hygienical quality of 40 raw cows' milk collected from dairy herds from four provinces: Huancayo (n = 13), Concepción (n = 11), Jauja (n = 9), and Chupaca (n = 7). Physicochemical properties were quantified by evaluating the fat content, density, non-fat-solids, protein, water add, freezing point, salts, total solids, lactose, and pH using the milk analyzer Lactoscan SP. Microbial quality was determined through viable mesophilic bacteria (VMB), total coliforms (TC), fecal coliforms (FC), and yeast and mold (YMC). In addition, antibiotic presence was measured by SNAPduo*ST plus test kit and Reduction time by Methylene Blue Dye Reduction (MBRT). The results found in this work indicate that physicochemical features of raw cow milk were adequate compared to standard levels. In microbial quality, only Chupaca showed higher values (6.28 log cfu/mL) than recommended (5.3 log cfu/mL). Likewise, total bacterial/mL in Huancayo (H, 19.12×10^5) and Concepcion (C, 1.18×10^5) were relatively high concerning the acceptable level (1×10^5 bacteria/mL of raw milk). Antibiotic presence was found in 37.5% (n = 15) from the total of samples (n = 40). MBRT analysis reported 32.5%, 45.0%, and 22.5%, as of excellent, good, and acceptable quality, respectively. Thus, it was concluded that physicochemical properties presented an appropriate level whereas microbial quality in the areas was good but is recommendable for enriched hygienic practices, personal hygiene in milk handling due to microbial presence, and educating the public on safety issues.

Keywords: milk quality, physicochemical characteristics, bacteriological quality, Andean dairy farming.

Resumen

El estudio se llevó a cabo en el Valle del Mantaro, Región Junín, Perú, con el objetivo de evaluar propiedades fisicoquímicas, calidad microbiana e higiénica de 40 muestras de leche cruda recolectada de rebaños bovinos lecheros de cuatro provincias: Huancayo (n = 13), Concepción (n = 11), Jauja (n = 9) y Chupaca (n = 7). Las propiedades fisicoquímicas se cuantificaron mediante la evaluación del contenido de grasa, densidad, sólidos no grasos, proteína, adición de agua, punto de congelación, sales, sólidos totales, lactosa y pH utilizando el analizador de leche Lactoscan SP. La calidad microbiana se determinó a través de bacterias mesófilas viables (VMB), coliformes totales (TC), coliformes fecales (FC) y levaduras y mohos (YMC). Además, la presencia de antibióticos se midió mediante el kit de prueba SNAPduo * ST plus y el tiempo de reducción mediante la reducción de colorante azul de metileno (MBRT). Los resultados reportados en este estudio indican que las propiedades fisicoquímicas de la leche cruda de vaca fueron adecuadas en comparación con los niveles estándar. En calidad microbiana, solo Chupaca mostró valores superiores (6,28 log ufc/mL) a los recomendados (5,3 log ufc/mL). Asimismo, las bacterias totales por mL en Huancayo (H, $19{,}12 \times 10^5$) y Concepción (C, $1{,}18 \times 10^5$) fueron relativamente altas en comparación con el nivel aceptable (1×10^5 bacterias por mL de leche cruda). La presencia de antibiótico se encontró en el 37,5% (n = 15) del total de muestras (n = 40). El análisis MBRT informó 32,5%, 45,0% y 22,5%, como de calidad excelente, buena y aceptable, respectivamente. Así, se concluyó que las propiedades fisicoquímicas presentaron nivel adecuado mientras que la calidad microbiana en las zonas fue buena pero recomendable para enriquecer las prácticas higiénicas, la higiene personal en el manejo de la leche por presencia de microbios y concienciar al público en temas de seguridad.

Palabras clave: calidad de la leche, características fisicoquímicas, calidad bacteriológica, ganadería lechera andina.

Suggested citation: Arauco Villar, F., Guzmán Estremadoyro, L., Pantoja Esquivel, R., Mayorga Sánchez, N., Unchupaico Payano, I. and Huamán de la Cruz, A. (2025). Assessment of Physicochemical, Microbial, and Hygienic Quality of Raw Cow Milk Produced in Dairy Herds from the Peruvian Andes. *La Granja: Revista de Ciencias de la Vida*. Vol. 41(1):121-132. https://doi.org/10.17163/lgr.n41.2025.8.

Orcid IDs:

Fernando Arauco Villar: https://orcid.org/0000-0002-1768-8388
Leonor Guzmán Estremadoyro: https://orcid.org/0000-0002-1817-1356
Rafael Pantoja Esquivel: https://orcid.org/0000-0001-7080-1426
Noemí Mayorga Sánchez: https://orcid.org/0000-0001-6157-468X
Ide Unchupaico Payano: https://orcid.org/0000-0001-6922-9311
Alex Huamán De La Cruz: https://orcid.org/0000-0003-4583-9136

1 Introduction

Cow´s milk has a complex biochemical composition and is by far the main type of milk consumed worldwide (Boudalia et al., 2016). Due to their characteristics of containing an important source of nutrients, proteins, vitamins, carbohydrates, and energy-containing fats is highly recommendable for immunological protection and the human diet (MINAGRI, 2005). Milk offers an excellent environment for microbial growth and zoonotic agents, which accelerated the degradation of milk quality and shelf-life (Gemechu and Amene, 2016; Kra et al., 2013). Milk freshly obtained from a healthy animal theoretically is safe for human consumption (Thorning et al., 2016). However, milk can be easily contaminated during or after being secreted from the udder by food-borne pathogens or spoilage microorganisms such as feed, soil, air, water, animal feces, equipment, and people (Elrahman et al., 2009; Owusu-Kwarteng et al., 2020).

Besides, the prevalence of spoilage microorganisms and pathogenic agents in milk and dairy products may be impacted by a great number of factors and their possible combinations. Among these factors are the hygiene level, the health condition of the cow, dairy herd and environment, prestorage and milking conditions, farm management practices, technologies, microbial hazards, animal feedstuffs and husbandry, season, and geographic location (Alhussien and Dang, 2018; Hnini et al., 2018; Owusu-Kwarteng et al., 2020). Food-safety risks linked with dairy products and cow milk consumption vary between developing (smallholder dairy farmers) and developed (industrialized with pasteurization technologies) countries. Thus, a high bacterial presence signifies poor production hygiene or ineffective milk pasteurization (Owusu-Kwarteng et al., 2020).

Peru produced about 2.8 million metric tons (MMT) of fluid milk per year, and its per capita milk consumption is 84 liters (USDA, 2019). Cajamarca (18%), Arequipa (18%), and Lima (13%) are the regions that concentrate on milk production with some modern dairy farms and technologies (Bernet et al., 2001). However, most milk production is by small herds (USDA, 2019). The Mantaro Valley produces about 80,000 liters of milk by day, with 7% intended for the production of cheese, butter, yogurt, and other derived products (Correo, 2019).

Thus, milk production in the Mantaro Valley is a key piece for the livelihood of the population. However, there is no published data on the composition and hygienic quality of raw cow's milk produced by small producers. Therefore, this investigation aims to evaluate the quality of milk through its physicochemical properties and its microbiological analysis. Previously, a survey was carried out on the owners and managers of dairy herds, and on the milk collectors to establish potential risk factors that may be influencing the quality of the milk.

2 Materials and Methods

2.1 Study area and population

The study was performed in the Mantaro Valley (MV) located in Junin region, Peru, at 3 200 masl, and constituted by Jauja (J), Concepción (C), Huancayo (H), and Chupaca (CH) provinces. The MV is a fluvial inter-Andean valley with a diversified agricultural activity that produces several crops (maize, potatoes, and vegetables), and it is not a very developed dairy farming; it has small herds of less than three cows; medium herds, between four and ten cows, and the largest, more than ten and up to a hundred cows.

2.2 Protocol of sampling

The study was performed between October 2019 - February 2020. Forty milk samples from dairy herds and collection centers (processing plant and food markets) were collected from four provinces: Huancayo (n =13), Concepción (n =11), Jauja (n =9), and Chupaca (n =7) located at the Mantaro Valley, Junín Region, Perú. Criterion selection was made through discretionary sampling, taking into consideration only herds with a cows' population greater than 5 cows.

The milk samples were collected aseptically with a sterile bucket directly from the milk can, randomly selected according to the production volume of the dairy herd, in sterile glass jars with a capacity of 500 mL, and transported to the laboratory inside a Styrofoam box with refrigerant (3°C- 9°C) (Brousett-Minaya et al., 2015), for the corresponding analyses; all equipment used for milk samples was sterilized and clean to avoid contamination or influence on the properties or composition (Brousett-Minaya et al., 2015).

2.3 Physicochemical analysis of raw cow milk samples

The milk constituents (protein, fat, solid and solids-non-fat (SNF), and lactose) and physical features (percentage water, freezing point, salts, and density) were quantified through a milk analyzer Lactoscan SP (Apple Industries services-La Roche Sur Foron, France). An amount of 25 mL of each milk sample was taken in the sample holder, placing the analyzer in the recess position and starting the measurement. After the measurement (45 s), the digital indicator (IED display) shows the obtained results; the procedure was performed in duplicate (Juárez-Barrientos et al., 2016).

Antibiotic residues (beta-lactam, tetracycline, and cephalexin) were measured using SNAP-duo*ST plus test kit, following the methodology described by Cardoso et al. (2019). The AOAC method was employed to measure the acidity in the samples (AOAC International, 2000). pH was quantified through an Orion pH – meter after calibrating (7.02 to 4.00) by soaking in a small volume of milk taken from a beaker.

2.4 Microbiological analysis

Microbial analysis of cow milk samples includes the quantification of colony-forming units per mL (CFUs) of viable mesophilic bacteria (VMB - ISO 4833-1:2013 reference method), fecal (FC) and total coliforms (TC), and yeast and fungi through adequate average (ISO, 2013). The determination of hygienic quality included the count of Viable Aerobic Mesophilic Microorganisms expressed in colony-forming units per mL, preparing and homogenizing the sample with successive decimal dilutions and using plate count agar (APC) and incubating for 24-48 hours at 37°C.

For the determination of Total Coliforms and Fecal Coliforms, indicative of product fecal contamination, the method consists of culturing milk samples according to protocol to determine the presence of total coliforms and the most probable number (MPN) which consisted of making serial tenfold dilutions, as mentioned above, reaching a 10^{-8} dilution. 1 mL of each dilution was added to each of the tubes, containing 10 ml of simple lactose broth with an inverted Durham tube to determine the presence of gas and were incubated for 24 hours at 37°C and, after this time, the tubes that showed gas formation were reviewed, i.e., those in which the presence of bubbles was observed in the Durham tubes and those that were negative to the presence of gas were incubated for a further 24 hours. After this time, the results were read, the highest dilution in which the presence of gas was observed in the three tubes with simple lactose broth was selected, and a roast was taken from the tubes with gas to seed in a MacConkey agar plate to determine if the gas was due to the presence of fecal coliform bacteria; this plate was incubated for 24 hours at 37°C and the presence of colonies of fecal coliform bacteria, which are characterized by a pink color, was determined. For determining Fungi and Yeasts, Sabouraud agar was used, with incubation at 25°C for 24 to 72 hours and with daily examination of the culture. All equipment used for analysis was previously sterilized and used according to the manufacturer's guidelines.

2.5 Hygienic quality of raw milk

The hygienic quality of milk refers to the quantity and type of bacteria present as a consequence of its handling during the milking process, storage and transport (12-24 hours) and for this purpose it was used the reductase assay in milk (Methylene Blue Reduction Time -MBRT) according to the peruvian technical standard NTP 202.014:2004 (MINAGRI, 2018), making the first reading at half an hour of incubation (37° C) and subsequent readings at one-hour intervals.

The Methylene blue reduction test is based on the color transmitted to the milk sample when a dye is added (1 % methylene blue solution in methanol) which disappears more or less quickly (Yadav et al., 2018). The color disappears because of the removal of oxygen and substances reduced by bacterial metabolism. Samples were evaluated as: Excellent (decolorized $>$ 4 hours), Good (decolorized between 3 to 4 hours), acceptable (decolorized of 0.5 to $<$3 hours), and unacceptable (decolorized $<$ 0.5 h). Reduction time for each cow milk sample was annotated in an excel format and processed statistically.

2.6 Statistical analysis

Data obtained were processed by the CRAN R free software, version 3.3.6 (R Team Core, 2019). Differences in physicochemical and microbial features for each province were performed by one-way variance analysis (ANOVA). After ANOVA, the Tukey test was applied with a significance of 95 %.

3 Results and discussions

3.1 Physicochemical characteristics of raw cow milk

Results of the physicochemical characteristics of raw cow milk obtained in Huancayo, Jauja, Concepción and Chupaca are shown in Table 1, where the fat content (%), ranged from 3.29- to 3.77, and the average for four provinces were 3.58 ± 0.50. Similar results were reported by Montes de Oca-Flores et al. (2019), Kra et al. (2013), and Asefa and Teshome (2019) with 3.46 %, 3.26 ± 1.18 %, 3.89 ± 0.58 %, respectively. In contrast, a greater average fat content of 6.02 ± 0.76 % was reported by Gemechu and Amene (2016) in Ethiopia.

There was an observed significant difference ($p< 0.05$) in fat content (%) among the four provinces, besides, there is no significant difference between Jauja and Chupaca. The fat content of milk can be affected by the time of year that affects the diet, as well as by management practices and the racial component (Desyibelew and Wondifraw, 2019). The European Union and the Food and Drug Administration (FDA) establish that the fat content in total fluid and unprocessed milk should not be less than 3.5 % and 3.25 %, respectively. The results obtained in this work are within the recommended standards.

Specific gravity (average 1.03 ± 0.01 g/dm^3) was under those revealed by Gwandu et al. (2018) and Gemechu and Amene (2016). Likewise, differences were not observed ($p> 0.05$) among the provinces studied.

The non-fat solids content of the milk ranged between 8.47 ± 0.51 % and 8.99 ± 0.72 %, with an overall mean of 8.82 ± 0.62 %, with significant differences (p <0 .05) between provinces (except Huancayo and Jauja). These results are higher than those reported by Gemechu and Amene (2016) in Ethiopia (8.08 ± 0.13 %) and by Mahmoudi and Norian (2015) in Iran (8.50 %). The European Union considers that the standard quality content of lean solids should not be lower than 8.59 % for raw milk (Tamime, 2008). The results found in this paper showed values higher than 8.59 % for three provinces (Huancayo, Jauja and Concepción), and 8.47 ± 0.51 % for Chupaca. These values, slightly lower than the EU quality standard, may be related to seasonality, feeding practices, lactation period and milking method.

The protein contents in milk were 3.28 ± 0.31 % in Huancayo, 3.27 ± 0.26 % in Jauja, 3.19 ± 0.15 % in Concepción and 3.28 ± 0.31 % in Chupaca, with a general average of 3.21 ± 0.25 %. There was a significant difference ($p< 0.05$) between Huancayo, Concepción and Chupaca but not between Huancayo and Jauja (p 0.05). The results found were similar to those reported by Asefa and Teshome (2019) and Mahmoudi and Norian (2015) with 3.16 ± 0.31 % and 3.40 %, respectively. The quality standard of the European Union (EU) and the Food and Drug Administration suggested values of not less than 2.73 % and 2.9 % for raw whole milk samples, respectively. In all cow's milk samples collected in the four provinces, values were found within the recommended standards.

In the milk samples from the provinces of Huancayo and Chupaca, the presence of water was detected (0.56 ± 2.03 % and 1.59 ± 2.98 %, respectively). According to Rasheed et al. (2018) and Tripathy et al. (2019), natural milk, being a food rich in nutrients, proteins and vitamins, should not suffer any type of adulteration, which could cause serious risks for the health. According to our results, the incorporation of water into milk is an adulteration practice that reflects one of the negative behaviors of some producers in Huancayo and Chupaca in order to increase the total volume of the product to be offered.

Total solid (TS) concentration ranged from 12.35 %- 12.91 % with an overall 12.52 ± 1.11 %, and Jauja province presented a significant difference ($p< 0.05$) concerning other provinces (p 0.05). It was higher than the reported by Desyibelew and Wondifraw (2019) (11.89 ± 0.40 %) and Hnini et al. (2018) (11.84 ± 0.28 %) in Ethiopia and Morocco, respectively. The European Union (EU) established that the total solid content should not have a value lower than 12.5 %. Thus, the average TS content in milk samples is slightly inside the recommended standard. The slightly lower values than those of the EU, found in Huancayo, Chupaca and Concepción, can be due to management practices and poor feeding that tend to affect milk quality, although this is not statistically significant (Picinin et al., 2019).

Table 1. Mean ± standard deviation (S.D) and Tukey test comparison of physicochemical characteristics of raw cow's milk samples obtained from four Provinces at Mantaro Valley (n= 40).

Variables	Huancayo (H) (n = 13)	Jauja (J) (n = 9)	Concepción (C) (n = 11)	Chupaca (CH) (n = 7)	Media global (n = 40)
Fat content (%)	3.29 ± 0.32^a	3.77 ± 0.50^b	3.63 ± 0.47^c	3.77 ± 0.67^b	3.58 ± 0.50
Specific gravity (g/dm^3)	1.03 ± 0.02^a	1.03 ± 0.01^a	1.03 ± 0.01^a	1.03 ± 0.02^a	1.03 ± 0.01
Non-fat solids (%)	8.96 ± 0.73^a	8.99 ± 0.72^a	8.75 ± 0.42^b	8.47 ± 0.51^c	8.82 ± 0.62
Protein (%)	3.28 ± 0.31^a	3.27 ± 0.26^a	3.19 ± 0.15^b	3.07 ± 0.18^c	3.21 ± 0.25
Water adds (%)	0.56 ± 2.03^a	0.00 ± 0.00^b	0.00 ± 0.00^b	1.59 ± 2.98^c	0.46 ± 1.72
Freezing point	560 ± 52^a	570 ± 32^a	561 ± 27^b	535 ± 51^c	558 ± 42
Salts (%)	0.72 ± 0.07^a	0.72 ± 0.07^a	0.71 ± 0.03^a	0.69 ± 0.04^a	0.71 ± 0.05
Total solids (%)	12.37 ± 1.24^a	12.91 ± 1.21^b	12.48 ± 0.85^a	12.35 ± 1.21^a	12.52 ± 1.11
Lactose (%)	4.97 ± 0.55^a	4.95 ± 0.41^a	4.83 ± 0.22^b	4.67 ± 0.28^c	4.88 ± 0.41
pH	6.67 ± 0.27^a	6.62 ± 0.29^a	6.78 ± 0.23^b	6.76 ± 0.11^b	6.70 ± 0.24

Values on each horizontal line followed by the same letter do not differ significantly at p <0.05, n= number of milk samples.

The lactose content ranged between 4.67 % and 4.97 % with an overall average of 4.88 ± 0.41 %. There were significant differences (p <0.05) between Huancayo, Concepción and Chupaca, but not (p 0.05) between Huancayo and Jauja. Elrahman et al. (2009) revealed lower lactose values (4.33 ± 0.02 %) in raw milk from cows in Sudan. However, Asefa and Teshome (2019) found similar results to those found in the present work in Ethiopian cows (4.77 ± 0.42 %). Unlike the fat concentration in milk, the lactose concentration is similar in all dairy breeds and cannot be easily altered by feeding practices. Lactose is very important as it influences the absorption of minerals such as copper, zinc and calcium, especially during breastfeeding.

The pH values of the milk samples from Jauja and Huancayo did not present significant differences (p> 0.05), the same as between Concepción and Chupaca, with the general average pH being 6.70 ± 0.24. By measuring the pH of milk, impurities, deterioration and signs of mastitis infection can be detected, which can help understand the causes of some changes in its composition.

Fresh milk has a pH value of 6.7; a lower value may be indicative of deterioration due to bacterial degradation, when lactose is broken down and lactic acid is formed due to the presence of lactic acid bacteria (LAB), which ends up producing coagulation or curds with a characteristic smell and flavor ("sour" milk). Milk with pH values higher than 6.7 may indicate the presence of cows with mastitis, so measuring pH can offer a quick way to detect this disease. Small variations in pH 6.7 can affect the time required for pasteurization and the stability of the milk after treatment.

3.2 Microbial quality of raw cow milk

Table 2 presents the microbial quality in raw cow milk samples collected from Mantaro Valley.

The total of viable mesophilic bacteria (VMB) counts expressed in logarithm showed an overall mean of Log 4.82 ± 6.49 CFU/100 mL (0.66 ± 30.76 × 10^5 CFU/mL). The results found in milk samples showed that in Huancayo the BMV exceeded the permissible level of Log 5.3 CFU/mL (5 × 10^5 CFU/mL) according to official standards (MINAGRI, 2017), since Log 6.28 ± 6.74 CFU/mL was determined (19.12 ± 54.78 × 10^5 CFU/mL). Microbial contamination is related to the handling chain and to the animal itself when it is infected (Gwandu et al., 2018); therefore, the milking process, the milking environment, the handling of the milk and its storage would be carried out in unhygienic conditions to a greater degree in Huancayo due to the presence of a high microbial count in the milk. Similar findings were reported by Gwandu et al. (2018) in Tanzania and Ogot et al. (2015) in Kenya.

The mean fecal coliform count (FC) from four provinces showed significant differences ($p < 0.05$) among them (Table 2). The FC showed an overall mean Log 2.06 ± 2.52 CFU/mL, ordered as follow: Chupaca (2.50 ± 2.73) Concepción (1.49 ± 1.81) Jauja (1.34 ± 2.69) Huancayo (0.84 ± 1.34). Similar results were revealed by Abdalla and Elhagaz (2011) who determined coliform counts of Log 2.23 ± 0.14 CFU/mL from cow milk samples obtained on farms in Sudan. In contrast, higher FC was reported by Gemechu and Amene (2016) with an overall mean of Log 5.10 ± 0.29 CFU/mL. In the present study, some cows are kept in a muddy barn, and under hygienic poor conditions. These conditions probably have influenced the milk sample contamination, which increases the microbial count.

Table 2. Mean ± standard deviation (S.D) and Tukey test comparison of microbial counts (log10 CFU/mL) belongings to milk samples studied from four Provinces at Mantaro Valley (n= 40).

Variables	Huancayo (H) (n = 13)	Jauja (J) (n = 9)	Concepción (C) (n = 11)	Chupaca (CH) (n = 7)	Media global (n = 32)
VMB (CFU/mL × 10^5)	19.12 ± 54.78^a	0.95 ± 1.24^b	1.18 ± 1.64^c	0.31 ± 0.42^d	0.66 ± 30.76
VMB Log	6.28 ± 6.74^a	4.98 ± 5.10^b	5.07 ± 5.21^b	4.48 ± 4.63^c	4.82 ± 6.49
TC (CFU/mL × 10^3)	0.25 ± 0.46	0.34 ± 0.47	0.27 ± 0.44	0.50 ± 0.56	0.33 ± 0.47
TC Log	2.39 ± 2.66^a	2.53 ± 2.67^b	2.44 ± 2.65^a	2.70 ± 2.75^c	2.52 ± 2.67
FC (CFU/mL × 10^3)	0.01 ± 0.02	0.22 ± 0.49	0.03 ± 0.06	0.32 ± 0.53	0.12 ± 0.32
FC Log	0.84 ± 1.34^a	1.34 ± 2.69^b	1.49 ± 1.81^c	2.50 ± 2.73^d	2.06 ± 2.52
YMC (CFU/mL × 10^5)	1.87 ± 5.81	0.67 ± 1.33	0.06 ± 0.06	0.47 ± 0.78	0.81 ± 3.27
YMC Log	2.76 ± 5.76^a	4.83 ± 5.12^b	3.77 ± 3.82^c	4.67 ± 4.89^d	4.01 ± 4.90

VMB = viable mesophilic bacteria, TC = total coliforms, FC = fecal coliforms, YMC = yeast and mould count. Means ± S.D followed by different superscript letters in the same row specify significant difference ($p < 0.05$), CFU= colony forming unit per mL, n = number of milk samples.

It is important to determine the total number of bacteria as well as the type of microorganisms present. Thus, coliform bacteria can grow at temperatures of 4°C to 7°C, resisting pasteurization and reducing the shelf life of milk and altering the quality of derived products such as cheese and yogurt. Therefore, it is important to cool the milk to maintain the hygienic quality of the product. Sources of contamination can come from bacteria inside the mammary gland, important in dairy herds with a high presence of mastitis and from bacteria coming from outside the animal, the main source of contamination of milk. The final number of microorganisms in the milk has to do with the environment (pastures, corrals, etc.), the level of bacterial contamination, favorable conditions for the development of bacteria in milk storage and hygiene practices.

The mean total coliform count presented a significant difference ($p < 0.05$) among cow milk samples obtained from dairy farms in each province, and overall mean was Log 4.82 ± 6.49 CFU/mL (ranging from 4.48– 6.28 CFU/mL). Thus, the overall mean count of total coliform of raw cow milk from four provinces was lower than the reported by Gemechu and Amene (2016) who reported an elevated presence of total bacterial Log count of 7.09 ± 0.34 CFU/mL in milk samples collected from dairy farms of Bench Maji-Zone, Ethiopia. On the other hand, total bacteria obtained in Huancayo (19.12×10^5) and Concepción (1.18×10^5) were relatively higher than the acceptable level (1×10^5 bacteria per mL of raw milk).

The higher count of microbial observed in Huancayo may be due to a lack of suitable preparation and knowledge about the use of clean milking utensils and material (plastic containers), maintaining clean the milk production area, correct udder treatment of the cow by milkers handling, and poor hygienic quality. Likewise, most milk production is carried out in small herds. The presence of fecal coliform bacteria indicates unsanitary conditions and non-well hygienic practices in storage or production (Martin et al., 2016). Through prevention programs in milking, the possibility of contamination with total coliforms and particularly fecal coliforms, which constitutes a risk to public health, can be reduced.

The yeast and mold count (YMC) mean were Log 2.76 ± 5.76, Log 4.83 ± 5.12, Log 3.77 ± 3.82, and Log 4.67 ± 4.89 CFU/mL for cow milk samples analyzed from H, J, C, and CH, respectively with an overall mean Log 4.01 ± 4.90 CFU/mL. Significant differences were observed between mold and yeast counts ($p > 0.05$) (Table 2). Among provinces, J was higher in YMC than CH, C, and H. Similar YMC values were reported by Gemechu and Amene (2016) based on three cities examined from Ethiopia with an overall mean of Log 3.90 ± 0.48. However, in other cities of Ethiopia, Habtamu et al. (2018) reported higher YMC values, with an overall mean of Log 7.21 ± 0.21 CFU/mL.

Ortiz-Durán et al. (2017) in Colombia, mention that the presence of fungi in milk can be an indicator of poor hygiene or disease in the mammary gland, evidencing the presence of *Candida* spp., and to a lesser percentage *Aspergillus* spp. in all milk samples evaluated, which suggests a factor that puts the safety and quality of milk and its derivatives at risk. The higher YMC values found in cow's milk analyzed in provinces J and CH could be related to poor personal hygiene, air contamination by organisms, uncleaned containers, and poor practices of milk handlers.

3.3 Hygienic quality of raw cow milk

The presence of antibiotic residues (betal-lactams, tetracycline and cephalexin) was found in 37.5% (n= 15) of the total samples (n= 40). The provinces of Huancayo (n= 13), Jauja (n= 9), Concepción (n= 11) and Chupaca (n= 7) showed the presence of antibiotics in 30.7%, 44.4%, 54.5%. 14.3%, respectively (Table 3). The cause of a high aerobic mesophilic count is due to the presence of bacteria in the milk residue left on the surface of the materials used for collecting or storing milk, dirty or unfurnished udders before milking and rapid non-cooling of the milk (Calderón et al., 2006).

The methylene blue reduction test is suitable for inferring the number of organisms contained in milk samples (Nandy and Venkatesh, 2010). As the bacterial load in milk increases, the oxidation-reduction indicator passes more quickly to its leucobase, thus representing an indirect metabolic count. However, if the number of microorganisms present in raw milk with a reducing effect is low, the test would not agree with the bacterial count obtained in plates, not reflecting, as already mentioned, the real microbial contamination of the milk, which makes it lose value as a tool within rapid tests (Luigi et al., 2013).

Of the 40 milk samples processed for MBRT (Table 2), 13 (32.5%) had excellent quality, 18 (45.0%) had good quality, 9 (22.5%) had acceptable quality, and no sample (0%) had poor quality. By province, Huancayo (n= 13) presented excellent, good and acceptable quality in 38.4% (H2, H3, H5, H6 and H7), 38.4% (H1, H4, H8, H9 and H11) and 23.2%. (H10, H12 and H13), respectively.

In Jauja (n= 9), 55.6% (n=5, J1, J2, J4, J7 and J8) of the samples had excellent quality, and 22.2% (n= 2) of the samples had good (J3 and J9) and acceptable quality (J5 and J6). For Concepción (n= 11), 27.3%, 54.6% and 18.1% had excellent (C2, C4 and C5), good (C1, C3, C6, C7, C8 and C10) and acceptable (C9 and C11) quality.

In Chupaca (n= 7), 71.4% had good quality (CH2, CH3, CH4, CH5 and CH7) and 28.6% acceptable quality (CH1 and CH6). In total, the quality of the Mantaro Valley was considered to have good quality (3.50 ± 1.26 hours).

Table 3. Presence of antibiotic residues, MBRT test (reduction time of methylene blue reduction time), and quality classification based on each collection point and its average.

Site	Point	Antibiotic residues presence	Reduction time (hours)	Reduction time average (hours)	Quality
Huancayo (H) (n = 13)	H1	No (-)	3.0 (Good)	3.54 ± 1.43	Good
	H2	No (-)	4.5 (Excellent)		
	H3	No (-)	4.5 (Excellent)		
	H4	Yes (+)	4.0 (Good)		
	H5	Yes (+)	5.0 (Excellent)		
	H6	Yes (+)	4.5 (Excellent)		
	H7	No (-)	5.5 (Excellent)		
	H8	No (-)	3.5 (Good)		
	H9	No (-)	4.0 (Good)		
	H10	Yes (+)	1.0 (Acceptable)		
	H11	No (-)	4.0 (Good)		
	H12	No (-)	1.5 (Acceptable)		
	H13	No (-)	1.0 (Acceptable)		
Jauja (J) (n = 9)	J1	No (-)	4.5 (Excellent)	3.33 ± 1.31	Good
	J2	No (-)	5.0 (Excellent)		
	J3	No (-)	3.5 (Good)		
	J4	Yes (+)	5.0 (Excellent)		
	J5	No (-)	1.5 (Acceptable)		
	J6	Yes (+)	1.5 (Acceptable)		
	J7	Yes (+)	3.5 (Excellent)		
	J8	Yes (+)	2.0 (Excellent)		
	J9	No (-)	3.5 (Good)		
Concepcion (C) (n = 11)	C1	Yes (+)	3.5 (Good)	3.54 ± 1.29	Good
	C2	Yes (+)	1.5 (Excellent)		
	C3	No (-)	3.0 (Good)		
	C4	No (-)	4.5 (Excellent)		
	C5	No (-)	4.0 (Excellent)		
	C6	Yes (+)	5.5 (Good)		
	C7	No (-)	5.0 (Good)		
	C8	Yes (+)	3.5 (Good)		
	C9	No (-)	4.0 (Acceptable)		
	C10	Yes (+)	3.5 (Good)		
	C11	Yes (+)	1.0 (Acceptable)		
Chupaca (CH) (n = 7)	CH1	No (-)	2.5 (Acceptable)	3.57 ± 0.68	Good
	CH2	No (-)	4.0 (Good)		
	CH3	No (-)	4.0 (Good)		
	CH4	No (-)	4.0 (Good)		
	CH5	No (-)	4.0 (Good)		
	CH6	Yes (+)	2.5 (Acceptable)		
	CH7	No (-)	4.0 (Good)		
Total (n = 40)				3.50 ± 1.26	Good

Table 3 shows the results of hygienic quality through antibiotic presence, methylene blue reduction time (MBRT), and quality classification of raw cow milk samples collected in four provinces from Mantaro Valley.

The recognition of the risk factors present throughout the biological and production process of poor quality milk should allow the different actors involved (producers, collectors and processors of milk) to rethink their respective work schemes in order to adopt corrective measures to improve the hygienic quality of milk.

4 Conclusions

As for the physicochemical properties of raw cow's milk samples from the four provinces of the Mantaro Valley, the values found were within national and international standards.

The determination of the hygienic quality of the milk sampled from the four provinces showed an acceptable level to the methylene blue reduction test (MBRT). The microbiological analysis detected the presence of viable mesophilic bacteria, total coliforms, fecal coliforms and yeast and mold counts, which may be related to poor sanitary conditions, dirty collection materials, bad milking environment, among others.

Recommendations to produce milk of good hygienic quality based on the Code of Hygienic Practice for Milk and Dairy Products CAC/RCP 57, published in 2004 by the Codex Alimentarius (MIDAGRI, 2004), are to improve general hygiene practices, both in the environment and milking, as well as in post-milking handling and hygienic storage of milk. Although it is true that the composition of milk varies due to a multiplicity of factors, genetics and nutrition play a determining role in its compositional quality and it is on them that dairy producers in the Mantaro Valley should focus more attention.

Declaration of interest

The authors declare not to have a conflict of interest.

Acknowledgments

The authors thank the owners, managers, and collaborators of the herds where the samples were collected. Likewise, to MSc Danny Cruz for his support in the statistical analysis

Authors' contribution

F.A.V.: conceptualized and designed the manuscript, L.G.E.: wrote the manuscript, N.M.S.; I.U.P.; ARHDLC: statistical analysis, interpretation, and edited the manuscript.

References

Abdalla, M. and Elhagaz, F. (2011). The impact of applying some hygienic practices on raw milk quality in khartoum state, sudan. *Research Journal of Agriculture and Biological Sciences*, 7(2):169–173. Online:https://n9.cl/79pdo4.

Alhussien, M. and Dang, A. (2018). Milk somatic cells, factors influencing their release, future prospects, and practical utility in dairy animals: An overview. *Veterinary world*, 11(5):562–577. Online:https://n9.cl/e54wk.

AOAC International (2000). *Official Methods of Analysis of AOAC International*, volume 15. AOAC International, 17th edition.

Asefa, Z. and Teshome, G. (2019). Physical properties and chemical compositions of raw cow milk in milk shades around addis ababa, ethiopia. *Journal of Natural Sciences Research*, 9(19):33–37. Online:https://n9.cl/au9ni.

Bernet, T., Staal, S., and Walker, T. (2001). Changing milk production trends in peru. *Mountain Research and Development*, 21(3):268–275. Online:https://n9.cl/phgd6.

Boudalia, S., Benati, D., Boukharoub, R., Chemakh, B., and Chemmam, M. (2016). Physicochemical properties and hygienic quality of raw and reconstituted milk in the region of guelma-algeria. *International Journal of Agricultural Research*, 11(2):77–83. Online:https://n9.cl/mhzy1.

Brousett-Minaya, M., Torre, A., Chambi, A., Villalba, M., Herán, and Samata, G. (2015). Physicochemical, microbiological and toxicological quality of raw milk in cattle basins of the region puno-peru. *Scientia agropecuaria*, 6(3):165–176. Online:https://n9.cl/zc2z1.

Calderón, A., García, F., and Martínez, G. (2006). Indicadores de calidad de leches crudas en diferentes regiones de colombia. *Revista MVZ Córdoba*, 11(1):725–737. Online:https://n9.cl/wqn38u.

Cardoso, C., de C Nunes, E., Barbosa, E., das GP Ribeiro, A., de M Souza, R., Liberal, M., and Castro, H. (2019). Farm test for rapid identification of antibiotic residues in raw milk. *Adv. Biotech. Microbiol*, 13(1):9–15. Online:https://n9.cl/eydss.

Correo (2019). En riesgo producción de 100 mil litros de leche de la región junín. Diario Correo website. Online:https://n9.cl/fsevw.

Desyibelew, W. and Wondifraw, Z. (2019). Evaluation of milk composition in zebu× hf crossbred dairy cows in different seasons and stage of lactations in amanuel town. *Ethiopia. Journal of Agricultural Science and Food Research*, 10(1):255. Online:https://n9.cl/nlmla.

Elrahman, S., Ahmad, A., El Zubeir, I., El Owni, A., and Ahmed, M. (2009). Microbiological and physicochemical properties of raw milk used for processing pasteurized milk in blue nile dairy company (sudan). *Australian Journal of Basic and Applied Sciences*, 3(4):3433–3437. Online:https://n9.cl/ucjtbk.

Gemechu, T. and Amene, T. (2016). Physicochemical properties and microbial quality of raw cow milk produced by smallholders in bench maji-zone, southwestern ethiopia. *Food Science and Quality Management*, 54(1):47–54. Online:https://n9.cl/a4dwm.

Gwandu, S., Nonga, H., Mdegela, R., Katakweba, A., Suleiman, T., and Ryoba, R. (2018). Assessment of raw cow milk quality in smallholder dairy farms in pemba island zanzibar, tanzania. *Veterinary Medicine International*, 1(1):1031726. Online:https://n9.cl/35ag2q.

Habtamu, K., Ajebu, N., , and Edessa, N. (2018). Microbiological quality and safety of milk production and marketing in hawassa district, ethiopia. *African Journal of Microbiology Research*, 12(25):587–594. Online:https://n9.cl/b8f5u.

Hnini, R., Ouhida, L., Chigr, M., Merzouki, M., Bahi, L., El Hansali, M., Najimi, M., and Chigr, F. (2018). Evalution of the microbiological quality of moroccan cow raw milk in dairy herds located in the beni mellal region. *World Journal of Research and Review*, 7(1):19–23. Online:https://n9.cl/h3czu.

Juárez-Barrientos, J., Díaz-Rivera, P., Rodríguez-Miranda, J., Martínez-Sánchez, C., Hernández-Santos, B., Ramírez-Rivera, E., Torruco-Uco, J., and Herman-Lara, E. (2016). Caracterización de la leche y clasificación de calidad mediante análisis cluster en sistemas de doble propósito. *Revista mexicana de ciencias pecuarias*, 7(4):525–537. Online:https://n9.cl/wivvz.

Kra, K., Mégnanou, R., Akpa, E., Assidjo, N., and Niamké, L. (2013). Evaluation of physico-chemical, nutritional and microbiological quality of raw cow's milk usually consumed in the central part of côte d'ivoire. *African Journal of Food, Agriculture, Nutrition and Development*, 13(3):7888–7904. Online:https://n9.cl/42pzv.

Luigi, T., Rojas, L., and Valbuena, O. (2013). Evaluación de la calidad higiénico-sanitaria de leche cruda y pasteurizada expendida en el estado carabobo, venezuelaleche, bacterias salmonella spp., calidad microbiológica. *Salus*, 17(1):25–33. Online:https://n9.cl/ebs8d.

Mahmoudi, R. and Norian, R. (2015). Physicochemical properties and frauds in the samples of raw cow milk produced in qazvin, iran. *Journal of Research and Health*, 5(3):340–346. Online:https://n9.cl/464x1.

Martin, N., Trmčić, A., Hsieh, T., Boor, K., and Wiedmann, M. (2016). The evolving role of coliforms as indicators of unhygienic processing conditions in dairy foods. *Frontiers in microbiology*, 7:1549. Online:https://n9.cl/sdqpe.

MIDAGRI (2004). Código de prácticas de higiene para la leche y los productos lácteos. cac/rcp 57–2004.

MINAGRI (2005). *Aspectos Nutricionales y Tecnológicos de la Leche*. Dirección General de Promoción Agraria - MINAGRI.

MINAGRI (2017). Decreto supremo n 007-2017-minagri. Online:https://n9.cl/qdbos.

MINAGRI (2018). Ntp 202.084:2004, leche y productos lacteos. Online:https://n9.cl/30id6.

Montes de Oca-Flores, E., Espinoza-Ortega, A., and Arriaga-Jordán, C. (2019). Technological and physicochemical properties of milk and physicochemical aspects of traditional oaxaca cheese. *Revista mexicana de ciencias pecuarias*, 10(2):367–378. Online:https://n9.cl/ybwh4.

Nandy, S. and Venkatesh, K. (2010). Application of methylene blue dye reduction test (mbrt) to determine growth and death rates of microorganisms. *African Journal of Microbiology Research*, 4(1):061–070. Online:https://n9.cl/iaa2s.

Ogot, H., Ochuodho, H., and Machoka, R. (2015). Microbial analysis of raw and boiled milk sold at baraton center in nandi county, kenya. In *Proceedings of the Second Annual Baraton International Interdisciplinary Research Conference Proceedings 2015 Emerging Issues in Globalization, Baraton Interdisciplinary Research Journal*, pages 1–8.

Ortiz-Durán, E., Pérez-Romero, R., and Orozco-Sanabria, C. (2017). Identificación de agentes micóticos en muestras de leche obtenidas de tanques de enfriamiento. *Ciencia y Agricultura*, 14(2):99–106. Online:https://n9.cl/pyb28.

Owusu-Kwarteng, J., Akabanda, F., Agyei, D., and Jespersen, L. (2020). Microbial safety of milk production and fermented dairy products in africa. *Microorganisms*, 8(5):752. Online:https://n9.cl/ngga4.

Picinin, L., Bordignon-Luiz, M., Cerqueira, M., Toaldo, I., Souza, F., Leite, M., Fonseca, L., and Lana, A. (2019). Effect of seasonal conditions and milk management practices on bulk milk quality in minas gerais state-brazil. *Arquivo Brasileiro de Medicina Veterinária e Zootecnia*, 71:1355–1363. Online:https://n9.cl/5q7gn.

R Team Core (2019). A language and environment for statistical computing. R Foundation for Statistical Computing, Vienna Austria. Retrieved from https://www.r-project.org/.

Rasheed, N., Mohammad, A., and Hafeez, H. (2018). A comparative assessment of the quality of milk-validation of standard brands versus local milk sold in market. *Global Journal of Pharmacy & Pharmaceutical Sciences*, 5(1):1–5. Online:https://bit.ly/3WDRppV.

Tamime, A. (2008). *Milk Processing and Quality Management*. Wiley Online Library.

Tripathy, S., Reddy, M., Vanjari, S., Jana, S., and Singh, S. (2019). A step towards miniaturized milk adulteration detection system: Smartphone-based accurate ph sensing using electrospun halochromic nanofibers. *Food Analytical Methods*, 12:612–624. Online:https://n9.cl/9351y.

USDA (2019). Peru an overview of peru's dairy sector. USADA. Online:https://n9.cl/25h0u.

Yadav, N., Yadav, R., and Pokharel, B. (2018). Bacteriological quality analysis of milk available in local market of janakpurdham, nepal. *J Microbiol*, 56:97–100. Online:https://n9.cl/0u1ok.

La granja: Revista de Ciencias de la Vida
pISSN:1390-3799; eISSN:1390-8596
https://doi.org/10.17163/lgr.n41.2025.09

Scientific paper/ Artículo científico

Agricultural Sciences

Improvement of the nutritional value of *Lupinus mutabilis* Sweet foliage meal by solid-state fermentation with *Aspergillus niger* J1 and *Trichoderma viride* M5-2 strains

Mejora del valor nutritivo de harina de follaje de *Lupinus mutabilis* Sweet mediante fermentación en estado sólido con las cepas *Aspergillus niger* J1 y *Trichoderma viride* M5-2

David Catagua*[1,2], Julio Dustet Mendosa[2] and Elaine Valiño Cabrera[3]

[1]*Escuela Superior Politécnica del Litoral, ESPOL, Centro de Investigaciones Biotecnológicas del Ecuador (CIBE), Campus Gustavo Galindo Km. 30.5 Vía Perimetral, P.O. Box 09-01-5863, Guayaquil, Ecuador.*
[2]*Universidad Tecnológica de La Habana "José Antonio Echeverría". 11901. Calle 114, s/n, Marianao, Ciudad de La Habana, Cuba.*
[3]*Instituto de Ciencia Animal, Apartado Postal 24, San José de las Lajas, Mayabeque, Cuba*

*Corresponding author: david.catagua@espol.edu.ec, catagua@quimica.cujae.edu.cu

Article received on May 12th, 2022. Accepted, after review, on September 14th, 2022. Published on March 1st, 2025.

Abstract

To increase the nutritive value of *Lupinus mutabilis* Sweet (chocho) foliage meal by solid-state fermentation with *Aspergillus niger* J1 and *Trichoderma viride* M5-2 strains, two laboratory experiments were carried out. A completely randomized design with 2×8 factorial arrangement and three replicates was used. The two strains of lignocellulolytic fungi and the fermentation times (0, 24, 48, 72, 96, 120, 144 and 168 h) were selected as factors. Samples were taken every 24 h for enzymatic analyses (exo β1-4 glucanase) and chemical composition (neutral detergent fiber (NDF), acid detergent fiber (ADF), cellulose and lignin). Substrate pH and moisture, as well as phenolic and flavonoid content composition were measured. Variations in the physicochemical properties of the flour studied were observed, with decreases in NDF, flavonoids and phenolic content by both strains, reaching a maximum of 12, 75 and 84% respectively in a maximum time of 168 hours in the fermentation with *A. niger* J1 ($P<0.01$). In enzyme kinetics, interaction was observed in all factors ($P<0.01$). High values of exo β 1-4 glucanase enzymes were recorded in *L. mutabilis* Sweet with strain *T. viride* M5-2 at 96 h and sustained this activity over time for *A. niger* J1 with 0.189 UPF/mL. *T. viride* M5-2 and *A. niger* J1 strains improve the nutritive value of legume meal.

Keywords: Legume, Solid Fermentation, antinutrients, monogastrics.

Resumen

Para incrementar el valor nutritivo de la harina de follaje de *Lupinus mutabilis* Sweet (chocho) por medio de una fermentación en estado sólido con las cepas *Aspergillus niger* J1 y *Trichoderma viride* M5-2 se efectuaron 2 experimentos a nivel de laboratorio. Se utilizó un diseño completamente aleatorizado, con arreglo factorial 2×8 y tres repeticiones. Como factores se seleccionaron las dos cepas de hongos lignocelulolíticos y los tiempos de fermentación (0, 24, 48, 72, 96, 120, 144 y 168 h). Se tomaron muestras cada 24 h para los análisis enzimáticos (exo β1-4 glucanasa) y composición química (fibra neutro detergente (FND), fibra ácido detergente (FAD), celulosa y lignina). Se midió el pH y la humedad en el sustrato, así como la composición de contenido fenólico y flavonoides. Se observaron variaciones en las propiedades físico-químicas de la harina estudiada, con disminución de la FND, flavonoides y el contenido fenólico por ambas cepas, alcanzando un máximo de 12, 75 y 84 % respectivamente en un tiempo máximo de 168 horas en la fermentación con *A. niger* J1 ($P<0,01$). En la cinética enzimática se observó interacción en todos los factores ($P<0,01$). Se registraron valores altos de enzimas exo β 1-4 glucanasa en *L. mutabilis* Sweet con la cepa *T. viride* M5-2 a las 96 h y sostenida esta actividad en el tiempo para *A. niger* J1 con 0,189 UPF/mL. Las cepas *T. viride* M5-2 y *A. niger* J1 mejoran el valor nutritivo de la harina de leguminosa.

Palabras clave: Leguminosa, Fermentación sólida, antinutrientes, monogástricos.

Suggested citation: Catagua, D., Dustet Mendosa, J. and Valiño Cabrera, E. (2025). Improvement of the nutritional value of Lupinus mutabilis Sweet foliage meal by solid-state fermentation with Aspergillus niger J1 and Trichoderma viride M5-2 strains. *La Granja: Revista de Ciencias de la Vida.* Vol. 41(1):133-143. https://doi.org/10.17163/lgr.n41.2025.09.

Orcid IDs:

David Catagua: https://orcid.org/0000-0002-9418-7253
Julio Dustet Mendosa: https://orcid.org/0000-0002-2044-0383
Elaine Valiño Cabrera: https://orcid.org/0000-0003-4178-3286

1 Introduction

Lupinus mutabilis Sweet (chocho) is a crop with low nutritional requirements that grows in marginal soils, and its grains have high nutritional value, providing valuable proteins in the human diet. This legume also preserves soil fertility through nitrogen fixation, it is rich in calcium and proteins, and its cultivation has spread throughout Ecuador, becoming a key component in development projects in indigenous regions of the country (Martínez Flores et al., 2016).

The grain of *L. mutabilis* Sweet is considered highly nutritious, with proteins and oils comprising more than half of its weight. Based on bromatological analyses, it contains an average of 35.5 % protein, 16.9 % oil, 7.65 % crude fiber, 4.15 % ash, and 35.77 % carbohydrates (Carvajal-Larenas, 2019). Additionally, it contains certain proteins that can help reduce blood glucose levels (Vargas-Guerrero et al., 2014; Gulisano et al., 2019).

Being a short-cycle crop, after harvesting, *L. mutabilis* Sweet leaves behind residues consisting of foliage and pods, which can represent up to 75 % of the plant's weight. These residues are often reincorporated into the soil, where natural degradation returns nutrients to the soil. Alternatively, this waste can be used as animal feed. This residue typically contains a high fiber content, consisting of crude fiber (CF), neutral detergent fiber (NDF), and acid detergent fiber (ADF).

Fiber can be defined as the plant components that have low digestibility and promote ruminal balance. Because of this, its use has mainly been directed toward ruminants, although it can be included in the diets of monogastric animals (Savón et al., 2005). However, its use requires an appropriate transformation strategy to achieve socially desirable and economically viable production systems (Savón et al., 2005; Trujillo and Escobar, 2012; Rodríguez García, 2017) due to the presence of antinutritional compounds (fiber, phenolic content, flavonoids, tannins) in such feedstuffs (Molina-Poveda et al., 2013; Díaz Sánchez et al., 2017; Martínez-Pérez et al., 2018). It is recommended that NDF content does not exceed 65 % and that ADF does not exceed 45 % (Linn and Martin, 1991). While polyphenols are known to have beneficial effects on animal health, a high content of these compounds can negatively affect the nutritional value of the substrate (Siddhuraju et al., 2000; Bessada et al., 2019).

Solid-state fermentation (SSF) is a transformation method involving the growth of microorganisms on a substrate under certain moisture, pH, and temperature conditions, using the substrate as a nutrient source to facilitate growth, development, and reproduction (Pandey, 2003). In this study, the microorganisms utilized the antinutritional compounds (ADF, NDF, polyphenols) as a food source for their growth, thereby reducing their levels. The use of SSF has demonstrated an increase in the nutritional value of fermented substrates and their safety for animal feed.

Valiño et al. (2015) increased the nutritional value of flour from four legumes using solid fermentation with *T. viride* M5-2 for use in monogastric species. Varadyova et al. (2018) published a review showing that substrates enriched through solid fermentation can increase the concentration of polyunsaturated fatty acids in the rumen. In 2019, Sugiharto and Ranjitkar demonstrated that fermentation, in addition to being an economical means of enhancing the nutritional value of ingredients used in broiler chicken feed, also has a beneficial influence on gut morphology, immune function, and bird growth performance (Valiño et al., 2015; Varadyova et al., 2018; Sugiharto and Ranjitkar, 2019).

The objective of this research is to improve the nutritional value of *L. mutabilis* Sweet foliage meal through solid fermentation with the strains *Aspergillus niger* J1 and *Trichoderma viride* M5-2.

2 Materials and Methods

2.1 Experimental Design and Statistical Analysis

A completely randomized design was used, with three replications and two inoculants (*A. niger* J1 and *T. viride* M5-2), with 8 sampling times (0, 24, 48, 72, 96, 120, 144, and 168 hours). Each biodigester was considered an experimental unit. Statistical analyses were performed using STATGRAPHICS XV CENTURION software.

2.2 Microorganisms

Two strains of lignocellulolytic fungi were used: *Aspergillus niger*, isolated from sugarcane bagasse at the Faculty of Chemical Engineering at the Technological University of Havana "José Antonio Echevería" (CUJAE), and *Trichoderma viride* M5-2, from the strain bank of the Animal Science Institute (Mayabeque, Cuba). These strains are known for their hydrolytic activity and secretion of cellulase enzymes in substrates with high fiber content, and both strains were evaluated through solid-state fermentation (Valiño et al., 2004a).

2.3 Fermentation Substrate

The plant substrate consisted of post-harvest *L. mutabilis* Sweet plants (leaves and stems) from the "Lupita" farm in the Riobamba canton, Chimborazo province. The material was dried at the Biotechnology Research Center of Ecuador (CIBE) in a HAFO SERIES 1 600 oven at 65 °C for 48 hours and then ground using a manual CORONA mill.

2.4 Fermentation process

For this experiment, 42 glass jars of 250 ml were used as biodigesters (21 for fermentation with*A. niger* J1 and 21 for fermentation with *T. viride* M5-2). Each was filled with 10 g of the dried substrate and then moistened with distilled water to achieve an initial moisture content of 70% (25 ml). The mixture was enriched with 2.5% urea (0.25 g), 5% potassium phosphate (KH_2PO_4, 0.5 g), and 10% ammonium sulfate ($(NH_4)_2SO_4$, 1 g) (Roussos et al., 1991), and the pH of the substrate was adjusted to 6. The wet substrate was sterilized with saturated steam in an autoclave for 20 minutes at 121 °C. Two spore suspensions were prepared for substrate inoculation: *A. niger* J1 was inoculated into the biodigesters containing the substrate at a concentration of 10^6 spores/g of dry substrate (Villena and Gutiérrez-Correa, 2003), and *T. viride* M5-2 was inoculated into the remaining biodigesters at a concentration of 10^7 spores/g of dry substrate (Valiño et al., 2004b).

The inoculated and homogenized jars were incubated at 30 °C for 168 hours. Samples were taken every 24 hours for the corresponding analyses, and fungal growth and substrate colonization were visually observed.

2.5 Chemical and Enzymatic Analyses

Three grams of fermented material were weighed at 0, 24, 48, 72, 96, 120, 144, and 168 hours, and 30 ml of distilled water was added. The sample was placed on a mechanical shaker at 140 rpm for 20 minutes, centrifuged at 5,000 rpm for 10 minutes, and filtered through Whatman No. 40 filter paper to obtain the enzymatic extract. The pH was measured, and the enzymatic analysis of exo 1,4 β-D glucanase activity (filter paper activity) was performed using the technique from the National Renewable Energy Laboratory NREL/TP-510-42628, January 2008 (Adney and Baker, 2008). This enzymatic activity was expressed in filter paper units per milliliter (FPU/ml).

The bromatological indicators studied included dry matter conversion (DM), calculated by gravimetry as the difference between the initial and final dry mass (Oliva et al., 2018), neutral detergent fiber (NDF), acid detergent fiber (ADF), lignin (LIG) using the ANSI/ASTM D1106-56 method, and cellulose (CEL) using the ANSI/ASTM D1103-60 method (1977). The content of phenolic compounds (mg of gallic acid/100 g of dry substrate) was analyzed according to the Folin-Ciocalteu method (Vera et al., 2022), and the flavonoid content was determined by the spectrophotometric method (mg of catechins/100 g of dry substrate) (Xu et al., 2017).

3 Results and discussion

The bromatological composition and granulometry of the substrate are detailed in Tables 1 and 2, respectively. Fiber, particularly that derived from forages, constitutes the main component of ruminant diets, although its use in monogastrics is limited due to the morphology of their digestive systems. Despite this, several studies have demonstrated the feasibility of using this type of substrate in their diets (Savón et al., 2005; Jha et al., 2019).

Phenolic compounds, particularly tannins, can precipitate certain proteins, thus reducing their digestibility and limiting the availability of amino acids, compromising the nutritional value of the substrate (Bessada et al., 2019).

Table 1. Composition of *L. mutabilis* Sweet foliage meal.

Component	%	mg/100 gr of DM*
Moisture	3.12	
Neutral Detergent Fiber (NDF)	71.05	
Acid Detergent Fiber (ADF)	53.84	
Lignin	13.28	
Cellulose	40.56	
Hemicellulose	17.21	
Flavonoids		55.53
Phenolic Content		9.78

* Dry Matter

Table 2. Granulometric Characterization of *L. mutabilis* Sweet Foliage Meal.

Mesh No. (U.S. STD. Sieve)	%
< 5	0.28
5 - 16	22.67
16 - 25	37.39
25 - 60	33.71
> 60	

In Table 3, it can be observed that both strains exhibited growth on the selected substrate, with differences in sporulation. *A. niger* J1 showed mycelial growth at 24 hours, began sporulation at 48 hours, and fully colonized the surface of the substrate by 72 hours. In contrast, *T. viride* M5-2 began sporulation at 72 hours and did not fully cover the substrate with spores throughout the experiment. An important factor influencing the observed mycelial growth could be particle size, as noted by Haldar and Purkait (2020) and Gao et al. (2020). Substrate colonization and sporulation are enhanced by the surface area available for contact, with larger surface areas favoring better colonization.

The pH variation during the 168-hour fermentation process is shown in Figure 1. For both strains, pH values between 6 and 8 were observed, corresponding to the optimal range for cellulolytic enzyme activity in fibrous substrates. It is known that the optimal initial pH values for the hydrolytic action of cellulase enzymes are between 5 and 6, although these may vary depending on the substrate being fermented, the incubation temperature, and even the strain from which the enzyme originates (Kaschuk et al., 2020).

In this study, the *T. viride* M5-2 strain showed low cellulolytic activity between pH 6 and 8 during the fermentation of *L. mutabilis* Sweet at 30°C, differing from results obtained in other studies with legumes (*Vigna unguiculata*), where the pH remained between 5 and 7 (Valiño et al., 2004b) (Figure 2). It was also observed that during fermentation with the *T. viride* M5-2 strain, the pH rose to levels above 8 after the third day of fermentation. This could be related to the α-amino groups present in the substrate's proteins, which ionize when dissolved in water, releasing a proton from the functional group that could raise the pH. Additionally, the substrate is rich in nitrogenous compounds that could also contribute to the pH increase (Villacrés et al., 2020).

Table 4 shows the fermentation process of *L. mutabilis* Sweet in relation to dry matter (DM) conversion, where an interaction between the studied factors is observed. The *A. niger* J1 strain converts up to 7.68 percentage points during the 168 hours of fermentation. On the other hand, the *T. viride* M5-2 strain converts only 1.3 percentage points in the same period. These values indicate the fermentation activity, with substrate conversion observed by the fungi. The difference in conversion between the strains may be attributed to the metabolism of the fungi (Lameiras et al., 2018), as well as the composition of soluble carbohydrates and, consequently, the functional food properties of legumes (Dustet and Izquierdo, 2004).

The determinations of exo β-1,4-glucanase activity (Figure 2) showed that the fungi produce cellulase enzymes, with most enzyme activity occurring during the initial hours of fermentation and remaining active throughout the 168-hour fermentation period. This hydrolytic activity presents a marked difference between strains. The *A. niger* J1 strain exhibited greater cellulolytic activity, increasing from 0.064 FPU/mL to 0.189 FPU/mL by the end of fermentation of *L. mutabilis*, which corresponds to the fungal colonization of the substrate and its sporulation. However, for the *T. viride* M5-2 strain, there was no significant increase in enzymatic activity, reaching a maximum of 0.106 FPU/mL on the second day of fermentation, followed by a decline to as low as 0.074 FPU/mL. These enzyme activity values were very low. This behavior could be related to the type of substrate, which may not have favored hydrolytic action (Malgas et al., 2017), and may also be influenced by the elevated pH, which can affect enzymatic activity (Villacrés et al., 2020).

Table 3. Growth of *A. niger* J1 and *T. viride* M5-2 during the fermentation dynamics of *L. mutabilis* Sweet at Temperature = 30°C, pH = 6, Humidity = 70 %.

Strain	Growth (Hours)						
	24	**48**	**72**	**96**	**120**	**144**	**168**
A. niger J1	X	XX	XXX	XXX	XXX	XXX	XXX
T. viride M5-2		X	XX	XX	XX	XX	XX

X: onset of mycelial growth, XX: sporulation, XXX: complete sporulation

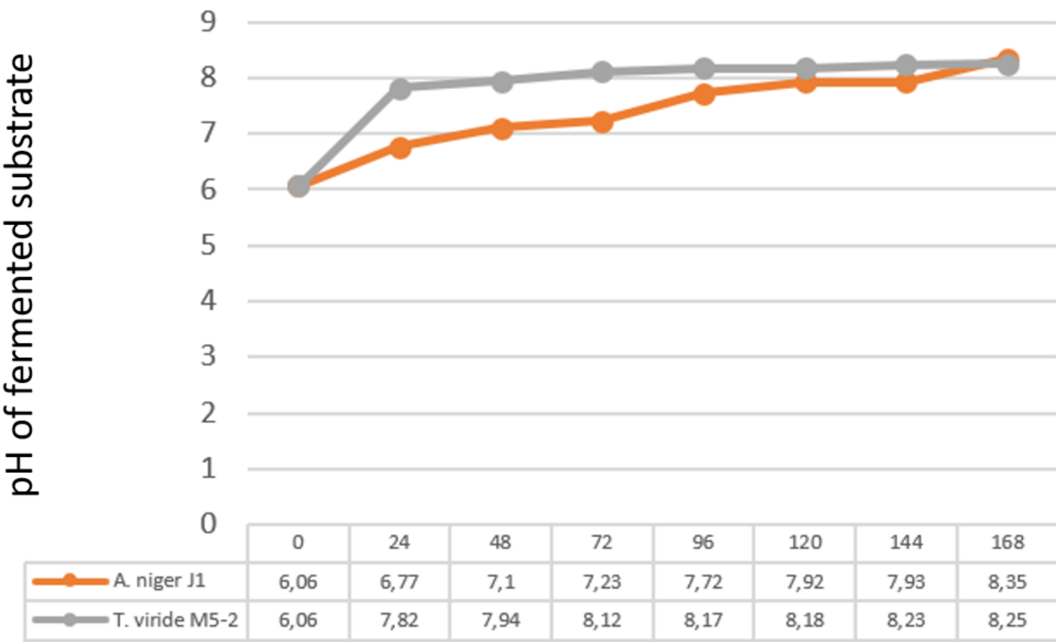

Figure 1. pH variation during the fermentation dynamics of *L. mutabilis* Sweet by *A. niger* J1 and *T. viride* M5-2. SE (±) 0.168, $P < 0.001$.

Table 5 shows the effect of the fermentation process on the fibrous fraction of the substrate. A notable reduction in NDF values by both strains and in ADF values by *A. niger* J1 was observed. This reduction could be related to the high nitrogen content associated with this indicator (Villacrés et al., 2020), as the studied strains, in addition to using the components of the cell wall, may have metabolized part of the nitrogen associated with fiber as a nutrient before beginning to degrade lignin (Valiño et al., 2015).

NDF, also known as insoluble fiber, is a good predictor of the substrate's energy value. Very low levels slow down intestinal transit, reduce productive yields, and increase the risk of digestive pathologies (Jiménez-Moreno et al., 2019). Conversely, excessive levels are related to poor digestibility, particularly in monogastric species whose digestive systems are not adapted to high-fiber feeds. Valiño et al. (2015) demonstrated that the *T. viride* M5-2 strain has valuable potential for the biotransformation of fibrous substrates that could later be included in animal feed.

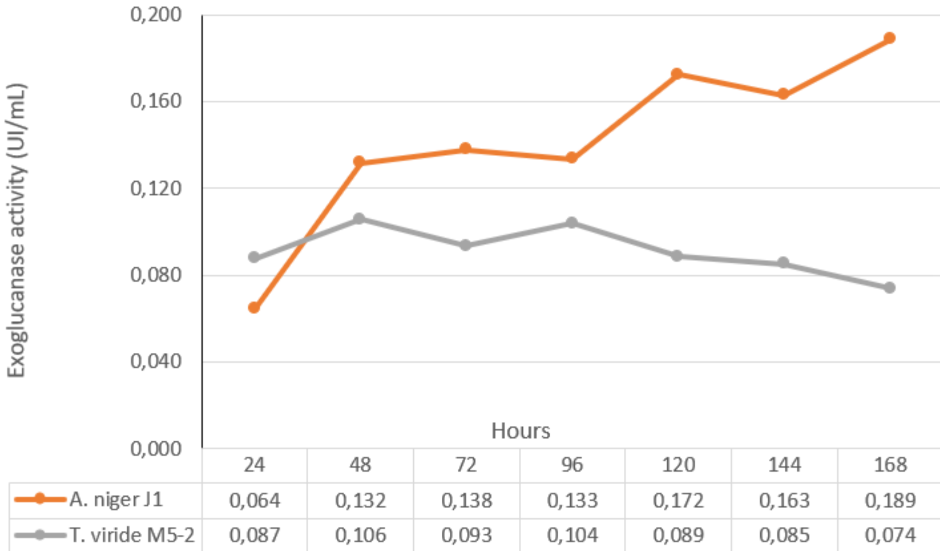

Figure 2. Exo β-1,4 glucanase enzymatic activity of *A. niger* J1 and *T. viride* M5-2 during the solid-state fermentation dynamics of *L. mutabilis* Sweet. SE (±) 0.038, P<0.001.

Table 4. Dry matter conversion during the solid fermentation process of *L. mutabilis* Sweet with *A. niger* J1 and *T. viride* M5-2. Initial conditions: Temperature = 30 °C, pH = 6, Humidity = 70 %.

Indicator	Strain	Fermentation Time (hours)								SE (±)
		0	24	48	72	96	120	144	168	Sign.
Dry Matter	*A. niger* J1	0^a	0.17^a	0.34^a	3.02^c	4.46^d	5.71^e	7.48^f	7.68^f	0.679
Conversion (%)	*T. viride* M5-2	0^a	0.9^b	0.93^b	0.94^b	0.95^b	1.16^b	1.23^b	1.3^b	P<0.001

^{a,b,c,d,e,f} Different letters indicate significant differences at P<<0.05, according to Duncan.

Both strains demonstrated the ability to degrade the fibrous fraction of the substrate. *A. niger* J1 reduced NDF and ADF by 12 percentage points, while *T. viride* M5-2 reduced NDF by 12 percentage points but only reduced ADF by 6 percentage points. The cellulolytic activity was greater in *A. niger*, which degraded cellulose by 11 percentage points, while *T. viride* M5-2 only degraded 4 percentage points.

The use of *L. mutabilis* Sweet as a substrate for solid fermentations has been scarcely reported in the literature. Other varieties of *Lupinus* have been used in fermentations with bacteria to improve their nutritional values (Starkute et al., 2016; Bartkiene et al., 2018).

Table 6 shows the effect of fermentation on secondary metabolites present and associated with the fibrous fraction of the analyzed substrate. From the analysis of phenolic content and its transformation, it was observed that the *A. niger* J1 strain reduced the phenolic content from 9.78 mg to 1.83 mg per 100 grams of dry substrate, with the greatest reduction occurring during the first three days. This reduction is consistent with the findings of Molina et al. (1990), who reported up to a 75 % reduction in polyphenol content using a different strain of *A. niger*.

On the other hand, *T. viride* M5-2 only reduced the phenolic content from 9.78 mg to 4.49 mg throughout the process. The *A. niger* J1 strain reduced flavonoids by 53% compared to the unfermented substrate, while the *T. viride* M5-2 strain reduced them by 22% during the first four days of fermentation. However, after the fifth day, the concentration of flavonoids likely increased due to the reduction in dry matter during fermentation.

It was observed, unlike other lignocellulosic substrates, that no pretreatment was required for the fermentation of Lupinus, as previously noted in laboratory experiments with other legumes (Pérez et al., 2016), which is not the case when sugarcane bagasse is used (De la Cruz et al., 2016).

Phytochemical studies on phenolic compounds conducted by Scull et al. (2015) on forage from other legumes with various fungal strains yielded similar results. However, the enzymatic potential of the T. viride M5-2 strain had a greater impact on the transformation of this seasonal legume, with a reduction of 32% in polyphenols, 18% in flavonoids, and 3% in fiber, without the addition of other mineral sources.

Table 5. Effect of the fermentation process on the fibrous fraction of the substrate with both strains. Temperature = 30°C, pH = 6, Humidity = 70%.

Indicators (%)	Strain	Fermentation Time (hours)								SE (±)
		0	24	48	72	96	120	144	168	Signific.
NDF	*A. niger* J1	71.05^{b}	61.26^{a}	59.25^{a}	61.60^{a}	60.73^{a}	60.55^{a}	57.62^{a}	59.37^{a}	0.773
	T. viride M5-2	71.05^{b}	61.67^{a}	59.87^{a}	61.26^{a}	60.14^{a}	60.70^{a}	60.64^{a}	58.97^{a}	P<0.001
ADF	*A. niger* J1	53.84^{d}	50.84^{d}	47.29^{abcd}	47.94^{abcd}	48.43^{abcd}	42.75^{ab}	43.04^{abc}	41.77^{a}	0.827
	T. viride M5-2	53.84^{d}	49.34^{bcd}	49.08^{abcd}	50.23^{cd}	48.60^{abcd}	49.19^{abcd}	47.87^{abcd}	47.89^{abcd}	P<0.001
Lignin	*A. niger* J1	13.28^{c}	10.80^{abc}	11.36^{abc}	12.62^{bc}	13.75^{c}	12.15^{abc}	13.01^{c}	12.01^{abc}	0.320
	T. viride M5-2	13.28^{c}	9.25^{a}	9.83^{ab}	11.16^{abc}	10.92^{abc}	11.62^{abc}	11.06^{abc}	11.06^{abc}	P<0.001
Cellulose	*A. niger* J1	40.56^{c}	40.04^{c}	35.93^{abc}	35.32^{abc}	34.68^{abc}	30.60^{ab}	30.03^{a}	29.76^{a}	0.939
	T. viride M5-2	40.56^{c}	40.09^{c}	39.25^{c}	39.07^{c}	37.68^{c}	37.57^{c}	36.81^{bc}	36.83^{bc}	P<0.001

^{a,b,c,d} Different letters indicate significant differences at P<0.05, according to Duncan.

Table 6. Effect of fermentation on flavonoids and polyphenols.

Indicator (mg / 100 g DM)	Strain	Fermentation time (hours)								SE (±)
		0	24	48	72	96	120	144	168	Signific.
Flavonoids	*A. niger* J1	55.53^{de}	46.82^{bc}	30.25^{a}	27.57^{a}	30.62^{a}	27.05^{a}	26.53^{a}	26.01^{a}	3.890
	T. viride M5-2	55.53^{de}	53.53^{de}	50.31^{cd}	44.57^{b}	43.28^{b}	56.35^{e}	64.23^{f}	72.17^{g}	P<0.001
Phenolic content	*A. niger* J1	9.78^{h}	5.35^{d}	1.96^{ab}	1.83^{a}	2.61^{ab}	2.16^{ab}	2.52^{b}	2.52^{b}	0.730
	T. viride M5-2	9.78^{h}	8.74^{g}	8.60^{g}	8.45^{g}	6.90^{f}	6.10^{e}	5.02^{d}	4.49^{c}	P<0.001

^{a,b,c,d,e,f,g,h} Different letters indicate significant differences at P<0.05, according to Duncan.

4 Conclusions

The results demonstrate that using solid-state fermentation can reduce antinutritional factors in *L. mutabilis* Sweet foliage meal to acceptable levels, thereby increasing its potential nutritional value. In this study, there was a significant reduction in NDF, ADF, flavonoids, and phenolic content during fermentation, improving its nutritional quality and enhancing its potential for use in monogastric species, while facilitating further processing. It is important to optimize the process for potential scaling.

The *T. viride* M5-2 and *A. niger* J1 strains enabled the development of a biologically feasible fermentation process for the foliage meal under study, improving its nutritional value, with the best results obtained using the *A. niger* J1 strain. It is recommended to optimize the process for scaling.

Authors' contribution

D.J.C.M.: Conceptualization, Formal analysis, Data processing, Funding acquisition, Investigation, Project administration, Resources, Supervision, Validation, Visualization, Writing – original draft. J.C.D.M: Conceptualization, Project administration, Supervision, Writing –review & editing. E.V.C.: Conceptualization, Project administration, Supervision, Writing –review & editing.

References

Adney, B. and Baker, J. (2008). Measurement of cellulase activities: laboratory analytical procedure (lap); issue date: 08/12/1996. Technical report, National Renewable Energy Laboratory. Online: https://n9.cl/049al5.

Bartkiene, E., Sakiene, V., Bartkevics, V., Juodeikiene, G., Lele, V., Wiacek, C., and Braun, P. (2018). Modulation of the nutritional value of lupine wholemeal and protein isolates using submerged and solid-state fermentation with *Pediococcus pentosaceus* strains. *International Journal of Food Science and Technology*, 53(8):1896–1905. Online: https://n9.cl/1o079.

Bessada, S., Barreira, J., and Oliveira, M. (2019). Pulses and food security: Dietary protein, digestibility, bioactive and functional properties. *Trends in Food Science and Technology*, 93:53–68. Online: https://n9.cl/meeep.

Carvajal-Larenas, F. (2019). Nutritional, rheological and sensory evaluation of *Lupinus mutabilis* food products-a review. *Czech Journal of Food Sciences*, 37(5):301–311. Online: https://n9.cl/4556o.

De la Cruz, K., Dustet-Mendoza, J., Pérez-Caballero, L., and Anaya-Villalpanda, M. (2016). Caracterización de enzimas celulasas de nuevas cepas fúngicas obtenidas a partir de bagazo de caña de azúcar. *ICIDCA. Sobre los Derivados de la Caña de Azúcar*, 50(2):35–42. Online: https://n9.cl/4lvc7.

Díaz Sánchez, M., Martín-Cabrejas, M., Martínez Pérez, M., Savón Valdés, L., Aguilera, Y., Benítez, V., Torres Cárdenas, V., Coto Valdés, G., González Conde, A., and Sarmiento Menéndez, M. (2017). Germinados de leguminosas temporales: Una alternativa para la alimentación animal. *Cuban Journal of Agricultural Science*, 51(3):381–390. Online: https://n9.cl/s4zip.

Dustet, J. and Izquierdo, E. (2004). Aplicación de balances de masa y energía al proceso de fermentación en estado sólido de bagazo de caña de azúcar con *Aspergillus niger*. *Biotecnología Aplicada*, 21(2):85–91. Online: https://n9.cl/rxp1c.

Gao, W., Lei, Z., Tabil, L., and Zhao, R. (2020). Biological pretreatment by solid-state fermentation of oat straw to enhance physical quality of pellets. *Journal of Chemistry*, 2020(1. Online: https://n9.cl/sed5n).

Gulisano, A., Alves, S., Martins, J., and Trindade, L. (2019). Genetics and breeding of *Lupinus mutabilis*: An emerging protein crop. *Frontiers in Plant Science*, 10:1385. Online: https://n9.cl/ol8z4.

Haldar, D. and Purkait, M. (2020). Lignocellulosic conversion into value-added products: A review. *Process Biochemistry*, 89:110–133. Online: https://n9.cl/lt7j10.

Jha, R., Fouhse, J., Tiwari, U., Li, L., and Willing, B. (2019). Dietary fiber and intestinal health of monogastric animals. *Frontiers in Veterinary Science*, 6(48. Online: https://n9.cl/l4fl3).

Jiménez-Moreno, E., González-Alvarado, J., de Coca-Sinova, A., Lázaro, R., Cámara, L., and Mateos, G. (2019). Insoluble fiber sources in mash or pellets diets for young broilers. 2. effects on gastrointestinal tract development and nutrient digestibility. *Poultry Science*, 98(6):2531–2547. Online: https://n9.cl/t1bt5.

Kaschuk, J., de Alexandria Santos, D., Frollini, E., Canduri, F., and Porto, A. (2020). Influence of ph, temperature, and sisal pulp on the production of cellulases from *Aspergillus* sp. cbmai 1198 and hydrolysis of cellulosic materials with different hemicelluloses content, crystallinity, and average molar mass. *Biomass Conversion and Biorefinery*, 10:483–494. Online: https://n9.cl/3mbvf.

Lameiras, F., Ras, C., Ten Pierick, A., Heijnen, J., and van Gulik, W. (2018). Stoichiometry and kinetics of single and mixed substrate uptake in *Aspergillus niger*. *Bioprocess and Biosystems Engineering*, 41:157–170. Online: https://n9.cl/uk1et.

Linn, J. and Martin, N. (1991). Forage quality analyses and interpretation. *The Veterinary Clinics of North America. Food Animal Practice*, 7(2):509–523. Online: https://n9.cl/tbn61.

Malgas, S., Thoresen, M., van Dyk, J., and Pletschke, B. (2017). Time dependence of enzyme synergism during the degradation of model and natural lignocellulosic substrates. *Enzyme and Microbial Technology*, 103:1–11. Online: https://n9.cl/pl4kx.

Martínez Flores, L., Ruivenkamp, G., and Jongerden, J. (2016). Fitomejoramiento y racionalidad social: los efectos no intencionales de la liberación de una semilla de lupino (*Lupinus mutabilis* sweet) en ecuador. *Antípoda. Revista de Antropología y Arqueología*, (26):71–91. Online: https://bit.ly/4fublCu.

Martínez-Pérez, M., Sarmiento-Franco, L., Santos-Ricalde, R., and Sandoval-Castro, C. (2018). Chemical composition and *in vitro* protein digestibility of processed *Mucuna pruriens* seeds. *Cuban Journal of Agricultural Science*, 52(3):313–319. Online: https://n9.cl/daxg4.

Molina, M., Lechuga, O., and Bressani, R. (1990). Valor nutritivo de la pulpa de café sometida a fermentación sólida usando *Aspergillus niger* en pollos y cerdos. *Agronomía Mesoamericana*, 1:79–82. Online: https://n9.cl/imwd4j.

Molina-Poveda, C., Lucas, M., and Jover, M. (2013). Evaluation of the potential of andean lupin meal (*Lupinus mutabilis* sweet) as an alternative to fish meal in juvenile *Litopenaeus vannamei* diets. *Aquaculture*, 410:148–156. Online: https://n9.cl/pe2tq.

Oliva, M., Valqui, L., Meléndez, J., Milla, M., Leiva, S., Collazos, R., and Maicelo, J. (2018). Influencia de especies arbóreas nativas en sistemas silvopastoriles sobre el rendimiento y valor nutricional de *Lolium multiflorum* y *Trifolium repens*. *Scientia Agropecuaria*, 9(4):579–583. Online: https://n9.cl/z7qw8.

Pandey, A. (2003). Solid-state fermentation. *Biochemical Engineering Journal*, 13(2-3):81–84. Online: https://n9.cl/1413a.

Pérez, H., Dustet, J., and Valiño, E. (2016). Incremento de la calidad nutritiva potencial de la harina de follaje de stizolobium niveum (mucuna) mediante fermentación en estado sólido con el hongo trichoderma viride m5-2. *Revista CENIC. Ciencias Químicas*, 47:30–33. Online: https://n9.cl/bbzls.

Rodríguez García, I. (2017). Potencialidades de *Tithonia diversifolia* (hemsl.) gray en la alimentación animal. *Livestock Research for Rural Development*, 29(4. Online: https://n9.cl/k43jr0).

Roussos, S., Olmos, A., Raimbault, M., Saucedo-Castañeda, G., and Lonsane, B. (1991). Strategies for large scale inoculum development for solid state fermentation system: conidiospores of *Trichoderma harzianum*. *Biotechnology Techniques*, 5:415–420. Online: https://n9.cl/yqhhe.

Savón, L., Gutiérrez, O., Ojeda, F., and Scull, I. (2005). Harinas de follajes tropicales: una alternativa potencial para la alimentación de especies monogástricas. *Pastos y Forrajes*, 28(1):69–79. Online: https://n9.cl/dqjuw.

Scull, I., Savón, L., Valiño, E., and Ramos, Y. (2015). Composición fitoquímica de la harina de forraje de mucuna (*Styzolobium aterrimum*) fermentada con el hongo *Trichoderma viride*. *Multiciencias*, 15(3):265–270. Online: https://n9.cl/srm4x.

Siddhuraju, P., Becker, K., and Makkar, H. (2000). Studies on the nutritional composition and antinutritional factors of three different germplasm seed materials of an under-utilized tropical legume, *Mucuna pruriens* var. *Utilis*. *Journal of Agricultural and Food Chemistry*, 48(12):6048–6060. Online: https://n9.cl/6dy5p.

Starkute, V., Bartkiene, E., Bartkevics, V., Rusko, J., Zadeike, D., and Juodeikiene, G. (2016). Amino acids profile and antioxidant activity of different *Lupinus angustifolius* seeds after solid state and submerged fermentations. *Journal of Food Science and Technology*, 53:4141–4148. Online: https://n9.cl/sh9y7.

Sugiharto, S. and Ranjitkar, S. (2019). Recent advances in fermented feeds towards improved broiler chicken performance, gastrointestinal tract microecology and immune responses: A review. *Animal Nutrition*, 5(1):1–10. Online: https://n9.cl/53y71.

Trujillo, A. and Escobar, A. (2012). Evaluación de la sustitución de concentrado comercial por harina de forrajeras en pollos de engorde ross. *Agroecología: Ciencia y Tecnología*, 1(1):6–12. Online: https://n9.cl/m7jeu.

Valiño, E., Elías, A., Torres, V., Carrasco, T., and Albelo, N. (2004a). Improvement of sugarcane bagasse composition by the strain *Trichoderma viride* m5-2 in a solid-state fermentation bioreactor. *Cuban Journal of Agricultural Science*, 38(2):143–150. Online: https://n9.cl/peo82j.

Valiño, E., García, R., and Albelo, N. (2004b). Efecto de la inoculación de la cepa de *Trichoderma viride* 137 mcxi en mezclas de *Vigna unguiculata* y bagazo de caña de azúcar para disminuir factores antinutricionales. *Revista Cubana de Ciencia Agrícola*, 38(1):65–72. Online: https://n9.cl/l09v6.

Valiño, E., Savón, L., Elías, A., Rodriguez, M., and Albelo, N. (2015). Mejora del valor nutritivo de las leguminosas temporales *Vigna unguiculata, Canavalia ensiformis, Stizolobium niveum, Lablab purpureus* mediante el procesamiento de sus granos con *Trichoderma viride* m5-2. *Cuban Journal of Agricultural Science*, 49(1):81–89. Online: https://n9.cl/l25tw.

Varadyova, Z., Certik, M., and Jalc, D. (2018). The possible application of fungal enriched substrates in ruminant nutrition. a review. *Journal of Animal and Feed Sciences*, 27(1):3–10. Online: https://n9.cl/9gn0c.

Vargas-Guerrero, B., García-López, P., Martínez-Ayala, A., Domínguez-Rosales, J., and Gurrola-Díaz, C. (2014). Administration of *Lupinus albus* gamma conglutin (cγ) to n5 stz rats augmented *Ins-1* gene expression and pancreatic insulin content. *Plant Foods for Human Nutrition*, 69:241–247. Online: https://n9.cl/hhs3c3.

Vera, J., Dueñas, A., Rodríguez, J., and Radice, M. (2022). Phytochemical characterization of the ethanolic extract, antioxidant activity, phenolic content and toxicity of the essential oil of *Curcuma longa* l. *Revista De La Facultad De Agronoma De La Universidad Del Zulia*, 39(1):1–7. Online: https://bit.ly/3Ag5diz.

Villacrés, E., Quelal, M., Jácome, X., Cueva, G., and Rosell, C. (2020). Effect of debittering and solid-state fermentation processes on the nutritional content of lupine (*Lupinus mutabilis* sweet). *International Journal of Food Science and Technology*, 55(6):2589–2598. Online: https://n9.cl/4zm84.

Villena, G. and Gutiérrez-Correa, M. (2003). Biopelículas de *Aspergillus niger* para la producción de celulasas: algunos aspectos estructurales y fisiológicos. *Revista Peruana de Biología*, 10(1):78–87. Online: https://n9.cl/h1dgl.

Xu, C., Wang, B., Pu, Y., Tao, J., and Zhang, T. (2017). Advances in extraction and analysis of phenolic compounds from plant materials. *Chinese Journal of Natural Medicines*, 15(10):721–731. Online: https://n9.cl/qdayb.

LA GRANJA:
REVISTA DE
CIENCIAS DE LA VIDA
pISSN:1390-3799; eISSN:1390-8596
https://doi.org/10.17163/lgr.n41.2025.10

Scientific paper/ Artículo científico
AGRICULTURAL SCIENCES

PLANTING DISTANCE IN *ZEA MAYS* L. DURING THE DRY AND RAINY SEASONS ON THE CENTRAL COAST OF ECUADOR

DISTANCIAMIENTO DE SIEMBRA EN *ZEA MAYS* L. DURANTE LA ÉPOCA SECA Y LLUVIOSA EN LA COSTA CENTRAL DEL ECUADOR

Camilo Alexander Mestanza Uquillas*[1], Pánfilo José Cedeño Cárcamo[2], Diana Verónica Véliz Zamora[1], Santiago Cristóbal Vásquez Matute[3] and John Jairo Pinargote Alava[4]

[1] *Universidad Técnica Estatal de Quevedo-(UTEQ), Quevedo, Los Ríos, Ecuador.*
[2] *Proyecto de Innovación de Asistencia Técnica y Extensión Rural (PIATER), Ministerio de Agricultura y Ganadería (MAG), Babahoyo, Los Ríos, Ecuador.*
[3] *Universidad Nacional de Loja (UNL), Loja, Ecuador.*
[4] *Universidad de Córdoba-(UCO), Córdoba, España.*

*Corresponding author: cmestanza@uteq.edu.ec

Received on January 12th, 2022. Accepted, after revision on July 04th, 2022. Published on March 1st, 2025.

Abstract

The research was carried out in Mocache, province of Los Ríos, where three experimental corn trials were established, one on the property of Mr. Fortunato Cedeño Diaz, located in the John F. Kennedy sector, and two located on the "La María" Campus of the Quevedo State Technical University (UTEQ), with the purpose of evaluating the effect of different planting distances of a commercial hybrid (hybrid ADV-9139) and a creole variety (Creole variety S/N) of corn during the dry and rainy seasons, in order to define optimal planting distances to achieve better yields. A completely randomized design (CRD) with a unifactorial arrangement was applied, with six treatments composed of a combination of two variables: varieties and planting distances. The first consisted of two genotypes: hybrid ADV-9139 and a creole variety S/N, and the second consisted of distances of 0.6 *times* 0.2 m; 0.7 × 0.2 m and 0.8 × 0.2 m. Each of these treatments had four replications. The results showed little influence of distances on plant height, stem diameter and ear insertion height. Regarding productive parameters such as yield, T4 (Hybrid ADV - 9139 + 0.6 X 0.2) and T5 (Hybrid ADV - 9139 + 0.7 X 0.2) stood out in trials 1 and 3, while only T4 stood out in trial 2.

Keywords: Maize, density, genotypes, agronomic response, yield parameters.

Resumen

La investigación se desarrolló en el cantón Mocache provincia de Los Ríos, donde se establecieron tres ensayos experimentales de maíz, uno en la propiedad del Sr. Fortunato Cedeño Diaz, ubicado en el sector John F. Kennedy, y dos ubicados en el Campus "La María" de la Universidad Técnica Estatal de Quevedo (UTEQ), con el fin de evaluar el efecto de distintos distanciamientos de siembra sobre el comportamiento agronómico de un híbrido comercial (híbrido ADV-9139) y una variedad criolla (Variedad criolla S/N) de maíz durante la época seca y lluviosa para definir distancias de siembra óptimas que permitan alcanzar mejores rendimientos. Se aplicó un Diseño completamente al azar (DCA) con arreglo unifactorial, con seis tratamientos compuestos por la combinación de dos variables: variedades y distanciamientos de siembra. La primera conformada por dos genotipos: híbrido ADV-9139 y una variedad criolla S/N, y la segunda por distancias de 0,6 × 0,2 m; 0,7 × 0,2 m y 0,8 × 0,2 m. Cada uno de estos tratamientos tuvo cuatro repeticiones. Los resultados registrados demostraron una escaza influencia de las distancias sobre la altura de planta, diámetro del tallo y altura de inserción de mazorca. Respecto a los parámetros productivos como el rendimiento se logró destacar T4 (Híbrido ADV – 9139 + 0,6 X 0,2) y T5 (Híbrido ADV – 9139 + 0,7 X 0,2) en los ensayos 1 y 3, mientras que únicamente destacó T4 en el ensayo 2.

Palabras clave: Maíz, densidad, genotipos, respuesta agronómica, parámetros productivos.

Suggested citation:	Mestanza Uquillas, C., Cedeño Cárcamo, P., Véliz Zamora, D., Vásquez Matute, S. and Pinargote Alava, J. (2025). Planting Distance in *Zea mays* L. during the dry and rainy seasons on the central Coast of Ecuador. *La Granja: Revista de Ciencias de la Vida.* Vol. 41(1):144-154. https://doi.org/10.17163/lgr.n41.2025.10.

Orcid IDs:

Camilo Alexander Mestanza Uquillas: https://orcid.org/0000-0001-9299-170X
Pánfilo José Cedeño Cárcamo: https://orcid.org/0000-0002-9411-8645
Diana Verónica Véliz Zamora: https://orcid.org/0000-0003-2039-8741
Santiago Cristóbal Vásquez Matute: https://orcid.org/0000-0002-3713-020X
John Jairo Pinargote Alava: https://orcid.org/0000-0002-8065-5124

1 Introduction

Maize (*Zea mays* L.) is one of the crops most susceptible to nutrient deficiency stress, particularly during the pre- and post-flowering period, known as the critical period. The extent to which the crop is affected during this stage is directly related to the agronomic practices employed and the availability of resources essential for plant growth (Videla et al., 2014).

One of the most significant factors in this regard is population density. Changes in population density can elicit different responses in productive parameters, which in turn depend on the genotype and environmental quality (Quevedo et al., 2015). This phenomenon is explained by the availability of resources per plant, which is influenced by crop processes such as light capture and utilization, as well as genotype-specific traits like reproductive plasticity and the stability of biomass partitioning during the critical period. It is well known that modern hybrids differ in the population density that maximizes their yield (Ogando et al., 2017).

However, given the modifications introduced in recent maize genotypes -such as reduced plant height, lower ear insertion height, decreased plant sterility, shorter anthesis-silking interval, plants with more upright leaves, and higher yield potential- it is necessary to reevaluate recommendations regarding spacing and planting density (Martínez et al., 2017).

A similar situation occurs with landrace varieties, which have been cultivated and selected by farmers over generations. These varieties retain unique identities and great adaptability but lack formal breeding programs (CIMMYT, 2014). Combined with the absence of appropriate practices, such as the implementation of optimal planting distances, this has hindered the full exploitation of the potential found in many of these materials.

Considering the above and the significant cultural, socioeconomic, and dynamic importance of this crop in municipalities like Mocache, as well as in the province of Los Ríos —which accounts for 43.81 % of the national maize production (1,479,770 tons) according to INEC (2020)— it is imperative to reconsider strategies to increase productivity. These strategies must aim to meet local demand, a critical factor in strengthening the productive chain in the region.

In this context, this paper aims to evaluate the effect of different planting distances on the agronomic performance of a commercial hybrid and a landrace maize variety under the agroclimatic conditions of Mocache during the dry and rainy seasons. The objective is to determine the optimal planting distance to achieve higher yields.

2 Material y Methods

2.1 Experiment location and crop management

The establishment of maize trials 1 and 2 cultivated during the rainy season took place in December 2020. Trial 1 was conducted on the property of Mr. Fortunato Cedeño Diaz, located in the John F. Kennedy sector of Mocache Canton, Los Ríos Province, with geographic coordinates: 1°15′57.3″ South Latitude and 79°29′43.8″ West Longitude, at an altitude of 71.4 meters above sea level. Trial 2 was carried out at the "La María" Campus of UTEQ, with geographic coordinates: 1°05′01″ South Latitude and 79°30′02″ West Longitude, at an altitude of 66 meters above sea level.

Trial 3 was established in the same location as Trial 2 but during the dry season in May 2021. Table 1 provides a description of the agroclimatic conditions present in Mocache Canton.

Table 1. Agroclimatic conditions of the Mocache canton, Los Ríos province

Agroclimatic data	Average values
Altitude	75 msnm
Temperature	24.9 °C
Relative Humidity (%)	84 %
Precipitation	2216.3 mm
Topography	Irregular

Regarding management, three experimental trials of 1,320 m^2 were established at the sites and during the seasons previously mentioned. Manual operations such as weeding, and plowing were carried out to prepare the fields. Experimental units were then randomly assigned.

Once the fields were prepared, sowing was performed manually using a planting stick (espeque). The following planting distances were employed: 0.6 × 0.2 m, 0.7 × 0.2 m and 0.8 × 0.2 m. Weed control was conducted conventionally, using selective pre-emergent and post-emergent herbicides to prevent collateral damage. Fertilization was performed using urea and diammonium phosphate (DAP). Similarly, pest control was carried out conventionally, applying systemic and contact insecticides. Fungicides were also used, proving essential given that the trials were conducted during the rainy season. Since the sowing for trials 1 and 2 was scheduled for December 2020, coinciding with the beginning of the rainy season, irrigation was not required, and the crop was grown under rainfed conditions. However, for trial 3, conducted during the dry season, sprinkler irrigation was applied to achieve field capacity. Finally, the harvest was performed manually once the plants had reached physiological maturity.

2.2 Experimental Design

The three trials were conducted using a Completely Randomized Design (CRD) with a unifactorial arrangement, consisting of six treatments formed by the combination of two variables: varieties and planting distances. The first variable included two genotypes: the ADV-9139 hybrid and a landrace variety (S/N), while the second variable comprised planting distances of 0.6 × 0.2 m, 0.7 × 0.2 m and 0.8 × 0.2 m. Each treatment had four replications. The effective area of each trial was 1320 m^2, consisting of 24 plots of 25 m^2 each.

2.3 Measurements and statistical analysis

Plant height was recorded 60 days after sowing (DAS) by randomly selecting 10 plants per plot (replication) and measuring the distance from the soil surface to the base of the plant's ear using a measuring tape. To determine the number of rows, ear diameter, and ear length, 10 ears were randomly selected, and measurements were taken and recorded for each parameter. Additionally, the 100-seed weight and grain yield were determined. This required threshing the ears harvested from the effective area of each experimental plot, followed by moisture standardization to 13 % using the following formula:

$$PU(13\,\%) = \frac{Pa(100 - Ha)}{100 - Hd}$$

Where:
PU represents the weight adjusted to 13 % moisture,
Pa is the actual weight,
Ha is the current moisture content,
Hd is the desired moisture content.

The data obtained from the three trials were subjected to analysis of variance (ANOVA), and treatment means were compared using Tukey's test (5 %). The statistical analysis was performed using InfoStat software, version 2019.

3 Results and Discussion

3.1 Plant height (m)

Plant height exhibited two distinct scenarios. The first occurred in Trials 1 and 2, where analysis of variance demonstrated statistically significant differences between treatments ($P<0.05$). In Trial 1, the highest values were observed in T1, T3, and T2, with measurements of 2.86, 2.82, and 2.81 m, respectively. In Trial 2, the treatment that stood out was T1, with a value of 2.98 m. On the other hand, in Trial 3, no statistically significant differences between treatments were found ($P>0.05$) (Table 2).

3.2 Number of rows per ear

Regarding the number of rows per ear, according to the ANOVA with a variation coefficient of 3.87 %, there were no significant statistical differences among the treatments that constituted trials 1, 2 and 3 ($P>0.05$), obtaining averages that ranged between 14 and 16 rows per ear in each of the cases (Table 3).

3.3 Cob diameter (mm)

According to the analysis of variance for ear diameter in trial 1, there were no significant statistical differences between treatments ($P>0.05$) (Table 4). This scenario was replicated in trial 2, where there were no statistical differences between treatments or factors ($P>0.05$). On the other hand, trial 3 obtained statistical differences, with T3 being the different treatment with a record of 47.85 mm.

Table 2. Plant height at 60 dds (m) in trial 1, 2 and 3. Mocache, Los Ríos province, Ecuador.

Plant height[1]				
	Location of trials	**John F. Kennedy, 2020 rainy season (test 1)**	**Campus "La María", 2020 rainy season (test 2)**	**Campus "La María", dry season 2021 (test 3)**
		60 dds[2]	**60 dds[2]**	**60 dds[2]**
Trat[3]	**Description**			
T1	Creole variety S/N + 0.6 X 0.2	2.86 a	2.98 a	2.34 a
T2	Creole variety S/N + 0.7 X 0.2	2.81 a	2.48 b	2.64 a
T3	Creole variety S/N + 0.8 X 0.2	2.82 a	2.40 b	2.52 a
T4	ADV Hybrid – 9139 + 0.6 X 0.2	2.40 b	2.31 b	2.30 a
T5	ADV Hybrid – 9139 + 0.7 X 0.2	2.37 b	2.38 b	2.50 a
T6	ADV Hybrid – 9139 + 0.8 X 0.2	2.35 b	2.29 b	2.26 a
C.V(%)		4.23	8.25	11.86
x̄		2.61	2.47	2.43

[1]equal letters are not significant according to Tukey's test (P>0.05).
[2]dds: Days after the sown,
[3]Trat: Treatment.

3.4 Cob length (cm)

According to the ANOVA results, statistically significant differences in cob length were observed among treatments in trials 1, 2, and 3 (P<0.05). Treatments T4, T5, and T6 exhibited distinct outcomes in each case, whereas treatments T1, T2, and T3 recorded lower values (Table 5).

3.5 Weight of 100 seeds (g)

Regarding the weight of 100 seeds, ANOVA revealed statistically significant differences among the treatments in trial 1 (P<0.05). Treatments T4, T5, and T6 showed distinct values, with averages of 43.75, 43.75, and 46.25 g, respectively, compared to T1, T2, and T3, which recorded lower values of 36.00, 37.25, and 36.50 g, respectively. In contrast, no statistically significant differences among treatments were observed in trials 2 and 3 (P>0.05) (Table 6).

Table 3. Number of rows per ear in trials 1, 2 and 3. Mocache, Los Ríos province, Ecuador.

Number of rows per ear[1]				
	Location of trials	**John F. Kennedy, winter of 2020 (test 1)**	**Campus "La María", winter of 2020 (test 2)**	**Campus "La María", summer of 2021 (test 3)**
Treatment	**Description**			
T1	Creole variety S/N + 0.6 X 0.2	15.25 a	14.50 a	14.40 a
T2	Creole variety S/N + 0.7 X 0.2	15.55 a	15.50 a	14.75 a
T3	Creole variety S/N + 0.8 X 0.2	15.60 a	15.00 a	15.35 a
T4	ADV Hybrid – 9139 + 0.6 X 0.2	15.25 a	15.50 a	14.47 a
T5	ADV Hybrid – 9139 + 0.7 X 0.2	15.30 a	14.00 a	14.27 a
T6	ADV Hybrid – 9139 + 0.8 X 0.2	14.95 a	15.00 a	14.47 a
C.V (%)		3.87	6.52	4.00
x̄		15.32	14.92	14.62

[1]equal letters are not significant according to Tukey's test (P>0.05).

3.6 Grain yield (kg/ha)

For the grain yield variable, the analysis of variance revealed statistically significant differences among the treatments in the evaluated trials (P<0.05). Treatments T4 and T5 stood out in trials 1 and 3, while in trial 2, only T4 demonstrated superior performance (Table 7).

Table 4. Ear diameter (mm) in trials 1, 2 and 3. Mocache, Los Ríos province, Ecuador.

Cob diameter (mm)[1]				
	Location of trials	**John F. Kennedy, 2020 rainy season (test 1)**	**Campus “La María”, 2020 rainy season (test 2)**	**Campus “La María”, dry season 2021 (test 3)**
Treatment	**Description**			
T1	Creole variety S/N + 0.6 X 0.2	48.75 a	44.50 a	43.43 cd
T2	Creole variety S/N + 0.7 X 0.2	49.44 a	46.13 a	45.00 bc
T3	Creole variety S/N + 0.8 X 0.2	49.49 a	46.20 a	47.85 a
T4	ADV Hybrid – 9139 + 0.6 X 0.2	48.27 a	45.40 a	43.43 cd
T5	ADV Hybrid – 9139 + 0.7 X 0.2	48.63 a	44.18 a	42.57 d
T6	ADV Hybrid – 9139 + 0.8 X 0.2	49.57 a	45.03 a	46.17 ab
C.V (%)		1.81	2.02	2.07
x̄		49.11	45.24	45.00

[1] equal letters are not significant according to Tukey’s test (P>0.05).

Table 5. Ear length (cm) in trials 1, 2 and 3. Mocache, Los Ríos province, Ecuador.

Cob length (cm)[1]				
	Location of trials	**John F. Kennedy, winter of 2020 (test 1)**	**Campus “La María”, winter of 2020 (test 2)**	**Campus “La María”, summer of 2021 (test 3)**
Treatment	**Description**			
T1	Creole variety S/N + 0.6 X 0.2	17.28 b	16.00 b	13.50 c
T2	Creole variety S/N + 0.7 X 0.2	17.16 b	15.93 b	14.50 bc
T3	Creole variety S/N + 0.8 X 0.2	17.63 b	15.96 b	15.00 b
T4	ADV Hybrid – 9139 + 0.6 X 0.2	20.51 a	18.08 a	17.44 a
T5	ADV Hybrid – 9139 + 0.7 X 0.2	20.25 a	19.01 a	17.42 a
T6	ADV Hybrid – 9139 + 0.8 X 0.2	20.25 a	19.01 a	18.79 a
C.V (%)		3.84	3.90	3.87
x̄		18.85	17.33	16.11

[1] equal letters are not significant according to Tukey’s test (P>0.05).

3.7 Discussion

The height data recorded for the ADV-9139 hybrid in the three evaluated trials align with those reported by Moreira (2019) for the same hybrid, established in the Mocache canton during the 2019 rainy season, with a value of 2.01 m at 52 days. However, it was observed in this research that the native variety S/N, across all spacing treatments, achieved higher height values than the hybrid, likely due to its wild traits. This behavior is commonly seen in native or mestizo varieties, as noted by authors such as Quiroz et al. (2017), Molina and Isasi (2018) and Cabrera et al. (2019), who found that mestizo plants (native × improved) exhibit greater height than hybrids, a finding corroborated by Rodríguez et al. (2016). Regarding planting spacing, Quiroz et al. (2017) recorded a similar scenario, where increased population densities did not result in significant phenotypic variability in plant height across genotypes.

Thus, both previous findings and the observations from this study suggest that marked differences exist between genotypes in growth traits such as height, attributed to distinct development patterns and genetic heritage expressed differently, even under similar environmental conditions (Sánchez et al., 2011). This was not the case with spacing, where it is commonly observed that closer row spacing enables plants to capture a greater proportion of total radiation due to an increase in the leaf area index and light interception efficiency per unit surface area, thereby promoting greater height development (Soltero et al., 2010). This phenomenon has been documented in various studies, including those by Campos (2022), Gómez et al. (2021) and Satorre (2021).

Despite this, it is important to clarify that plants with reduced height are generally the result of the genetic improvement process these materials undergo. This is supported by authors such as Bastidas et al. (2015) and Gordón and Camargo (2021), who note that this characteristic can be seen as an advantage during harvest, as well as reducing lodging of both roots and stems.

On the other hand, Velez (2019) highlights the influence of planting distance. In his study, he analyzed the effects of three spacings (0.80 × 0.25m, 0.80 × 0.30m and 0.80 × 0.35m) on maize cultivation using the Somma, ATL 400, and Pioneer hybrids, observing better results in productive parameters with a spacing of 0.80 m × 0.25m. This finding aligns with the conclusions of Millán, cited by Pérez (2015).

Regarding cob diameter, similar results were observed in trials 1 and 2 of Quimi (2015) study, conducted in nearby cantons such as Quevedo and Balzar. This research evaluated experimental and commercial hybrids, with the former achieving diameters of 48.9 mm compared to 46.7 mm for the latter. Concerning spacing, Zamudio et al. (2015) cited by Sánchez (2017), reported larger cob diameters in double-row systems using a commercial hybrid (AS-722), attributing this to lower population density per hectare. This is consistent with results from trial 3, where the 0.8 × 0.2 m spacing outperformed other densities.

Table 6. Weight of 100 seeds (g) in trials 1, 2 and 3. Mocache, Los Ríos Province, Ecuador.

Weight of 100 seeds (g)[1]				
	Location of trials	**John F. Kennedy, winter of 2020 (test 1)**	**Campus “La María”, winter of 2020 (test 2)**	**Campus “La María”, summer of 2021 (test 3)**
Treatment	**Description**			
T1	Creole variety S/N + 0.6 X 0.2	36.00 b	30.00 a	39.15 a
T2	Creole variety S/N + 0.7 X 0.2	37.25 b	30.00 a	38.85 a
T3	Creole variety S/N + 0.8 X 0.2	36.50 b	30.00 a	39.28 a
T4	ADV Hybrid – 9139 + 0.6 X 0.2	43.75 a	37.50 a	39.27 a
T5	ADV Hybrid – 9139 + 0.7 X 0.2	43.75 a	37.50 a	38.97 a
T6	ADV Hybrid – 9139 + 0.8 X 0.2	46.25 a	37.50 a	42.77 a
C.V (%)		7.39	10.48	5.17
$\bar{x}$		40.58	34.50	39.83

[1]equal letters are not significant according to Tukey’s test (P>0.05).

This is consistent with the results of Oyervides et al. (1990) cited by Cervantes et al. (2014), who determined negative effects on yield components such as cob diameter, by increasing population density; a pattern that is repeated in the research of Otahola and Rodríguez (2001).

Regarding cob length, the results obtained in this study are consistent with those of Martínez et al. (2017), who found no pronounced influence of spacing on cob length, despite observing a gradual reduction as maize plant population increased per hectare. This scenario was replicated in this study and is consistent with findings reported by Silva et al. (2009). Differences were attributed to genotypic variation among the evaluated lines, as the high heritability of these traits has been demonstrated in multiple studies, including those by Alonso et al. (2022) and Bueno and Tolentino (2022).

According to authors such as Hidalgo et al. (2020), Sandal (2014), Quevedo et al. (2015) and Cifuentes (2014), grain yield is positively and significantly associated with the number and weight of kernels, which are highly influenced by increased plant density due to reduced planting distance. This suggests that narrower row spacing leads to higher 100-seed weight. However, this pattern was not observed in any of the trials evaluated in this study.

On the other hand, Shapiro and Wortmann (2006), cited by Soltero et al. (2010), found that reducing row spacing from 0.76 to 0.51 m resulted in a 4% increase in maize grain yield. A similar trend was observed in trial 1 of this study. Specifically for the ADV-9139 hybrid, comparing the spacing used in T6 (0.8 × 0.2 m) with that in T4 (0.6 × 0.2 m), corresponding to a 0.20 m row-spacing reduction, a 17% yield increase per hectare was recorded. However, this trend did not hold for the native variety S/N, where no consistent pattern was observed in trials 1 and 3.

Nonetheless, this does not imply that narrower spacings for native genotypes would necessarily result in higher yields. León et al. (2018) caution that an irrational increase in population density could lead to yield decline due to grain abortion and an increase in sterile plants. Conversely, low densities reduce vegetative and reproductive compensation.

Table 7. Grain yield (kg/ha) in trials 1, 2 and 3. Mocache, Los Ríos province, Ecuador.

	Grain yield (Kg/ha)[1]			
	Location of trials	**John F. Kennedy, winter of 2020 (test 1)**	**Campus “La María”, winter of 2020 (test 2)**	**Campus “La María”, summer of 2021 (test 3)**
Trat[2]	**Description**			
T1	Creole variety S/N + 0.6 X 0.2	7699.11 c	10300.00 bcd	6770.97 b
T2	Creole variety S/N + 0.7 X 0.2	8139.39 c	9731.75 cd	6893.00 b
T3	Creole variety S/N + 0.8 X 0.2	7384.27 c	8632.50 d	7562.50 b
T4	ADV Hybrid – 9139 + 0.6 X 0.2	12707.42 a	13724.00 a	11278.01 a
T5	ADV Hybrid – 9139 + 0.7 X 0.2	12002.87 a	12036.50 ab	10437.63 a
T6	ADV Hybrid – 9139 + 0.8 X 0.2	10599.01 b	10864.50 bc	8452.66 b
C.V (%)		4.33	7.53	8.76
$\bar{x}$		9755.345	10881.54	8565.80

[1]equal letters are not significant according to Tukey’s test (P>0.05).
[2]Trat: Treatment.

4 Conclusions

Regarding the agronomic performance of the materials studied across the three trials, planting spacings showed minimal influence. Plant height (m), stem diameter (cm), and cob insertion height did not exhibit statistically significant differences. Yield components such as cob length, cob diameter, and 100-seed weight clearly contributed to the increase in yield per unit area. However, this increase was not driven by the weight or dimensions achieved but rather by the reduced planting distance, which allowed for a higher number of plants per unit area, resulting in more cobs and, consequently, a greater quantity of kernels.

Planting distance affected yield only in the ADV-9139 hybrid, which achieved higher yields with a row spacing of 0.60 m compared to spacings of 0.70 m and 0.80 m.

Acknowledgments

The authors extend their gratitude to the Faculty of Agricultural Sciences of the Technical State University of Quevedo for the support provided in carrying out this research, and to Engineers Jonathan Cedeño and William Sarabia for their assistance with data collection.

The activities conducted in this research are part of the FOCICYT 7th Call Project titled Aerospace Technology Applied to Spectral Responses of Tropical Crops as a Technical Element for Crop Improvement. Phase I: Maize (*Zea mays* L.).

Author's contribution

C.A.M.U.: Conceptualization, data curation, formal analysis. P.J.C.C.: Research, methodology, drafting -original draft. D.V.V.Z.: Project management, resources, and supervision. S.C.V.M.: Software, validation. J.J.P.A.: Visualization, writing - review and editing.

References

Alonso, H., Tadeo, M., Espinosa, A., Zamudio, B., Zaragoza, J., and López, C. (2022). Water and agronomic evaluation of maize hybrids in response to different environments and nitrogen doses. *Agrociencia*, 56(i1.2698):1–12. Online:https://n9.cl/2zjyt.

Bastidas, Y., Chassaigne, A., Alezones, J., and Hernández, A. (2015). Comportamiento agronómico y fitopatológico de variedades de maíz (zea mays l.) en los estados yaracuy y guárico, venezuela. *Bioagro*, 27(1):17–26. Online:https://n9.cl/int42.

Bueno, E. and Tolentino, L. (2022). Adaptabilidad de cinco híbridos de maíz amarillo duro (zea mays l.) bajo condiciones edafoclimáticas de los anitos-valle de barranca. Master's thesis, Universidad Nacional de Barranca.

Cabrera, J., Carballo, A., Mejía, J., and Vaquera, H. (2019). Caracterización de poblaciones sobresalientes de maíz de la raza zapalote chico. *Revista fitotecnia mexicana*, 42(3):269–279. Online:https://n9.cl/0qdm3.

Campos, L. (2022). Efecto del distanciamiento entre surcos y plantas sobre el rendimiento de grano de la línea de alta endogamia de "maíz amarillo duro" zea mays l.(poaceae) cml 297. Master's thesis, Universidad Privada Antenor Orrego.

Cervantes, F., Gasca, M. adn Andrio, E., Mendoza, M. adn Guevara, L., Vázquez, F., and Rodríguez, S. (2014). Densidad de población y correlaciones fenotípicas en caracteres agronómicos y de rendimiento en genotipos de maíz. *Ciencia y Tecnol. Agrop. México*, 2(1):9–16. Online:https://n9.cl/p0wavd.

Cifuentes, E. (2014). Características agronómicas y rendimiento de once híbridos de maíz, retalhuleu, retalhuleu. Master's thesis, Universidad Rafael Landívar.

CIMMYT (2014). El maíz criollo vuelve a casa 50 años después. CIMMYT. Online:https://n9.cl/h4vq4.

Gómez, L., Arteaga, M., and Acosta, E. (2021). Evaluación de tres distancias de siembra y quitomax en el cultivo del maíz (original). *Investigación*, 6(1):314–326. Online:https://n9.cl/ns6dh.

Gordón, R. and Camargo, I. (2021). Herramientas estadisticas para la evaluacion y seleccion de hibridos de maiz a traves de multiples ambientes y años. *Ciencia Agropecuaria*, (32):12–37. Online:https://n9.cl/x4b3g.

Hidalgo, M., González, V., Mendoza, L., Cruz, N., and Ramírez, I. (2020). Desempeño de arquetipos de maíz (zea mays l.) en dos densidades de población. *Agrociencia*, 54(4):491–504. Online:https://n9.cl/vy9hnl.

INEC (2020). Encuesta de superficie y producción agropecuaria continua (espac) 2019. Technical report, INEC. Online:https://n9.cl/x8fg.

León, R., Torres, A., Ardisana, E., Fosado, O., Véliz, F., and Pin, W. (2018). Comportamiento productivo del maíz híbrido agri-104 en diferentes sistemas, densidades de siembra y riego localizado. 9(2):124–130. Online:https://n9.cl/7eagh.

Martínez, R., Kölln, O., and de Castro, G. (2017). Evaluación de la densidad de plantas, componentes fenológicos de producción y rendimiento de granos en diferentes materiales genéticos de maíz. *Idesia (Arica)*, 35(3):23–30. Online:https://n9.cl/oaq3e3.

Molina, J. and Isasi, C. (2018). Abonamiento orgánico y microorganismos eficientes en la absorción de fósforo por maíz morado (zea mays l.)-ayacucho. *Investigación*, 26(1):11–16. Online:https://n9.cl/eiaqb.

Moreira, B. (2019). Evaluación agronómica de híbridos de maíz (zea mays l.), en la época lluviosa en el cantón mocache, provincia de los ríos. Master's thesis, Universidad Técnica Estatal de Quevedo.

Ogando, F., Raspa, F., Pita, M., Alvarez, C., and Vega, C. (2017). Influencia de la interacción entre la densidad poblacional y la disponibilidad de nitrógeno sobre el rendimiento de maíz sembrado en verano. In *III Workshop Internacional de Ecofisiología de cultivos*.

Otahola, V. and Rodríguez, Z. (2001). Comportamiento agronómico de maíz (zea mays l.) tipo dulce bajo diferentes densidades de siembra en condiciones de sabana. *Revista Científica UDO Agrícola*, 1(1):18–24. Online:https://n9.cl/szt23.

Oyervides, A., Ortíz, J., González, V., and Carballo, A. (1990). El número de mazorcas por planta y la formación de arquetipos de maíz. *Agrociencia Serie Fitotecnia*, 1(4):103–118. Online:https://bit.ly/4jMqUbL.

Pérez, P. (2015). Comportamiento agronómico de nuevos materiales de maíz (zea mays l) comparados con testigos comerciales, sembrados durante la época lluviosa del 2014 en fumisa. Master's thesis, Universidad Técnica Estatal de Quevedo.

Quevedo, Y., Barragán, E., and Beltrán, J. (2015). Efecto de altas densidades de siembra sobre el híbrido de maíz (zea mays l.) impacto. *Revista Scientia Agroalimentaria*, 2:18–24. Online:https://n9.cl/83bhk.

Quimi, D. (2015). Interacción genotipo-ambiente de híbridos triples experimentales de maíz (zea mays l.), en dos zonas del litoral ecuatoriano. Master's thesis, Universidad Técnica Estatal de Quevedo.

Quiroz, J., Pérez, D., González, A., Rubí, M., Gutiérrez, F., Franco, J., and Ramírez, J. (2017). Respuesta de 10 cultivares de maíz a la densidad de población en tres localidades del centro mexiquense. *Revista mexicana de ciencias agrícolas*, 8(7):1521–1535. Online:https://n9.cl/vev3z.

Rodríguez, L., Guevara, F., Ovando, J., Marto, J., and Ortiz, R. (2016). Crecimiento e índice de cosecha de variedades locales de maíz (zea mays l.) en comunidades de la región frailesca de chiapas, méxico. *Cultivos Tropicales*, 37(3):137–145. Online:https://n9.cl/le4fyl.

Sánchez, J. (2017). Comportamiento agronómico y rendimiento del cultivo de maíz (zea mays l.), con sistema de siembra a doble hilera en la zona de vinces-ecuador. Master's thesis, Universidad de Guayaquil.

Sánchez, M., Aguilar, C., Valenzuela, N., Sánchez, C., Jiménez, M., and Villanueva, C. (2011). Densidad de siembra y crecimiento de maíces forrajeros. *Agronomía mesoamericana*, 22(2):281–295. Online:https://n9.cl/le4fyl.

Sandal, M. (2014). Comportamiento agronómico de tres híbridos de maíz (zea mays l.) en el cantón pueblo viejo provincia de los ríos. Master's thesis, Universidad Técnica Estatal de Quevedo.

Satorre, E. (2021). Variabilidad de la distancia entre plantas dentro de la hilera de siembra y su efecto sobre el rendimiento del cultivo de maíz (zea mays l.) en argentina, brasil y estados unidos. *Agronomía y Ambiente*, 41(1):49–57. Online:https://n9.cl/r4wbnj.

Silva, W., Alfaro, Y., and Jiménez, R. (2009). Evaluación de las características morfológicas y agronómicas de cinco líneas de maíz amarillo en diferentes fechas de siembra. *Revista Científica UDO Agrícola*, 9(4):743–755. Online:https://n9.cl/3sydsm.

Soltero, L., Garay, C., and Ruiz, J. (2010). Respuesta en rendimiento de híbridos de maíz a diferentes distancias entre surcos y densidades de plantas. *Revista mexicana de ciencias agrícolas*, 1(2):149–158. Online:https://n9.cl/qyzykq.

Velez, M. (2019). Efecto de tres distancias de siembra en tres híbridos de maíz (zea mays l.). Master's thesis, Universidad de Guayaquil.

Videla, H., Canale, A., and Muñoz, S. (2014). Evaluación de diferentes densidades de plantas de maíz en siembras tempranas en ambientes contrastantes del territorio sudeste de córdoba. In *13 Curso Internacional de Agricultura de Precisión y Máquinas Precisas*.